Proteomic Characterization of Embryonic Epicardial-Myocardial Signaling

BY

Yanyang Li

B.S., China Agricultural University, 2010

THESIS

Submitted as partial fulfillment of the requirements
for the degree of Doctor of Philosophy in Biological Sciences
in the Graduate College of the
University of Illinois at Chicago, 2017

Chicago, Illinois

Defense Committee:

Peter Okkema, Chair
Brian Kay, Advisor
Q. Tian Wang, Congressionally Directed Medical Research Programs
Teresa Orenic
Hans-Georg Simon, Northwestern University

ACKNOWLEDGEMENTS

I thank my advisor, Q. Tian Wang, for all the time and resources she has invested in me and this research. Under her guidance, I have learned to think critically, pay attention to details while always keep the big picture in mind. This thesis and my professional development would not have been possible without her mentorship. I thank my committee members, Teresa Orenic and Pete Okkema for all their help, encouragement and critical comments to my work. I thank my committee member Brian Kay for stepping in as my official advisor. I am incredibly grateful to my committee member Hans-Georg Simon for "adopting" me to his lab during the past two years and providing valuable insights and feedbacks. A team of researchers contributed to this work. I cannot possibly list them all here, but I offer my sincere gratitude to all researchers who helped me along the way. I thank Robert Dettman for generously sharing his time and knowledge in avian heart development and epicardial biology. I thank the Hanley lab in the chemistry department, especially Yang and Gulsah as well as Shey lab at Vanderbilt University, especially Jamie, for sharing their expertise and resources in imaging mass spectrometry. I thank the members of the Wang lab (Hsiao-Lei, Andrea, Rachel, Farida and Zana), the members of Simon lab (Devin, Alex and Erin) and my fellow graduate students for their friendship and company. I thank the Schmidt lab, Orenic lab and Kay lab for sharing reagents and equipment. Lastly, I thank my family, especially my parents, Yinfeng and Shanshi, for their endless and unconditional love, support and trust.

LYY

CONTRIBUTION OF AUTHORS

For chapter II to chapter IV, Qun-Tian Wang, Hans-Georg Simon and Yanyang Li conceived and designed the experiments. Yanyang Li performed the bulk of experiments and data analysis with contributions from Qun-Tian Wang, Alexander Urban, Devin Midura, and Hans-Georg Simon. Qun-Tian and Hans-Georg assisted in interpretation of data. Devin made contribution to data presented in Figure 4 and 6. Alexander made contribution to data presented in Figure 23, 26 and 27. For chapter V, Qun-Tian Wang, Hans-Georg Simon and Yanyang Li conceived and designed the experiments. Yanyang Li performed the bulk of experiments and data analysis with contributions from Qun-Tian Wang, Jamie Wenke, Yang Cui, Gülsah Uygur, Luke Hanley and Kevin Shey. Jamie Wenke assisted in generation of Figure 38. Yang Cui and Gülsah Uygur assisted in generation of Figure 36 and Figure 39. Luke Hanley and Kevin Shey contributed reagents and materials.

TABLE OF CONTENTS

CHAPTER PAGE

I . General introduction 1
1.1 Chicken and mouse as animal models for congenital heart defects 1
1.2 Vertebrate heart development: insights from chicken and mouse embryos 2
1.2.1 Cardiogenesis: cell lineages that form the heart 2
1.2.2 Cardiac morphogenesis: trabeculation and compaction 4
1.3 Epicardial-myocardial signaling in vertebrate heart development 7
1.3.1 Cellular contribution of the epicardium to heart formation 7
1.3.2 Epicardial-myocardial signaling in the regulation of epithelial-to-mesenchymal transition and coronary vessel development 8
1.3.3 Epicardial-myocardial signaling in the regulation of cardiomyocyte proliferation and maturation 9
1.4 Epicardial-myocardial signaling in heart repair or regeneration 12
1.5 Mass spectrometry identification of cell secretomes to elucidate cellular signaling events 13
1.5.1 Defining cell secretomes 13
1.5.2 The necessity for spatially resolved *in vivo* proteomics 15
1.6 The canonical NF-κB signaling pathway 15
1.6.1 Overview of the canonical NF-κB signaling pathway 15
1.6.2 NF-κB pathway in the regulation of epithelial cell behavior 18
1.7 Purpose of this study 18

II . Mass spectrometry identification of proteins in EPDC-heart explant-conditioned medium .. 20
2.1 Introduction 20
2.2 Materials and methods 21
2.2.1 Animals 21
2.2.2 Tetrahydrofuran-Sodium lauroyl sarcosinate precipitation of proteins from conditioned medium 21
2.2.3 Preparation of EHE-conditioned medium 21
2.2.4 Silver staining 22
2.2.5 Two-dimensional liquid chromatography mass spectrometry/mass spectrometry . 22
2.2.6 *In silico* determination of the EHE secretome 24
2.2.7 Reverse transcription PCR 24
2.2.8 Enzyme-linked immunosorbent assay 25
2.2.9 Western blotting 25
2.2.10 Measurement of cytotoxicity 26
2.3 Results 26
2.3.1 Establish the EHE co-culture system 26
2.3.2 Mass spectrometry and determination of the EHE secretome 32
2.3.3 Confirmation of the presence of selected proteins in EHE-CM 34
2.4 Discussion 36
2.4.1 The EHE co-culture system 36
2.4.2 Evaluation of the proteomic approach 37

III . Bioinformatics analyses of the EHE secretome 39
3.1 Introduction 39

TABLE OF CONTENTS (continued)

CHAPTER PAGE

3.2 Materials and methods 39
3.2.1 Gene Ontology 39
3.2.2 Ingenuity pathway analysis 40
3.3 Results 40
3.3.1 Gene Ontology analysis 40
3.3.2 Pathway and network analysis 43
3.4 Discussion 57
3.4.1 The EHE secretome database: a rich source of information 57
3.4.2 A deeper look into the network and pathway analysis 57

IV . Functional characterization of the NF-κB signaling pathway in epicardial EMT 60
4.1 Introduction 60
4.2 Material and methods 61
4.2.1 Cell line and reagents 61
4.2.2 Cell culture and immunocytochemistry 61
4.2.3 Quantitative real-time RT-PCR (qRT-PCR) 62
4.2.4 Immunocytochemistry of MEC1 cells 63
4.2.5 Immunohistochemistry 63
4.2.6 NF-κB p65 nuclear translocation assay 64
4.3 Results 66
4.3.1 TGFβ2 and PDGFBB activate NF-κB signaling in primary EPDCs 66
4.3.2 NF-κB signaling is necessary for cellular and molecular changes associated with EMT 71
4.3.3 NF-κB p65 is expressed in the epicardium during embryonic EMT 75
4.4 Discussion 78
4.4.1 NF-κB in the regulation of epicardial EMT 78
4.4.2 Potential Species Difference in the Mechanism of NF-κB Activation 83

V . Protocol development of Matrix-Assisted Laser Desorption/Ionization Imaging Mass Spectrometry for the visualization and/or identification of proteins/peptides on murine heart sections 84
5.1 Introduction 84
5.1.1 Basic principles of matrix-assisted laser desorption/ionization imaging mass spectrometry in protein analysis 84
5.1.2 Current status of MALDI-IMS for *in situ* protein analysis 85
5.2 Materials and methods 89
5.2.1 Reagents 89
5.2.2 *In situ* protein identification from adult mouse heart 89
5.2.2.1 Sample preparation 89
5.2.2.2 Instrumentation and spectrums acquisition 92
5.2.2.3 Database searching 93
5.2.3 MALDI-IMS of intact proteins 93
5.3 Results 94
5.3.1 MALDI-IMS of intact proteins on embryonic mouse heart sections 94

TABLE OF CONTENTS (continued)

CHAPTER PAGE

5.3.2 *In situ* protein identification using MALDI-IMS 97
5.4 Discussion 103
5.4.1 Summary of results 103
5.4.2 Limitations of MALDI-IMS from the perspective of present study 103

VI. GENERAL DISCUSSION 106
6.1 EHE secretome: summary and perspectives 106
6.2 NF-κB signaling pathway in epicardial EMT 112
6.3 Identify secreted proteins in active sub-epicardial niche 112

APPENDICES 114
Appendix A. Proteins identified in EHE-CM 114
Appendix B. EHE secretome 151
Appendix C. Over-represented IPA Canonical Pathways in the EHE secretome 158
Appendix D. Primers used in qRT-PCR 161
Appendix E. Primers used for reverse-transcriptase PCR 162
Appendix F. Investigation of ASXL2's protein interactions 163
Appendix G. Establish culture of a cardiac muscle cell line HL-1 166
Appendix H. Creative Commons Attribution License 171
Appendix I. Animal care committee letter of approval 176

CITED LITERATURE 177

VITA 195

LIST OF TABLES

TABLE PAGE

Table I. LIST OF IDENTIFIED PROTEINS FROM ADULT MOUSE HEART SECTION ... 101

Table II. POTENTIAL CANDIDATES FOR INVOLVEMENT IN EPICARDIAL EMT 109

Table III. PROTEINS IDENTIFIED IN EHE-CM 114

Table IV. EHE SECRETOME 151

Table V. OVER-REPRESENTED IPA CANONICAL PATHWAYS[1] (P-VALUE < 0.05) IN THE EHE SECRETOME 158

Table VI. PRIMERS USED IN QRT-PCR 161

Table VII. PRIMERS USED FOR REVERSE-TRANSCRIPTASE PCR 162

LIST OF FIGURES

FIGURE PAGE

Figure 1. Summary of heart development. 5
Figure 2. Epicardium development. 11
Figure 3. Schematic representation of the canonical NF-κB signaling pathway. 17
Figure 4. Preparation of EHE-CM for mass spectrometry. 28
Figure 5. Expression and localization of the tight junction protein ZO1 in primary chicken EPDCs. 29
Figure 6. Quality control of EHE co-culture. 30
Figure 7. Compareson of TCA precipitation with ultrafiltration. 31
Figure 8. Overlap between proteins identified in triplicate EHE-CM samples. 33
Figure 9. Confirmation of 2D-LC-MS/MS results. 35
Figure 10. Gene Ontology (GO) analysis of the EHE secretome. 42
Figure 11. Graphical representation of the Wnt and TGFβ pathways. 45
Figure 12. IPA-predicted functional networks in the EPDC-heart explant secretome. 46
Figure 13. Collagen network (A) and network components (B). 47
Figure 14. Akt network (A) and network components (B). 48
Figure 15. CALR network (A) and network components (B). 49
Figure 16. PI3K network (A) and network components (B). 50
Figure 17. APP network (A) and network components (B). 51
Figure 18. Jnk network (A) and network components (B). 52
Figure 19. Immunoglobulin network (A) and network components (B). 53
Figure 20. p38 MAPK network (A) and network components (B). 54
Figure 21. TGFB1 network (A) and network components (B). 55
Figure 22. The NF-κB regulatory network. 56
Figure 23. Image analysis workflow for the quantification of signal intensity in subcellular compartments. 65
Figure 24. Response of mouse epicardial cell line MEC1 to TGFβ2 treatment. 68
Figure 25. NF-κB p65 subcellular localization in primary mouse epicardial cells after TGFβ2 and PDGFBB treatment. 69
Figure 26. NF-κB p65 subcellular localization in primary chicken epicardial cells after TGFβ2 and PDGFBB treatment. 70

LIST OF FIGURES (continued)

FIGURE PAGE

Figure 27. Inhibition of NF-κB blocks TGFβ2- and PDGFBB-induced EMT in primary chicken epicardial cells. 72

Figure 28. Inhibition of NF-κB blocks TGFβ2- and PDGFBB-induced EMT in the mouse epicardial cell line MEC1. 73

Figure 29. NF-κB inhibitor JSH-23 blocks TGFβ2/PDGFBB-induced EMT in MEC1 cells. 74

Figure 30. NF-κB p65 is expressed in mouse embryonic epicardium. 76

Figure 31. NF-κB p65 is expressed in chicken embryonic epicardium. 77

Figure 32. Proposed model for the function of NF-κB signaling in epicardial EMT. 80

Figure 33. Many targets of NF-κB pathway are present in the EHE secretome. 81

Figure 34. Gene Ontology (GO) analysis of NF-κB regulated proteins identified in the EHE secretome. 82

Figure 35. Schematic representation of the MALDI-IMS process. 88

Figure 36. CHCA matrix deposition. 91

Figure 37. H&E staining of an E13.5 mouse heart section. 95

Figure 38. Representative ion images of embryonic mouse heart using MALDI-IMS at 30 µm resolution. 96

Figure 39. Representative averaged MALDI spectrum from frozen adult mouse heart section. . 99

Figure 40. Tandem MS (MS/MS) spectrum of the peptide at m/z 2093. 100

Figure 41. MALDI imaging of frozen adult mouse section at 150 µm resolution. 102

Figure 42. Biochemical characterization of ASXL2 and ZMIZ1 interaction. 165

Figure 43. Culture and characterization of HL-1 cells. 170

LIST OF ABBREVIATIONS

µg	microgram
µl	microliter
2D-LC–MS/MS	two-dimensional liquid chromatography tandem mass spectrometry
BP	biological process
CHCA	α-cyano-4-hydroxycinnamic acid
CHDs	congenital heart defects
CM	conditioned medium
CNC	cardiac neural crest
Cre	Cre Recombinase
DAPI	4',6-diamidino-2-phenylindole
DAVID	Database for Annotation, Visualization and Integrated Discovery
DMEM	Dulbecco's Minimal Essential Media
E	embryonic day
ECM	extracellular matrix
EHE	EPDC-heart explant
ELISA	Enzyme-linked immunosorbent assay
EMT	epithelial-to-mesenchymal transition
EPDCs	epicardial-derived cells
FBS	fetal bovine serum
FGF	fibroblast growth factor
FGFR	fibroblast growth factor receptor
FHF	first heart field

LIST OF ABBREVIATIONS (continued)

GO	gene ontology
H&E	hematoxylin and eosin staining
HH	Hamburger and Hamilton
IκB	Inhibitor of kappa B protein
IKK	I kappa B kinase
IPA	ingenuity pathway analysis
LCM	laser capture microdissection
LDH	lactate dehydrogenase
m/z	mass-to-charge
MALDI-IMS	matrix-assisted laser desorption/ionization imaging mass spectrometry
MAPK	mitogen-activated protein kinase
MEM	Minimum Essential Media
ml	milliliter
mM	millimolar
MS	mass spectrometry
ng	nanograms
ºC	degree Celsius
NF-κB	Nuclear Factor- kappa B
PBS	phosphate-buffered saline
PDGF	platelet-derived growth factor
PDGFR	platelet-derived growth factor receptor
PFA	paraformaldehyde

LIST OF ABBREVIATIONS (continued)

PI3K	Phosphoinositol 3 Kinase
RNA-seq	Ribonucleic Acid sequencing
qRT-PCR	quantitative real-time polymerase chain reaction
RT-PCR	reverse transcription polymerase chain reaction
SDS-PAGE	sodium dodecyl sulfate polyacrylamide gel electrophoresis
SHF	second heart field
TGFβ	Transforming Growth Factor beta
TGFβR3	Type III TGFβ receptor
TOF	time of flight
UTD	untreated
WB	western blotting
WT1	Wilm's Tumor-1
ZO1	Zonula Occludins-1

Summary

The communication between the epicardium and the underlying myocardium is crucial not only for proper heart development but also for homeostasis and response to injury in the adult heart. Epicardial-myocardial signaling is mediated in part by proteins secreted by the myocardium and/or epicardium, such as growth factors, cytokines, and matrix proteins. Studies of epicardial-myocardial signaling using targeted approaches have yielded many insights into the molecular basis of this communication. Still, the complex molecular interactions and regulatory networks involved in the epicardial-myocardial crosstalk are not well understood.

To obtain a comprehensive, unbiased perspective on epicardial/myocardial signaling, we used a discovery-based proteomics approach that complements traditional targeted approaches. This thesis details the generation of an unbiased dataset of proteins secreted into the media by embryonic chicken epicardial-derived cells (EPDC)-heart explant (EHE) co-cultures. A 150-protein secretome dataset was then generated by integrating mass spectrometry with bioinformatics. The majority of the proteins in this dataset have not been shown to function in the context of epicardial-myocardial development. The large size of the dataset enabled bioinformatics analysis to deduce networks for the regulation of specific biological processes and predicted signal transduction nodes within the networks. Functional analysis was performed on one of the predicted nodes, NF-κB, and demonstrated that NF-κB activation is an essential step in TGFβ2/PDGFBB-induced cardiac epithelial-to-mesenchymal transition. Taken together, we have generated an unbiased EHE secretome dataset for the first time. Bioinformatics analysis of the dataset successfully predicted an essential role for NF-κB in epicardial EMT, indicating that this dataset can be used to guide functional, and targeted investigation. Further analysis of the secretome

dataset and networks may yield important insights into signaling pathways regulating epicardial-myocardial communication.

Epicardial-myocardial crosstalk occurs *in vivo* in the sub-epicardial niche. To complement our *ex vivo* culture system-based proteomic study, I explored the feasibility of developing a matrix-assisted laser desorption/ionization imaging mass spectrometry (MALDI-IMS) protocol for untargeted detection and imaging of endogenous proteins/peptides on mouse heart sections. Intact protein imaging on embryonic heart sections demonstrated the feasibility of achieving images with sufficient spatial resolution targeted to the epicardium/subepicardium area. However, *in situ* protein identification only detected the most abundant proteins, with no additional secreted proteins identified. These results suggest further technology development is needed to identify low abundance proteins directly from tissue sections.

I. GENERAL INTRODUCTION

1.1 Chicken and mouse as animal models for congenital heart defects

The heart is the first organ to form during development. From embryonic stages on, the heart continuously pumps blood through the body to sustain life. Congenital heart defects (CHDs) are the most common birth defects and affect over 1% of live births (Hoffman and Kaplan, 2002). Although many CHDs can be surgically corrected, accumulating evidence shows that there are long-term health consequences, including higher risk of heart disease later in life (Greutmann et al., 2015). Among adults, heart disease is the leading cause of death in developed countries. There is a great need to improve our ability to treat the many impairments of this vital organ, such as preventing CHDs in children and replacing scar tissue after a heart attack in adults.

Heart development among different vertebrates is a highly conserved process: beginning with the formation of linear heart tube to the early stages of looping and chamber formation (Warkman, 2009). Hence multiple model organisms, including mouse, chicken, frog and zebrafish, have been used to investigate the molecular and cellular mechanisms of heart development to provide insights into the mechanisms of CHDs. The mature chicken heart comprises four chambers with separate pulmonary and systemic circulation paths, and identival to other vertebrates, the wall of the heart chambers is comprised of epicardium, myocardium and endocardium (Moynihan et al., 2010). The anatomy of the chicken heart actually resembles that of the human heart more closely than other non-mammalian model organisms except that the ventricles of the bird heart have more muscle

mass and less chamber space due to the high physiological demand from flight (Jensen et al., 2013). The chicken cardiac muscle bands are much shorter in diameter and express more myosin isoforms than those of mammals (Moorman and Christoffels, 2003). With regard to heart development, the major difference between chicken and mouse is that the timing of fusion and differentiation of the heart fields is more rapid in the mouse so that the mouse has a cardiac crescent (Fig 1) while the chick does not (Abu-Issa and Kirby, 2008). Otherwise, early cardiac development events including the formation of heart tube, looping, formation of chambers and the development of coronary vasculature are highly similar in chicken and mouse (Jensen et al., 2013; Poelmann and Lie-Venema, Heleen; Gittenberger-de Groot, 2002). Like mammalian hearts, the chicken heart displays rhythmic posterior-to-anterior contractions very early in development (Christoffels et al., 2010; Moynihan et al., 2010).

1.2 Vertebrate heart development: insights from chicken and mouse embryos

1.2.1 Cardiogenesis: cell lineages that form the heart

The heart is composed of different tissue components originating from multiple cardiac cell lineages. Embryonic heart cells are derived from three major sources: the cardiogenic mesoderm, the cardiac neural crest and the proepicardium. Here I will give a brief overview of the early developmental events of the chicken and mouse heart. Hamburger and Hamilton (HH) staging is used to describe the chicken cardiac developmental events.

Heart development starts with a subset of precardiac mesoderm cells migrating to the anterior lateral plate mesoderm and forming bilateral heart fields (chicken) or cardiac crescent (mouse) during gastrulation (Abu-Issa and Kirby, 2008; Meilhac et al., 2014). Subsequently, the heart fields or cardiac crescent split into somatic and splanchnic layers; the cardiogenic progenitors reside in the latter (Wittig and Münsterberg, 2016). The bilateral cardiac fields or cardiac crescent

fuse at the midline to form a primitive heart tube by HH9 in the chicken and E8 in the mouse (Martinsen, 2005). The forming heart tube has an outer myocardial layer and an inner endothelial layer, which are divided by cardiac jelly. The first heart field (FHF) contributes the earliest cells that are committed to the cardiac fate. After the formation of the FHF, movement of cells from the pharyngeal mesoderm into the growing arterial pole or venous pole continues until HH22 in the chicken and E11 in the mouse (Brand, 2003; Kelly and Buckingham, 2002). These cells form the second heart field (SHF), which is localized anterior and dorsal to the linear heart tube. It is now generally accepted that in mammalian hearts, the FHF primarily contributes to the left ventricle myocardium (Kelly, 2012), while the SHF is the primary source of the outflow tract (OFT) and right ventricle (Meilhac et al., 2014). Both lineages contribute to the atria and other parts of the heart (Meilhac et al., 2014). For chicken hearts, the SHF primarily contributes to the outflow tract (Waldo et al., 2005, 2001). It is unclear whether the SHF also colonizes other parts of the avian cardiac tube. The two-layered heart tube then loops to the right to adopt a spiral shape and now the atrium is above the developing ventricles. Concomitantly, the future chambers balloon outward and become recognizable, eventually forming the mature four-chambered heart after a complex remodeling process (Fig 1).

The cardiac neural crest cells are derived from the dorsal neural tube and migrate into the heart at HH15 in chicken and E9 in mouse. This migratory cell population contributes to the vascular smooth muscle cells of the aortic arch and outflow tract. Additionally, neural crest cells contribute to the parasympathetic innervation of the heart (Harvey, 2002; Keyte and Redmond, 2012).

Another group of migratory cells that contribute to the heart is the pro-epicardium. The pro-epicardium is a transient organ that develops from the mesenchyme of the septum transversum (Fig 1D and Fig 2A) between E8.5-E9.75 in mouse and between HH14-17 in chicken. At E11,

proepicardial cells migrate towards and envelope the myocardium from dorsal to ventral, forming an epithelial sheet - the epicardium - in all vertebrates. An epicardial sheet covering the entire myocardium is formed by HH23 in chicken and E11.5 in mouse. The space between the epicardium and the myocardium is called the sub-epicardial space. This space is rich in sub-epicardial cells, hemangioblasts and primitive blood vessels along with various forms of ECM, exosomes and proteins secreted by neighboring cells. The exact makeup and source of the ECMs or proteins contained in the sub-epicardial space is unknown. The pro-epicardial cells migration and their subsequent attachment to the heart is regulated by myocardium-derived BMP signaling (Ishii et al., 2010).

1.2.2 Cardiac morphogenesis: trabeculation and compaction

Starting at HH16 in chicken and E9.5 in mouse, following heart looping, cell proliferation promotes rapid ventricular myocardium growth and development into the inner trabecular myocardium and the outer compact zone myocardium (Fig 2B). Trabeculae are ridge-like myocardial protrusions along the myocardial wall (Fig 2B), which increase surface to volume ratio and permit nutrition and oxygen uptake prior to establishment of a coronary circulation without increasing heart size. Trabeculation, the formation of trabeculae, is regulated by signaling between endocardium and myocardium. For example, endothelin, neuregulin (Gassmann et al., 1995), and Notch signaling pathways have been shown to operate across the close conjunction of endocardium and myocardium to induce proliferation and morphogenic remodeling into trabeculation (Brutsaert, 2003; Grego-Bessa et al., 2007). Between E13-E14 in mouse and HH31-HH36 in chicken (Brand, 2003), the basal portions of the trabeculae undergo a compaction process. In both mouse and chicken, these trabecular myocytes rejoin the compact myocardial layer, resulting in a dramatically thicker compact layer (Sedmera, David; McQuinn, 2008).

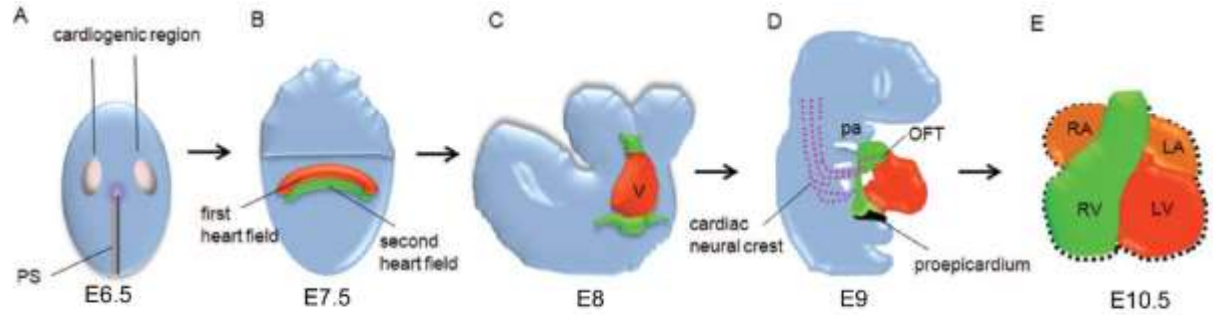

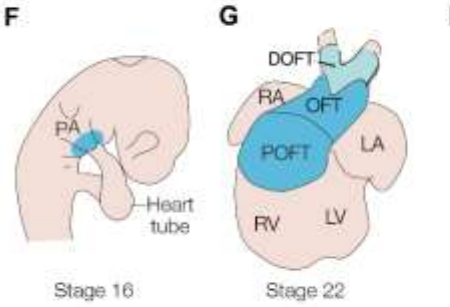

H

	Chicken (HH)	Mouse (Embryonic Day)
Gastrulation	4	7
Heart fields	5	7
Heart tube	11	8.5
Looping	13-18	8.5-10.25
Myocardial contraction	10	8.5
Arterial/Venous pole addition	14-18	8.5-10.25
Proepicardium	14-15	9-11.5
CNC migration start	14	9
Trabeculation start	16	9.5
Septation complete	34	14.5

Figure 1. Summary of heart development. (A) Cardiac progenitor stage. At approximately E6.5, myocardial progenitor cells, which originate in the primitive streak (PS), start to migrate to the anterior bilateral fields of the embryo. (B) Cardiac crescent stage. At approximately E7.5, myocardial progenitor cells form the cardiac crescent. The first heart field (FHF) starts to give rise to differentiated myocardial cells. The second heart field (SHF) is located medially to the cardiac crescent at this stage. Shown in red: FHF location and contribution. Shown in green: SHF location and contribution (the same color coding as here for the lineage contributions to the heart at later stages in C to E). (C) Linear heart tube stage. At approximately E8.0, the cardiac crescent fuses at the midline of the embryo and forms a linear cardiac tube. SHF cells start extending anteriorly and dorsally at E8.0 to E8.5 to add to the heart tube. (D) Heart looping stage. The linear heart tube subsequently undergoes looping at approximately about E8.5. At approximately E9.0, the cardiac neural crest (CNC) cells (shown in purple) start to migrate into the outflow tract (OFT) and contribute to the developing heart tube. The proepicardium (PE) (shown in black) located at the

cardiac venous pole also starts to migrate onto the looping heart tube to form the epicardium. (E) Chamber formation stage. At approximately E10.0, the heart starts to form four well-defined chambers. The location (F) and contribution (G) of the second heart field (blue) in chicken embryo. LA, left atrium; LV, left ventricle; Pa, pharyngeal arches; OFT, outflow tract (D, distal; P, proximal); RA, right atrium; RV, right ventricle; PS, primitive streak. (H) Cardiac development and associated stages in chicken and mouse heart (Martinsen, 2005).

1.3 Epicardial-myocardial signaling in vertebrate heart development

1.3.1 Cellular contribution of the epicardium to heart formation

Soon after the formation of the epicardial sheet, a subset of cells of the epicardium undergo an epithelial-to-mesenchymal transition (EMT), delaminating from the epicardial epithelium and migrating into the sub-epicardial space between the epicardium and compact myocardium. The EMT process includes several key molecular and cellular changes, including dissolution of intercellular adhesion, reorganization of cytoskeleton, acquisition of a front-rear polarity, and degradation of the extracellular matrix. Multiple cell tracing studies in the chicken and genetic lineage tracing in the mouse have determined the fate of epicardium-derived cells (EPDCs) (Miquerol and Kelly, 2013). In mice, lineage tracing using different epicardial marker (Wt1, Gata5 and Tbx18) Cre lines showed contribution to smooth muscle cells of the coronary vasculature and to cardiac fibroblasts (Merki et al., 2005; Wessels et al., 2012). Another lineage tracing study in mice showed that *Tcf21*$^{+}$ cells give rise to intracardiac fibroblasts, but not to coronary smooth muscle (Acharya et al., 2012, 2011). Cell labeling analysis of the chicken epicardium also showed contributions to perivascular fibroblast and smooth muscle cell lineages (Dettman et al., 1998). Whether epicardial cells differentiate into myocytes or coronary endothelial cells *in vivo* is a subject of on-going debate in both mouse and chicken (Mikawa and Brand, 2005; Tian et al., 2015; von Gise et al., 2012). These controversies are largely due to the challenge in generating Cre alleles with highly restricted epicardial expression. Since currently available Cre drivers may only label a subset of epicardium, the possibility of an endothelial or myocyte cell fate cannot be excluded. Additional work is required to establish a full EPDC lineage map and to discover the signals that govern EPDCs differentiation.

Physical inhibition of epicardial outgrowth to the developing heart blocked coronary vascular development in chicken (Groot et al., 2000). Similarly, loss of genes essential for epicardium formation (Wt1 and Gata4) or attachment to the myocardium in mice (interaction between myocardial Vcam1 and epicardial α4 integrin) resulted in defects in coronary development (Crispino et al., 2001; Kwee et al., 1995; Moore et al., 1999; Yang et al., 1995). These data together with the epicardium fate studies revealed that the epicardium and EPDCs contribute to coronary vasculature components, myocardial interstitial cells and/or serve as a critical developmental signaling center (Mikawa and Brand, 2005; Olivey and Svensson, 2010; Pérez-Pomares et al., 2011) in heart development.

1.3.2 Epicardial-myocardial signaling in the regulation of epithelial-to-mesenchymal transition and coronary vessel development

Epicardial EMT and subsequent coronary vessel development can be regulated by epicardial or myocardial derived signals (Germani et al., 2015; Lavine and Ornitz, 2007; Olivey and Svensson, 2010; von Gise et al., 2012). Here I will highlight 4 of the most studied pathways as described below.

FGF10 has been shown to be expressed in the compact myocardium and FGF10 treated heart explants displayed increased EPDCs migration. Epicardial-specific deletion of FGFR1/2b results in abnormal EMT and defects in EDPCs differentiation (Vega-Hernández et al., 2011), suggesting the FGF10 signals to epicardial FGFR1/FGFR2b to promote epicardial EMT, enhance EPDCs motility, and stimulated their differentiation into cardiac fibroblasts. Multiple Wnt ligands are expressed in the developing myocardium (Gessert and Kühl, 2010). WT1 mutant mice showed reduced expression of epicardial β-catenin and down-stream targets of canonical Wnt/ β-catenin signaling (von Gise et al., 2011). Treatment of EPDCs with canonical Wnt inhibitors such as Dkk1

or Sfrp2 led to diminished EMT (von Gise et al., 2011), suggesting that Wnt signaling originating from the myocardium promote epicardial EMT.

Both *Tgfβ2* and *Pdgfb* are primarily expressed in the epicardium and/or sub-epicardium before E12.5 during the developmental EMT processes (Cooley et al., 2014; Molin et al., 2003; Van Den Akker et al., 2005). *Pdgfb* mutant mice developed blood vessel dilation and thin wall in the right ventricule (Levéen et al., 1994). Epicardial deletion of both PDGF receptors resulted in failure of epicardial EMT and EPDC formation. Specifically, epicardial loss of PDGFRβ blocked differentiation of EPDCs into vascular smooth muscle cells while loss of PDGFRα in epicardium impaired EPDCs differentiation into fibroblasts. TGFβ1, TGFβ2 and TGFβ3 have been shown to promote epicardial EMT in both chicken and mouse *in vitro* (Compton et al., 2006; Sánchez and Barnett, 2012). While TGFβ ligand knockout models do not have coronary vessel abnormalities (Arthur and Bamforth, 2011), deletion of *Tgfβr2* in both the myocardium and the epicardium results in impaired coronary vasculogenesis. Similarly, homozygous deletion of *Tgfβr3* resulted in reduced epicardial proliferation and impairment of EPDCs invasion. Furthermore, specific disruption of epicardial ALK5 causes defective formation of a smooth muscle cell (Sridurongrit et al., 2008), demonstrating that TGFβ signaling via ALK5 is important in epicardial development and function *in vivo*.

1.3.3 Epicardial-myocardial signaling in the regulation of cardiomyocyte proliferation and maturation

The embryonic heart grows primarily via proliferation of cardiomyocytes (Foglia and Poss, 2016). The rate of cardiomyocyte proliferation is highest at E12 and E15, then slows down during late fetal development (Walsh et al., 2010), coinciding with the time window of epicardial EMT. Both physical and genetic inhibition of epicardium formation in chicken and mouse leads to decrease in

myocyte proliferation and results in a thinner compact myocardium (Groot et al., 2000; Pennisi et al., 2003; Sucov et al., 2009). EPDC-conditioned media treatment has been shown to promote proliferation and maturation of isolated neonatal cardiomyocytes (Weeke-Klimp et al., 2010). These data demonstrated that epicardial-myocardal signaling is pivotal to proliferation and maturation of the developing myocardium (Pennisi et al., 2003; Sucov et al., 2009).

Fgf9 is expressed in the epicardium at E10.5 (Lavine et al., 2005). Myocardial-specific deletion of FGFR1/FGFR2 or complete loss of FGF9 resulted in decreased myocardial proliferation and premature differentiation of cardiomyocytes. (Lavine et al., 2005; Stuckmann et al., 2003; Wu et al., 1999). A recent study suggests epicardial-derived adrenomedullin drives cardiomyocyte proliferation during mouse heart development (Wetzel-Strong et al., 2014). Furthermore, RA signaling has been shown to indirectly stimulate myocardial growth by activating the epicardial secretion of IGF2. Compact zone cardiomyocyte proliferation was reduced upon loss of IGF2 ligand and myocardial loss of the receptors IGF1R/INSR (Brade et al., 2011; Li et al., 2011). This study also indicates that there might be additional epicardial mitogenic activity other than IGF signaling, highlighting the importance of further characterizing epicardial-myocardial signaling components.

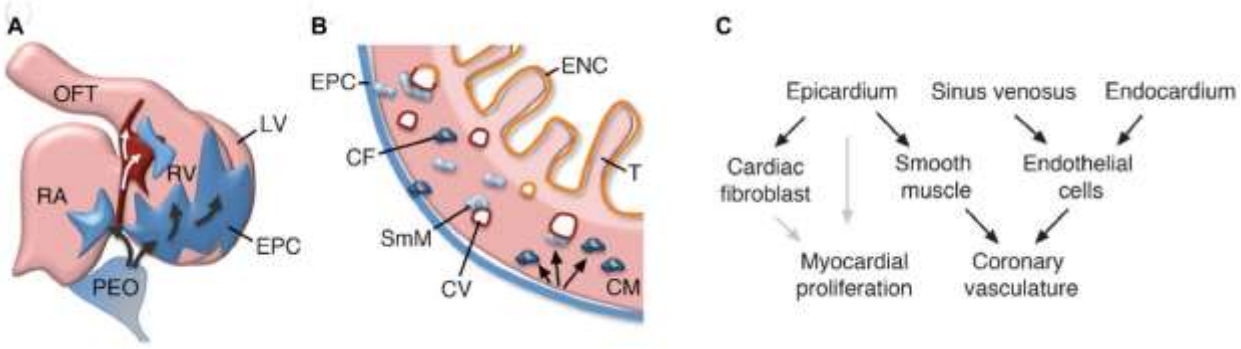

Figure 2. Epicardium development. (A) Right lateral view of a midgestation heart showing attachment of cells derived from the proepicardial organ (PEO) and spreading of epicardial cells (blue) over the external surface of the heart (black arrows). Endothelial progenitor cells originating from the sinus venosus (red) also spread over the surface of the heart (white arrows). (B) Cartoon showing epicardial-derived (black arrows) cardiac fibroblasts (CF) and smooth muscle cells (SmM) in the ventricular wall associated with coronary endothelial cells (red, orange). (C) Scheme showing epicardial contributions to myocardial proliferation and coronary vasculature. Proliferative signals are indicated by gray arrows. CM, compact ventricular myocardium; CV, coronary vascular endothelial cells; ENC, endocardium; EPC, epicardium; LV, left ventricle; OFT, outflow tract; RA, right atrium; RV, right ventricle; T, trabeculae.

1.4 Epicardial-myocardial signaling in heart repair or regeneration

Epicardial activation after cardiac injury has been shown in both adult lower vertebrates and neonatal mice, and is characterized by upregulation of epicardial marker genes that have been shown to be significantly down-regulated in postnatal epicardium, such as Tbx18 or Raldh2 (Darehzereshki et al., 2015; Masters and Riley, 2014; Smart et al., 2012). It was reported that inhibition of epicardial FGFR blocked epicardial cell integration into the wound area and neovascularization (Kikuchi, 2014). Another key epicardial response is to establish a pro-regenerative ECM environment. For example, epicardium associated Tenascin C was shown to support cell cycle reentry in adult newt cardiomyocytes (Mercer et al., 2013). In addition, epicardial fibronectin was enriched of the injury site, and in zebrafish, Fibronectin1 deletion resulted in defective heart regeneration (Mercer et al., 2013; Wang et al., 2013). Together these findings highlight the important roles of epicardium-myocardium communication for heart regeneration (Porrello and Olson, 2014).

Unlike adult zebrafish, newts or neonatal mice, adult mammalian hearts are unable to efficiently regenerate lost cardiomyocytes and are mended by fibrotic scars instead. The mammalian adult heart epicardium is normally quiescent. However, it can respond to cardiac injury by re-activating part of its embryonic program, producing paracrine factors that promote angiogenesis, reduce infarct size and improve short-term heart function (Zhou et al., 2011). A recent study reported a role for epicardial activation in suppressing the post-infarct inflammatory response through paracrine mechanisms, thus limiting deleterious remodeling following myocardial injury. (Ramjee et al., 2017). Furthermore, transplantation of human EPDCs into infarcted mouse hearts markedly upregulated angiogenesis and improved heart function (Winter et al., 2007), highlighting the contribution of EPDCs to the adult heart repair.

The regenerative potential of the adult mammalian epicardium was further demonstrated in a recent study (Wei et al. 2015). The investigators observed a maladaptive shift of epicardial follistatin-like 1 (FSTL1) to the myocardium following injury and showed that epicardial delivery of FSTL1 can induce proliferation of existing cardiomyocytes. Another example is that priming with Thymosin β4, a myocardium-derived peptide, before myocardial infarction may activate the epicardium and induce adult epicardial progenitor mobilization and act as a source of cytokines capable of promoting neovascularization (Smart et al., 2007; Zhou et al., 2012).

Taken together, these studies support the view that if provided with the correct combination of signals and cues, the adult mammalian epicardium may be re-programmed to function like its counterpart in embryonic/neonatal mice, zebrafish or newt hearts to enhance the regenerative capacity of the heart in later stages of life.

1.5 Mass spectrometry identification of cell secretomes to elucidate cellular signaling events

1.5.1 Defining cell secretomes

The proteome is the repertoire of proteins produced by a particular cell, tissue type or an organism at a specific time point. The genome of an organism is more or less constant. The transcriptome has certain variability, but the proteome is dynamic and complex, varying from cell to cell and reflecting the effects of both internal and environmental signals. Thus, the advantage of proteomics over transcriptomics is that the real functional molecules of the cell are being studied.

A secretome consists of proteins that are released into the extracellular enviroment or remain attached to the cell surface (transmembrane proteins). Secreted proteins are the major players in paracrine/autocrine signaling in a specific microenvironment. Systematic characterization of secretomes will provide resources for the identifying basic components and investigating complex

interactions involved in many signaling networks. Thus, the characterization of the secretome is critical for understanding of biological processes such as cell migration, cell signaling and communication.

Extracellular proteins in tissue culture are secreted through the protein secretion pathways. Proteins in the extracellular space are either secreted by continuous exocytosis of transport vesicles or by release of secretory vesicle after receiving regulatory signals. The secreted proteins mostly contain N-terminal signal peptides (SP) that direct them to the endoplasmic reticulum (ER). The SP is cleaved from nascent proteins during post-translational modification and the mature protein is released into the ER lumen. The proteins are transported to the Golgi and then to the plasma membrane, where they are released into extracellular space. This well-characterized secretory pathway is also known as the "classical secretory pathway" (Gilmore, 1993; Mellman and Warren, 2000). Alternatively, proteins can be exported by various ER/Golgi-independent pathways, also known as the "non-classical secretory pathway". For example, proteins can also be secreted through releasing exosomes or by direct translocations across the plasma membrane using distinct transport systems (Nickel, 2010).

Mass spectrometry (MS) is the most powerful approach to characterize proteomes including secretomes. In this dissertation, we performed gel-free two-dimensional liquid chromatography tandem mass spectrometry (2D-LC–MS/MS) to achieve a systematic protein identification of the chicken EPDC-heart explant (EHE) co-culture conditioned medium. In this widely-used bottom-up approach, individual protein identification is realized by identifying its unique peptides. The detailed workflow of the experiment is described in Chapter II and III.

1.5.2 The necessity for spatially resolved *in vivo* proteomics

Although a LC-MS/MS analysis using an *ex vivo* culture system has clear advantages over targeted approaches such as immunohistochemistry, it cannot directly interrogate signaling *in vivo* and thus cannot capture the full complexity of the microenvironments in which epicardial-myocardial signaling events take place. Epicardial-myocardial crosstalk occurs *in vivo* at the extracellular space between epicardium and myocardium - the sub-epicardial niche. Therefore, another approach to study the *in vivo* proteome within a targeted histological area is required. One technology that can directly measure analytes with spatial resolution from tissue sections is matrix-assisted laser desorption/ionization imaging mass spectrometry (MALDI-IMS). Specifically, MALDI-IMS combined with on-tissue digestion is used in protein identification *in situ*. The ultimate goal of this type of MALDI-IMS experiment is to directly correlate the detected peptides and the original precursor protein with their spatial distribution. While this technology represents an important step forward to achieve a spatially resolved proteome, several important hurdles - such as spatial resolution, sensitivity and dynamic range - stand between current MALDI-IMS techniques and their routine use on biological samples. Chapter V of this dissertation describes the basic principle of MALDI imaging technology and my effort to develop a protocol for *in situ* protein identification from heart tissue.

1.6 The canonical NF-κB signaling pathway

1.6.1 Overview of the canonical NF-κB signaling pathway

The avian and mammalian NF-κB transcription factors consist of five Rel domain homology proteins: NFκB1/p50, NFκB2/p52, RelA/p65, RelB, and c-REL. The functional units of NF-κB are dimer protein complexes, with p65/p50 being the most prevalent form (Ghosh et al., 1998). These proteins share a Rel homology domain (RHD), which is important for DNA

binding/dimerization and interaction with IkB proteins. NF-κB proteins form homo- or heterodimers can bind to target genes and have different activities depending on subunit composition. A schematic representation of the canonical NF-κB pathway is shown in Fig 3. In the absence of activating signals, NF-κB is sequestered in the cytoplasm via interaction with inhibitory proteins of the IκB family such as IκBα and IκBβ. Upon stimulation, the IκB kinase (IKK) phosphorylates IκB proteins, which causes ubiquitination and proteosomal degradation of IκB and in turn nuclear translocation of NF-κB, activating target genes. The IKK complex consists of two catalytic subunits, IKKα and IKKβ, and the NEMO/IKKγ scaffolding protein. Thus, in the canonical NF-κB pathway, the transcriptional activity of mammalian NF-κB is primarily regulated by change of subcellular localization (Hayden and Ghosh, 2012; Kanegae et al., 1998; Ryzhakov et al., 2013; Verma et al., 1995). The activation of NF-κB is also regulated by negative feedback inhibition through the expression of IκBα, which is NF-κB-dependent. If the stimulus remains, the inhibitor degradation and re-synthesis cycles can lead to oscillations of NF-κB nuclear translocations.

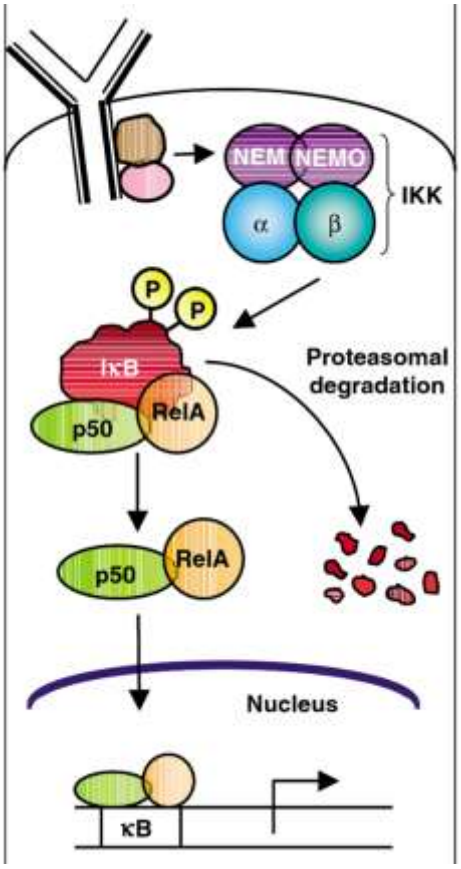

Figure 3. Schematic representation of the canonical NF-κB signaling pathway. NF-κB dimers such as p50/p65 are maintained in the cytoplasm by interaction with IκB molecule (often IκBα). In many cases, the binding of a ligand to a cell surface receptor recruits adaptors to the cytoplasmic domain of the receptor. In turn, these adaptors often recruit an IKK complex directly onto the cytoplasmic adaptors. This clustering of molecules at the receptor activates the IKK complex. IKK then phosphorylates IκB, which leads to its degradation by the proteasome. NF-κB then enters the nucleus to turn on target genes. The auto-regulatory aspect of the canonical pathway, wherein NF-κB activates expression of the IκBα gene that leads to re-sequestration of the complex in the cytoplasm by the newly synthesized IκB protein is not shown.

Adapted by permission from Macmillan Publishers Ltd: [Oncogene] (Gilmore, 2006), copyright (2006).

1.6.2 NF-κB pathway in the regulation of epithelial cell behavior

The NF-κB pathway has been shown to regulate multiple biological processes such as cell proliferation, differentiation and survival, as well as immune responses. With particular interest for this present work, I will highlight the role of NF-κB family in regulating epithelial cell behavior in both pathological and physiological contexts. NF-κB has been shown to promote EMT, migration and invasion of pancreatic carcinoma cells (Maier et al., 2010) and breast cancer cells (Huber et al., 2004). NF-κB signaling has been reported to be involved in epithelial-mesenchymal interactions in the developing chick limb (Kanegae et al., 1998). Overexpression of NF-κB targeted to the lung epithelium decreased apoptosis of epithelial cells (Londhe et al., 2008), and deletion of IKKβ in alveolar epithelium enhances cell apoptosis (Londhe et al., 2011). Knockdown of IKKβ in mouse lung epithelial cells significantly decreased expression of VEGF, a known factor regulating epithelial-mesenchymal transition (Londhe et al., 2011). Furthermore, recent research shows that NF-κB is required downstream of TGFβR3 for invasion of an immortalized epicardial cell line (DeLaughter et al., 2016). Together these studies suggest that NF-κB plays a regulatory role in EMT.

1.7 Purpose of this study

Signaling between the epicardium and underlying myocardium is crucial for proper heart development. In addition, activation of the epicardium plays an essential role during heart regeneration in both adult lower vertebrates and neonatal mice. The complex molecular interactions and regulatory networks involved in the epicardial-myocardial crosstalk are not well understood. A comprehensive understanding of these interactions and networks holds the potential to translate into mechanisms to enhance cardiac repair. In this study, mass spectrometry was integrated with bioinformatics to systematically characterize the secretome of embryonic chicken

EPDC-heart explant (EHE) co-cultures. The MS dataset was analyzed with bioinformatics tools to deduce networks present in the secretome and predict signal transduction nodes within predicted networks. We then tested one of the predicted nodes, NF-κB, by functional assays and demonstrated that NF-κB activation is an essential step in TGFβ2/PDGFBB-induced epicardial EMT. Taken together, our proteomic-bioinformatics approach opens exciting new avenues for investigating the molecular basis of heart development and regeneration.

The purpose of this work was to achieve the following goals:

Objective 1: To generate an unbiased dataset of proteins in the conditioned media of embryonic chicken EPDC-heart explant (EHE) co-culture system.

Objective 2: To present a case study of how the dataset can be used to guide functional, targeted investigation.

Objective 3: To develop a protocol of Matrix-Assisted Laser Desorption/Ionization Imaging Mass Spectrometry (MALDI-IMS) for the visualization and/or identification of proteins/peptides in murine heart sections.

II. MASS SPECTROMETRY IDENTIFICATION OF PROTEINS IN EPDC-HEART EXPLANT-CONDITIONED MEDIUM

2.1 Introduction

Signaling within and between the epicardium and underlying myocardium is essential for proper shaping and function of the heart. Experimental studies in murine and avian models have shown that perturbation of epicardial-myocardial signaling results in cardiac malformations reminiscent of those presented in human CHDs, including abnormal coronary vasculogenesis, annulus fibrosis, and compaction of the cardiac wall (Arthur and Bamforth, 2011; Kolditz et al., 2008; Ruiz-Villalba and Pérez-Pomares, 2012; Zhou et al., 2010).

Epicardial-myocardial signaling is mediated in part by proteins secreted by the myocardium and/or epicardium, such as growth factors, cytokines and matrix proteins. These proteins either directly regulate epicardial EMT or affect the underlying myocardium, which also has a paracrine role in regulating coronary vessel development. Studies of epicardial-myocardial signaling using targeted approaches have identified important roles for a number of growth factors, including TGFβ, PDGF, Wnt9b, Shh, VEGF, IGF, and several FGFs (reviewed in (Olivey and Svensson, 2010; Pérez-Pomares et al., 2011)). In this study, we aim to obtain a comprehensive and unbiased picture of epicardial-myocardial signaling, complementing targeted approaches that investigate specific molecules. Towards this goal, we first established an *ex vivo* chicken epicardial-derived cells (EPDC)-heart explant (EHE) co-culture system that partially preserves the complexity of epicardial-myocardial communication at the chosen developmental stage. Then we used unbiased

discovery proteomics to systematically identify proteins secreted into the medium by the EHE co-culture. To our knowledge, this study is the first proteomic characterization of epicardial-myocardial signaling.

2.2 Materials and methods

2.2.1 Animals

All animal studies were performed in accordance with the Animal Care Committee (ACC) and Institutional Animal Care and Use Committee (IACUC) policies at University of Illinois at Chicago (IACUC protocol number 13-002) and Northwestern University (IACUC protocol number 13-035). All experimental mice are on a C57BL/6J genetic background.

2.2.2 Tetrahydrofuran-Sodium lauroyl sarcosinate precipitation of proteins from conditioned medium

HEK293 cells and AREC (adult rat epicardial cells) were cultured in Dulbecco's modified Eagle's medium (DMEM, Invitrogen) supplemented with 10% fetal bovine serum (FBS, HyClone) and penicillin/streptomycin (10 μg/ml) in a 5% CO_2 tissue culture incubator. Cells were washed with PBS and DMEM three times after removing full medium and then cultured for another 24 hours in DMEM. The conditioned medium was collected and centrifuged to remove dead cells. Proteins were precipitated by adding Sodium lauroyl sarcosinate (NLS) and TCA (tetrahydrofuran) to 0.1% and 7.5%, respectively, and incubating at 4°C overnight. The precipitates were dissolved in 2 ml tetrahydrofuran and stored in -80°C.

2.2.3 Preparation of EHE-conditioned medium

Fertilized eggs of White Leghorn chicken (Gallus gallus) were incubated in a humidified bird hatching incubator at 37°C for 4 days before heart isolation. Embryos were staged according to Hamburger and Hamilton (HH; Hamburger and Hamilton, 1951). HH22-24 hearts were dissected

into sterile PBS. 10 hearts were placed onto a 35 mm plate covered with MEM (Corning, 17305-CV) supplemented with primocin (Invivogen) and cultured for 24 hours in a 5% CO2 tissue culture incubator at 37°C. Primary EPDC cultures were washed with fresh MEM to remove blood cells pumped out of the hearts. After the final wash, fresh medium was added and the cells were incubated for another 12 hours. Conditioned medium was then collected.

For each mass spectrometry sample, conditioned medium from 4 plates was pooled and centrifuged at 1,000g for 10 min at 4°C to remove dead cells. The supernatant was further centrifuged at 100,000g for 1 hour at 4°C to remove small debris. The supernatant was concentrated to approximately 60µl using Amicon ultrafiltration units (Millipore, UK) with a 3KD cutoff membrane and washed with 50mM Ammonium Bicarbonate for three times. Concentrated EHE-CM was subjected to mass spectrometry analysis, silver staining, and/or Western blotting.

2.2.4 Silver staining

A 2µl aliquot from each sample was analyzed by sodium dodecyl sulfate polyacrylamide gel electrophoresis (SDS-PAGE) and the protein content was detected by silver staining as previously described (Chevallet et al., 2006).

2.2.5 Two-dimensional liquid chromatography mass spectrometry/mass spectrometry

Two-dimensional liquid chromatography tandem mass spectrometry (2D-LC-MS/MS) service was provided by Duke University School of Medicine. Protein concentrations were measured by Bradford assay and 20 µg of protein from each sample was denatured and reduced by addition of 0.2% (w/v) acid labile surfactant (ALS-1) and 10 mM DTT and heating at 80°C for 10 minutes. Next, 25 mM iodoacetamide was added, and samples were incubated at room temperature in the dark for 30 minutes. Next, 1:50 (w/w) Sequencing Grade Modified Trypsin (Promega, Fitchburg, WI, USA) was added, and samples were incubated at 37°C overnight. After digestion, a final

concentration of 1% trifluoroacetic acid (TFA) and 2% acetonitrile (MeCN) were added and incubated with samples at 60°C for 2 hours. Samples were centrifuged at 20,000g for 5 minutes and lyophilized. Finally, peptides were reconstituted in 100 mM ammonium formate (pH 10), containing 50 fmol of MassPrep ADH standard (Waters, Milford, MA, USA) per μg and transferred to Total Recovery LC Vials (Waters, Milford, MA, USA).

Three micrograms of digests were analyzed by 2D-LC-MS/MS as previously described (Foster et al., 2015; Hoos et al., 2013). The 2D-LC used a nanoACQUITY with 2D Technology (Waters). Briefly, peptides were first trapped at pH 10 on a 5 μm XBridge BEH130 C18 300 μm x 50 mm column (Waters) and eluted from the first dimension column with step gradient of MeCN (10.8%, 14.0%, 16.7%, 20.4% and 50.0%). For the second dimension separation, peptides were trapped on a 5 μm Symmetry C18 180 μm × 20 mm column (Waters), and analytical separation used a 1.7 μm Acquity BEH130 C18 75 μm × 150 mm column (Waters) with a linear gradient of 7 to 35% MeCN over 37 minutes, at a flow rate of 0.5 μl/min. For MS data collection, the LC was interfaced to a Synapt G2 HDMS mass spectrometer (Waters) via a nanoelectrospray source. Data was acquired in ion mobility assisted data-independent analysis (HDMSE) mode using a 0.6-second cycle time alternating between low collision energy (6 V) and high collision energy ramp in the transfer region (27 to 50 V).

Data was searched using Protein Lynx Global Server (Waters) against a refseq *Gallus gallus* database (downloaded on 10/24/13), which contained additional reference standards and an equal number of reverse sequences (73,696 total entries). Searches were performed using the trypsin enzyme (with up to 2 missed cleavages). Fixed modifications for carbamidomethyl (C) as well as variable modifications for deamidation (NQ) and oxidation (M) were used in the database searches. Results were imported into Scaffold (Proteome Software Inc., Portland, OR) and annotated at a 1%

protein false discovery rate. Data from two 2D-LC-MS/MS experiments with triplicates in each experiment were compiled into a single data set. All proteins that meet the search criteria were included. Only one protein per gene name was kept in the final data set.

2.2.6 *In silico* determination of the EHE secretome

To build the EGE secretome database, we used SignalP4.1 (Petersen et al., 2011), DAVID (Database for Annotation, Visualization and Integrated Discovery) v. 6.7 (Huang et al., 2009) and Ingenuity Pathway Analysis (QIAGEN, Redwood City, CA) software to assign secreted and/or plasma membrane-associated proteins. Amino acid sequences from all identified proteins were submitted to the SignalP4.1 server online database to identify predicted cleavable signal peptides. The default settings were used and the eukaryotes organism group was chosen. Proteins reached the significance threshold of SignalP4.1 were included in the EHE secretome database. All proteins annotated as being extracellular by DAVID v6.7 were added to the database. All proteins annotated as "extracellular space" and "plasma membrane" by the IPA software were also added to the database. Finally, the combined dataset was cleaned up of redundancies. Of note, to reduce false positives, we excluded proteins that were predicted to be secretory using unconventional secretion pathway (Nickel, 2010) but were not validated by experiments.

2.2.7 Reverse transcription PCR

Total RNA was extracted from chicken heart explants, chicken EPDCs or MEC1 cells using the RNeasy mini kit (Qiagen, CA, USA). EPDCs were allowed to grow 24 hours before RNA isolation. The OneStep RT-PCR kit (Qiagen, CA, USA) was used for the reverse transcription PCR (RT-PCR). QuantumRNA Universal 18S Internal Standard (Applied Biosystems, Foster City, CA) was used to analyze 18s rRNA.

2.2.8 Enzyme-linked immunosorbent assay

Chicken EHE-CM was collected as described above. To prepare mouse EHE-CM, E11.5 mouse hearts were cultured on collagen (BD 354236) coated tissue culture dishes in DMEM supplemented with 10% FBS and Primocin. After 48 hours, medium was replaced with fresh DMEM and EPDCs were cultured for additional 12 hours before collection of CM. Enzyme-linked immunosorbent assay (ELISA) was performed following a standard protocol (Huang et al., 2016). Briefly, Nunc microtiter plates (Thermo Fisher Scientific Inc., Waltham, MA) were coated with CM or control medium (MEM or DMEM) overnight at 4°C in triplicates and then blocked with 5% BSA in PBS for 1 hour. Primary antibodies used were: anti-Thymosin β4 (Abcam, ab14335), anti-MMP2, anti-TGFβ2, anti-DKK3, anti-IGFBP7 and anti-SPARC. After overnight incubation in primary antibody in 0.5% Tween-20 in PBS (PBST) at 4°C, the wells were washed for 5 times with PBST and incubated with appropriate HRP-conjugated secondary antibodies in PBST for 1 hour. The wells were then washed for 5 times with 0.5% Tween-20 in PBS. The chromogenic substrate, 2,2'-azino-bis(3-ethylbenzthiazoline-6-sulfonic acid) (ABTS), was added in the presence of 3% hydrogen peroxide and incubate for 5-30 minutes. Absorbance was determined at 405 nm with a microtiter plate spectrophotometer (BMG Labtech, Germany).

2.2.9 Western blotting

Chick hearts were lysed and homogenized by passing through 21-gauge needle in RIPA buffer (Sigma, St. Louis, MO) supplemented with protease inhibitors cocktail (EMD Millipore, Billerica, MA). Chick hearts lysate or concentrated EHE-CM was suspended with 2x Laemmli sample buffer, separated by SDS-PAGE and detected using the following primary antibodies: anti-Beta Amyloid (Covance, SIG-39320), anti-ApoA1 (ThermoFisher, PA5-21166), anti-MMP2 (Abcam, ab37150), anti-TGFβ2 (Santa Cruz, sc-90) and anti-TGFβ3 (Santa Cruz, sc-82). Appropriate

HRP-conjugated secondary antibodies (Jackson ImmunoResearch) were then used. The reactivity was revealed by Immobilon Western chemiluminescence (Millipore).

2.2.10 Measurement of cytotoxicity

Lactate dehydrogenase (LDH) activity was measured using Cytotoxicity Detection Kit (Roche), according to manufacturer's instructions, at 36 and 48 hours of culturing. Total LDH in the EHE culture was determined by adding Triton X-100 solution to the medium 2% to lyse all EPDCs and tissue in the culture. Assessment of cytotoxicity was calculated according to the formula: % of total LDH release=[(A–B)/(C–B)] ×100, with A=LDH measurement of EHE-conditioned medium, B=LDH measurement of fresh medium, and C=total LDH in the EHE culture. Propidium iodide (Life Technology) staining was performed at 36 hours of culturing. Briefly, after conditioned medium was collected, the EPDC monolayer was stained with 0.3 μg/ml propidium iodide solution for 30 minutes, washed with PBS and fixed with 4% PFA before imaging with a Leica DM-IRB inverted microscope.

2.3 Results

2.3.1 Establish the EHE co-culture system

EHE co-cultures were established from embryonic day 4 (E4) chicken hearts (Fig 4A-C). At this developmental stage (HH22-24), *in vivo* EPDCs are beginning to undergo EMT, invade into the myocardium, and differentiate (Hiruma and Hirakow, 1989; Martinsen, 2005). In a heart explant culture, EPDCs migrate off the surface of the heart and form a monolayer of primary cells. These EPDCs proliferate but remain joined by tight junctions, showing a cobblestone-like appearance (Fig 4B,C and Fig 5). The heart separated from the EPDCs contains primarily cardiomyocytes (>90%), a small fraction (~6%) of endothelial cells, and even smaller fraction of other cell types

(Welikson et al., 2007). Hence the predominant cellular players in the co-culture system are EPDCs and the myocardium.

Conditioned media (CM), especially those collected from primary cell cultures, are inevitably contaminated by intracellular proteins derived from apoptotic cells (Blanco et al., 2012; Chevallet et al., 2007). To minimize cell apoptosis and maximize secreted protein enrichment, we monitored cell viability at different time points during culture by propidium iodide staining and lactate dehydrogenase assay (Fig 6). The cultured epicardial cells are negative for propidium iodide staining, indicating these cells are healthy. The explanted heart revealed positive staining, though, indicating cell apoptosis (Fig 6B, C). LDH assay indicated that the level of apoptosis is significally higher after 48 hours of culture than at 36 hours (Fig 6D). Thus the conditioned medium was collected after 36 hours of culture.

Two protein concentration methods were tested, including TCA precipitation and molecular weight cutoff filters. The ultrafiltration method was chosen over TCA precipitation method because it generated a much higher yield (Fig 7). CM samples produced using the above collection scheme and concentration method exhibited highly reproducible protein bands on silver-stained SDS-PAGE (Fig 4D). Western blotting confirmed the presence of TGFβ2 and TGFβ3, two growth factors that have been reported to mediate epicardial-myocardial signaling (Molin et al., 2003; Olivey and Svensson, 2010; Sanford et al., 1997), in CM samples (Fig 4E).

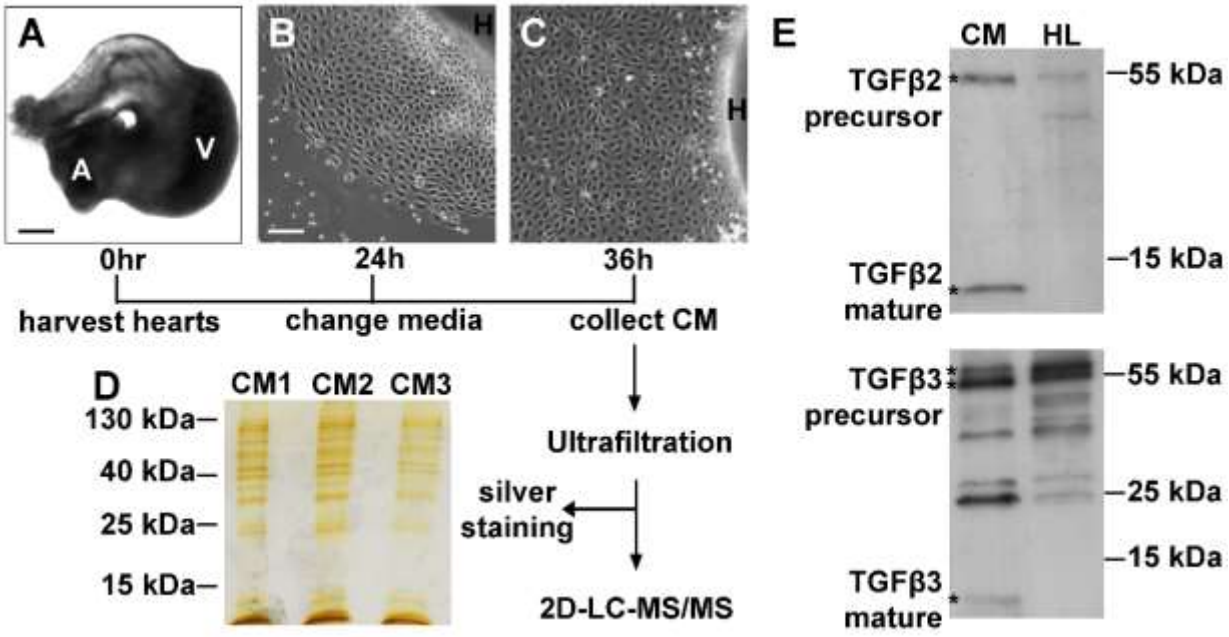

Figure 4. Preparation of EHE-CM for mass spectrometry. Representative images of chicken heart explant at 0 hour (A), EHE co-culture at 24 hours (B) and 36 hours (C). Scale bar: 80 μm in (A); 40 μm in (B-C). (D) Silver-stained SDS-PAGE gel of 3 independent preparations, CM1-3. (E) Western blot of TGFβ2 and TGFβ3 in CM preparations. CM, conditioned medium; H, heart explant; HL, heart lysate; A, atria; V, ventricle.

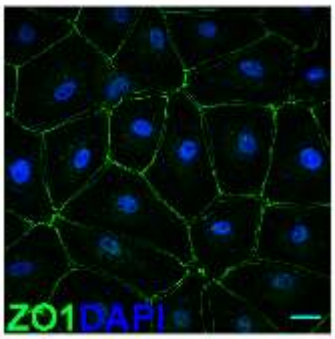

Figure 5. Expression and localization of the tight junction protein ZO1 in primary chicken EPDCs. Cultured primary chicken EPDCs were stained for ZO1 (green) and DAPI (blue). Scale bar: 20 μm.

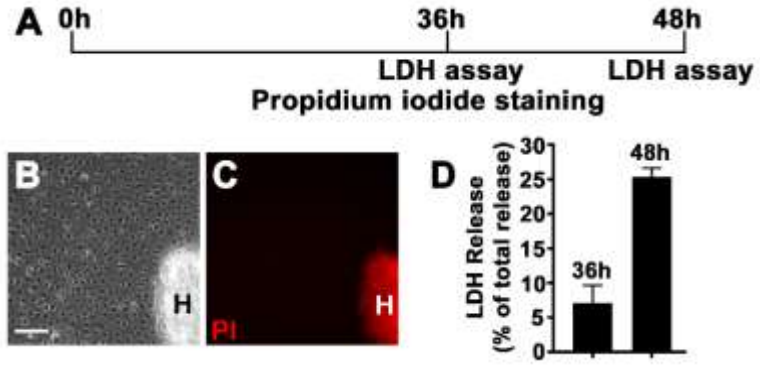

Figure 6. Quality control of EHE co-culture. (A) The experimental timeline, starting at the time of heart harvest (0h). (B) Phase contrast image of EHE co-culture at 36 hours. H: heart. (C) Corresponding propidium iodide (PI) staining (red) of the same field. (D) Lactate dehydrogenase (LDH) levels in the CM, measured at 36 hours and 48 hours and normalized to total LDH in whole-culture lysate. Data are shown as mean ± standard deviations (n=3). Scale bar: 40 μm.

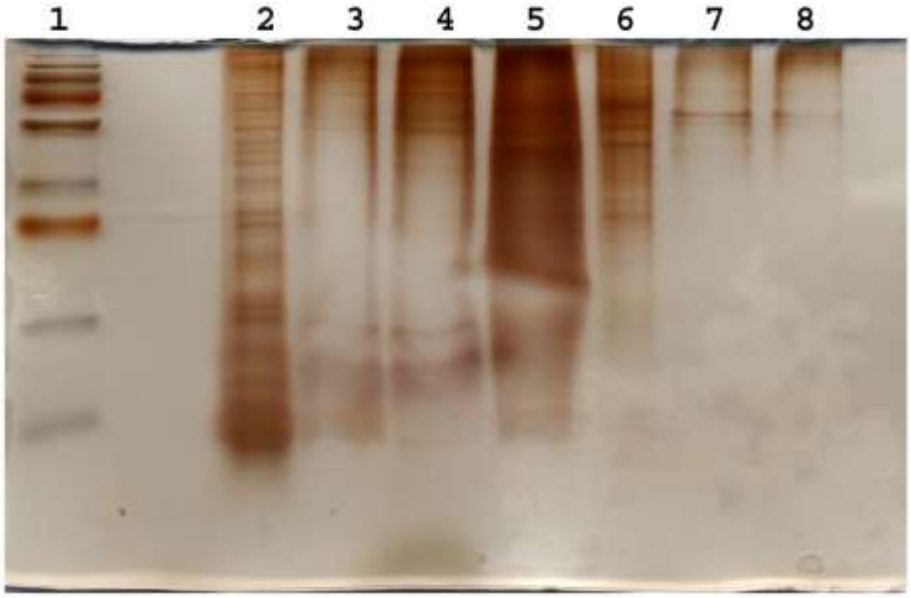

Figure 7. Compareson of TCA precipitation with ultrafiltration. Lane 1: protein ladder. Lane 2: 50% of protein concentrated by ultrafiltration from 3ml 293 cell conditioned medium. Lane 3: 50% of protein precipitated by 15% TCA-NLS from 3ml 293 cell conditioned medium. Lane 4: 50% of protein precipitated by 20% TCA-NLS from 3ml 293 cell conditioned medium. Lane 5: 1.3ug AREC cell lysate. Lane 6: 50% of protein concentrated by ultrafiltration from 1.3ug AREC cell lysate. Lane 7: 50% of protein precipitated by 15% TCA-NLS from 1.3ug AREC cell lysate. Lane 8: 50% of protein precipitated by 20% TCA-NLS from 1.3ug AREC cell lysate.

2.3.2 Mass spectrometry and determination of the EHE secretome

A gel-free shot-gun proteomics approach was chosen over a gel-based method to minimize contamination from the environment, such as Keratin. 2D-LC-MS/MS analyses were performed on three independently collected samples to increase proteome coverage (Durr et al., 2004). Combination of all three samples identified a total of 663 unique proteins (Fig 8; Table III, Appendix A). The overlap between the triplicates ranged between 56.9%, 61.4% and 62.2%, respectively (Figure 8). Among the 663 proteins, 150 proteins were either experimentally observed to be extracellular, localized to the plasma membrane or contain secretion motifs and thus were predicted secreted factors. This group of proteins is referred to as the EHE secretome hereafter (Table IV, Appendix B). The fraction of secreted factors among all proteins identified is approximately 23%, comparable to the percentages (20%-40%) reported by other MS studies of CM (Blanco et al., 2012; Ma et al., 2013). We anticipate that the EHE secretome contains factors mediating or regulating epicardial-myocardial communication.

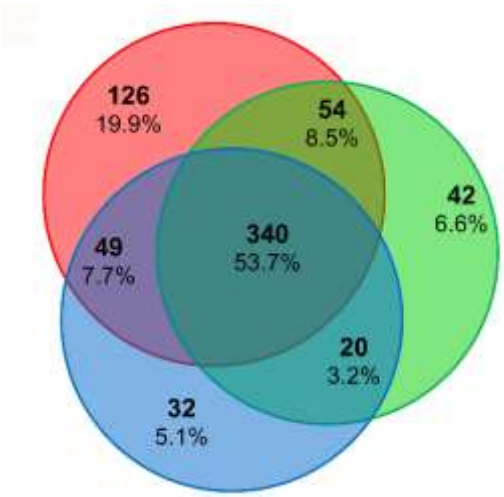

Figure 8. Overlap between proteins identified in triplicate EHE-CM samples. Venn diagram showing the numbers of common and unique proteins identified in the three biological replicates.

2.3.3 Confirmation of the presence of selected proteins in EHE-CM

To assess the accuracy of protein identification by MS, we verified the presence of 5 selected proteins by Western blot and ELISA (Fig 9A-B) and that of 17 selected RNA transcripts by RT-PCR (Fig 9D). Moreover, taking advantage of antibodies available for homologous mouse proteins, we used ELISA to verify the presence of DKK3, IGFBP7 and SPARC in mouse EHE-CM at an equivalent developmental stage (Fig 9C).

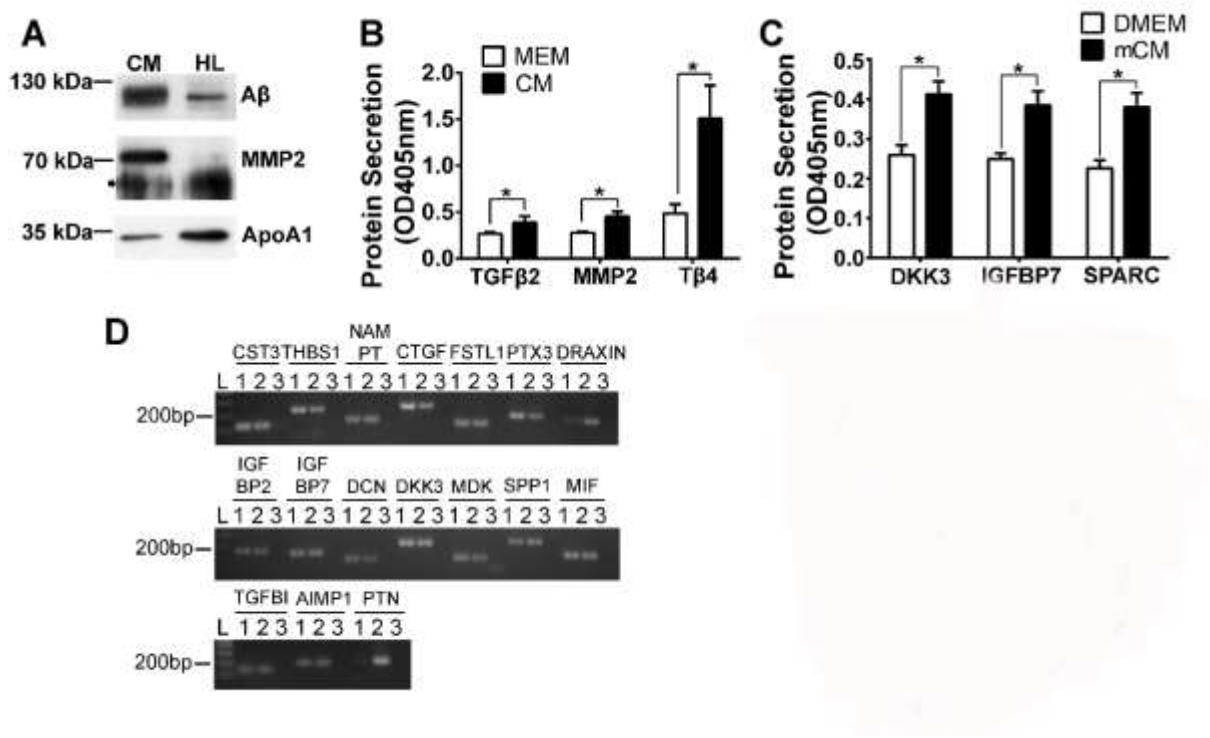

Figure 9. Confirmation of 2D-LC-MS/MS results. Western blot analysis of chicken EHE-CM for Amyloid-β1 (Aβ), MMP2 and ApoA1. Arrow: background band. (B) ELISA analysis of chicken EHE-CM for TGFβ2, MMP2 and Thymosin β4 (Tβ4). (C) ELISA analysis of E11.5 mouse EHE-CM for DKK3, IGFBP7 and SPARC. ELISA data in (B) and (C) are shown as mean±standard deviations (n=3); *P<0.05 (student's t Test). CM: chicken EHE-CM; HL: chicken heart lysate; MEM and DMEM: medium; mCM: mouse EHE-CM. (D) RT-PCR analysis of chicken EPDCs and heart explant for transcription of select genes that encode proteins detected in EHE-CM. L: 100bp DNA ladder. For each gene, lane 1 = RNA isolated from EPDCs; lane 2 = RNA isolated from heart explants; lane 3 = mock RT-PCR without RNA template.

2.4 Discussion

2.4.1 The EHE co-culture system

Past research suggests that factors secreted by the epicardium regulate the expression of genes and proteins in the myocardium, and vice versa (Krainock et al., 2016; Olivey and Svensson, 2010; von Gise et al., 2012). In order to extract the *in vivo* protein expression profile of the developing heart, it is important to use a system that preserves the crosstalk between the epicardium and myocardium. Hence we chose to profile the secretome of EHE co-cultures. Embryonic chicken hearts were used to establish the EHE co-culture because primary chicken epicardial cells can be maintained in serum-free media (Garriock et al., 2014), hence removing serum as a complicating factor in downstream mass spectrometry analysis. In adopting and optimizing this explant co-culture scheme, we sought a balance of preserving biological signaling between EPDCs and the heart myocardium, the minimum time needed for secreted factors to accumulate in the media in sufficient amounts, and apoptotic activities in the heart explant that increased with culture time. We applied a wash step to remove blood cells in the primary tissue culture and harvested the conditioned medium within 36 hours to minimize intracellular protein contamination (Fig 4; Fig 7). These factors shall be considered when interpreting the presence and absence of specific proteins and their biological meaning.

The EHE model does not per se distinguish between autocrine versus paracrine signaling. In some cases, spatiotemporal expression profiles reported elsewhere can help close this information gap. For example, both TGFβ2 and PDGFBB are primarily localized in the epicardium and/or subepicardium during the developmental EMT processes (Cooley et al., 2014; Molin et al., 2003; Van Den Akker et al., 2005). In other cases, additional studies are needed to identify the source of the signal and understand the direction of signaling.

2.4.2 Evaluation of the proteomic approach

In this study, we used a state-of-the-art proteomics approach to identify the secretome of the described EHE co-culture system, which is the first attempt to interrogate communication between the epicardium and the myocardium in a systematic way. 2D-LC-MS/MS analysis of the chicken EHE-CM generated the EHE secretome dataset: a collection of 150 proteins that are targeted to extracellular space or cell membranes. The secretome dataset highlights known proteins secreted from the epicardium and/or myocardium, such as TGFβ2 and FSTL1, as well as previously unidentified candidates (Table IV, Appendix B), establishing validity of our approach. This dataset greatly expands the current knowledge of secretory factors produced by the epicardium and myocardium, providing a valuable resource for investigators of cardiac development (discussed in more details in Chapter III).

Surprisingly, we could not detect several growth factors that are known to be secreted by the embryonic chicken heart, such as FGFs (Morabito et al., 2001), PDGFs (Bax et al., 2009) and Wnt9a (Person et al., 2005) in our data set. One possible explanation for their absence could be that many growth factors are produced and secreted in minute quantities. Furthermore, a number of secreted proteins can bind to and become sequestered by ECM proteins, resulting in a rather low concentration of protein fractions soluble in the medium (Sarkar et al., 2012). This makes detection by MS challenging, especially when the sample is complex and contains hundreds of proteins, some of which are significantly more abundant than the growth factors of interest. However, it is worth noting that even when MS failed to detect a particular secreted factor, our bioinformatics analysis tool (see Chapter III for further details) was able to model pathways and networks based on more abundant interacting or related proteins detected (see Chapter III for further details). In this way bioinformatics can predict the presence of a factor, which can then be

confirmed by other experimental means. As MS technology advances, we anticipate that both the sensitivity and the dynamic range of detection will improve in the future, facilitating an ever-increasing resolution of the global protein interaction network.

III. BIOINFORMATICS ANALYSES OF THE EHE SECRETOME

3.1 Introduction

In the last chapter, I introduced our unbiased EHE secretome dataset, which consists of 150 secreted proteins. To better understand and interpret this dataset, it has to be organized and connected to biological themes. This chapter describes the bioinformatics analysis strategy used to generate testable, targeted hypotheses on embryonic epicardial-myocardial signaling events. Our bioinformatics analysis includes two steps. The dataset was first subjected to GO term annotation analysis to classify them into different categories based on their molecular functions. This provided a general overview of the types of proteins and functions present in the dataset. Then we zoomed out from individual proteins and subjected the dataset to pathway and network analysis. The second step provided a mechanism for the identification of molecular drivers that enabled the organization of corresponding networks.

3.2 Materials and methods

3.2.1 Gene Ontology

DAVID v. 6.7 was used to perform Molecular Function classifications of the EHE secretome. Human orthologous genes were used to achieve maximum coverage and all level 2 GO terms are presented. DAVID v. 6.8 was used to perform Biological Process enrichment analysis. The reference dataset used is whole *Gallus gallus* genome.

3.2.2 Ingenuity pathway analysis

For pathway and network analysis, the EHE secretome dataset was loaded into IPA and analyzed using Ingenuity Knowledge Base (Genes only) as reference set. Only experimentally observed relationships were considered and endogenous chemicals were not included. The canonical pathway module of IPA identified the pathways that are over-represented in the EHE secretome from the IPA library of canonical pathways. The over-represented pathways are ranked by the probability calculated by Fisher's exact test. The probability represent the likelihood that chance alone can explain the association between the proteins in the EHE secretome and the canonical pathway. Ratio represents the number of proteins in the EHE secretome overlapping with the canonical pathway divided by the total number of proteins in that pathway. The networks module of IPA generated networks showing experimentally confirmed relationships between "focus molecules" (proteins that were present in our list) and other " interconnecting" gene products added by its network-generating algorithm to grow the network (Calvano et al., 2005). Scores were calculated for each network based on Fisher's exact test of enrichment relative to networks generated from genes selected randomly from Ingenuity's knowledge base and used to rank networks on the Ingenuity analysis.

3.3 Results

3.3.1 Gene Ontology analysis

Classification of molecular functions using DAVID (Huang et al., 2009) revealed that the EHE secretome proteins are mainly involved in protein binding, extracellular matrix remodeling, and enzymatic activity regulation (Fig 10A). The top 10 Biological Process annotations can be grouped into four main categories: adhesion, extracellular structure organization, movement and cardiovascular system development (Fig 10B). These biological functions and processes are

pertinent to mediating epicardial-myocardial signaling. Within the EHE secretome we found factors that have been reported to play roles in epicardial-myocardial signaling, such as TGFβ2 (Craig et al., 2010; Molin et al., 2003; Sanford et al., 1997), Tβ4 (Olivey and Svensson, 2010; Smart et al., 2007), and FSTL1 (van den Berg et al., 2007; Wei et al., 2015) (Table IV, Appendix B), providing further confidence that our dataset reflects the full range of biological processes in cardiac tissue crosstalk.

A

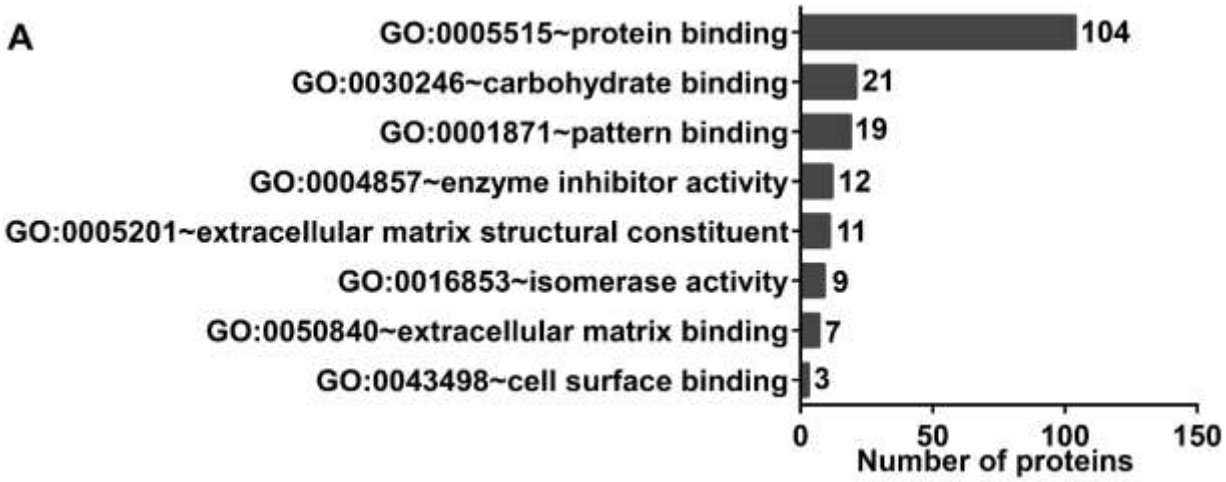

B

Term	Count	%	PValue	FDR
GO:0007155~cell adhesion	40	27.58621	9.23E-15	1.65E-11
GO:0022610~biological adhesion	40	27.58621	1.06E-14	1.91E-11
GO:0030198~extracellular matrix organization	18	12.41379	1.91E-12	3.43E-09
GO:0043062~extracellular structure organization	18	12.41379	1.91E-12	3.43E-09
GO:0006928~movement of cell or subcellular component	33	22.75862	3.34E-07	5.99E-04
GO:0040011~locomotion	30	20.68966	6.69E-07	0.001199
GO:0001944~vasculature development	19	13.10345	6.71E-07	0.001203
GO:0072359~circulatory system development	24	16.55172	6.82E-07	0.001222
GO:0072358~cardiovascular system development	24	16.55172	6.82E-07	0.001222
GO:0006457~protein folding	12	8.275862	8.40E-07	0.001507

Figure 10. Gene Ontology (GO) analysis of the EHE secretome. (A) Molecular function classifications of EHE secretome by DAVID v. 6.7. All level-2 GO terms are shown. (B) Top 10 enriched Biological Process (from DAVID BP-FAT).

3.3.2 Pathway and network analysis

The large size of the EHE dataset made it possible to explore more complex interactions between individual factors. Employing the Canonical Pathway module of the IPA Core Analysis software (IPA, QIAGEN), we identified 60 pathways that are over-represented in the EHE secretome (Table V, Appendix C). The list includes multiple pathways with well-known roles in regulating heart development, such as the Wnt, IGF1, and integrin pathways (Brade et al., 2006; Ieda et al., 2009; Li et al., 2011; Pae et al., 2008). For nine of these pathways, our analysis not only corroborated previous findings, but also implicated additional players that contribute to their functional roles. For example, we identified three Wnt pathway regulators - DKK3, PTK7, and CTHRC1 (Bin-Nun et al., 2014; Kelley, 2008; Niehrs, 2006) - in the EHE dataset (Fig 11). All three are implicated in epicardial-myocardial signaling for the first time, providing new entry points for further investigations. Furthermore, although the confidence level of the canonical TGFβ pathway is not above statistical threshold, several regulators of the TGFβ pathway were identified (Fig 11). In addition, we identified 18 pathways for which none of the components has been previously considered to play a role in epicardial-myocardial signaling (marked by asterisks in Table V, Appendix C).

The Networks module of IPA allowed us to go a step further and explore functional relationships between proteins in the EHE secretome. The network analysis uses proteins in the dataset as "focus molecules" and analyzes how they could be functionally or physically connected, either between two "focus molecules" or through "interconnecting molecules", which are added by IPA due to their high-specificity connections with neighboring focus molecules (Fig 12). An examination of the top ten protein regulatory networks showed that these networks are associated with various functions in the context of epicardial-myocardial signaling (Fig 12-21). For example,

the Collagen Network and the Akt Network (Fig 13, 14) are enriched for molecules regulating ECM remodeling and those regulating cell signaling and adhesion, respectively. The NF-κB network consists of 16 focus molecules and 20 interconnecting molecules, including TGFβ2, an important known regulator of epicardial EMT and coronary vessel development (Craig et al., 2010; Olivey and Svensson, 2010; Sánchez and Barnett, 2012), as well as Integrin alpha 3 beta 1, a laminin receptor involved in the regulation of cell migration (Ross and Borg, 2001) (Fig 22). These findings would suggest that a primary function of this network is EMT regulation. Of note, each network contains several highly connected nodes that together form the framework of the network (Fig 12-21). We hypothesize that such nodes play central roles in the network's primary biological function. To test this hypothesis and to evaluate the potential of the EHE dataset in guiding functional investigations, we examined the function of the most connected node in the third-ranking network, NF-κB (Fig 12; Fig 22).

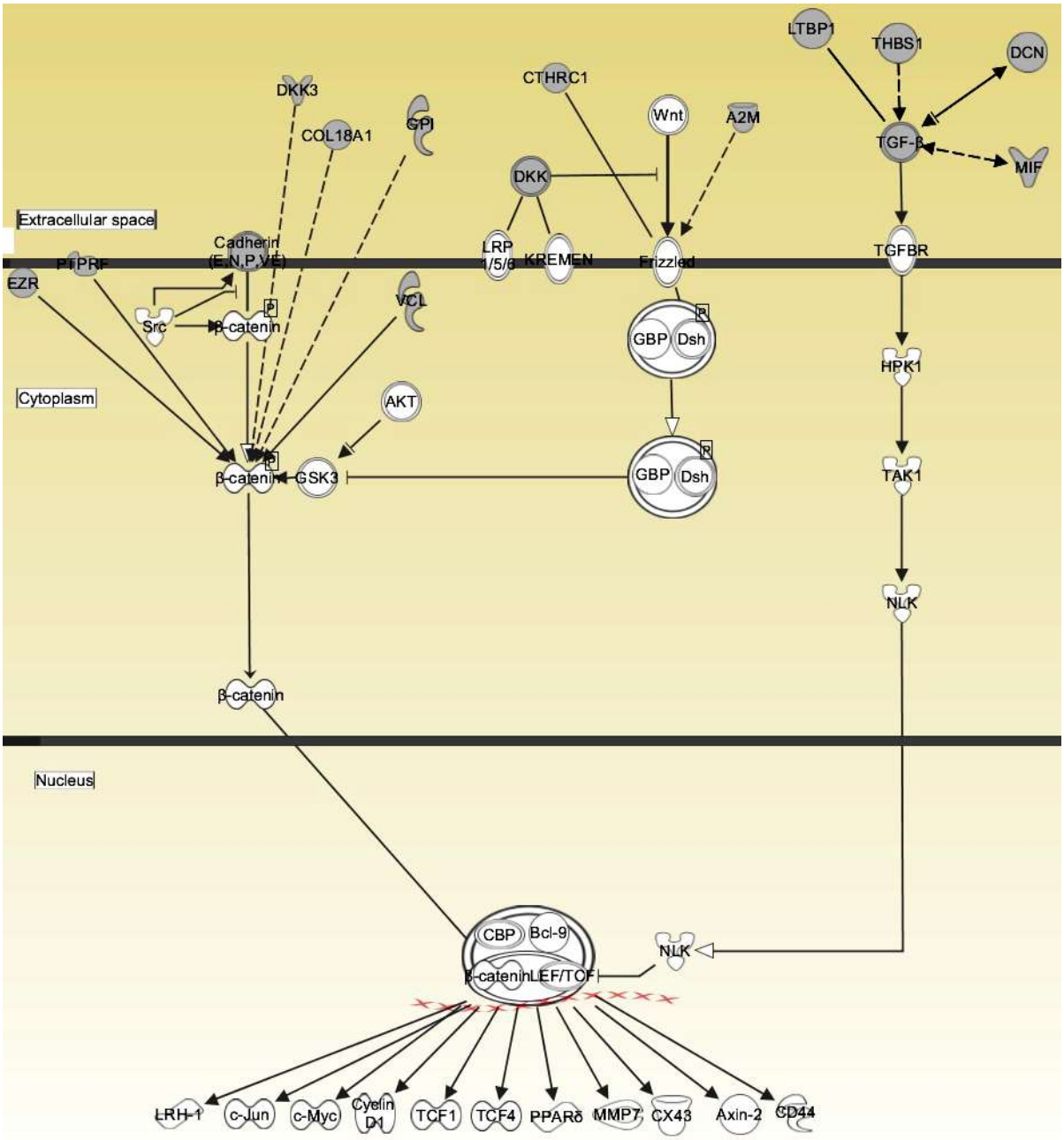

Figure 11. Graphical representation of the Wnt and TGFβ pathways. Shaded shapes represent molecules in uploaded EHE secretome dataset and open shapes represent molecules were not present in our dataset but placed by IPA due to their presence in the canonical pathway. Solid lines denote a direct relationship between gene products while dotted lines indicate an indirect relationship.

Network[1]	Score	Focus Molecules[2]	Nodes with >10 connectors	Top functional roles
Collagen	44	23	Collagen(s) (21); ERK1/2 (12)	Connective Tissue Disorders, Organismal Injury and Abnormalities
Akt	32	18	Akt (17); VCL (14)	Cell-to-Cell Signaling and Interaction, Cellular Movement, Cell Morphology
NF-κB	27	16	NF-κB (20)	Cardiovascular System Development and Function, Embryonic Development, Organismal Development
CALR	27	16	CALR (9)[3]	Cell-to-Cell signaling and Interaction, Skeletal and Muscular System Development and Function
PI3K	27	16	PI3K (16); CD3 (13); Ras homolog (13); MMP2 (12)	Carbohydrate Metabolism, Small Molecule Biochemistry
APP	27	16	APP (17); FN1 (11); Vegf (11)	Cell-to-Cell Signaling and Interaction, Skeletal and Muscular System Development and Function, Cell Death and Survival
Jnk	17	11	Jnk (20); ApoA1 (15); HDL (12); AMPK (12)	Molecular Transport, Lipid Metabolism, Small Molecule Biochemistry
Immunoglobulin	13	9	Immunoglobulin (19); Pkc(s) (14); IL-2 complex (13); Interferon alpha (13); IL-1 (12); Hsp70 (12); Hsp90 (12); HSPA5 (11); SOD1 (11)	Protein Degradation, Protein Synthesis, Cellular Movement
p38 MAPK	13	9	p38 MAPK (19); MAPK (19); Ap1 (17); Ras (17); PDGF (16); Insulin (16); RAC1 (16); PDGFBB (15); NPPA (12)	Cellular Assembly and Organization, Cellular Compromise, Cellular Function and Maintenance
TGFB1	9	7	TGFB1 (13); CD3 (12)	Cell Death and Survival, Organismal Injury and Abnormalities

[1]Networks are named after the node with the most connectors;

[2]Molecules that are from EHE secretome dataset;

[3]The most connected node CALR has 9 connectors

Figure 12. IPA-predicted functional networks in the EPDC-heart explant secretome.

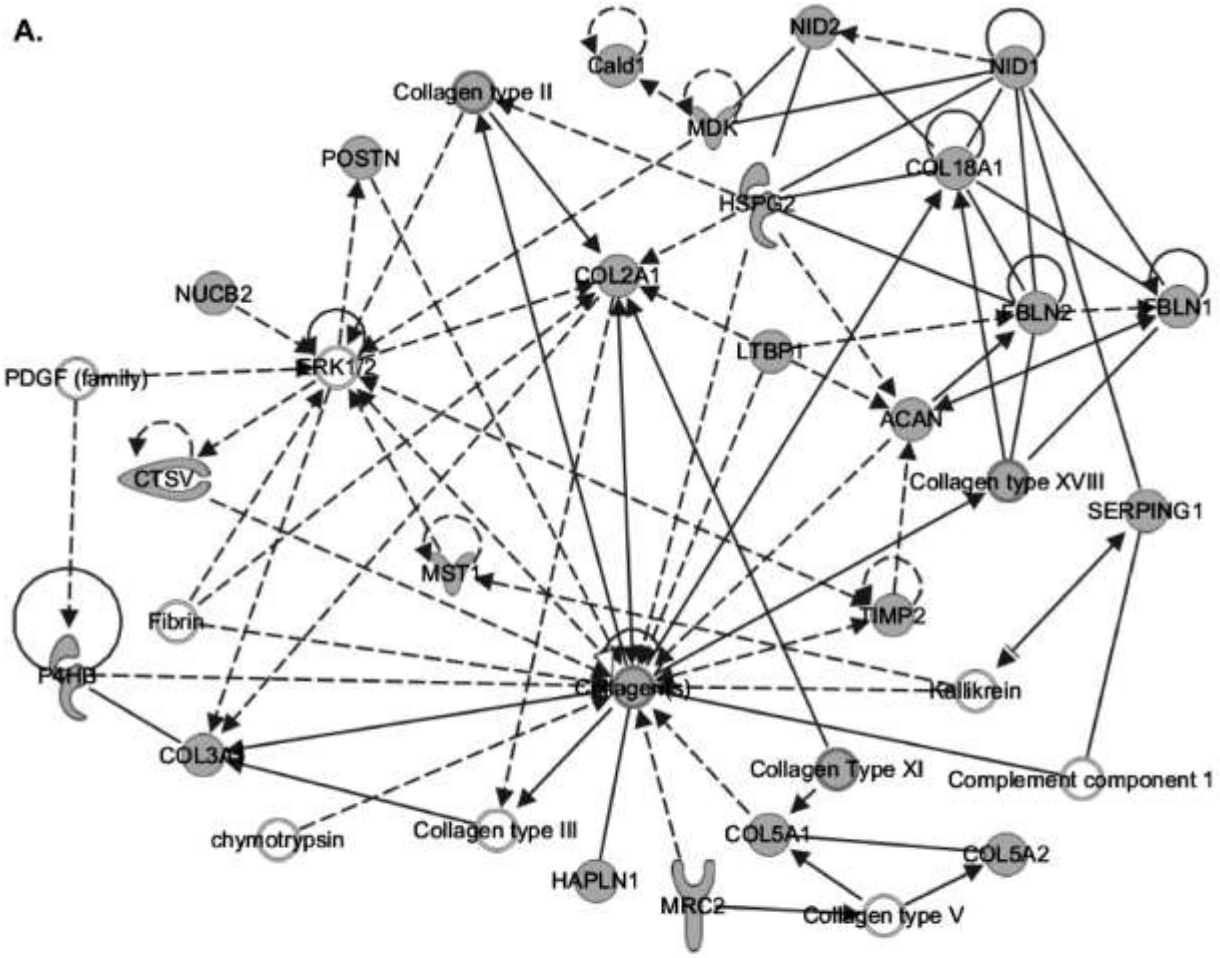

B

Network components
ACAN, CALD1, COL18A1, COL2A1, COL3A1, COL5A1, COL5A2, CTSV, FBLN1, FBLN2, HAPLN1, HSPG2, LTBP1, MDK, MRC2, MST1, NID1, NID2, NUCB2, P4HB, POSTN, SERPING1, TIMP2, chymotrypsin, complement component 1, ERK1/2, Fibrin, Kallikrein, PDGF

Figure 13. Collagen network (A) and network components (B).

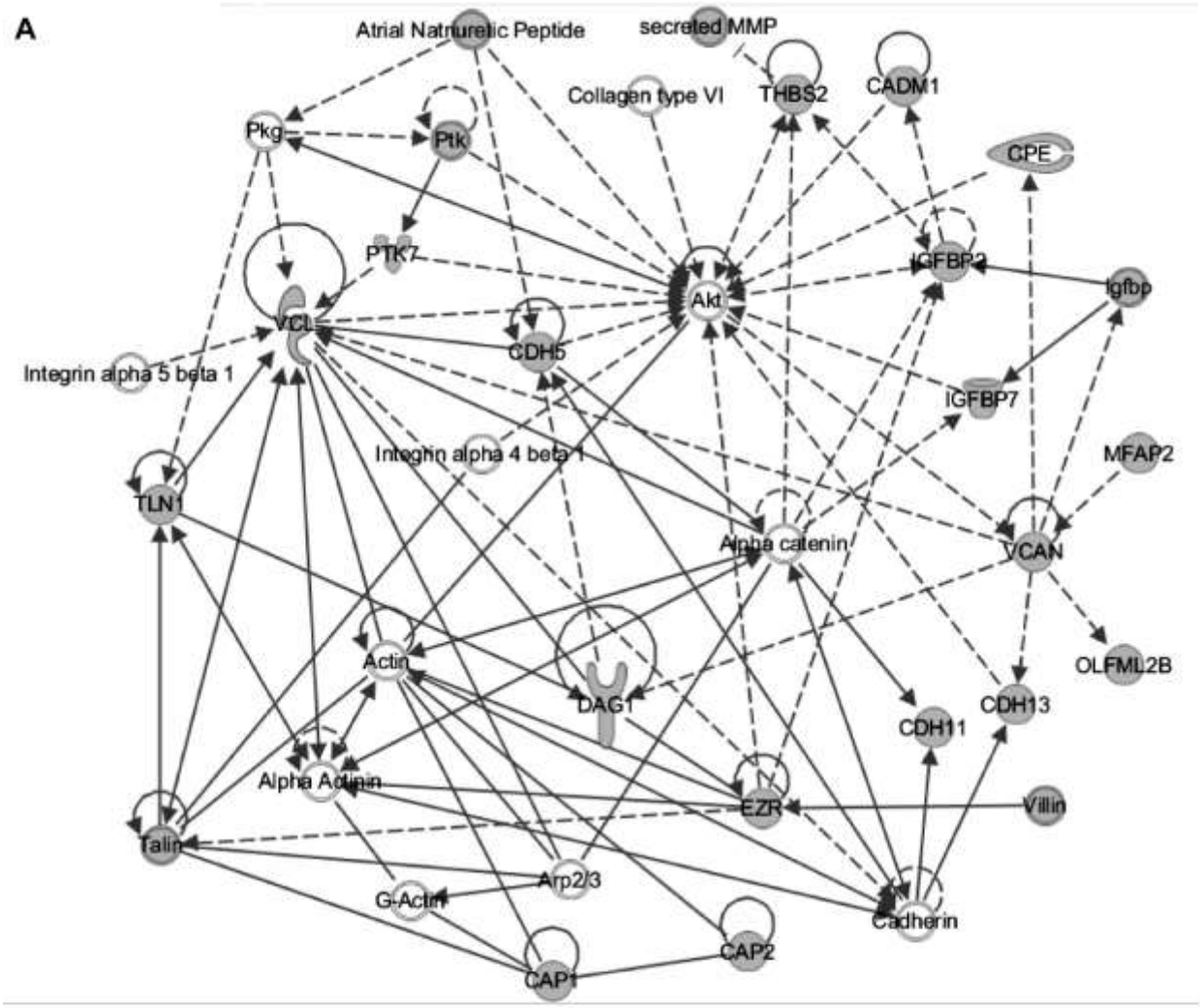

B

Network components
Actin, Akt, Alpha Actinin, Alpha catenin, Arp2/3, Atrial Natrieretic Peptide, Cadherin, CADM1, CAP1, CAP2, CDH5, CDH11, CDH13, Collagen type IV, CPE, DAG1, EZR, G-Actin, Igfbp, IGFBP2, IGFBP7, Intergin alpha 4 beta 1, Intergin alpha 5 beta 1, MFAP2, OLFML2B, Pkg, Ptk, PTK7, secreted MMP, Talin, THBS2, TLN1, VCAN, VCL, Villin

Figure 14. Akt network (A) and network components (B).

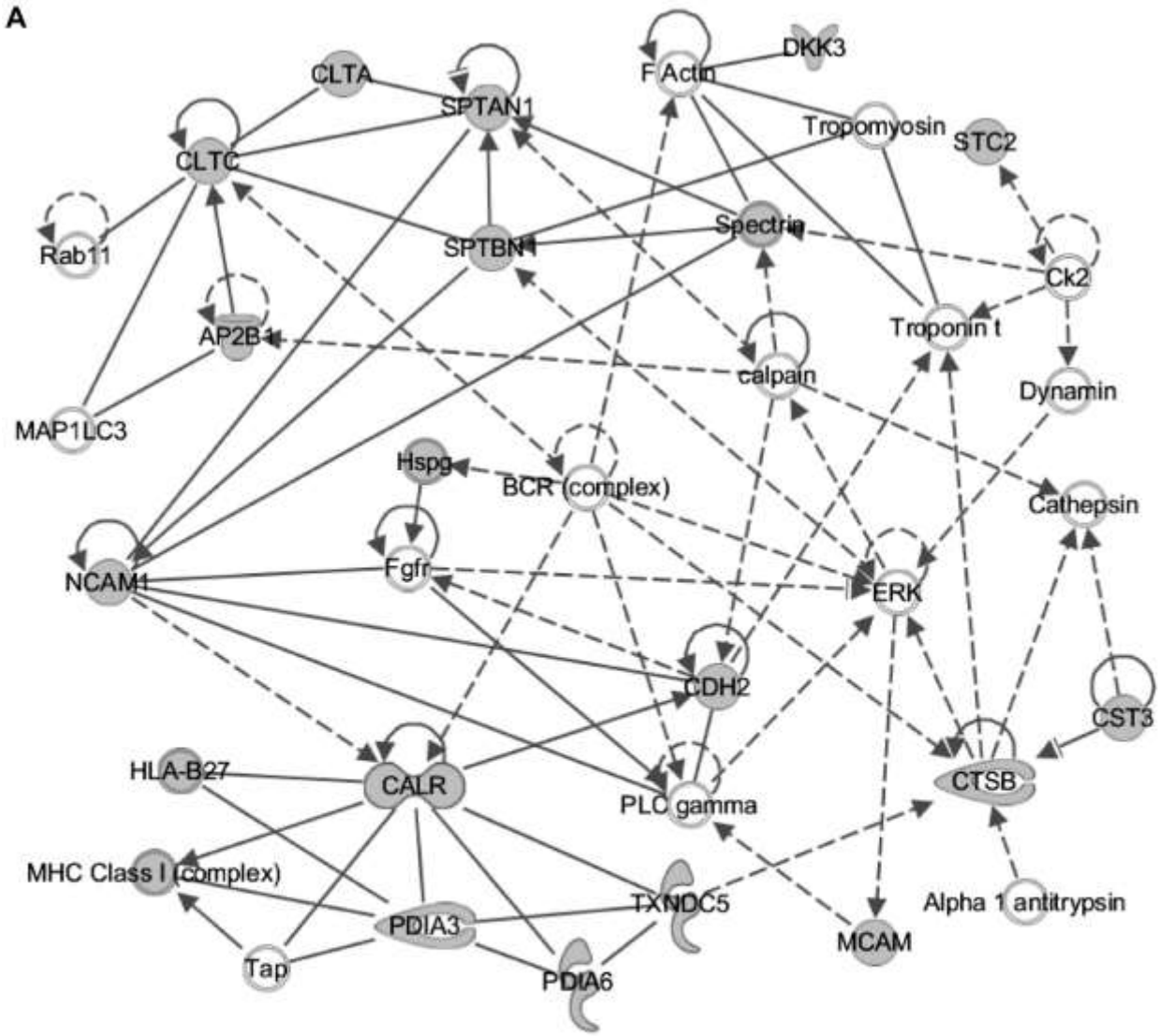

B

Network components
Alpha 1 antitrypsin, AP2B1, BCR (complex), calpain, CALR, Cathepsin, CDH2, Ck2, CLTA, CLTC, CST3, CSTB, DKK3, Dynamin, ERK, F Actin, Fgfr, HLA-B27, Hspg, MAP1LC3, MCAM, MHC Class I (complex), NCAM1, PDIA3, PDIA6, PLC gamma, Rab 11, Spectrin, SPTAN1, SPTBN1, STC2, Tap, Tropomyosin, Troponin t, TXNDC5

Figure 15. CALR network (A) and network components (B).

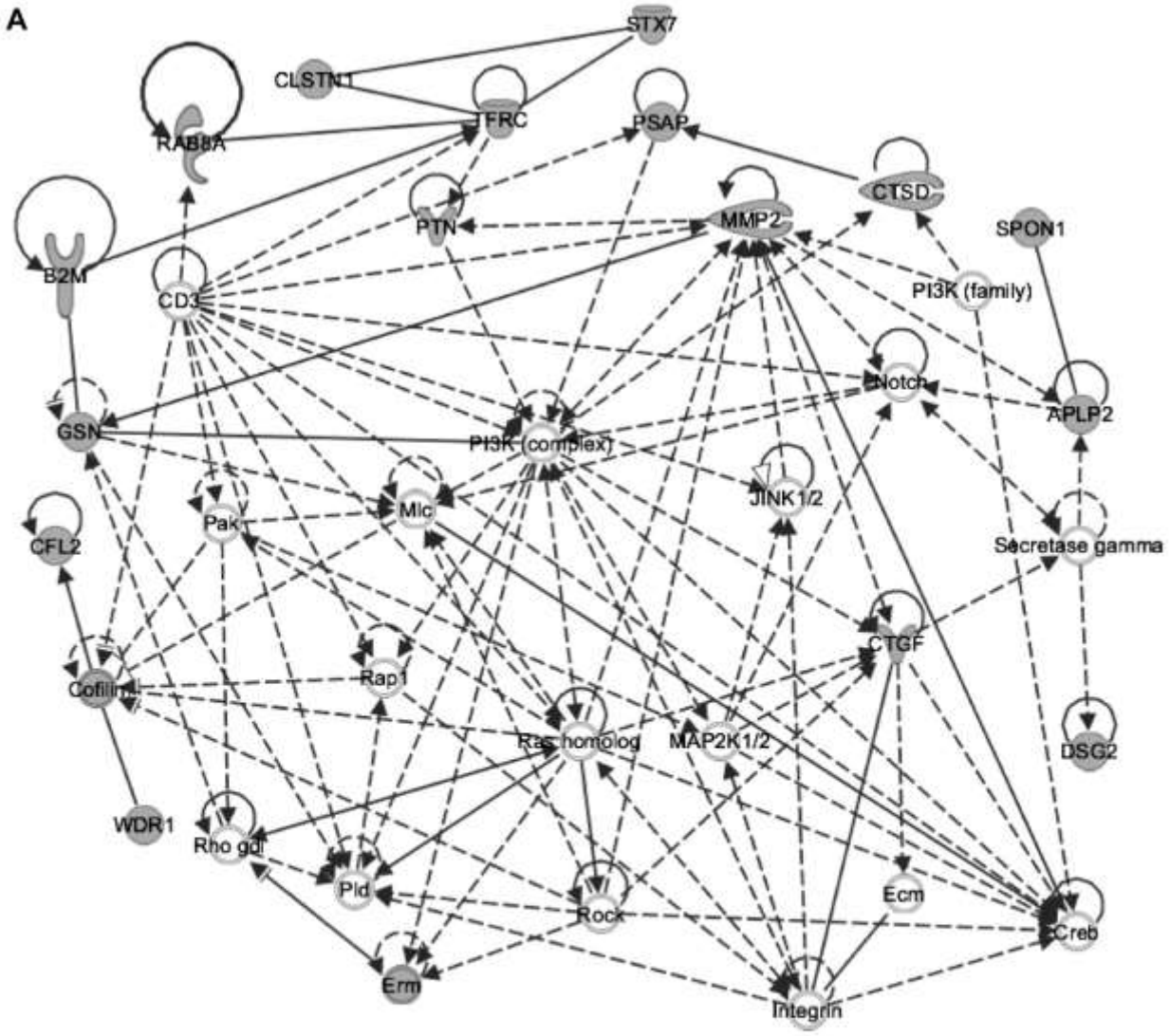

B

Network components
APLP2, B2M, CD3, CFL2, CLSTN1, Cofilin, Creb, CTGF, CTSD, DSG2, Ecm, GSN, Intergin, JINK1/2, MAP2K1/2, Mlc, MMP2, Notch, Pak, PI3K (complex), PI3K (family), Pld, PSAP, PTN, RAB8A, Rap1, Ras homolog, Rho gdi, Rock, Secretase gamma, SPON1, STX7, TFRC, WDR1

Figure 16. PI3K network (A) and network components (B).

A

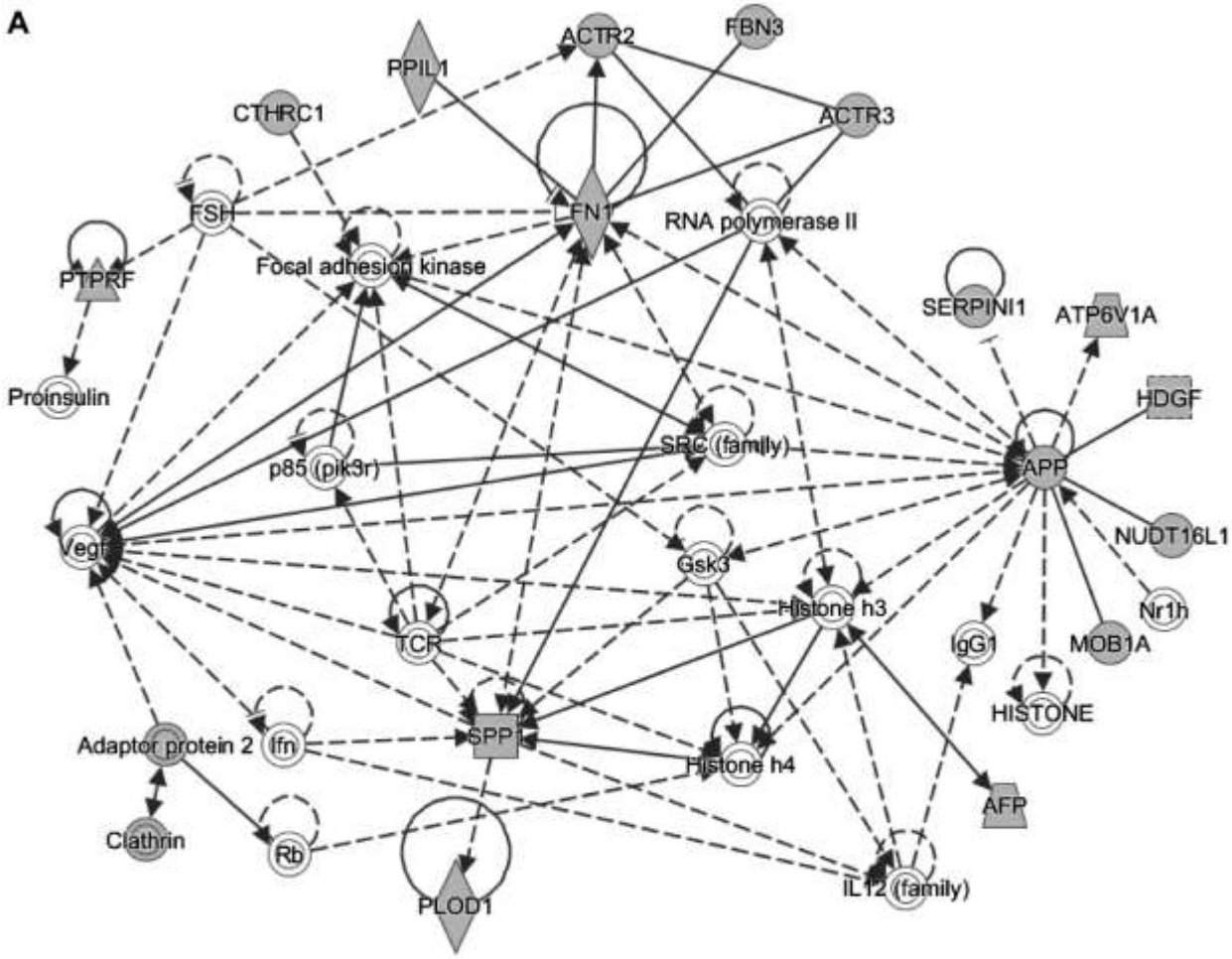

B

Network components
ACTR2, ACTR3, Adaptor protein 2, AFP, APP, ATP6V1A, Clathrin, CTHRC1, FBN3, FN1, Focal adhesion kinase, FSH, Gsk3, HDGF, HISTONE, Histone h3, Histone h4, Ifn, IgG1, IL12 (family), MOB1A, Nr1h, NUDT16L1, p85 (pik3r), PLOD1, PPIL1, Proinsulin, PTPRF, Rb, RNA polymerase II, SERPINI1, SPP1, SRC (family), TCR, Vegf

Figure 17. APP network (A) and network components (B).

A

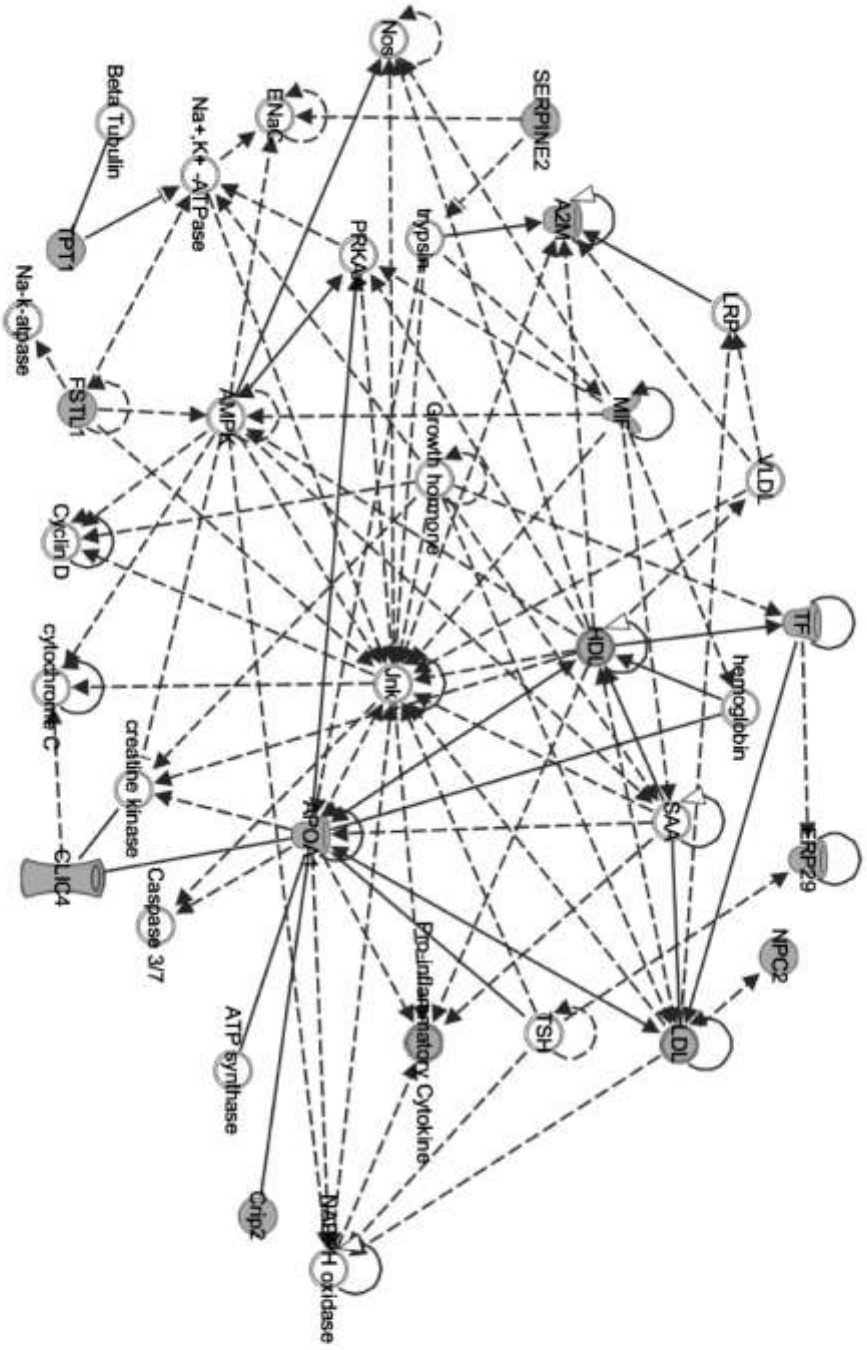

B

Network components
A2M, AMPK, APOA1, ATP synthase, Beta Tubulin, Caspase 3/7, CLIC4, creatine kinase, Crip2, Cyclin D, cytochrome C, ENaC, ERP29, FSTL1, Growth hormone, HDL, hemoglobin, Jnk, LDL, LRP, MIF, Na+,K+ -ATPase, Na-k-atpase, NADPH oxidase, Nos, NPC2, PRKAA, Pro-inflammatory Cytokine, SAA, SERPINE2, TF, TPT1, trypsin, TSH, VDL

Figure 18. Jnk network (A) and network components (B).

A

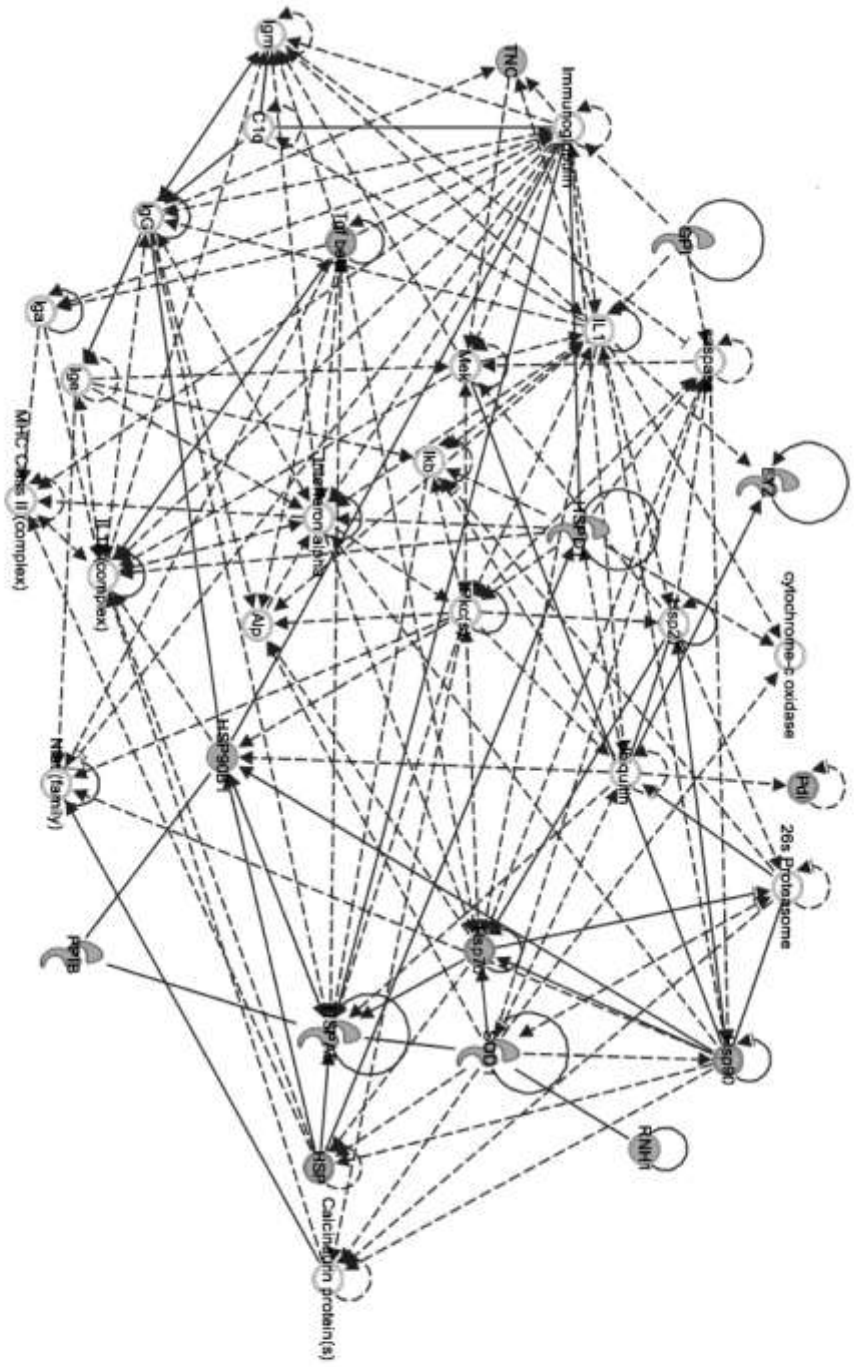

B

Network components
26s Proteasome, Alp, C1q, Calcineurin protein(s), caspase, cytochrome-c oxidase, GPI, HSP, Hsp27, Hsp70, Hsp90, HSP90B1, HSPA5, HSPD1, Iga, Ige, IgG, Igm, Ikb, IL1, IL12 (complex), Immunoglobulin, Interferon alpha, LYZ, Mek, MHC Class II (complex), Nfat (family), Pdi, Pkc(s), PPIB, RNH1, SOD1, Tgf beta, TNC, Ubiquitin

Figure 19. Immunoglobulin network (A) and network components (B).

A

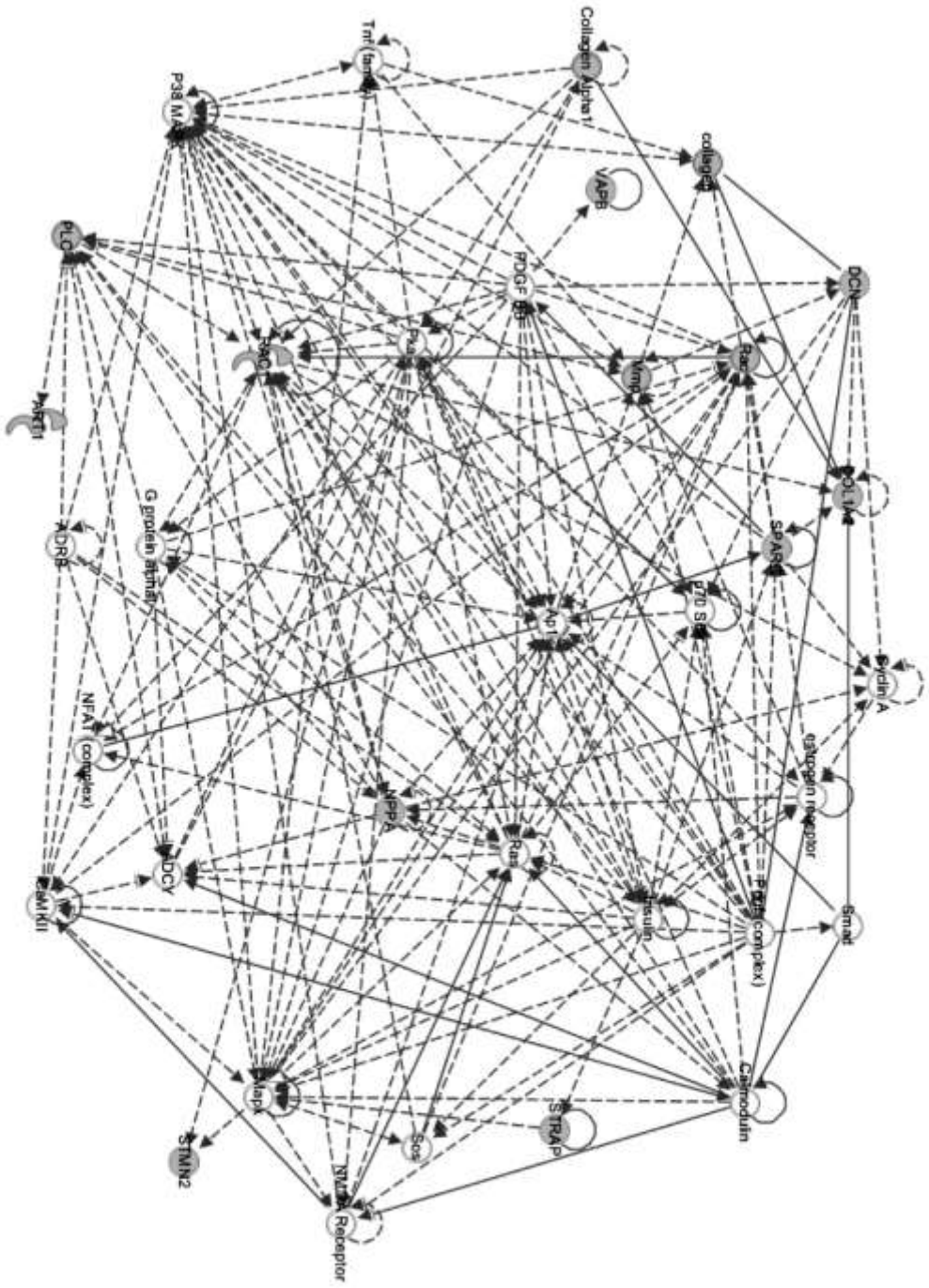

B

Network components
ADCY, ADRB, Ap1, ART1, Calmodulin, CaMKII, COL1A2, collagen, Collagen Alpha1, Cyclin A, DCN, estrogen receptor, G protein alphai, Insulin, Mapk, Mmp, NFAT (complex), NMDA Receptor, NPPA, P38 MAPK, p70 S6k, Pdgf (complex), PDGF BB, Pka, PLC, Rac, RAC1, Ras, Smad, Sos, SPARC, STMN2, STRAP, Tnf (family), VAPB

Figure 20. p38 MAPK network (A) and network components (B).

A

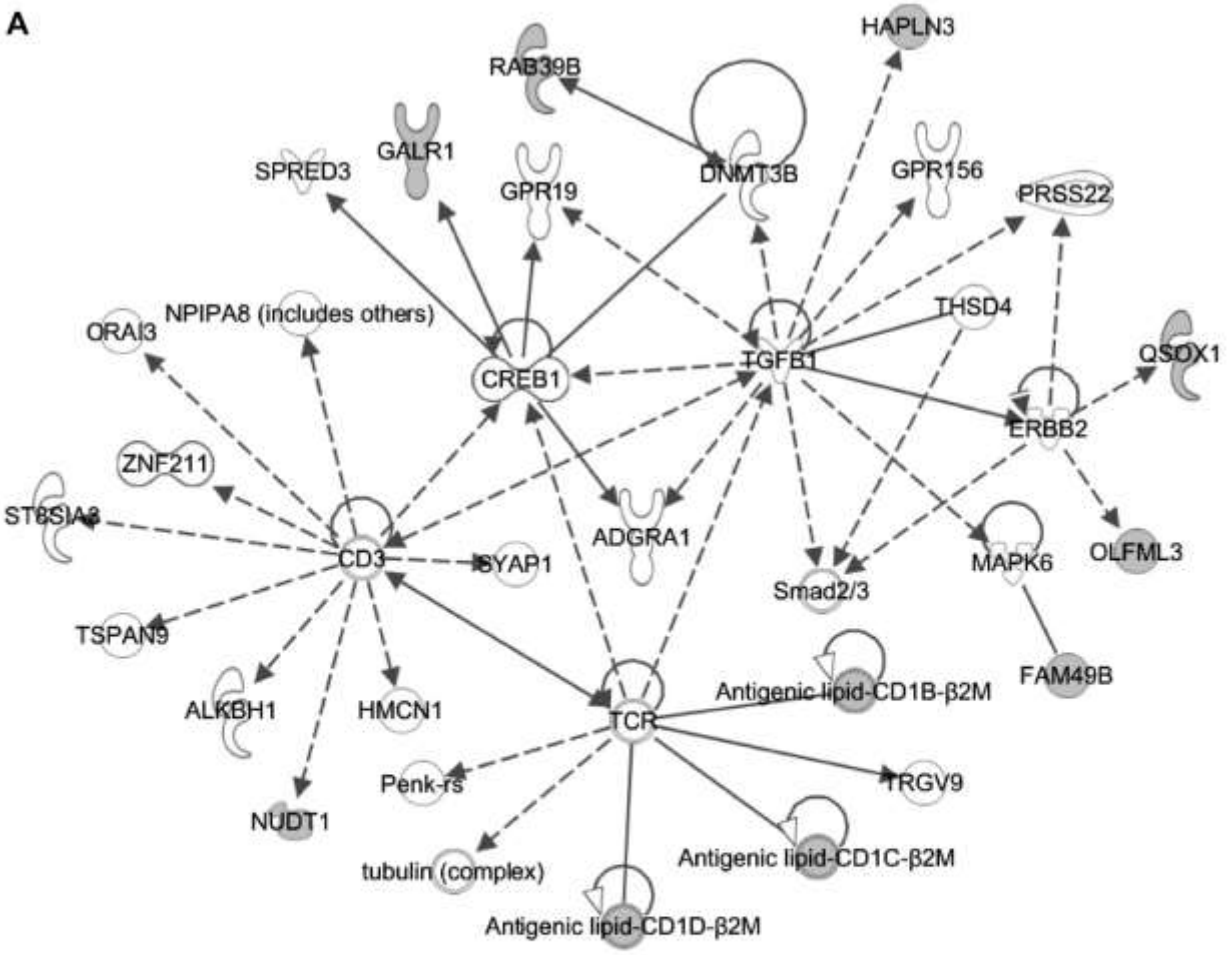

B

Network components
ADGR1, ALKBH1, Antigenic lipid-CD1B-β2M, CD3, CREB1, DNMT3B, ERBB2, FAM49B, GALR1, GPR19, GPR156, HAPLN3, HMCN1, MAPK6, NPIPA8 (include others), NUDT1, OLFML3, ORAI3, Penk-rs, PRSS22, QSOX1, RAB39B, Smad2/3, SPRED3, ST8SIA3, SYAP1, TCR, TGFB1, THSD4, TRGV9, TSPAN9, tublin (complex), ZNF211

Figure 21. TGFB1 network (A) and network components (B).

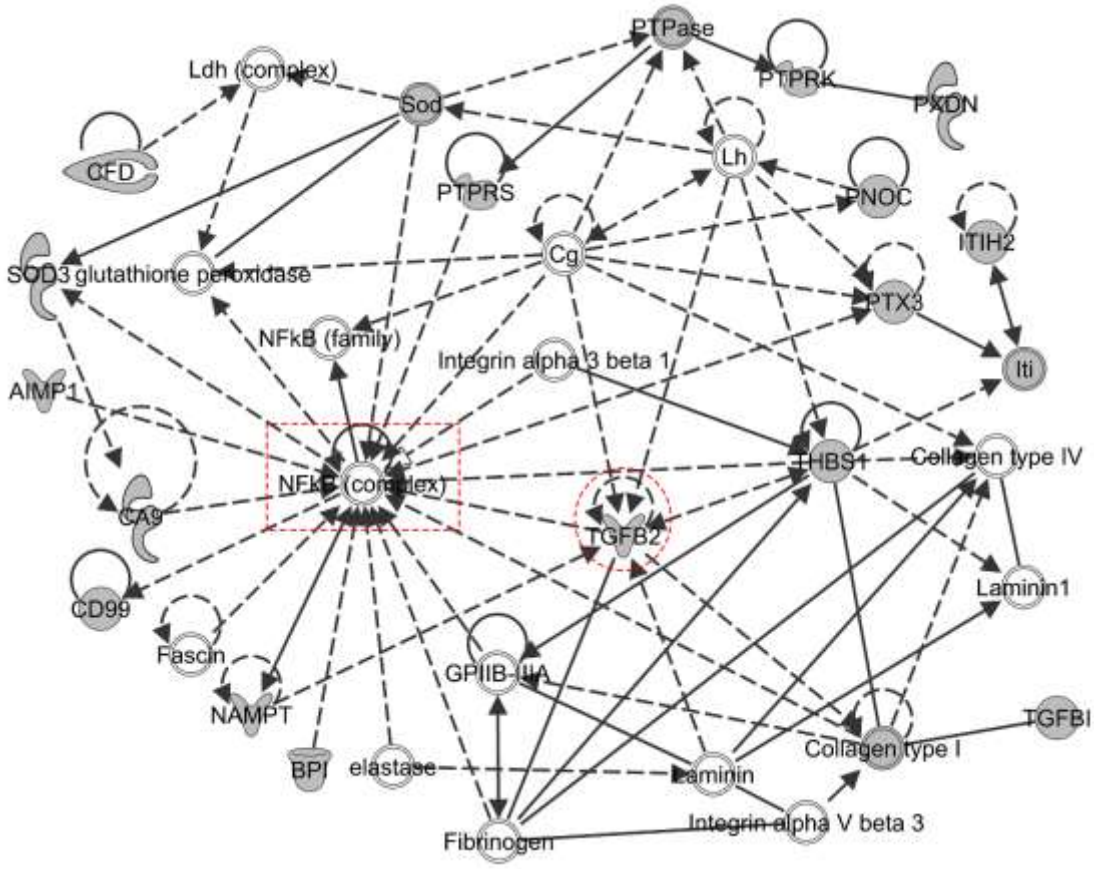

Figure 22. The NF-κB regulatory network. Ingenuity Pathway Analysis was utilized to generate network connections of the EHE secretome. In the depicted network NF-κB was identified as a central node. Nodes are depicted as molecule names over shapes. Shaded shapes represent focus molecules and open shapes represent molecules were not present in our dataset but placed by IPA due to their connections to the focus molecules. Single lines represent protein–protein interactions and arrows indicate regulatory relationship(s) between connected molecules. Solid lines denote a direct relationship between gene products while dotted lines indicate an indirect relationship. TGFβ (circle) and NF-κB (square) connectivity nodes are marked.

3.4 Discussion

3.4.1 The EHE secretome database: a rich source of information

The EHE secretome not only greatly expands the currently reported number of potential players in epicardial-myocardial signaling, but it also allows modeling relationships between identified proteins via pathway and network analysis. Applying bioinformatics, we identified new regulators of the Wnt, IGF and TGFβ pathways (Table V, Appendix C; Fig 11; Fig 22). Pathways that are implicated in epicardial-myocardial signaling for the first time were also identified, such as the Regulation of Cellular Mechanics by Calpain Protease pathway. Calpain has been implicated in regulating cell migration in cancer (Cortesio et al., 2008; Franco and Huttenlocher, 2005), but its role in heart development has not been explored. Together, these findings represent exciting new entry points for further investigations. The regulatory networks generated have clear recognizable functional themes, such as connective tissue remodeling (Fig 12; Fig 13), cell movement (Fig 12; Fig 13; Fig 20), and cell metabolism (Fig 12; Fig 18; Fig 19). For each network, a small number of proteins emerged as "nodes" whose extensive connections form the framework of the network. As exemplified by the functional studies of the NF-κB node described in Chapter IV, network modeling is can predict important regulators of specific biological functions. In this study, we have focused on the regulatory role of the NF-κB pathway in epicardial EMT (see chapter IV). The NF-κB pathway comprises only a small fraction of multiple networks with different biological themes, and future efforts should encompass in hypothesis generation and investigations into these functional roles.

3.4.2 A deeper look into the network and pathway analysis

Pathway analysis software has become a popular strategy for extracting functional and biological information from large proteomic datasets, including the cardiovascular research field (O'Meara

et al., 2015; Stastna and Van Eyk, 2012). Here we chose to use the Ingenuity Pathway Analysis software because it is relatively user friendly and its knowledge base contains literature supported and manually curated molecular interactions and functional annotations. The IPA core analysis module can provide insights into multiple aspects of the examined biological system, including molecular interactions, cellular functions and disease processes. Tools used included pathway analysis, upstream regulator and downstream effects prediction, network generation and functional effects prediction. Specifically, the “Canonical Pathways” and “Networks” models of IPA were ued in this study. It should be noted that the analysis is qualitative since the uploaded list only contains protein identifiers. Table V in Appendix C only indicates the level of overlap between identified proteins with the curated canonical pathway components, with no information about the pathway being either up-regulated or down-regulated.

Although the network and pathway analyses assisted in presenting the EHE secretome list as a well-curated resource and provided guide for hypothesis generation, there are several factors that need to be considered in interpreting the analysis results, as listed below.

1. Because some of the pre-constructed canonical pathways in IPA contain more than one pathway branch, members of the over-represented canonical pathways are highly redundant (Table V, Appendix C). Therefore, this type of output could only be viewed as a rough map to the dataset useful as supplemental information. Making more detailed/precise maps would require zooming in to individual pathways-of-interest and fine-tuning.
2. Currently, the boundaries of many signaling pathways are not very clearly defined scientifically. For example, the pathway "Hepatic Fibrosis/Hepatic Stellate Cell Activation" has no clear and consistent described definitions, causing the inclusion of

genes to be very subjective (Green and Karp, 2006). Thus, it is recommended to modify the canonical pathways during analysis. For example, the regulators of Wnt and TGFβ pathways were added to the canonical pathways (Fig 11).

3. Over-representation analyses consider pathways as mere sets of genes and completely ignored the biological roles of the genes in the pathways. For example, TGFβ2 was identified in the proteomics study, but the TGFβ pathway is not "over-represented" in IPA analysis.
4. Networks with high degree of connectivity are likely to represent significant biological function and we chose to focus on a node in the top third network in this study. However, the score of a network only indicates the number of focus molecules in that network, it does not necessarily indicate the quality or biological significance of it. Candidate selection still needs to be complemented by biological questions and the information from literature mining of the biological system.

IV . FUNCTIONAL CHARACTERIZATION OF THE NF-KB SIGNALING PATHWAY IN EPICARDIAL EMT

4.1 Introduction

In the previous chapters, I described our EHE secretome dataset, which is generated by proteomic analysis of medium conditioned by an EHE co-culture system that was intended to mimic the epicardial-myocardial interaction in development. I also described our bioinformatics strategy for predicting canonical pathways and modeling molecular and genetic interaction networks. An advantage of the IPA network analysis lies in the ability to predict functionally connected molecules, including intracellular proteins as well as low-abundance secreted proteins, both of which are expected to be absent from the secretome database but are essential in signal transduction. The networks provide both known proteins involved in epicardial-mycardial signaling and novel candidate proteins that warrant further validation.

I next wanted to explore whether the network analysis could aid new hypothesis generation. Specifically, I wanted to test the idea that the highly connected nodes likely play important roles in regulating heart development. For this purpose, NF-κB - the most connected node in the NF-κB network (Fig 12; Fig 22) - was selected to be tested for a potential role in regulation epicardial EMT, for several reasons. First, NF-κB has been shown to promote EMT in other systems such as cancer cells. Secondly, the role of NF-κB in regulating epicardial cell behavior has not been

investigated. Thirdly, many proteins that are directly or indirectly connected with NF-κB are identified in the EHE secretome, including proteins known to be important in epicardial EMT, such as TGFβ2, collagens and fibronectin (Fig22; Fig 29). Finally, specific small molecule inhibitors of NF-κB signaling are commercially available and can be used to manipulate NF-κB activity in functional assays.

This chapter describes functional studies to confirm the regulatory role of NF-κB in epicardial EMT. We observed increased NF-κB activity in cultured chicken and mouse epicardial cells in response to TGFβ2/PDGFBB treatment. Further investigations validated an essential role of NF-κB, acting downstream of TGFβ2/PDGFBB, to induce chicken and mouse epicardial cells to undergo morphological and gene expression changes consistent with acquiring of a mesenchymal fate. We further show that NF-κB's expression pattern in the developing epicardium is consistent with it playing a similar role *in vivo*.

4.2 Material and methods

4.2.1 Cell line and reagents

Mouse embryonic epicardial cell line MEC1 cells (gift from Dr. Hery Sucov lab, USC) were cultured in DMEM supplemented with 10% FBS and penicillin/streptomycin (10 μg/ml) in a 5% CO2 tissue culture incubator. JSH-23 (Santa Cruz, sc-222061) and BMS345541 (Millipore, 401480) were used at a final concentration of 8 μmol and 6 μmol, respectively. Recombinant TGFβ2 (Pepro Tech, 100-35B) and PDGFBB (Pepro Tech, 315-18) were used at a final concentration of 10 ng/ml and 50 ng/ml, respectively.

4.2.2 Cell culture and immunocytochemistry

Primary chicken EPDC cultures were established as described previously (Dokic and Dettman, 2006; Pae et al., 2008). Briefly, HH22-24 (E4) hearts were cultured on fibronectin coated

coverslips (Discovery Labware, 354088) and covered with M199 medium supplemented with Primocin. EPDC monolayers were allowed to grow for 24 hours before hearts were removed. MEC1 cells were seeded into a 35mm dish containing a fibronectin and gelatin coated coverslip to approximately 20% confluency. Cells were cultured for 24 hours before they were washed with PBS 3 times and cultured in serum-free medium for another 2 hours. For chicken EPDCs and MEC1 cells, growth factors and/or NF-κB inhibitors were then added to the medium at the final concentrations described above. After 48 hours of treatment, cells were fixed with 4% PFA, permeabilized with 0.2% PBT (0.2% Triton X-100 in PBS) and blocked with 3% BSA in PBS. Primary antibodies used are: anti-β-Catenin (BD Transduction Labs, 610153), anti-ZO1 (Invitrogen, 40-2200, 1:100) and anti-SMAα (Sigma-Aldrich, A5228, 1:200). Cells were washed and fluorescently labeled with goat anti-rabbit AlexaFluor 488 (Life Technology, 1:400) and Texas Red-X phalloidin (5 U/ml, Life Technology). Coverslips were mounted using Vectashield mounting media with DAPI (Vector Labs, H-1200) and were imaged on a Zeiss LSM510 confocal microscope. All images used for comparisons within an experiment were obtained with identical settings on the microscope. Experiments were repeated at least three times for both chicken and mouse epicardial cells.

4.2.3 Quantitative real-time RT-PCR (qRT-PCR)

Total RNA was extracted from cultured chicken primary EPDCs (untreated or treated with TGFβ2/PDGFBB and/or BMS345541for 48 hours) using the RNeasy macro kit (Qiagen, CA, USA). Quantitative real-time PCR (qRT-PCR) was performed on a StepOnePlus Real-Time PCR system (Applied Biosystems) using the Power SYBR Green RNA-to-CT One-Step kit (Invitrogen). Relative gene expression was normalized to GAPDH and calculated using the ΔΔCt method. Primer pairs are listed in Table VI, Appendix D.

4.2.4 Immunocytochemistry of MEC1 cells

After seeding, MEC1 cells were cultured for 24 hours before switching to serum-free medium for another 2 hours. MEC1 cells were then treated with recombinant TGFβ2 for 1 hour or left untreated before fixation. Cells were stained with anti-Smad2/3 (gift from Dr. Guofei Zhou, University of Illinois at Chicago, 1:100). Or, MEC1 cells were treated with recombinant TGFβ2 and/or 2.5μmol SB431542 (gift from Dr. Douglas E Vaughan lab, Northwestern University) for 72 hours after the 2 hour starvation and co-stained with anti-ZO1 and anti-SMAα. Coverslips were mounted using Vectashield mounting media with DAPI (Vector Labs, H-1200) and were imaged on a Zeiss LSM880 confocal microscope. Pixel intensity of nuclear Smad2/3 fluorescence signal was quantified with Image J. At least 110 cells were scored per treatment group within 3 independent experiments. All images used for comparisons within an experiment were obtained with identical settings on the microscope and then used for quantitation without any manipulation. All images were selected by viewing the DAPI channel.

4.2.5 Immunohistochemistry

HH22, HH26 and HH30 chick embryos as well as E11.5 and E13.5 mouse embryos were fixed in 4% PFA, cryoprotected in 30% sucrose and cryosectioned. Sections were permeabilized with 0.2% PBT and blocked with Image-iT FX Signal Enhancer (ThermoFisher, I36933). The following primary antibodies were used: anti-NF-κB p65 (Santa Cruz, sc-372 or Abcam, ab16502, 1:100), anti-Troponin T, cardiac (ThermoFisher, MS-295-P1, 1:200), anti-MF20 (Developmental Studies Hybridoma Bank, 1:200) and anti-SM22α (Abcam, ab10135, 1:100). Sections were washed with 0.1% Tween-20 (in PBS) and incubated with appropriate secondary antibodies. Tissues were mounted in Vectashield mounting media with DAPI (Vector Labs, H-1200). Images were taken on a Zeiss LSM880 confocal microscope.

4.2.6 NF-κB p65 nuclear translocation assay

Primary mouse EPDC cultures were established from E12.5 mouse hearts as described previously (Austin et al., 2008). Briefly, hearts were placed on fibronectin coated coverslips and covered with DMEM supplemented with 10% FBS and Primocin. After 48 hours, hearts were removed and epicardial monolayers were washed with PBS and left to culture in DMEM only with Primocin for another 2 hours. Primary chicken EPDCs were isolated from E5 chick hearts as described above. For either chicken or mouse EPDCs, growth factors and/or BMS345541 were added to the medium at the final concentrations described above. After 8 hours of treatment, cells were fixed with 4% PFA, permeabilized with 0.2% PBT, blocked with Image-iT FX Signal Enhancer (ThermoFisher, I36933), and stained with p65-directed antibodies (Abcam ab16502 for chicken and Santa Cruz sc-372 for mouse). Primary antibodies were detected with goat anti-rabbit AlexaFluor 488 (Life Technology, 1:400). Texas Red-X phalloidin was included during incubation of the secondary antibody to label F-actin. Coverslips were mounted using Vectashield mounting media with DAPI (Vector Labs, H-1200) and were imaged on a Zeiss LSM510 confocal microscope.

The nuclear: cytoplasmic ratio of p65 fluorescence signal for each image was quantified with Image J (Fig 23). For chicken EPDCs, >800 cells were scored per treatment group within 5 independent experiments. For mouse EPDCs, >250 cells scored per treatment group within 3 independent experiments. All images used for comparisons within an experiment were obtained with identical settings on the microscope and then used for quantitation without any manipulation. All images were selected by viewing the F-actin channel to identify intact epicardial monolayer.

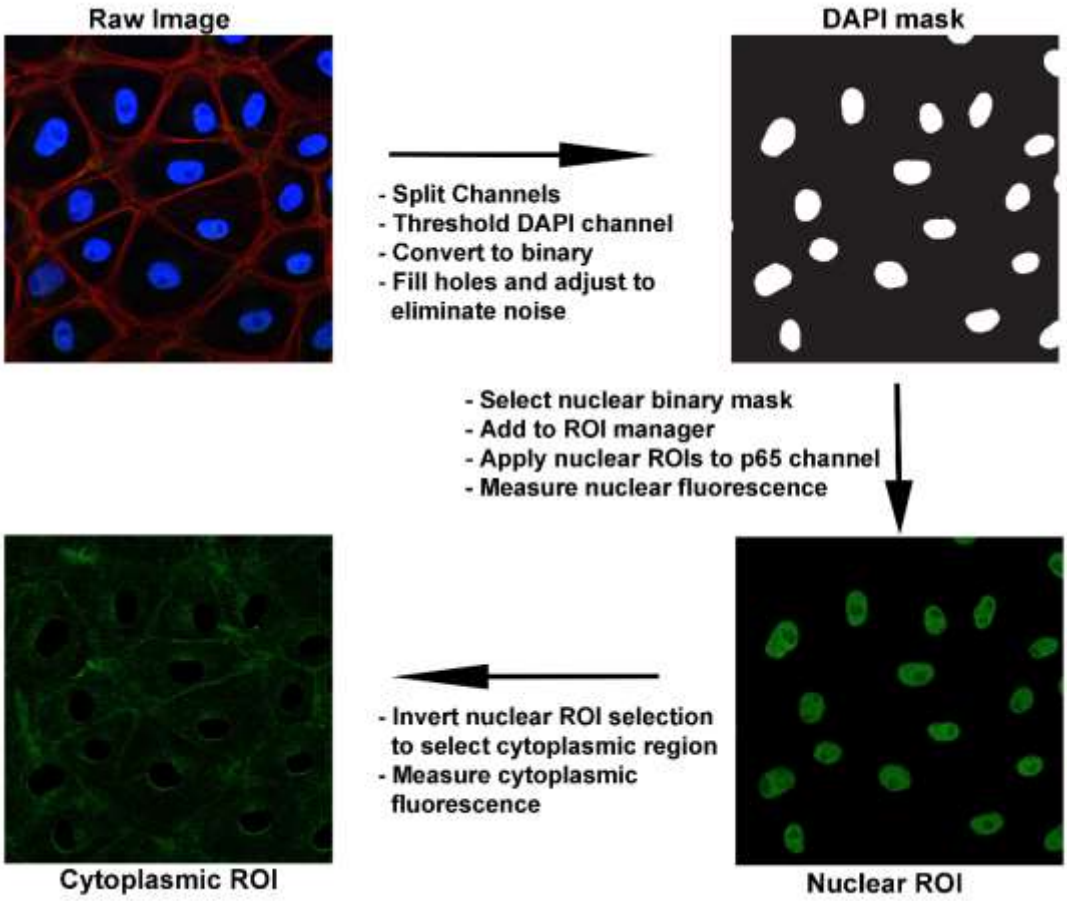

Figure 23. Image analysis workflow for the quantification of signal intensity in subcellular compartments.

4.3 Results

4.3.1 TGFβ2 and PDGFBB activate NF-κB signaling in primary EPDCs

The transcriptional activity of mammalian NF-κB is regulated by change of its subcellular localization (Hayden and Ghosh, 2012; Kanegae et al., 1998; Ryzhakov et al., 2013; Verma et al., 1995). In the absence of activating signals, NF-κB is sequestered in the cytoplasm via interaction with IκB. NF-κB becomes activated upon IκB phosphorylation, which causes proteosomal degradation of IκB and in turn nuclear translocation of NF-κB. To determine whether NF-κB has a function in epicardial EMT, we asked whether conditions that induce epicardial EMT would also activate NF-κB. The growth factor TGFβ2 is commonly used to induce EMT in cultured cells. In addition, the PDGFRα receptor, which binds PDGFBB, was shown to be important for TGFβ2-induced EMT in human adult epicardial cells (Bax et al., 2011). In our hands, a combined TGFβ2/PDGFBB treatment induces a robust EMT response in the mouse epicardial cell line MEC1 within 48 hours, resulting in characteristic morphological, cellular and molecular changes (additional details in the next section). Treatment with TGFβ2 alone also induced EMT, but the response was found to be less robust (Fig 24). Hence, the combinatorial treatment was used in all subsequent analyses. The functional units of NF-κB are dimer protein complexes, with p65/p50 being the most prevalent form (Ghosh et al., 1998). Before TGFβ2/PDGFBB treatment of primary mouse epicardial cells, we observed perinuclear p65 in the majority of cells, with a subset of cells exhibiting nuclear staining (arrows in Fig 25A). TGFβ2/PDGFBB treatment led to nuclear accumulation of p65 (Fig 25E-H and M). This nuclear accumulation was blocked by BMS345541 (Fig 25I-L and M), a specific inhibitor of NF-κB nuclear translocation by inhibiting signal-induced phosphorylation of IκBα (Burke et al., 2003).

The mechanism for NF-κB activation in chicken is less well understood. Interestingly, we observed a basal level of nuclear p65 in primary chicken epicardial cells (Fig 26A-D). Visual inspection alone could not unambiguously determine nuclear accumulation above this basal level after TGFβ2/PDGFBB treatment (Fig 26E-H). However, quantification of p65 fluorescence in the nucleus versus cytosol compartments revealed enhanced nuclear accumulation of p65 in treated chicken cells with statistically significance ($p<0.05$; Fig 26M). This enhancement was also blocked by BMS345541 (Fig 26I-L and M).

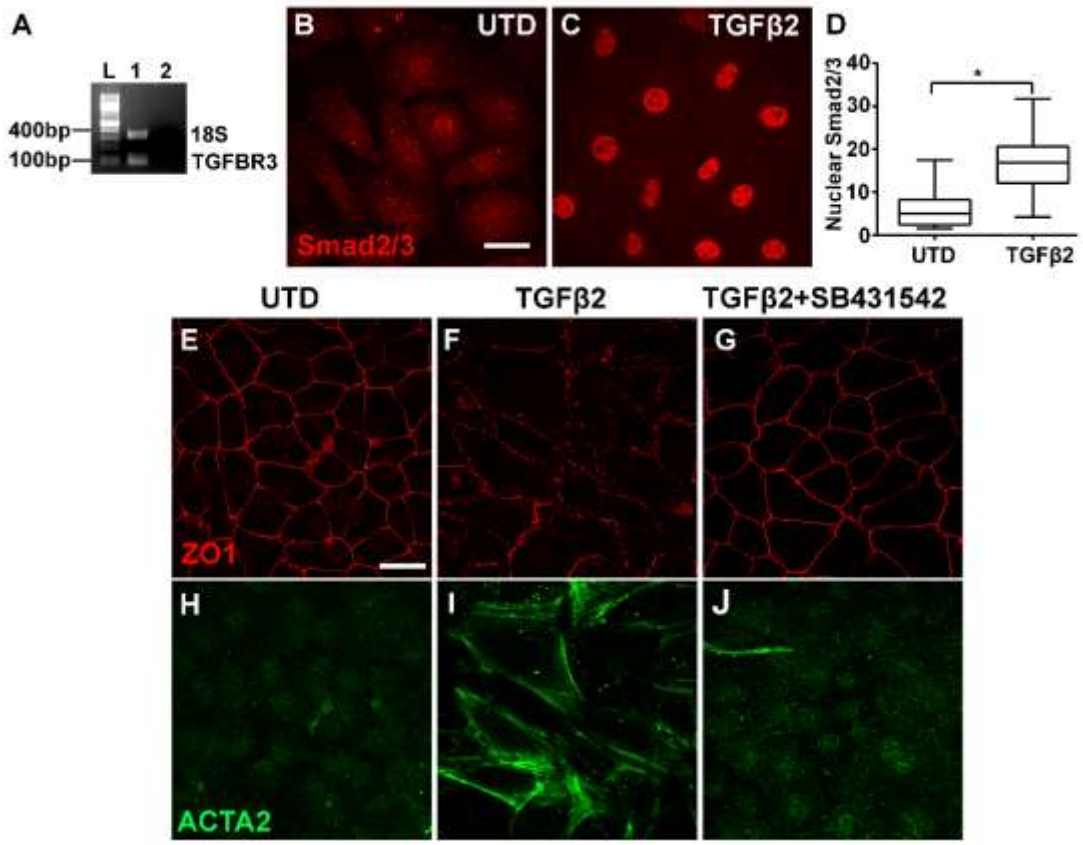

Figure 24. Response of mouse epicardial cell line MEC1 to TGFβ2 treatment. (A) RT-PCR analysis of TGFBR3 expression in MEC1 cells. The type III TGFβ receptor is essential for TGFβ2-induced epicardial invasion *in vivo* (Hill et al., 2012). L: ladder. 1: RT-PCR reaction using 100 ng MEC1 total RNA, 0.6 μmol *Tgfbr3* primers, and 0.1 μmol 18S rRNA primers (positive control). 2: mock RT-PCR reaction without MEC1 RNA. (B-C) TGFβ2 treatment of MEC1 cells induces nuclear accumulation of Smad2/3, indicating TGFβ pathway activation. (D) Box-and-Whisker plots (Min to Max method, Graphpad Prism) of nuclear Smad2/3 pixel intensity. The whiskers go down to the smallest value and up to the largest and the line in the middle of the box is plotted at the median. *$p < 0.0001$. (E-J) TGFβ2 treatment induces loss of ZO1 at cell-cell junction (F) and ACTA2 protein expression (I). Both responses are blocked by the TGFβ2 inhibitor SB431542 (G, J). Scale bar: 40 μm.

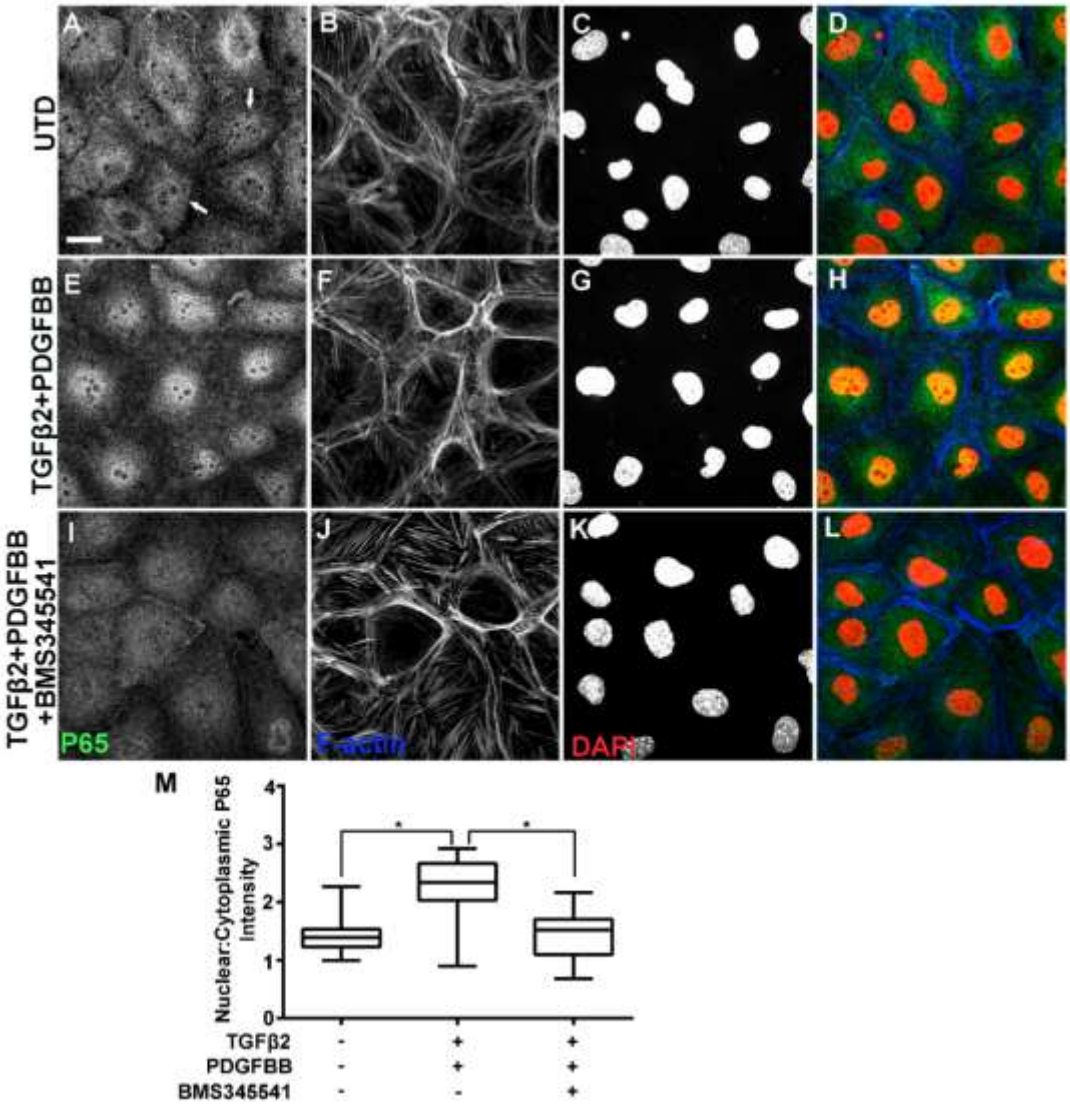

Figure 25. NF-κB p65 subcellular localization in primary mouse epicardial cells after TGFβ2 and PDGFBB treatment. Immunofluorescent detection of p65 in untreated (UTD) cells (A-D), cells treated with TGFβ2/PDGFBB for 8 hours (E-H), and cells co-treated with TGFβ2/PDGFBB and BMS345541 (I-L). Arrows point to untreated cells with elevated nuclear p65 staining as compared to cytoplasmic staining levels. Scale bar: 20 μm. Box-and-Whisker plots (Min to Max method, Graphpad Prism) of p65 nuclear:cytoplasmic ratio (M). The whiskers go down to the smallest value and up to the largest and the line in the middle of the box is plotted at the median. *$p < 0.0001$ (Mann–Whitney test).

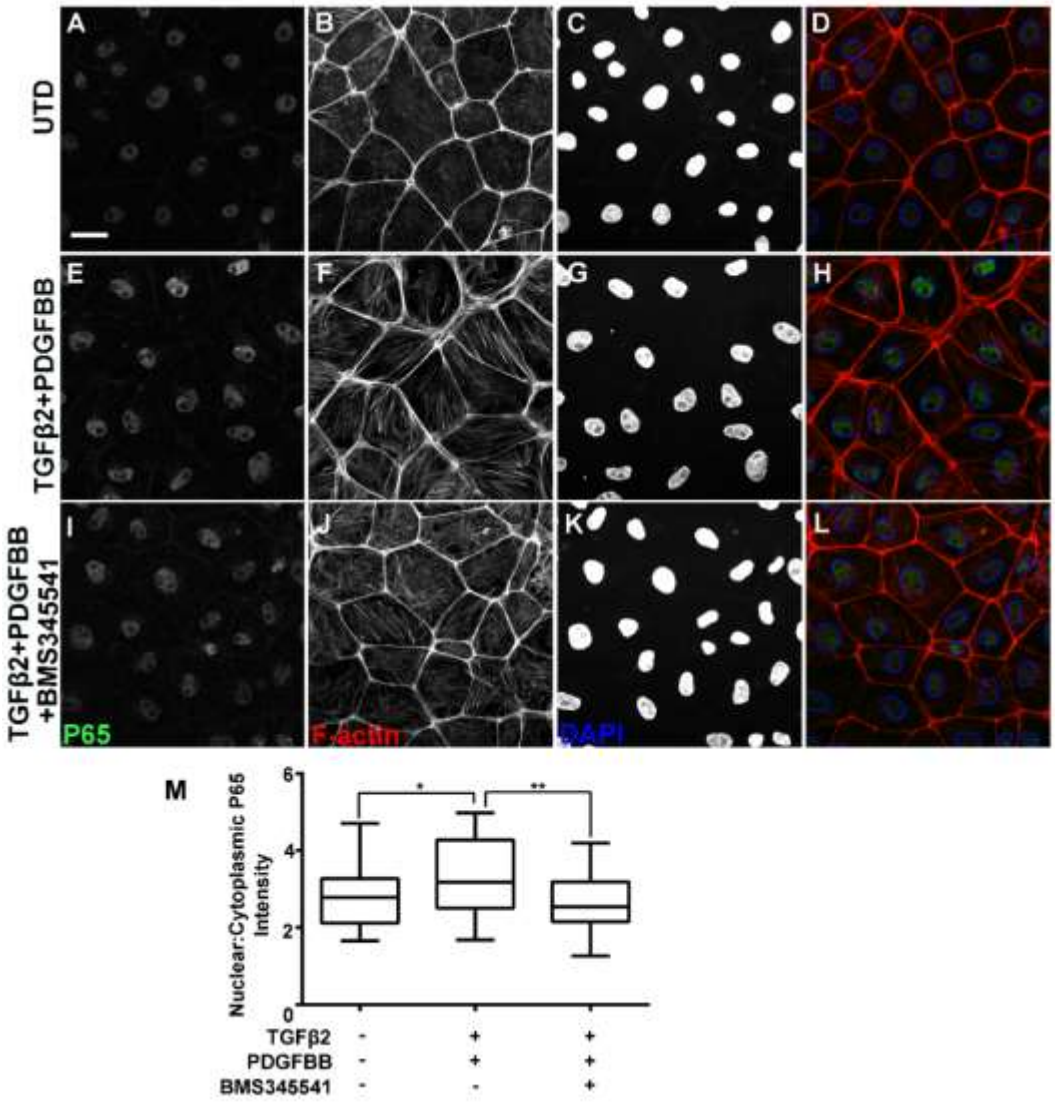

Figure 26. NF-κB p65 subcellular localization in primary chicken epicardial cells after TGFβ2 and PDGFBB treatment. Immunofluorescent detection of p65 in untreated (UTD) cells (A-D), cells treated with TGFβ2/PDGFBB for 8 hours (E-H), and cells co-treated with TGFβ2/PDGFBB and BMS345541 (I-L). Nuclei in the DAPI channel were outlined to enhance the visibility of nuclear p65 (D, H, L). Scale bar: 20 μm. Box-and-Whisker plots (Min to Max method, Graphpad Prism) of p65 nuclear:cytoplasmic ratio (M). The whiskers go down to the smallest value and up to the largest and the line in the middle of the box is plotted at the median. *$p < 0.05$, **$p < 0.01$ (Mann–Whitney test).

4.3.2 NF-κB signaling is necessary for cellular and molecular changes associated with EMT

Next we asked whether NF-κB signaling is necessary for epicaridal cells to undergo EMT. Primary chicken epicardial cells exhibit a tightly packed and cobblestone-like morphology typical for epithelial cells (Fig 27A). Cell-cell boundaries are clearly delineated by cortical F-actin (Fig 27E), and the cell adhesion protein β-catenin (Fig 27E'). Within 48 hours of TGFβ2/PDGFBB treatment, cell shape changed to an elongated morphology (Fig 27B) with accumulation of actin stress-fibers (Fig 27F). β-catenin was lost from cell boundaries and formed intracellular puncta instead (Fig 27F'), indicating an alteration in cell adhesion. Along with the morphological changes, quantitative RT-PCR demonstrated that TGFβ2/PDGFBB treatment resulted in downregulation of the epicardial marker gene *WT1* and concomitant upregulation of mesenchymal genes *MMP2* and *DCN* (decorin) (Fig 27I). Similar changes were observed in the TGFβ2/PDGFBB-treated mouse epicardial cell line, MEC1 (Fig 28A-B; A'-B'; E-F; E'-F'). In chicken and mouse cells, co-treatment with BMS345541 effectively blocked the TGFβ2/PDGFBB-induced cellular changes, including cell shape elongation (Fig 28C, G, G' and Fig 28C, C'), actin stress fiber formation (Fig 27G and Fig 28C, G'), and relocation of cell adhesion molecules (Fig 27G' and Fig 28C', G). BMS345541 also blocked *WT1* down-regulation and *MMP2*/*DCN* up-regulation in chicken epicardial cells (Fig 27I). Similar effects were observed using a second NF-κB inhibitor JSH-23. JSH-23 inhibits NF-κB nuclear translocation without affecting IκB degradation, which is different from the inhibitory mechanism of BMS345541 (Shin et al., 2004) (Fig 29).

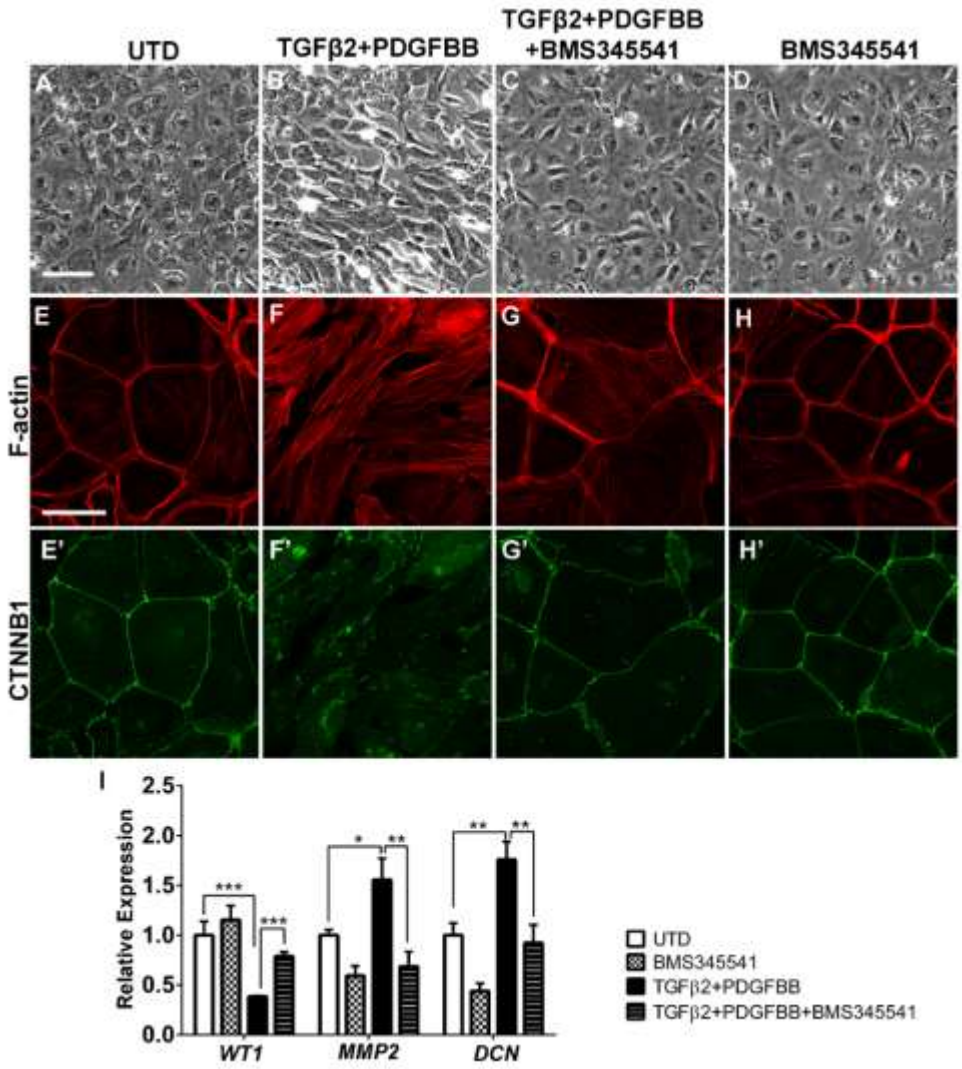

Figure 27. Inhibition of NF-κB blocks TGFβ2- and PDGFBB-induced EMT in primary chicken epicardial cells. Primary chicken epicardial cells cultured in the absence or presence of TGFβ2/PDGFBB and/or BMS345541for 48 hours. Determination of cell morphology using phase contrast (A-D). F-actin stress fiber formation (E-H) and β-catenin localization in the same cells (E'-H') were visualized by immunofluorescence. Scale bar: 80 μm in (A-D); 40 μm in (E-H, E'-H'). qRT-PCR analysis of WT1, MMP2 and DCN in untreated cells versus cells treated with TGFβ2/PDGFBB and/or BMS345541 (I). Error bars represent the means ± s.e.m. n=3. *$p < 0.05$; **$p < 0.01$; ***$p < 0.001$ (student's t Test).

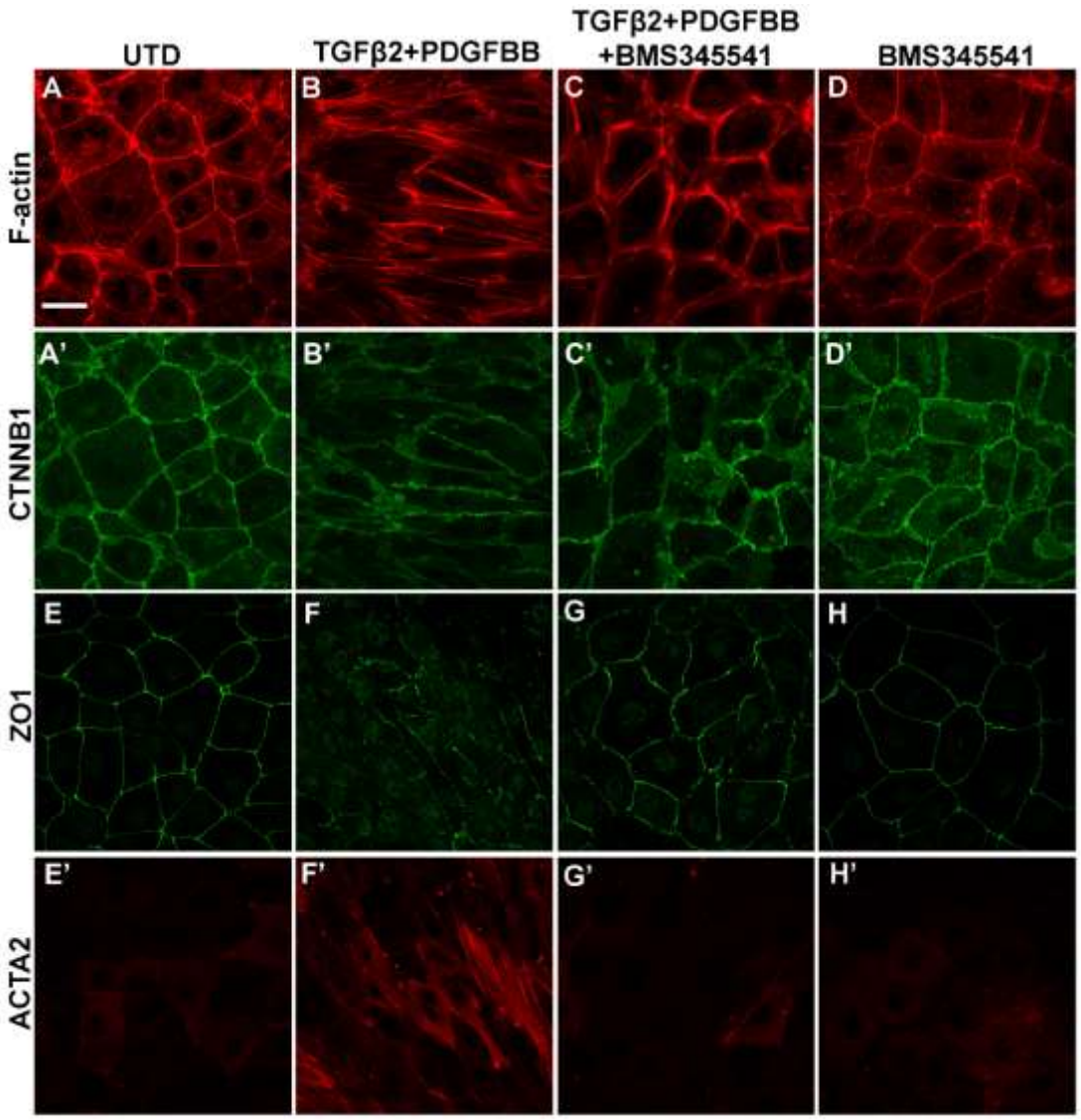

Figure 28. Inhibition of NF-κB blocks TGFβ2- and PDGFBB-induced EMT in the mouse epicardial cell line MEC1. MEC1 cells cultured in the absence or presence of TGFβ2/PDGFBB and/or BMS345541 for 48 hours. Immunodetection of F-actin (A-D) and β-catenin localization (A'-D') in the same cells. In addition, expression of ZO1 (E-H) and ACTA2-positive stress fiber formation (E'-H') was determined in the same cells. Scale bar: 40 μm.

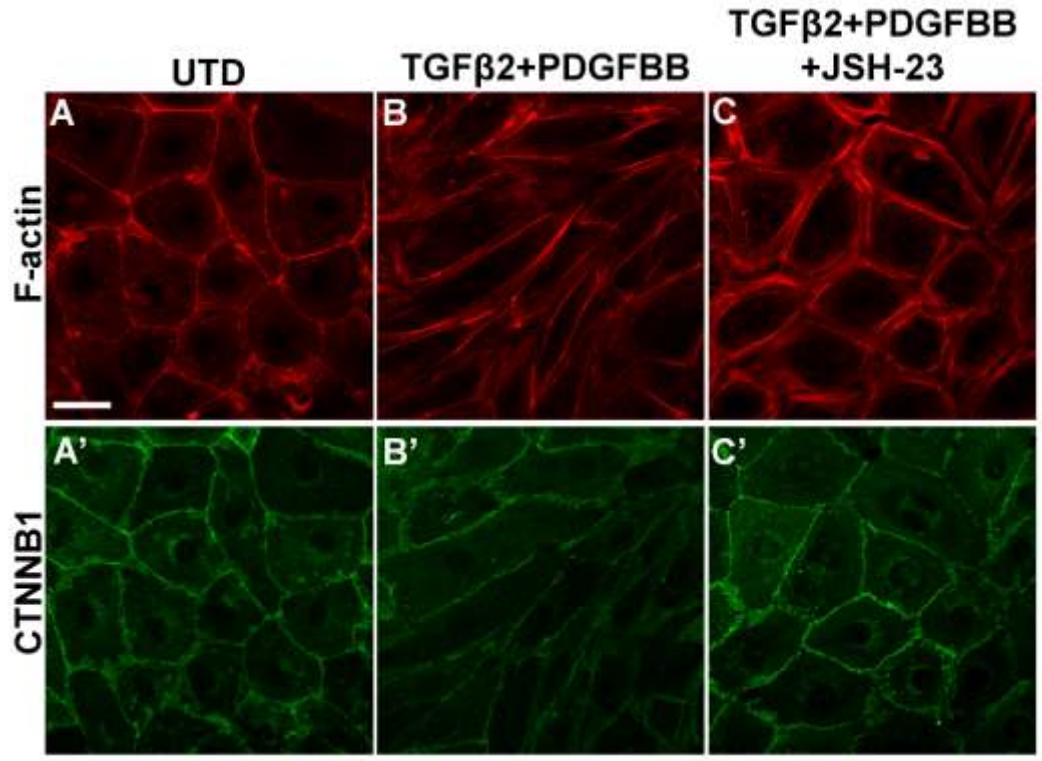

Figure 29. NF-κB inhibitor JSH-23 blocks TGFβ2/PDGFBB-induced EMT in MEC1 cells. MEC1 cells were cultured in the absence or presence of TGFβ2/PDGFBB and/or JSH-23 for 48 hours. F-actin stress fiber formation (A-C) and β-catenin localization (A'-C') were examined by immunocytochemistry. Scale bar: 40 μm.

4.3.3 NF-κB p65 is expressed in the epicardium during embryonic EMT

NF-κB p65 has been reported to be expressed in the developing chicken and mouse heart (Hernandez-Gutierrez. et al., 2006; Kraut et al., 2015). However, its spatiotemporal expression pattern in the heart has not been characterized at the cellular level, nor has a role for NF-κB in the developing heart been established. To examine whether NF-κB components are expressed in a manner consistent with regulating epicardial EMT, we investigated expression of NF-κB p65 in mouse and chicken hearts during time windows when epicardial cells are actively differentiating and communicating with the myocardium (Martinsen, 2005; Wu et al., 2010). We detected a broad expression of p65 in the developing heart, with more intense levels in the epicardium/subepicardium and endocardium compared to the myocardium (Fig 30; Fig 31). In the mouse heart, we found p65 to be perinuclear in the majority of epicardial cells, with a small subset of cells displaying nuclear accumulation (Fig 30). In contrast, chicken NF-κB revealed a predominantly nuclear localization in epicardial/subepicardial cells (Fig 31). This species difference in NF-κB subcellular localization is intriguing and reminiscent of the staining patterns in primary cells (Fig 25 and Fig 26).

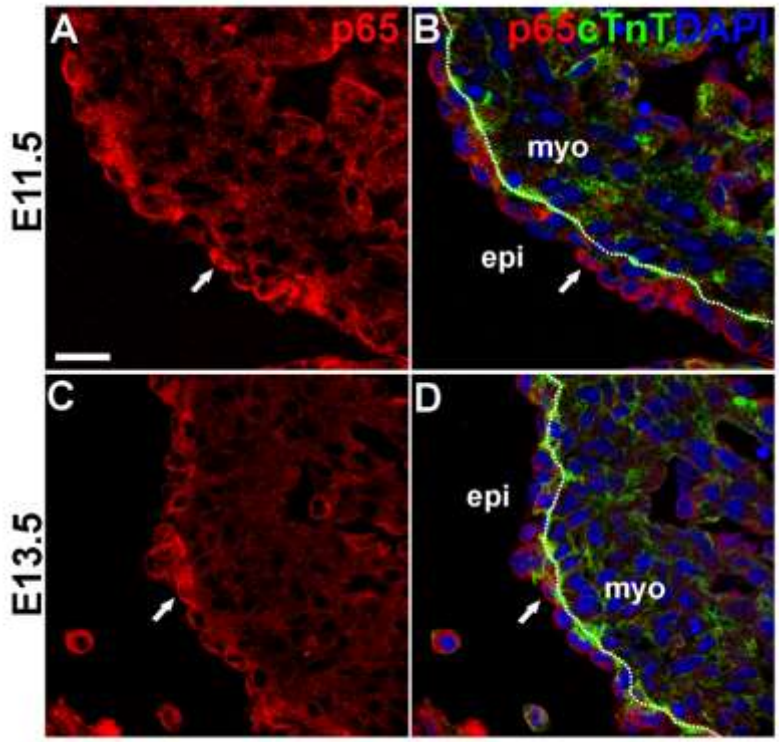

Figure 30. NF-κB p65 is expressed in mouse embryonic epicardium. Immunofluorescence imaging of mouse E11.5 (A-B) and E13.5 (C-D) sections using antibodies directed against p65 (red) and cTnT (green). Nuclei identified by DAPI (blue) staining. p65 proteins were found enriched in the epicardium and endocardium. Nuclear staining was observed in a subset of epicardial cells (arrows). Dotted lines delineate the border between the myocardium and the epicardium. Scale bars: 20 μm.

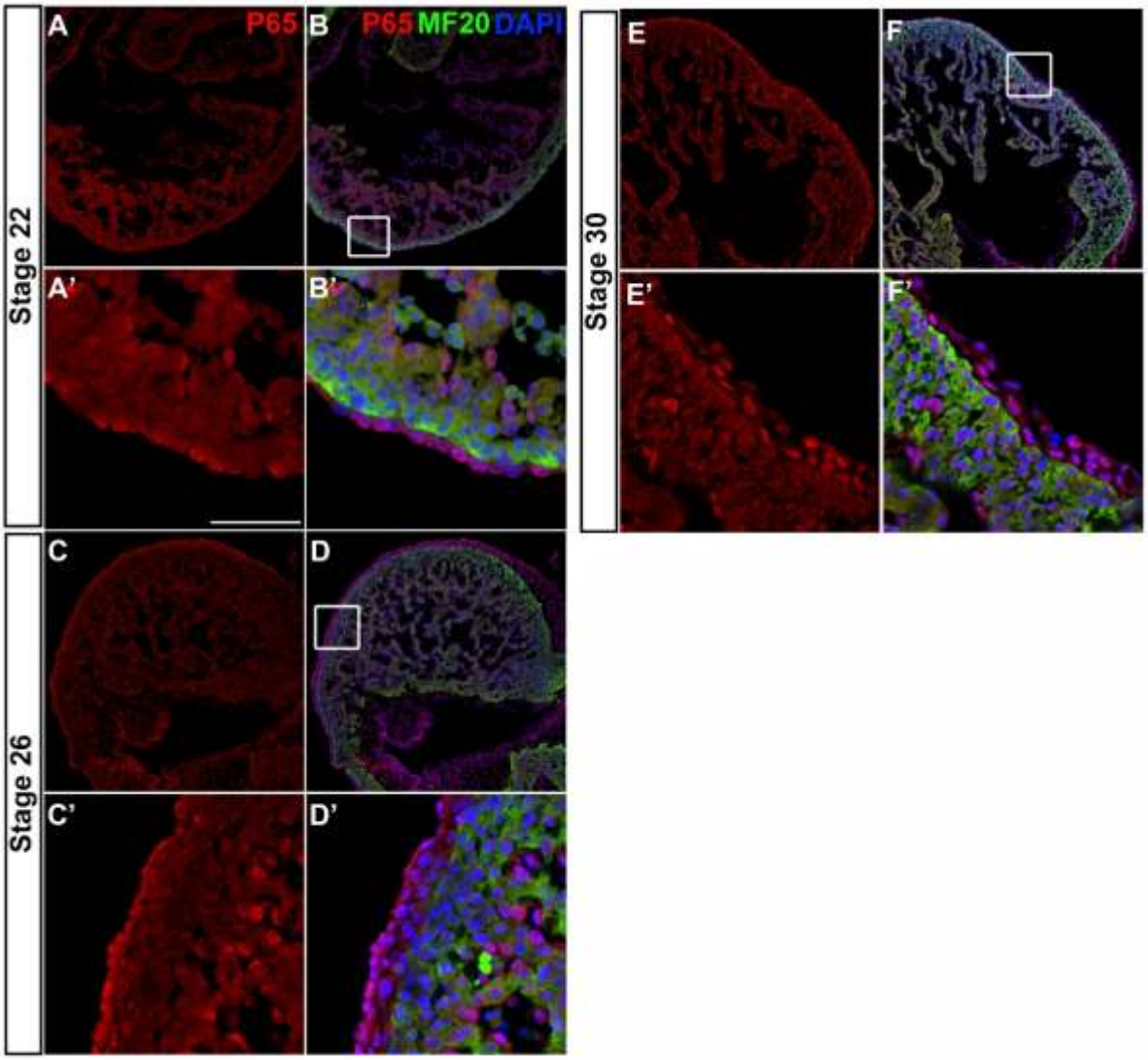

Figure 31. NF-κB p65 is expressed in chicken embryonic epicardium. Cryosections from HH22 (A, A', B, B'), HH26 (C, C', D, D') and HH30 (E, E', F, F') chick embryos were processed for immunohistochemistry using antibodies specific for p65 (red) and anti-sarcomeric myosin (MF20). The cardiomyocyte marker MF20 (green) labels the myocardium. Nuclei are detected by DAPI (blue). Rectangles mark the regions that are magnified in the lower panel for each stage. Scale bar: 50 μm for (A', B', C', D', E', F'); 315 μm for (A, B, C, D, E, F).

4.4 Discussion

4.4.1 NF-κB in the regulation of epicardial EMT

NF-κB has been reported to be required for IL-1b/TGFβ2-induced endothelial-to-mesenchymal transition (EndoMT) in human umbilical vein endothelial cells (Maleszewska et al., 2013). Here, we identified NF-κB as a central signaling node in the EHE dataset and predicted a functional role for NF-κB in epicardial EMT. We further demonstrated that NF-κB activation is necessary for chicken and mouse epicardial cells to transition from epithelial to mesenchymal fate in response to TGFβ2/PDGFBB treatment (Fig 27; Fig 28; Fig 29). These results of our functional studies in primary epicardial cells not only confirmed the bioinformatics prediction, but also complement two recent reports showing that NF-κB is required for TGFβR3-mediated collagen-invasion of epicardial cell lines (Clark et al., 2016; DeLaughter et al., 2016). Together, these studies are the first to establish a crucial role for NF-κB in growth factor-induced epicardial EMT in primary and immortalized cells, respectively. A model for the proposed role of NF-κB in epicardial EMT is shown in Fig 32. Consistent with a role in EMT, our immunostainings of developing chicken and mouse hearts revealed NF-κB p65 expression in the epicardium and subepicardial cells (Fig 30 and Fig 31), corroborating and extending previous reports of NF-κB expression in HH23-24 chicken (Hernandez-Gutierrez. et al., 2006) and E11.5 mouse hearts (Kraut et al., 2015). Therefore, NF-κB has the potential to play a similar role in EMT regulation during heart development in the embryo. Furthermore, IPA Upstream Regulator analysis revealed that many known targets of NF-κB signaling are present in the EHE secretome (Fig 33). GO analysis indicated that these targets are involved in multiple biological functions (Fig 34), suggesting that NF-κB may regulate other aspects of epicardial-myocardial signaling beyond EMT. Finally, Like the epicardium, chicken and mouse endocardium also exhibit NF-κB p65 staining (Fig 30 and Fig 31). This would suggest

that NF-κB may also regulate EndoMT in the embryonic endocardium, as has been demonstrated for human umbilical vein endothelial cells (Maleszewska et al., 2013).

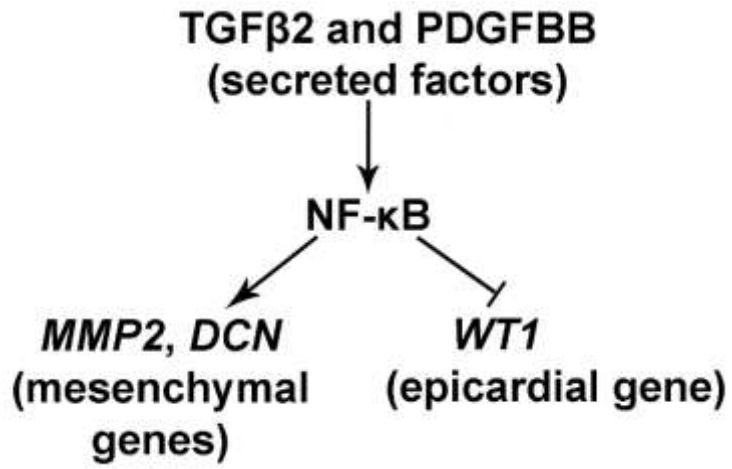

Figure 32. Proposed model for the function of NF-κB signaling in epicardial EMT. TGFβ2 and PDGFBB induce the activation of epicardial NF-κB and consequently upregulation of mesenchymal genes MMP2 and DCN as well as downregulation of epicardial cell marker gene WT1.

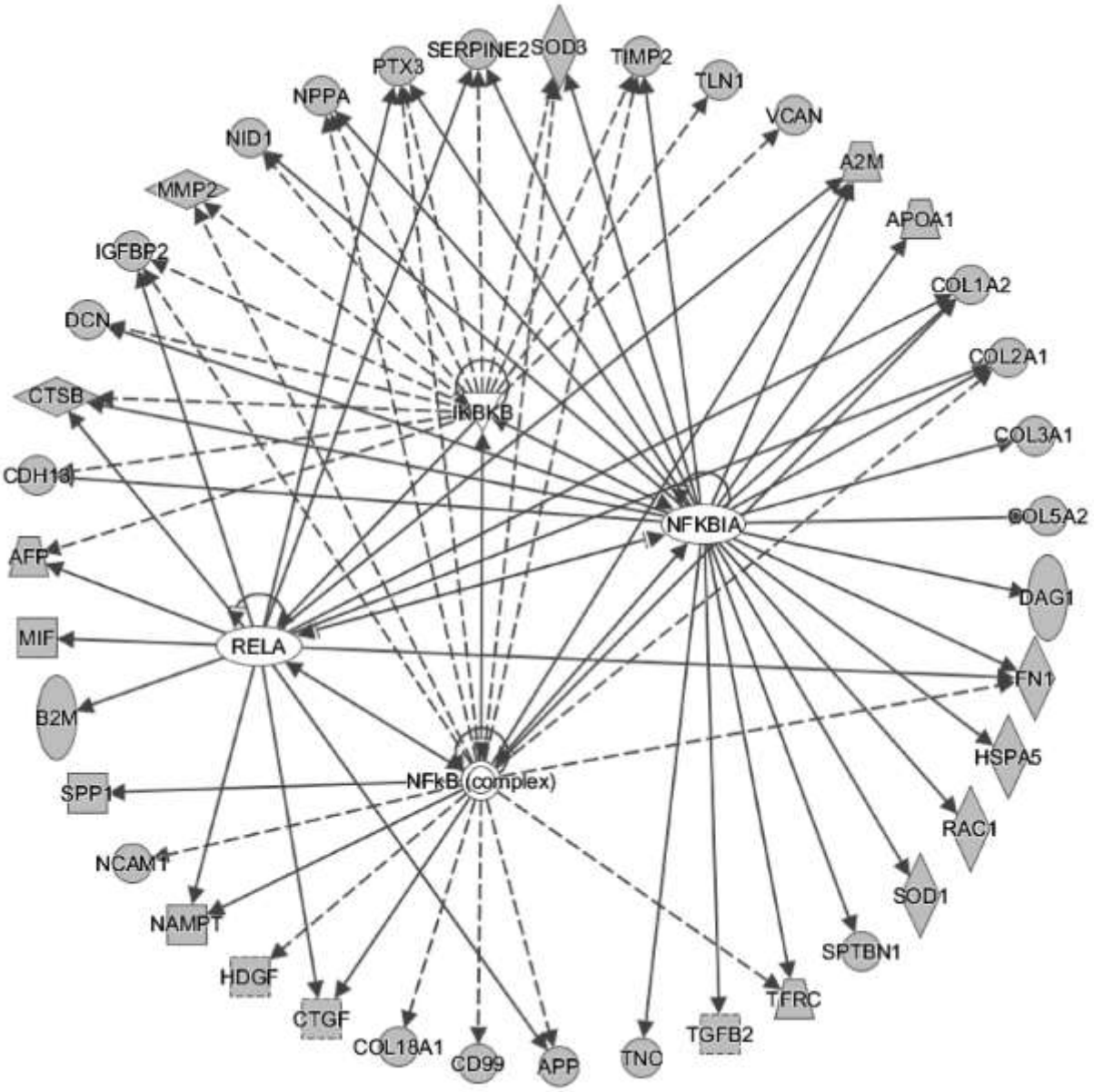

Figure 33. Many targets of NF-κB pathway are present in the EHE secretome. Solid lines denote a direct relationship between gene products while dotted lines indicate an indirect relationship.

Term	PValue	Genes
GO:0007155~cell adhesion	1.27E-07	NCAM1, COL18A1, TLN1, CTGF, TNC, VCAN, SPP1, FN1
GO:0051496~positive regulation of stress fiber assembly	0.00203	APOA1, CTGF, RAC1
GO:0030199~collagen fibril organization	0.002228	COL1A2, COL5A2, TGFB2
GO:0071230~cellular response to amino acid stimulus	0.003603	COL1A2, MMP2, COL5A2
GO:0051668~localization within membrane	0.006439	CDH13, RAC1
GO:0001501~skeletal system development	0.006909	COL1A2, VCAN, COL5A2
GO:0001666~response to hypoxia	0.012496	MMP2, SOD3, TGFB2
GO:0007016~cytoskeletal anchoring at plasma membrane	0.012837	TLN1, DAG1
GO:0061037~negative regulation of cartilage development	0.012837	MMP2, TGFB2
GO:0019430~removal of superoxide radicals	0.012837	SOD1, SOD3

Figure 34. Gene Ontology (GO) analysis of NF-κB regulated proteins identified in the EHE secretome. Top 10 enriched Biological Process (from DAVID BP-DIRECT) are shown.

4.4.2 Potential Species Difference in the Mechanism of NF-κB Activation

Interestingly, while NF-κB activation is necessary for growth factor-induced epicardial EMT in chicken and mouse, our data indicate the activation mechanisms may be different. In mouse cells NF-κB is primarily cytoplasmic (Fig 25A-D). The growth factors induced a clearly visible p65 nuclear accumulation (Fig 25E-H), which is blocked by BMS345541 (Fig 25I-L). In contrast, chicken cells exhibit a significant basal level of nuclear p65 (Fig 26A-D). The increase of nuclear p65 induced by growth factors was more subtle (Fig 26E), but reproducible and quantifiable (Fig 26M). Studies in Drosophila have shown that small differences in nuclear concentrations of NF-κB can have profound physiological consequences (Govind, 1999). Therefore, it is possible that a subtle change in p65 nuclear concentration or nuclear-to-cytoplasmic ratio is sufficient for the activation of downstream effectors that promote EMT. However, our observations also raise the question whether nuclear translocation is the only or the primary mechanism of NF-κB activation in chicken cells. It has been previously shown that chicken NF-κB is capable of interacting with IκB (Kanegae et al., 1998; Muraoka et al., 2000); however, whether the direct interaction controls the localization of chicken NF-κB has not been examined. Rather, it has been shown that IκB and IKK2 regulate the DNA binding activity of chicken NF-κB (Muraoka et al., 2000). It is therefore possible that TGFβ2/PDGFBB activates chicken NF-κB at the level of DNA binding, and the inhibitor BMS345541 interferes with this binding.

V. PROTOCOL DEVELOPMENT OF MATRIX-ASSISTED LASER DESORPTION/IONIZATION IMAGING MASS SPECTROMETRY FOR THE VISUALIZATION AND/OR IDENTIFICATION OF PROTEINS/PEPTIDES ON MURINE HEART SECTIONS

5.1 Introduction

5.1.1 Basic principles of matrix-assisted laser desorption/ionization imaging mass spectrometry in protein analysis

Matrix-assisted laser desorption/ionization imaging mass spectrometry (MALDI-IMS) essentially modifies established MALDI to acquire molecular information in a spatially defined manner. In a typical MALDI analysis, the matrix (small conjugated organic compounds facilitating molecules desorption and ionization process) co-crystallizes with the analytes on a sample plate. The matrix usually is dissolved in a solvent solution before being applied to the tissue section. The solvent aids in the extraction of analytes, increasing their availability for detection. After laser radiation, the matrix absorbs laser light energy, which causes the matrix-analyte mixture to vaporize and the matrix acts as a proton donor and receptor, ionizing the analytes. MALDI has been broadly used for the analysis of metabolites, lipids, peptides and proteins due to the extended mass range and low fragmentation of ionized molecules. In this present work, only peptides and proteins were analyzed.

MALDI can be interfaced with different mass analyzers (Chughtai and Heeren, 2011). Time-of-flight (TOF) mass analyzer was used in the present study. After acceleration, ions drift through a field-free drift region and subsequently reach the detector. All ions begin with the same kinetic energy. The TOF of the ion is proportional to the square root of its mass-to-charge (m/z) when

they travel a fixed distance. Each laser pulse generates a mass spectrum, which is a graph of ion intensity plotted against the mass-to-charge (m/z) ratio of ions (Tanaka et al., 1988). The usefulness of MALDI-TOF for IMS was first demonstrated by *Caprioli et al* decades ago (Caprioli et al., 1997). In IMS, a homogeneous coating of matrix was applied to the tissue surface followed by MALDI analysis with an imaging mode. In this mode, the laser rasters across the tissue surface or within one chosen region in a pre-defined manner by moving the sample plate and keeping the laser beam in a fixed position. At the same time, a mass spectrum from each discrete spatial spot or 'pixel' is acquired. Softwares have been developed to reconstruct these pixels into images displaying the molecular distribution throughout the tissue for given m/z values. Multiple images representing the spatial distribution of each detected ion within an analysis area can be extracted from one data set. A schematic representation of a typical MALDI-IMS workflow is presented in Fig 35 (Seeley and Caprioli, 2011).

5.1.2 Current status of MALDI-IMS for *in situ* protein analysis

MALDI-IMS is a young and rapidly expanding technology with many opportunities for analysis of biological samples. Applications include the molecular histology of tissue sections (Nimesh et al., 2013; Schwamborn and Caprioli, 2010; Watrous, 2011). With particular interest for this present work, I will summarize the advances in MALDI-IMS sample preparation for protein analysis from tissue sections.

For any MALDI-IMS analysis, the ultimate goal is to achieve high resolution images and high quality spectrums. However, because a reduction of the irradiated sample area naturally reduces the ion yield, improving image resolution would inevitably lead to loss in spectral quality and MALDI image brightness. Thus, it is important to find a balance between the amount of analyte incorporation into matrix crystals and the level of analyte migration. Proteins can be digested,

generating peptides to be analyzed, or intact proteins and naturally occurring protein fragments of up to 25 kDa are measured (Meding and Walch, 2013). A typical MALDI-IMS includes tissue section preparation, matrix application, trypsin application if direct protein identification with a bottom-up approach is needed, instrumentation and data analysis. All these steps need to be fine-tuned and carefully controlled to generate high resolution images in a reproducible manner.

For sample preparation, fresh frozen sections are known to best maintain their molecular properties while containing many salts and lipids that can contribute to signal suppression. Thus, wash procedures reducing salts, metabolites and lipids are absolutely essential for protein detection. A couple of wash procedures have been developed for protein analysis. The key point of this sample handling procedure is to maintain the integrity and localization of the proteins in sections. In this study, a relatively stringent wash protocol was used to enhance signal to noise ratios for proteins.

Another important aspect in sample preparation is matrix application, which should also be optimized. Ideal matrix application methods should create homogeneous and condensed matrix crystals that sufficiently extract the analytes of interest. Current matrix application methods include sublimation, spraying or spotting with decreasing spatial resolution and increasing spectral signal intensity. The spraying method has been suggested as a good compromise resulting in sufficient analyte incorporation under reduced migration conditions (Werner Bouschen and Schulz, 2010). The migration of biomolecules can be minimized by applying the matrix in cycles with drying between cycles. Spraying is capable of producing a spatial resolution of about 25 μm but is less efficient in protein extraction as compared to the spotting method.

For *in situ* protein identification, another pivotal factor is on tissue digestion. Similar to matrix application, popular trypsin application methods include spraying and spotting. The key point is to precisely maintain the digestion peptide locations while achieving the best digestion efficacy.

Then images of proteins can be deduced from the images generated from the peptide ion signals (Lemaire et al., 2007). Although the spotting method has been shown to achieve better spectral quality than spraying, spraying can generate images with higher spatial resolution.

Besides crystal size, the resolution of a protein image also depends on the instrumentation, especially laser spot size and sample stage movement. MALDI laser spot sizes are typically 30-200 μm. In this study, a linear TOF was used for protein imaging and the instrument parameters were tuned for targeted mass range.

An equally important aspect that needs further attention is the development of data analysis methods, especially informatics tools, such as quality checking of the acquired data, that are accessible to non-specialists (Watrous, 2011). In this protocol development study, only basic data processing and visualizing tools were used. Ideally, real-time evaluation should be incorporated throughout the whole process, for example the tissue wetness and drying rate during on tissue digestion. However, real-time evaluation was not feasible for the semi-automated sprayer used in this study.

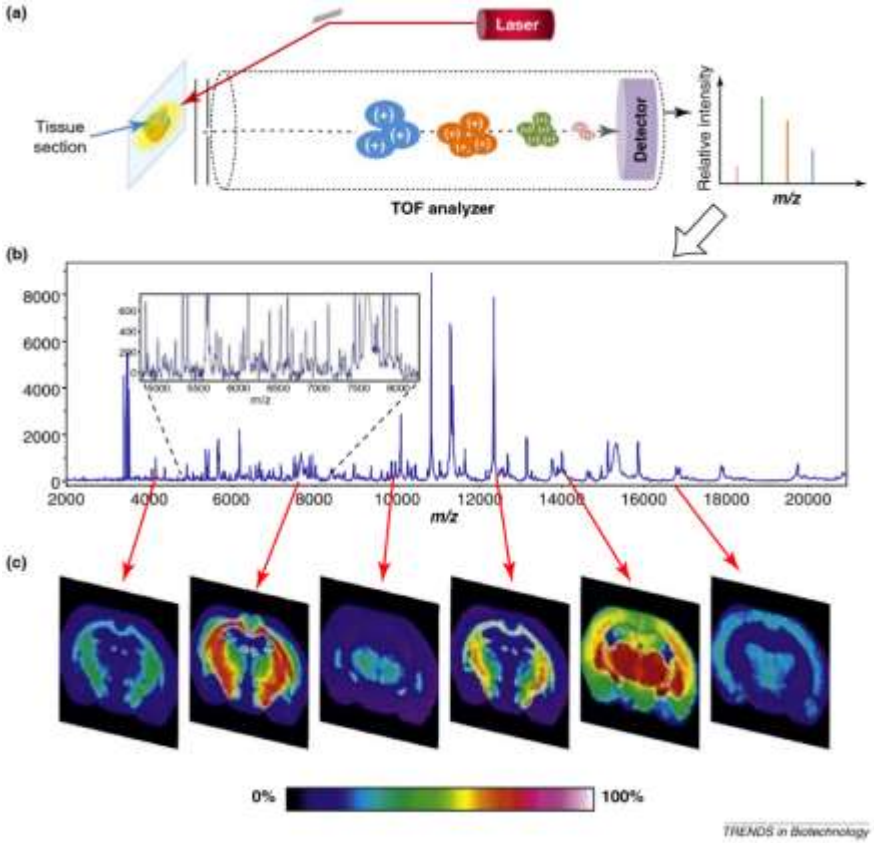

Figure 35. Schematic representation of the MALDI-IMS process. (a) A tissue section on a conductive slide is placed in the source of the instrument and a laser is fired at the surface to desorb and ionize molecules. Analytes from each spot are separated in the TOF analyzer, their flight times converted to m/z ratio, and a spectrum recorded. (b) A representative mass spectrum collected from a tissue section. Inset shows detail and complexity of the spectrum collected. A tissue imaging experiment might result in thousands of such spectra. (c) Using an average spectrum from the entire section, ion images can be generated from each peak. Each m/z value of interest can be displayed as a function of position in the tissue section and relative intensity. Hundreds of such images can be created from a single tissue section.

Reprinted from reference (Seeley and Caprioli, 2011). Copyright (2011), with permission from Elsevier.

5.2 Materials and methods

5.2.1 Reagents

Sequencing Grade Modified Trypsin was purchased from Promega (Madison, WI). High-performance liquid chromatography (HPLC)-grade acetonitrile, ethanol, Acetic acid, ammonium bicarbonate, chloroform and 2,5-DHA were from Fisher Scientific (Pittsburgh, PA). α-cyano-4-hydroxycinnamic acid (CHCA) was from Protea Biosciences (#CMS-100).

5.2.2 *In situ* protein identification from adult mouse heart

5.2.2.1 Sample preparation

Adult mouse hearts were dissected, wrapped in aluminum foil and directly frozen with liquid nitrogen. Frozen hearts were sectioned on a cryostat at 10 μm thickness and thaw mounted onto stainless steel MALDI plates (AB Sciex, Framingham, MA, #4347684). Heart tissue sections were washed in 70% ethanol for 30s, 100% ethanol for 30s, Carnoy's fluid (a 6:3:1 solution of 100 % ethanol/chloroform/acetic acid) for 2 min, 100% ethanol for 30s, and water for 30s, and then 100% ethanol for 30s (Yang and Caprioli, 2011). Slides were then stored in a desiccator until further processing on the same day.

After washing, 40 μl trypsin (final concentration at 0.08 μg/μl in 100 mM ammonium bicarbonate/10% acetonitrile, Promega, #V5117) was spray coated on each MALDI plate using an airbrush attached to a nitrogen gas tank, at 20 psi. The spraying cycle was 0.1 sec spray, 20 sec dry for 6 cycles; 0.2 sec spray, 60 sec dry for 6 cycles; 0.25 sec spray, 60 sec dry for 6 cycles. After spraying, the MALDI plate was incubated in a sealed humidified chamber for 6 hours at 36°C for on-tissue digestion. Spraying and incubation conditions were optimized for highest digestion efficiency and minimal delocalization. After digestion, the plates were dried completed in dessicator for 30 min. 300 μl matrix (14 mg/mL CHCA in 6:4 v/v mixture of acetonitrile and

0.1% trifluoroacetic acid) was applied with airbrush at 22 psi, the sections were completed dried, then another 400 μl MALDI matrix (20 mg/mL CHCA in 6:4 v/v mixture of acetonitrile and 0.1% trifluoroacetic acid) was applied. The spraying cycle was 0.2 sec spray, 20 sec dry for 6 cycles; 0.3 sec spray, 60 sec dry for 10 cycles; 0.35 sec spray, 80 sec dry for 6 cycles. The plates were stored in a dessicator until subject to MS analysis on the same day. The apparatus was set up as shown in Fig 36. The airbrush was controlled by a computer application built in-house.

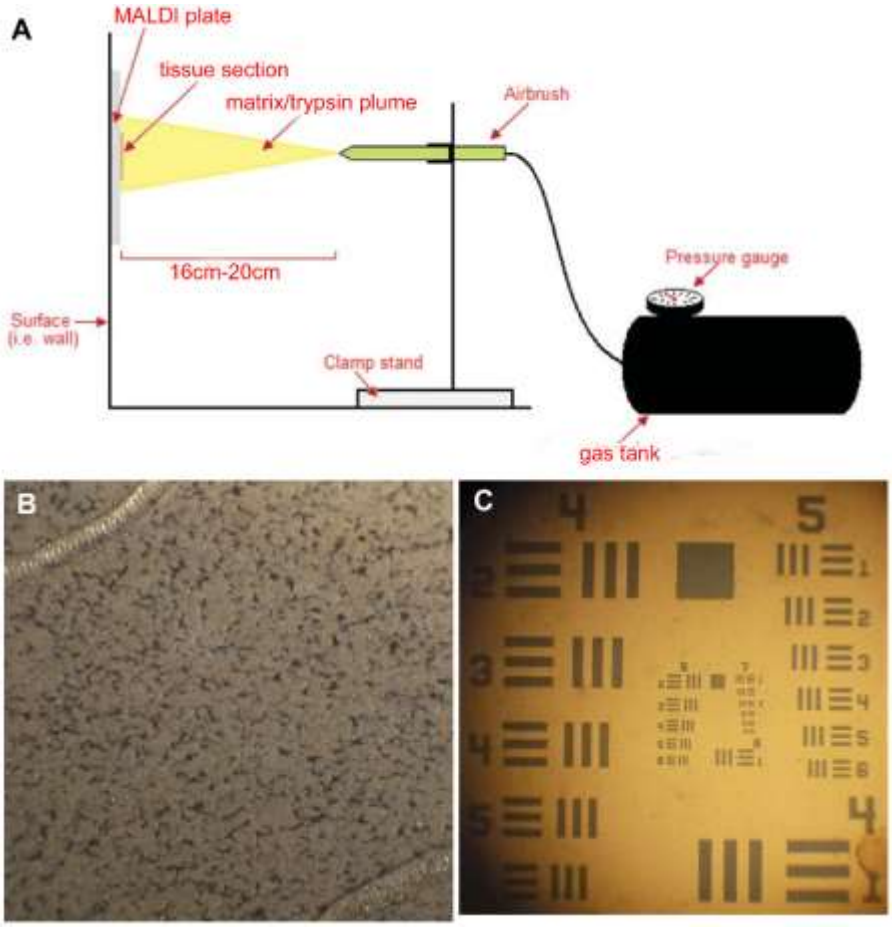

Figure 36. CHCA matrix deposition. (A) Schematic representation of spraying apparatus set up. (B) Optical images of CHCA matrix crystals applied by spraying. (C) USAF resolution test target was shown to demonstrate the lateral resolution.

Panel (A) is adapted with permission from reference (Gregson, 2009).

5.2.2.2 Instrumentation and spectrums acquisition

For mass spectrometry experiments without imaging, MALDI-MS was performed with a 4700 TOF/TOF (AB SCIEX, Foster City, CA, USA) in reflectron positive mode. MS coupled MS/MS method was used for *in situ* protein identification while MS coupled with imaging method was used for peptide imaging. The MALDI instrument has been described previously (Blaze et al., 2012). The instrument is equipped with a 200 Hz 355 nm Nd:YAG laser. The laser spot size is ~150 μm. Laser power was set to 2200-2600 arbitrary units. The collision gas for MS/MS experiments is Helium. A built-in software (4000 Series Explorer V3, AB SCIEX) was used for spectrum acquisition. It was calibrated using the standard calibration mixture (mass standards kit for calibration, 4333604, AB SCIEX) according to manufacturer's instruction (Blaze et al., 2012).

Digestion peptide profiles from the heart section were acquired using the following parameters: m/z range 600-3000 with focus m/z 2000, 2000 laser shots with laser intensity set at 2200. Peaks with relatively intensity were manually selected for MS/MS fragmentation via collision-induced dissociation (CID) using following parameters: metastable suppressor set as ON, laser intensity set at 3500 laser shots.

MS image acquisition was performed using the built-in software (4000 Series Explorer V3, AB SCIEX) coupled with an open source software (4700 Imaging V3, http://maldi-msi.org), which allows the acquisition of images in MS/MS mode. The following parameters were used: a raster size of 150 μm and 100 or 200 laser shots per spot depending on the size of imaging area. The imaing spectrums were processed and displayed using open source software (BioMap V3803, http://maldi-msi.org). All spectra were visualized and/or processed (baseline correction and smoothing with Savitzky Golay algorithm) with an open source mass spectrometry tool mMass (http://www.mmass.org/) before presenting.

5.2.2.3 Database searching

MS/MS spectra were submitted to the protein database MASCOT V 2.2.04 (licensed to the University of Illinois at Chicago, National Center for Data Mining, P0127504) to match tryptic peptide sequences to their respective intact proteins. Search parameters were set as follows, based on a published tutorial (Cottrell, 2011). MS/MS spectra were searched against the mouse subset of SwissProt databases (16281 sequences). Additional parameters are: trypsin enzyme specificity, monoisotopic masses were used for searching product ions, peptide tolerance within ±200 ppm and a fragment mass tolerance of ±0.5 Da, one missed cleavage, no fixed modifications (since no chemical modification was expected during digestion) and no variable modification selected. Probability-based scoring for peptide match is used in MASCOT. MASCOT scores are reported as -10*LOG10 (P). P is the absolute probability that the observed match is a random event.

5.2.3 MALDI-IMS of intact proteins

Embryonic mouse hearts (E14.5) wrapped by aluminum foil were directly frozen in liquid nitrogen. 10 µm heart cryosections were thaw mounted on to indium-tin-oxide (ITO) coated glass slides (Delta Technologies, Stillwater, MN, USA). Heart tissue sections were washed as described above except with modified Carnoy's fluid (6:3:1 solution of 100 % ethanol/chloroform/water). The matrix application and imaging are conducted similar to that described previously (Wenke et al., 2017). DHA matrix has been shown to provide good sensitivity for protein imagining (Zavalin et al., 2015). The matrix (150 mg DHA dissolved in 7 ml ACN, 2ml H2O, 200 µl TFA and 200µl acetic acid) was applied in 8 passes by a TM Sprayer (HTX Technologies, Carrboro, NC, USA) using the following parameters: 0.08 ml/min, 30°C, 2.5 mm track. A Bruker Autoflex Speed II TOF instrument (Bruker Daltonics, Billerica, MA) was used for MALDI protein imaging (m/z 3,000-30,000) and images were viewed in FlexImaging software. DHA matrix was then washed

off with ethanol and acetone and H&E staining were performed to gain histological information. H&E stained sections were viewed with a Leica microscope at ×5 magnification. H&E staining was performed as previously described (Casadonte and Caprioli, 2011).

5.3 Results

5.3.1 MALDI-IMS of intact proteins on embryonic mouse heart sections

The width of the embryonic mouse epicardial space is usually 2-4 cell layers (Fig 37). With a typical mammalian cell size of 10 μm, a 30 μm resolution is required to image the sub-epicardial space. In the present work, embryonic mouse heart sections were coated with DHA matrix by spraying which produced a uniform coating with crystal sizes ~25 μm. In the spraying techniques used here, matrix were applyed in cycles with drying between each cycle, thus the dislocalization of analytes on tissue surface can be minimized.

Molecular images reconstructed from three spatially distinct m/z signals in a single embryonic mouse heart section are presented in Fig 38. The same tissue section was then stained with H&E (Fig 38D). It is worth noting that even after irradiating the tissue with a high number of laser shots, the tissue appeared not altered in its morphology. Fig 38E shows the average spectra from a heart section. A signal at m/z 6804 was found at intermediate levels in the ventricular myocardium and localized strongly to the edge of the heart. m/z 7684 and m/z 13802 are more broadly localized in the myocardium and the interventricular septum. The interpretation of mass spectrometric images is intrinsically quantitative. Therefore it is worth noting that as a result of the tissue complexity induced ion-suppression effect, the intensity for each peak in the mass spectrum is not only associated with the concentration of proteins, but also to the efficiency of protein extraction and ionization. This is the first time that protein images have been generated directly from embryonic mouse heart sections by MALDI-IMS while retaining localization to histological features.

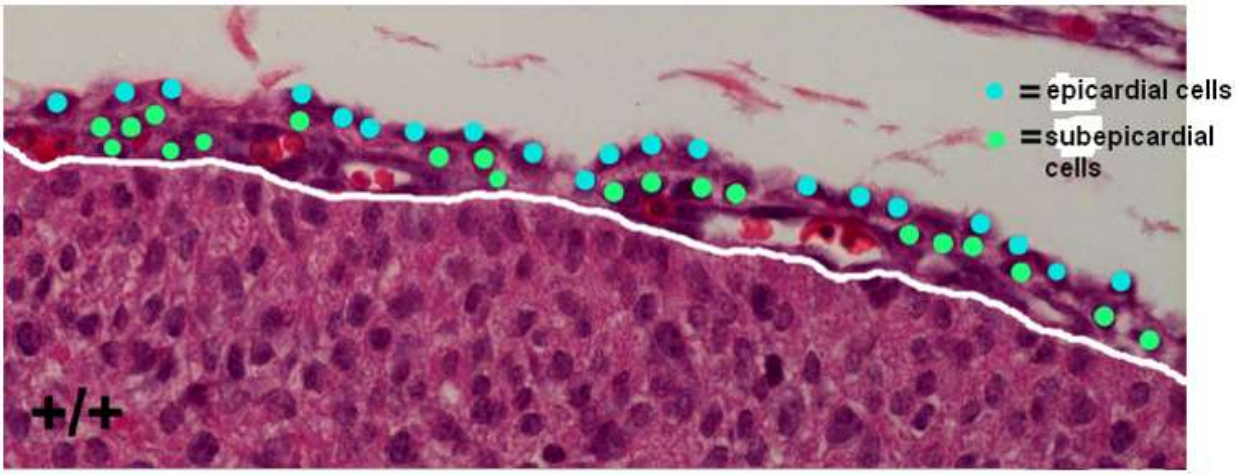

Figure 37. H&E staining of an E13.5 mouse heart section. Blue dots mark epicardial cells and green dots mark subepicardial cells. White line delineates the border between the myocardium and the subepicardium.

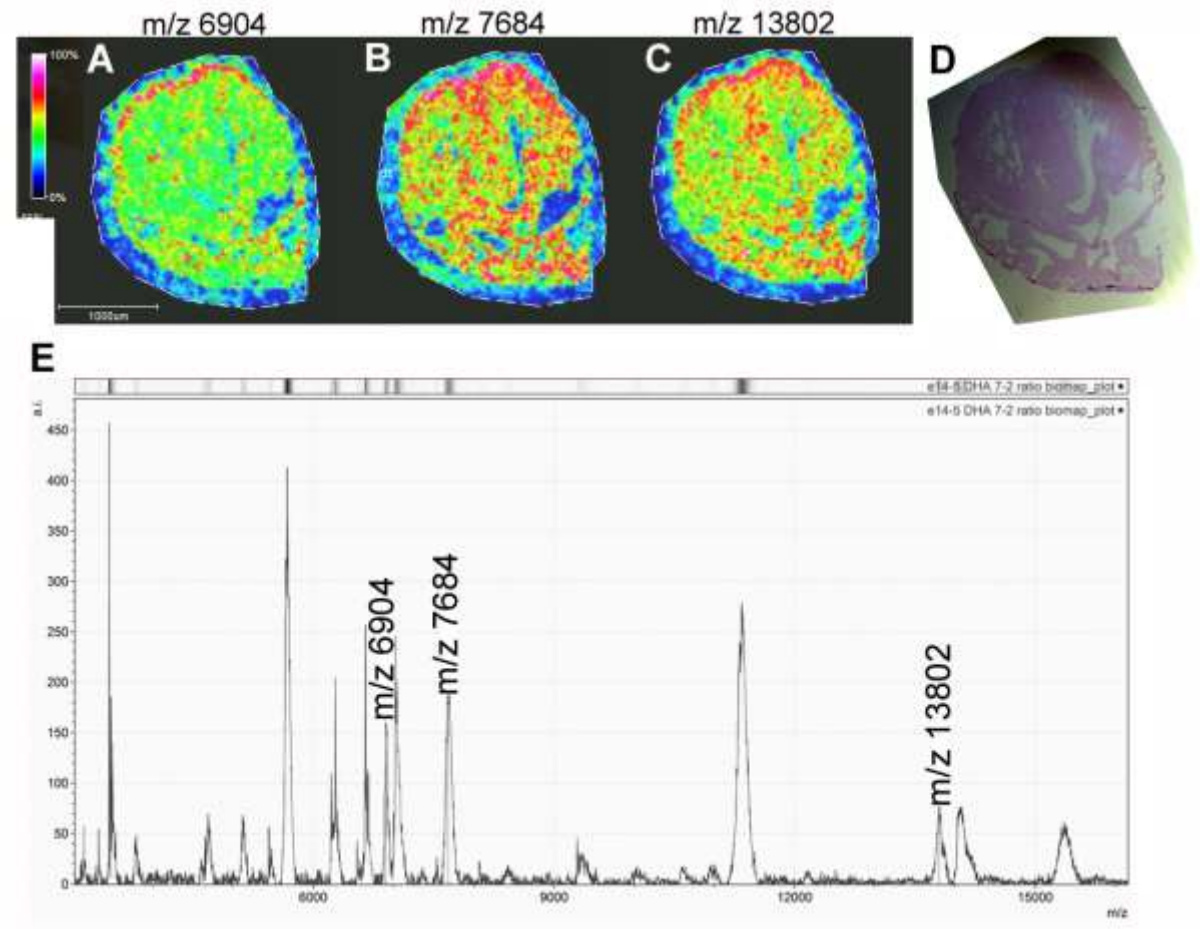

Figure 38. Representative ion images of embryonic mouse heart using MALDI-IMS at 30 µm resolution. (A) m/z 6904. (B) m/z 7684. (C) m/z 13802. (D) H&E stained E14.5 heart section following MS image acquisition. (E) Imaging spectrum with imaged peaks labeled.

5.3.2 *In situ* protein identification using MALDI-IMS

Generating high resolution ion images directly from tissue sections without the need of labels is a big step forward. However, it can only provide limited information for biological questions without the identity of these molecules, especially for unbiased study. Due to the molecular weight restriction of top down proteomics, a bottom up approach is more commonly used (Chughtai and Heeren, 2011). Here I will describe my efforts to combine on-tissue digestion with MALDI imaging for spatially resolved *in situ* protein identification. After extensive washing to remove molecules such as lipids and salts, embryonic mouse heart sections were sprayed with trypsin to generate spatially-localized peptides that reflect the distribution of their intact precursor. Fig 39 shows a typical average spectra from frozen adult heart section digested with trypsin. On tissue MS/MS analysis of selected peptide peaks identified several proteins listed in Table I. This protein list includes myosin, actin and hemoglobin subunits, which are all expected to be detected on heart sections. The number of proteins identified parallels previously reported protein number (4 proteins) identified by MALDI-IMS (Schober et al., 2011). A representative MS/MS spectrum (m/z 2093) is shown in Fig 40. Proteins were only called "identified" when they were detected in at least two biological samples.

Many peaks generated low MASCOT scores due to low signal-to-noise ratios or the assigned peptide sequences were questionable. Therefore, those peaks could not be reliably assigned to a specific protein. This is not surprising given the tissue complexity induced ion suppression effects. This complexity may also cause multiple peptides at each nominal mass, which further complicate the sequence assignment. The distribution of selected MS signals are presented in Fig 41, which shows that different peptide signals have different patterns of distribution. The spatial resolution

(150 μm) for MS images acquired in this study was dependent on the laser spot size (~150 μm diameter).

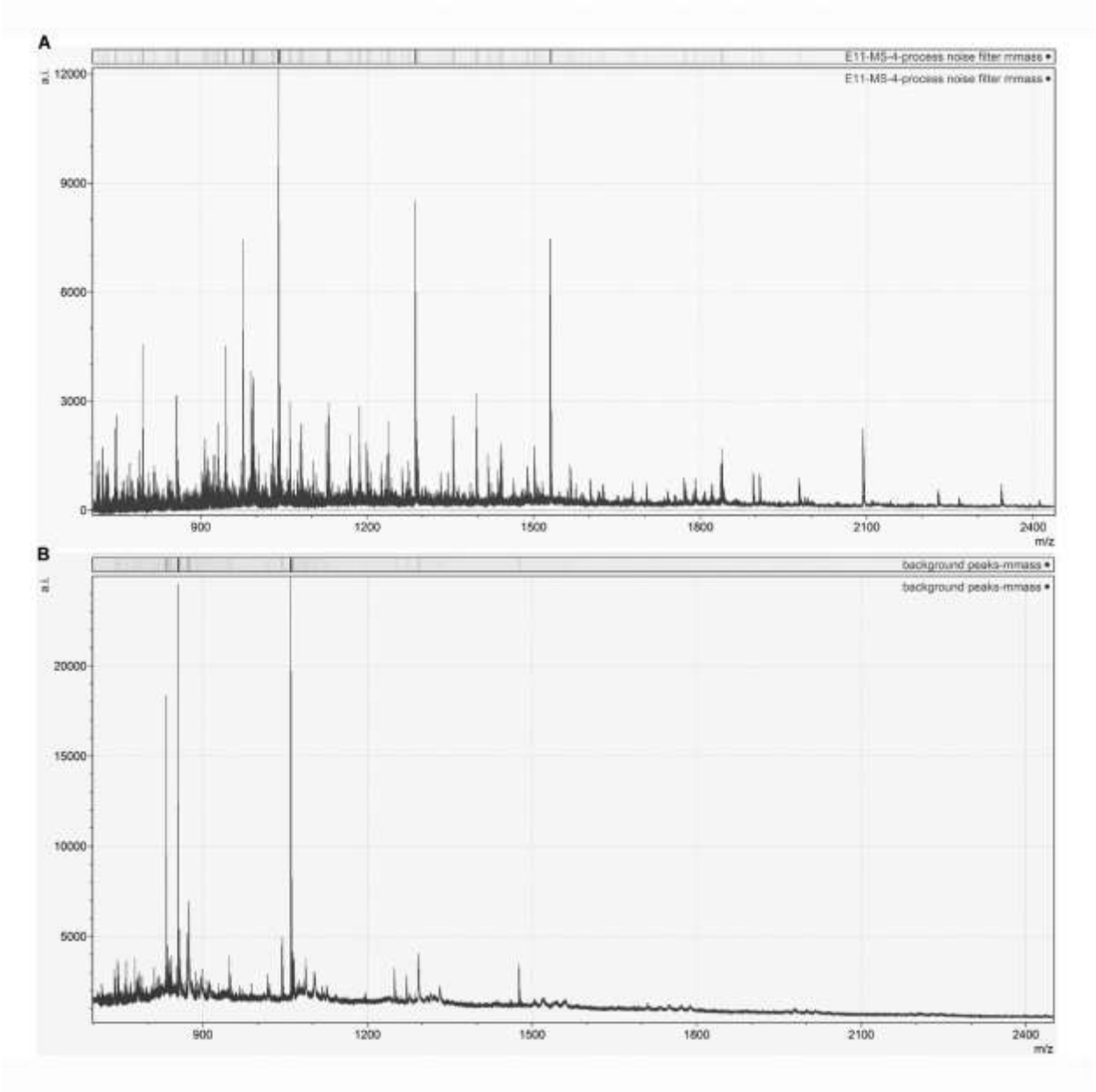

Figure 39. Representative averaged MALDI spectrum from frozen adult mouse heart section.

(A) Averaged MALDI MS spectrum of tryptic peptides from a selected spot on adult heart section.

(B) Background spectrum from a spot without tissue.

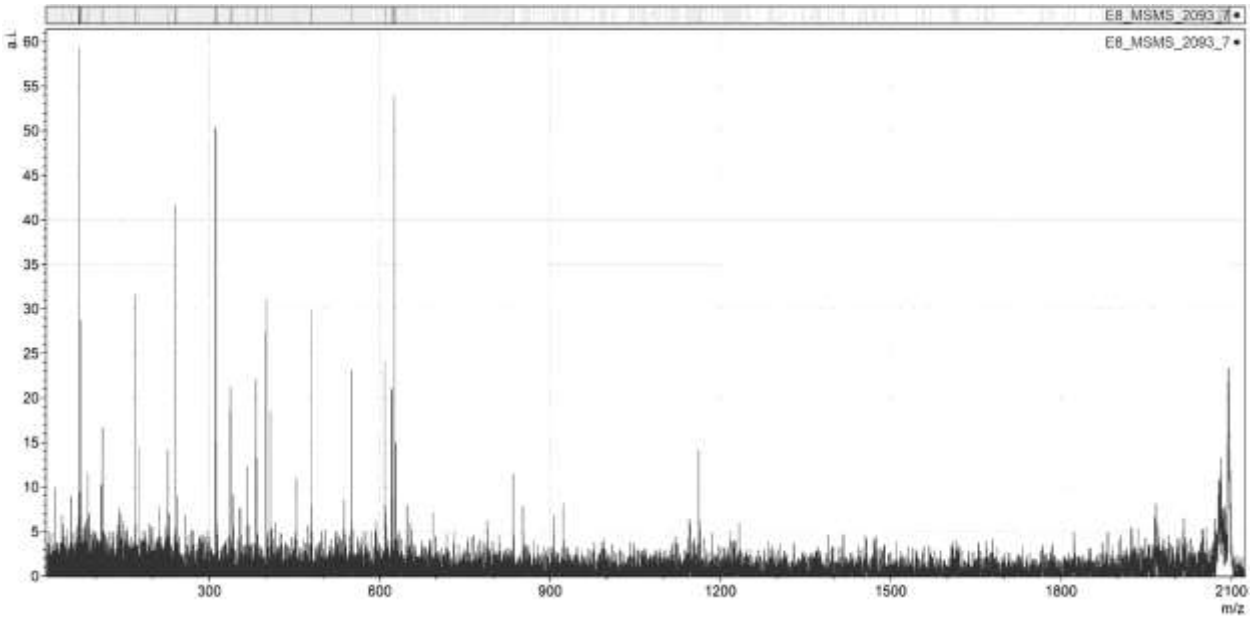

Figure 40. Tandem MS (MS/MS) spectrum of the peptide at m/z 2093. This peptide was identified as a tryptic fragment of myosin light chain 3 by searching the mouse SwissProt database with MASCOT software.

TABLE I. LIST OF IDENTIFIED PROTEINS FROM ADULT MOUSE HEART SECTION

Database	Protein	Peptide m/z used	Theoretical mol. wt	MASCOT score[a]
SwissProt	Myosin light chain 3	2093.0, 2093.0[b], 1396.7	22407	61, 52, 45
SwissProt	Actin	976.4, 1198.8	41710	38, 31
SwissProt	Hemoglobin subunit beta 1/2	1126.5, 1274.7	15830	39, 28
SwissProt	Myosin 4/1/7/6/8	1894.9	222720	53
SwissProt	Serum albumin	1439.7	68648	29
SwissProt	Hormone sensitive lipase	1081.45	83295	21
SwissProt	E3 ubiquitin-protein ligase	1977.9	110018	17

a. all MASCOT scores are higher than the homology threshold or identity threshold scores ($p<0.05$).
b. m/z 2093.0 was identified in two different biological samples.

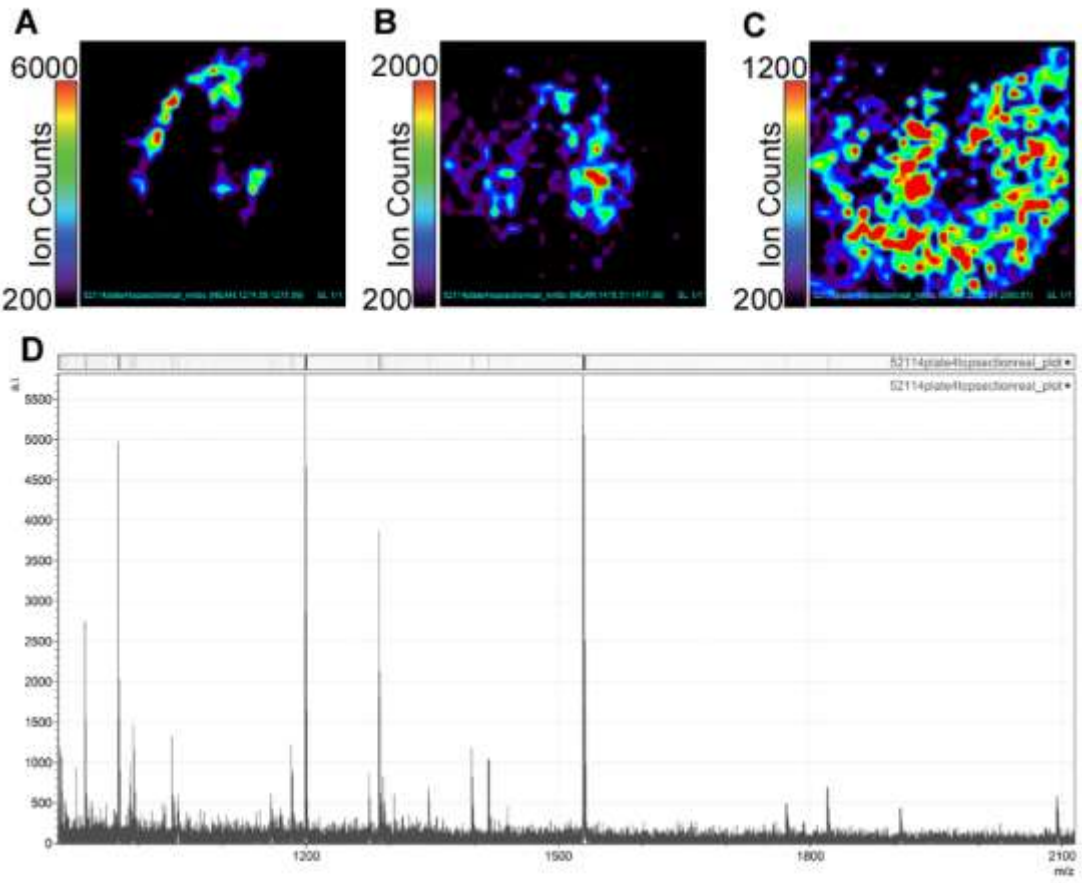

Figure 41. MALDI imaging of frozen adult mouse section at 150 µm resolution. Spatial distribution of three selected ions: (A) m/z 1276, (B) m/z 1416 and (C) m/z 2092. (D) Imaging spectrum.

5.4 Discussion

5.4.1 Summary of results

The objective of this study was to explore the feasibility of developing a MALDI-IMS protocol for untargeted detection and imaging of endogenous proteins/peptides on mouse heart sections. Intact protein imaging on embryonic heart sections demonstrated the feasibility of achieving images of intact proteins with a 30μm resolution, just sufficient for the spatial resolution required for imaging epicardium/subepicardium in the embryonic mouse heart (Fig 37). To correlate the intact protein images to protein identities, a top-down approach that fragments intact proteins for sequence information without further enzymatic digestion is recommended. (Angel et al., 2016).

However, *in situ* protein identification experiments only identified 7 highly abundant proteins directly on tissue. The low number of proteins identified indicated that direct on-tissue protein identification by MALDI-IMS will not identify additional low abundance secreted proteins in the epicardium/subepicardium region *in vivo*. The number of proteins identified in this study is consistent with previous reported protein identification number (4 proteins) (Groseclose et al., 2007; Schober et al., 2011). One study reported a strategy to improve the on-tissue identification of tryptic peptides by performing a complementary liquid chromatography-electrospray ionization-tandem mass spectrometry (LC/ESI-MS/MS) analysis on an adjacent section. This approach enhanced the number of identified proteins from 4 to 106 by mapping peptides identified in LC/ESI-MS/MS to the imaged peptides (Schober et al., 2011).

5.4.2 Limitations of MALDI-IMS from the perspective of present study

Although many methodological papers over the last decade described guidelines for sample preparation in protein analyses (Diehl et al., 2015; Schwartz et al., 2003; Seeley et al., 2008), the technology development for MALDI-IMS has yet to fulfill the potential that researchers hope for.

Most importantly, a simple and reproducible workflow has not been established for protein/peptide analysis. Although state-of-the-art instruments are essential for experiments requiring high resolving power, most mass spectrometers can generate high quality data for MALDI-MSI experiments, therefore tissue preparation and data analysis are the limiting factors (Cillero-Pastor and Heeren, 2013). This chapter describes a protocol development project for a qualitative MALDI-MSI study. Thus, I will discuss the limitations of MALDI-IMS in signal sensitivity and reproducibility from the perspective of sample preparation.

A major and unavoidable challenge in IMS is reproducibility, which mainly depends on three factors: tissue heterogeneity, sample preparation, and ion suppression effects (Lietz et al., 2008). In the present study, sample preparation processes were optimized and instrument parameters were tuned until spectra with similar quality could be obtained each time. However, for the spraying system built in-house, I found that the performance of the matrix and enzyme spray varied between spray cycles and resulted in heterogeneous coating even when exactly the same parameters were applied. This inhomogeneous coating of matrix can create local ionization biases that may cause extensive signal suppression (Lietz et al., 2008) and inconsistency. In this case, the variation in signals at different spatial points are not due to different concentrations of analytes, but rather due to differences in ionization efficiency or uneven matrix coating. Therefore, it is recommended to validate the molecular imaging data by immunohistochemistry whenever possible.

In situ identification of proteins corresponding to m/z detected by IMS is still challenging due to multiple reasons. First, there is no gold standard on the tissue digestion protocol. Second, the chemical complexity of tissue may generate several peptides of the same mass. Consequently, except for highly abundant peptides, identification by on-tissue MS/MS may lead to ambiguous results due to fragments from different peptides. Furthermore, the ionization process is generally

much less efficient then LC-MS, causing reduction of the quality of the IMS data (Heeren et al., 2009; Watrous, 2011). Thus, direct MALDI-MS/MS is only capable of detecting rather abundant proteins and peptides due to the absence of a fractionation procedure before the mass spectrometry analysis. Additionally, computational methods for data analysis of IMS needs to be greatly improved and informatics tools that are user friendly to other non-IMS scientists need to be developed. Besides, there are no established standard procedures for data processing. It is generally considered to be only a semi-quantitative technique.

VI . GENERAL DISCUSSION

6.1 EHE secretome: summary and perspectives

In this dissertation, I described a qualitative proteomic study that takes an unbiased approach to systematically identify proteins involved in epicardial-myocardial signaling. The study uses an EPDC-heart explant (EHE) co-culture system that is established from chicken embryos at HH22-24, when epicardial EMT is on-going. The research reported in this dissertation has accomplished two important goals: generate an unbiased dataset of the EHE secretome; and conduct a case study in which the dataset was used to guide a targeted functional investigation. The large number of proteins in the EHE secretome dataset indicates the complex nature of the epicardial-myocardial communication. GO analysis revealed that the 150 proteins in the EHE secretome are implicated in multiple biological processes that are pertinent to EMT, including cell migration, and cell invasion. Data analysis revealed that 60 protein pathways (defined by IPA) are over-represented in the EHE secretome, including 9 pathways with well-known roles in regulating heart development, such as the Wnt pathway. For these 9 pathways, additional proteins that could serve as regulators in the context of epicardial-myocardial signaling were identified, for example, three Wnt pathway regulators (DKK3, PTK7, and CTHRC1) were implicated for the first time. Additionally, the list includes 18 pathways for which none of the identified components has been previously considered to play a role in epicardial-myocardial signaling (Table 5, Appendix C). Further network analysis defined network structure that provides insights on the molecular

interactions of proteins involved in epicardial-myocardial signaling. This analysis identified ten protein regulatory networks, including the NF-κB network, to be associated with various biological themes in the context of epicardial-myocardial signaling (Fig 12).

To further assess the value of the dataset in guiding functional studies, we performed cell-based assays to validate the role of the NF-κB pathway in epicardial EMT. The functional data showed that activation of the NF-κB pathway is necessary for TGFβ and PDGFBB to induce EMT in cultured epicardial cells. This supports our bioinformatics analysis of the EHE secretome dataset, which identifies NF-κB as a node linked to TGFβ signaling.

The identification of novel factors and pathways mediating epicardial-myocardial signaling is an important step toward understanding the molecular mechanisms that promote epicardial EMT, regulate differentiation of EPDCs, or provide cardio-protection. In addition, the proteomics-bioinformatics approach established in this study provides a framework for future research. Starting from the established dataset, there are multiple lines of investigations that may be conducted in future studies. Here I propose a few examples.

1. The scope of this study was limited to protein identification. The experiments were not designed to quantitate the secreted proteins or to pinpoint their sources. Future studies should expand this proteomics/bioinformatics-based discovery pipeline to quantitative measurements of the expression levels of secreted proteins and the determination of their tissue origin. In addition, the work could be expanded to different model systems to verify evolutionary conservation, or different developmental stages. In addition, distinct epicardial mono-cultures, or using different growth factors could be employed to induce EMT. It is worth noting that for tissue explant cultures, the quantitation and determination of cell/tissue origin both present great challenges. It would require a large amount of

starting material and a robust method to harvest and purify epicardial and/or myocardial cells without altering the signaling pathways, so that the secreted factors as well as the receiving and signal transduction end. Most comparative quantitative MS studies entail isotopic labeling of peptides in the experimental groups (Bakalarski and Kirkpatrick, 2016). It was reported that longer culture time - usually > 72 hours - is needed for high labeling percentage. Labeling percentage in *ex vivo* explant cultures is significantly lower than in monoculture of cell lines (30% compared to 90%) (Polacek et al., 2010). Thus, the long culture times and use of primary cells pose currently a hurdle to perform quantitative studies close to the *in vivo* situation.

2. The functional analysis of the NF-κB pathway presented here validated the pathway analysis of the EHE secretome dataset, which predicted that NF-κB is a signaling node regulating epicardial EMT. We anticipate that the EHE secretome dataset can guide the functional evaluation of additional novel regulators of EMT, EPDC differentiation, cardiomyocyte proliferation or angiogenesis. For example, there are multiple proteins in the dataset (Table II) that have not been previously implicated in epicardial or endocardial EMT. They have been previously shown to be expressed in epicardium and/or myocardium and importantly, they are involved in EMT or cell migration in other contexts (for example, cancer). The initial test for functionality of the identified proteins included administration of commercially available protein to our primary epicardial cultures. Although treatment with recombinant proteins listed in Table II in chicken epicardial explant cultures did not result in consistent cell morphological changes (data not shown), it does not exclude the possibility that one or several proteins may be required to stimulate epicardial EMT. Loss-

of-function studies (e.g. shRNA-mediated knockdown) could be performed to explore this possibility.

3. Through functional assays of NF-κB, described in Chapter IV. I have shown that IPA networks can provide useful lead in the identification of important regulators of epicardial-myocardial interaction and development. In the future, functional assays should be extended to other networks, in particular other nodes that we have identified. For example, the node APP in the APP network is a good candidate for functional study based on the following considerations. Like NF-κB, more edges are associated with APP than other nodes in the APP network (Fig 12; Fig 17). We have biochemically confirmed the presence of APP by embryonic chicken hearts (Fig 9). APP has also been shown to be expressed in embryonic mouse heart at E10.5 (Reymond et al., 2002) and E14.5 (Visel et al., 2004). Importantly, the APP network includes known regulators of epicardial-myocardial signaling such as Fibronectin (Masters and Riley, 2014) and VEGF (Tao et al., 2013). Other nodes in this network include molecules related to cell motility and ECM remodeling such as focal adhesion kinase, SRC family (Mitra et al., 2005) and SPP1 (also known as OPN) (Singh et al., 2010), providing clues to what processes APP may regulate. Additional clues are provided by literature showing that APP promotes cancer cell growth and migration (Lim et al., 2014). Finally, while APP has been extensively studied in the context of cancer, Alzheimer's disease or neurological development, its role in heart development has not been investigated. Our data on APP expression, network analysis, together with known role of APP in the literature, suggest that it would be interesting to examine whether APP has a role in regulating EPDC proliferation, migration and/or invasion. A similar

experimental setup as the functional study of NF-κB could be utilized for investigating the influence of APP on EMT or EPDC proliferation.

TABLE II. POTENTIAL CANDIDATES FOR INVOLVEMENT IN EPICARDIAL EMT

Gene	Signaling Pathway	involved in general EMT	Expression in heart	References
CST3	TGFβ	Inhibit EMT (mammary epithelial cell)	RT-PCR	(Sokol et al., 2005)
TSP-1	TGFβ	Promote tumor cell migration	RNA seq	(Firlej et al., 2011)
NAMPT	TGFβ	promote EMT (mammary epithelial cell)	RT-PCR	(Soncini et al., 2014)
CTGF	TGFβ	Promote EMT in skin and epithelial cell	ELISA	(Sonnylal et al., 2013)
FSTL1	BMP4	Promote EMT in keratinocyte	RT-PCR	(Sundaram et al., 2013)
PTX3	FGF	Inhibits EMT (Melanoma Cells)	RT-PCR	(Ronca et al., 2013)
DRAXIN	Netrin	Inhibit neurons cell migration	RT-PCR	(Ahmed et al., 2011)
IGFBP2	IGF	Promote EMT in glioma cells	RT-PCR	(Wang et al., 2006)
IGFBP7	IGF	Promote EMT in glioma cells	ELISA, IF	(Jiang et al., 2008)
DCN	EGF/ErbB	Inhibit or promote EMT	RT-PCR	(Sofeu Feugaing et al., 2013)
DKK3	WNT	Inhibit or promote EMT	ELISA, IF	(Das et al., 2013)
MDK	Notch	Promote EMT in tumor cells and keratinocyte	RT-PCR	(Huang et al., 2008)
PTN	RPTP	Promote EMT in glioma cell line	RT-PCR	(Perez-Pinera et al., 2006)
OPN	Integrin	Promote EMT in hepatocytes	RNA seq	(Kale et al., 2013)
MIF	Erk/Akt	Promote EMT in tumor cells	RT-PCR	(Ohta et al., 2012)

6.2 NF-κB signaling pathway in epicardial EMT

In Chapter IV, I present experimental data that TGFβ2/PDGFBB treatment activated the NF-κB pathway and that NF-κB activation is necessary for epicardial cells to undergo EMT. It has been previously shown that epicardial cells with loss of PDGFRα and PDGFRβ were unresponsive to EMT-inducing growth factor TGFβ (Smith et al., 2011). Furthermore, we observed that a combined TGFβ2/PDGFBB treatment induced a more robust EMT response than TGFβ2 alone within 48 hours (Fig 24). These observations suggest a functional cross-talk between the PDGF and TGFβ pathways in regulating epicardial EMT and further studies are needed to address the underlying mechanism.

Previous studies of mutant mice lacking NF-κB family proteins - p65, p50, IKK1 or IKK2 - did not report obvious heart developmental phenotypes (Beg et al., 1995; Li et al., 1999; Sha et al., 1995). Interestingly, while cardiomyocyte-specific ablation of IKK2 does not affect normal heart development, cardiomyocyte-specific activation of IKK2 results in congenital heart defects (Dawn et al., 2001; Hikoso et al., 2009; Kraut et al., 2015). These observations demand a re-examination of NF-κB's role(s) in heart development using current tissue-specific knockout/transgenic mouse lines and genetic lineage tracing to expand the investigation from an *ex vivo* to a *in vivo* system. It is possible that abolishment of NF-κB signaling in the epicardium may result in decreased epicardial EMT. It would also be valuable to investigate whether activation of the NF-κB pathway is sufficient to induce epicardial EMT. One strategy could be through *in ovo* injection of plasmids expressing NF-κB or IKKs into the chicken embryo followed by examination of heart EMT.

6.3 Identify secreted proteins in active sub-epicardial niche

Epicardial-myocardial crosstalk occurs *in vivo* in the sub-epicardial niche, which is the extracellular space between epicardium and myocardium. Because *ex vivo* culture systems do not

fully recapitulate *in vivo* events, it would be ideal to identify secreted proteins of the appropriate time window in the sub-epicardial niche *in vivo*. In chapter V, I reported the development of a protocol for MALDI-IMS using heart tissue. The successful development of this imaging technique would facilitate mapping of a wide range of proteins and peptides without the need for labeling reagents or prior knowledge of the protein. However, my results showed that the MALDI-IMS technology is not yet at the stage where it can be used to identify secreted proteins in the sub-epicardial niche directly on embryonic heart tissue.

An attractive alternative strategy would be laser-capture microdissection (LCM) coupled to downstream proteomics analysis. Microdissected epicardium/subepicardial tissue may be analyzed against myocardium as a control. Embryonic chicken hearts again could be a good choice for LCM-based proteomic analysis, because the epicardium/subepicardium layer is thicker in chicken hearts compared to mouse, allowing more material to be collected for proteomics-based experimentation.

APPENDICES

Appendix A. Proteins identified in EHE-CM

TABLE III. PROTEINS IDENTIFIED IN EHE-CM

GI Number	Protein Name	Molecular Weight	#Unique Peptide	Percent Coverage[a]
311213923	ref|NP_001185641.1 fibronectin precursor [Gallus gallus]	273 kDa	86	38.50%
313661476	ref|NP_001186354.1 spectrin beta chain, brain 1 [Gallus gallus]	274 kDa	64	23.10%
110227609	ref|NP_001036003.1 spectrin alpha chain, non-erythrocytic 1 [Gallus gallus]	285 kDa	94	30.90%
46048882	ref|NP_990118.1 versican core protein precursor [Gallus gallus]	388 kDa	69	16.00%
157954047	ref|NP_001103255.1 heat shock protein HSP 90-alpha [Gallus gallus]	84 kDa	51	44.10%
94536813	ref|NP_001001876.1 basement membrane-specific heparan sulfate proteoglycan core protein precursor [Gallus gallus];	433 kDa	32	7.59%
71896431	ref|NP_001025512.1 filamin-B [Gallus gallus]; Duplicate proteins: gi|392018	276 kDa	38	13.10%
45382123	ref|NP_990772.1 vinculin [Gallus gallus]; Duplicate proteins: gi|212873	117 kDa	43	35.90%
45383033	ref|NP_989904.1 filamin-C [Gallus gallus]; Duplicate proteins: gi|15341204	280 kDa	25	9.18%
48675901	ref|NP_001001615.1 cadherin-2 precursor [Gallus gallus]	100 kDa	28	29.10%
114326309	ref|NP_001041541.1 vimentin [Gallus gallus]	53 kDa	26	49.10%
45384370	ref|NP_990334.1 heat shock cognate 71 kDa protein [Gallus gallus]	71 kDa	32	47.10%
45382453	ref|NP_990699.1 elongation factor 2 [Gallus gallus]	95 kDa	36	40.90%
330417943	ref|NP_001193425.1 fructose-bisphosphate aldolase C [Gallus gallus]	39 kDa	26	58.80%
113206112	ref|NP_001038129.1 transitional endoplasmic reticulum ATPase [Gallus gallus];	89 kDa	39	56.30%
46048768	ref|NP_990451.1 alpha-enolase [Gallus gallus]	47 kDa	27	58.50%
513226445	ref|XP_418173.4 PREDICTED: fibrillin-2 [Gallus gallus]	325 kDa	26	8.44%

GI Number	Protein Name	Molecular Weight	#Unique Peptide	Percent Coverage[a]
45384364	ref|NP_990335.1 rab GDP dissociation inhibitor beta [Gallus gallus];	51 kDa	29	59.60%
118097631	ref|XP_414655.2 PREDICTED: heat shock 70 kDa protein 4 isoformX2 [Gallus gallus]	94 kDa	33	34.90%
45383890	ref|NP_989441.1 protein disulfide-isomerase A3 precursor [Gallus gallus]	56 kDa	26	44.20%
46048687	ref|NP_990654.1 alpha-actinin-2 [Gallus gallus]	104 kDa	47	42.00%
45385813	ref|NP_990635.1 ovotransferrin precursor [Gallus gallus];	78 kDa	23	34.30%
45382061	ref|NP_990782.1 triosephosphate isomerase [Gallus gallus]	27 kDa	22	86.30%
45383766	ref|NP_989508.1 L-lactate dehydrogenase B chain [Gallus gallus]	36 kDa	22	64.90%
45382429	ref|NP_990216.1 ezrin [Gallus gallus]; Duplicate proteins: gi|4514720	69 kDa	30	32.10%
45384000	ref|NP_990596.1 nucleolin [Gallus gallus]	76 kDa	25	34.00%
45383127	ref|NP_989854.1 talin-1 [Gallus gallus]	272 kDa	29	14.20%
71896385	ref|NP_001025712.1 periostin precursor [Gallus gallus];	94 kDa	32	39.20%
57524920	ref|NP_001006128.1 glucose-6-phosphate isomerase [Gallus gallus];	62 kDa	25	39.10%
45382651	ref|NP_990800.1 pyruvate kinase muscle isozyme [Gallus gallus]	58 kDa	19	34.20%
513235208	ref|XP_001234986.3 PREDICTED: puromycin-sensitive aminopeptidase isoform X1 [Gallus gallus]	102 kDa	29	28.30%
55741616	ref|NP_001006219.1 14-3-3 protein epsilon [Gallus gallus]	29 kDa	18	55.30%
45384004	ref|NP_990509.1 bifunctional purine biosynthesis protein PURH [Gallus gallus]	64 kDa	22	44.70%
45384202	ref|NP_990616.1 lamin-B2 [Gallus gallus]	68 kDa	26	39.20%
45384348	ref|NP_990652.1 aspartate aminotransferase, cytoplasmic [Gallus gallus]	46 kDa	20	41.00%
52138683	ref|NP_001004390.1 hemoglobin subunit rho [Gallus gallus]	17 kDa	19	85.70%
45384486	ref|NP_990316.1 phosphoglycerate kinase [Gallus gallus]	45 kDa	25	52.30%
71895483	ref|NP_001025754.1 lysine--tRNA ligase [Gallus gallus];	68 kDa	20	28.80%

GI Number	Protein Name	Molecular Weight	#Unique Peptide	Percent Coverage[a]
513161428	ref|XP_004938226.1 PREDICTED: follistatin-related protein 1 [Gallus gallus]	37 kDa	20	49.50%
52138693	ref|NP_001004402.1 WD repeat-containing protein 1 [Gallus gallus]	67 kDa	25	39.60%
363737594	ref|XP_413868.3 PREDICTED: hyaluronan and proteoglycan link protein 3 [Gallus gallus]	41 kDa	22	54.60%
50758110	ref|XP_415765.1 PREDICTED: malate dehydrogenase, mitochondrial [Gallus gallus]	37 kDa	18	56.70%
45383035	ref|NP_989905.1 filamin-A [Gallus gallus]; Duplicate proteins: gi|15341202	273 kDa	15	9.27%
513233472	ref|XP_423059.4 PREDICTED: proliferation-associated protein 2G4, partial [Gallus gallus]	42 kDa	21	52.40%
482845617	ref|NP_001264828.1 aldo-keto reductase family 1, member B10 (aldose reductase) [Gallus gallus]	36 kDa	20	55.40%
57530355	ref|NP_001006395.1 malate dehydrogenase, cytoplasmic [Gallus gallus]	37 kDa	23	56.60%
71896197	ref|NP_001026768.1 polyadenylate-binding protein 1 [Gallus gallus];	71 kDa	23	29.50%
45384340	ref|NP_990641.1 creatine kinase B-type [Gallus gallus]	43 kDa	20	44.60%
52138651	ref|NP_001004374.1 hemoglobin subunit pi [Gallus gallus];	16 kDa	23	90.80%
296011017	ref|NP_001171603.1 fascin [Gallus gallus];	54 kDa	21	40.00%
513194584	ref|XP_004942895.1 PREDICTED: LOW QUALITY PROTEIN: desmin [Gallus gallus]	55 kDa	19	27.10%
513197844	ref|XP_001235060.3 PREDICTED: LOW QUALITY PROTEIN: nuclear autoantigenic sperm protein [Gallus gallus]	88 kDa	12	16.60%
44969651	gb|AAS49610.1 calreticulin [Gallus gallus]	47 kDa	13	19.80%
45384104	ref|NP_990457.1 alpha-actinin-4 [Gallus gallus]	104 kDa	33	37.40%
45383738	ref|NP_989519.1 aconitate hydratase, mitochondrial [Gallus gallus];	86 kDa	19	19.00%
45382977	ref|NP_990858.1 agrin [Gallus gallus];	211 kDa	8	3.73%
47604960	ref|NP_996842.1 heat shock cognate protein HSP 90-beta [Gallus gallus]	83 kDa	24	37.80%

GI Number	Protein Name	Molecular Weight	#Unique Peptide	Percent Coverage[a]
261490820	ref|NP_001159798.1 peptidyl-prolyl cis-trans isomerase A [Gallus gallus];	18 kDa	14	70.30%
363733410	ref|XP_420577.3 PREDICTED: insulin-like growth factor binding protein 7 [Gallus gallus]	33 kDa	20	52.20%
71895985	ref|NP_001026727.1 phosphoglycerate mutase 1 [Gallus gallus]	29 kDa	15	62.60%
513174222	ref|XP_004940228.1 PREDICTED: reticulon-4-like [Gallus gallus]	90 kDa	12	15.10%
513178768	ref|XP_004940554.1 PREDICTED: peroxidasin homolog isoform X4 [Gallus gallus]	164 kDa	29	28.00%
45384208	ref|NP_990615.1 L-lactate dehydrogenase A chain [Gallus gallus]	37 kDa	15	47.30%
513172079	ref|XP_004939875.1 PREDICTED: desmoglein-2 isoform X3 [Gallus gallus]	110 kDa	16	14.20%
57530288	ref|NP_001006410.1 prolyl endopeptidase [Gallus gallus];	81 kDa	20	21.10%
45384434	ref|NP_990290.1 myomesin-1 [Gallus gallus];	182 kDa	4	3.19%
45382953	ref|NP_990854.1 aspartate aminotransferase, mitochondrial precursor [Gallus gallus]	47 kDa	16	36.90%
513217491	ref|XP_417331.4 PREDICTED: adenosylhomocysteinase [Gallus gallus]	45 kDa	17	38.50%
132626770	ref|NP_001006309.3 heterogeneous nuclear ribonucleoprotein R [Gallus gallus]	71 kDa	17	26.70%
60302800	ref|NP_001012594.1 heat shock 70 kDa protein 4L [Gallus gallus];	95 kDa	19	30.20%
45383950	ref|NP_990587.1 transferrin receptor protein 1 [Gallus gallus];	86 kDa	19	20.80%
363735591	ref|XP_421787.3 PREDICTED: eukaryotic translation initiation factor 3 subunit A [Gallus gallus]	164 kDa	4	2.84%
513175427	ref|XP_004935469.1 PREDICTED: latent-transforming growth factor beta-binding protein 1 isoform X4 [Gallus gallus]	138 kDa	20	19.50%
124339781	ref|NP_001073586.1 clathrin heavy chain 1 [Gallus gallus]	192 kDa	16	8.96%
45383321	ref|NP_989751.1 72 kDa type IV collagenase preproprotein [Gallus gallus]	75 kDa	14	23.10%
383387814	ref|NP_001122300.2 neural cell adhesion molecule 1 isoform 1 precursor [Gallus gallus]	119 kDa	10	11.30%

GI Number	Protein Name	Molecular Weight	#Unique Peptide	Percent Coverage[a]
45383984	ref|NP_990594.1 poly [ADP-ribose] polymerase 1 [Gallus gallus];	114 kDa	12	12.40%
71897035	ref|NP_001026514.1 14-3-3 protein zeta [Gallus gallus]	28 kDa	13	58.40%
86129578	ref|NP_001034418.1 peroxiredoxin-6 [Gallus gallus]	25 kDa	14	49.10%
56119054	ref|NP_001007840.1 14-3-3 protein eta [Gallus gallus]	28 kDa	16	53.40%
513230934	ref|XP_004949260.1 PREDICTED: heterogeneous nuclear ribonucleoprotein K-like isoform X5 [Gallus gallus]	47 kDa	14	41.50%
312283582	ref|NP_001185639.1 protein disulfide-isomerase precursor [Gallus gallus]	57 kDa	16	28.70%
45382769	ref|NP_990822.1 78 kDa glucose-regulated protein precursor [Gallus gallus]	72 kDa	18	30.50%
513196353	ref|XP_422248.3 PREDICTED: 4-trimethylaminobutyraldehyde dehydrogenase [Gallus gallus]	64 kDa	12	16.10%
45382723	ref|NP_990811.1 myristoylated alanine-rich C-kinase substrate [Gallus gallus]	28 kDa	11	63.00%
118082590	ref|XP_425458.2 PREDICTED: histone H4-like [Gallus gallus];	11 kDa	12	64.10%
45382961	ref|NP_990856.1 apolipoprotein A-I preproprotein [Gallus gallus]	31 kDa	17	50.00%
57525441	ref|NP_001006250.1 peptidyl-prolyl cis-trans isomerase FKBP4 [Gallus gallus];	50 kDa	17	38.90%
310772215	ref|NP_001185571.1 phosphatidylethanolamine-binding protein 1 [Gallus gallus]	21 kDa	10	79.10%
50755288	ref|XP_414685.1 PREDICTED: betaine--homocysteine S-methyltransferase 1 [Gallus gallus]	45 kDa	10	34.10%
513217562	ref|XP_004947034.1 PREDICTED: glutathione synthetase isoform X4 [Gallus gallus];	52 kDa	22	43.50%
52138645	ref|NP_001004375.1 hemoglobin subunit alpha-D [Gallus gallus];	16 kDa	11	80.90%
71896753	ref|NP_001026156.1 heterogeneous nuclear ribonucleoproteins A2/B1 [Gallus gallus];	37 kDa	19	42.70%
513193827	ref|XP_004942739.1 PREDICTED: isocitrate dehydrogenase [NADP] cytoplasmic isoform X6 [Gallus gallus]	47 kDa	16	35.70%

GI Number	Protein Name	Molecular Weight	#Unique Peptide	Percent Coverage[a]
513205037	ref|XP_004944620.1 PREDICTED: transketolase isoform X3 [Gallus gallus]	64 kDa	17	29.70%
156119330	ref|NP_001095200.1 neurofilament medium polypeptide [Gallus gallus]	96 kDa	7	10.40%
363727569	ref|XP_416078.3 PREDICTED: cullin-associated NEDD8-dissociated protein 1 isoform 2 [Gallus gallus]	134 kDa	22	15.50%
363742669	ref|XP_001236427.2 PREDICTED: hepatoma-derived growth factor [Gallus gallus]	26 kDa	15	53.00%
54111425	ref|NP_001005618.1 procollagen-lysine,2-oxoglutarate 5-dioxygenase 1 precursor [Gallus gallus]	84 kDa	16	16.20%
350537089	ref|NP_001232856.1 tropomyosin alpha-3 chain [Gallus gallus];	29 kDa	14	32.30%
118100855	ref|XP_417486.2 PREDICTED: probable aminopeptidase NPEPL1 isoform X3 [Gallus gallus]	56 kDa	16	32.90%
45383790	ref|NP_989496.1 fibulin-1 precursor [Gallus gallus]	78 kDa	13	23.60%
45382959	ref|NP_990855.1 multifunctional protein ADE2 [Gallus gallus]	47 kDa	15	37.30%
45384044	ref|NP_990490.1 myosin light chain 1, cardiac muscle [Gallus gallus]	22 kDa	10	36.10%
54020687	ref|NP_989488.2 elongation factor 1-alpha 1 [Gallus gallus];	50 kDa	11	26.80%
308081945	ref|NP_001183979.1 calsyntenin-1 precursor [Gallus gallus]	109 kDa	10	10.20%
57529439	ref|NP_001006303.1 6-phosphogluconate dehydrogenase, decarboxylating [Gallus gallus];	53 kDa	16	36.90%
363742292	ref|XP_417784.3 PREDICTED: splicing factor, proline- and glutamine-rich isoform X5 [Gallus gallus]	70 kDa	11	22.60%
513209023	ref|XP_003642190.2 PREDICTED: eukaryotic translation initiation factor 3 subunit B, partial [Gallus gallus]	85 kDa	23	30.40%
45383015	ref|NP_989916.1 protein DJ-1 [Gallus gallus]	20 kDa	13	59.30%
45384260	ref|NP_990378.1 nucleoside diphosphate kinase [Gallus gallus]	17 kDa	12	73.20%
45384494	ref|NP_990318.1 60S acidic ribosomal protein P0 [Gallus gallus]	34 kDa	12	54.40%

GI Number	Protein Name	Molecular Weight	#Unique Peptide	Percent Coverage[a]
118405198	ref|NP_001072946.1 cytochrome c [Gallus gallus]	12 kDa	9	57.10%
45383337	ref|NP_989741.1 SPARC precursor [Gallus gallus]	34 kDa	12	44.00%
57530409	ref|NP_001006385.1 cytosolic non-specific dipeptidase [Gallus gallus];	53 kDa	14	28.60%
57530789	ref|NP_001006374.1 thioredoxin domain-containing protein 5 precursor [Gallus gallus];	46 kDa	10	24.60%
71896825	ref|NP_001026464.1 plasminogen activator inhibitor 1 RNA-binding protein [Gallus gallus];	46 kDa	13	41.90%
57530180	ref|NP_001006431.1 plastin-3 [Gallus gallus]; Duplicate proteins: gi|53136550	71 kDa	9	13.90%
47825387	ref|NP_001001469.1 trifunctional purine biosynthetic protein adenosine-3 [Gallus gallus]	107 kDa	11	12.40%
45384298	ref|NP_990364.1 nestin [Gallus gallus];	202 kDa	15	11.00%
57530301	ref|NP_001006405.1 T-complex protein 1 subunit alpha [Gallus gallus];	60 kDa	16	26.00%
513204938	ref|XP_425156.4 PREDICTED: fibulin-2 [Gallus gallus]	134 kDa	11	11.40%
57530349	ref|NP_001006398.1 bifunctional aminoacyl-tRNA synthetase [Gallus gallus];	180 kDa	2	1.50%
57525483	ref|NP_001006260.1 eukaryotic translation initiation factor 2 subunit 3 [Gallus gallus]	51 kDa	12	23.10%
57529674	ref|NP_001006535.1 far upstream element-binding protein 1 [Gallus gallus];	66 kDa	8	12.80%
45383852	ref|NP_989458.1 alpha-actinin-1 [Gallus gallus];	103 kDa	18	34.70%
50760475	ref|XP_418038.1 PREDICTED: probable C->U-editing enzyme APOBEC-2 [Gallus gallus]	26 kDa	12	49.50%
55742654	ref|NP_001006686.1 heat shock 70 kDa protein [Gallus gallus]	70 kDa	16	37.20%
119331076	ref|NP_001073185.1 xaa-Pro dipeptidase [Gallus gallus];	55 kDa	9	17.90%
60302808	ref|NP_001012599.1 UDP-glucose 6-dehydrogenase [Gallus gallus]	55 kDa	16	26.50%
363743802	ref|XP_424048.3 PREDICTED: thimet oligopeptidase isoform X4 [Gallus gallus]	78 kDa	15	21.50%

GI Number	Protein Name	Molecular Weight	#Unique Peptide	Percent Coverage[a]
195539501	ref|NP_001124213.1 inter-alpha-trypsin inhibitor heavy chain H2 precursor [Gallus gallus]	107 kDa	18	15.70%
308081909	ref|NP_001007824.1 40S ribosomal protein SA [Gallus gallus]	33 kDa	11	39.20%
50053682	ref|NP_001001858.1 stathmin [Gallus gallus]	17 kDa	12	48.60%
52138701	ref|NP_001004406.1 cofilin-2 [Gallus gallus];	19 kDa	9	45.80%
118094764	ref|XP_422542.2 PREDICTED: cystathionine gamma-lyase [Gallus gallus]	44 kDa	13	25.30%
45383788	ref|NP_989495.1 collagen, type XVIII, alpha 1 precursor [Gallus gallus];	137 kDa	13	11.90%
57530768	ref|NP_001006370.1 protein disulfide-isomerase A4 [Gallus gallus];	71 kDa	12	17.40%
57525373	ref|NP_001006234.1 leukotriene A-4 hydrolase [Gallus gallus];	69 kDa	17	22.10%
296090736	ref|NP_001171688.1 DNA-(apurinic or apyrimidinic site) lyase [Gallus gallus];	33 kDa	13	43.00%
45383329	ref|NP_989745.1 nuclease-sensitive element-binding protein 1 [Gallus gallus];	36 kDa	11	41.70%
513209917	ref|XP_004945584.1 PREDICTED: polyubiquitin-C isoform X3 [Gallus gallus]	17 kDa	6	35.90%
513236841	ref|XP_004950342.1 PREDICTED: heterogeneous nuclear ribonucleoprotein A1 [Gallus gallus]	34 kDa	10	25.70%
57529989	ref|NP_001006473.1 ribonuclease inhibitor [Gallus gallus];	50 kDa	11	37.10%
513215584	ref|XP_004946568.1 PREDICTED: AP-1 complex subunit beta-1 isoform X10 [Gallus gallus]	102 kDa	13	15.90%
513199731	ref|XP_004943473.1 PREDICTED: eukaryotic translation initiation factor 4 gamma 1 isoform X7 [Gallus gallus]	178 kDa	5	1.86%
45384514	ref|NP_990659.1 heterogeneous nuclear ribonucleoprotein A/B [Gallus gallus];	32 kDa	14	32.80%
45382221	ref|NP_990753.1 extracellular fatty acid-binding protein precursor [Gallus gallus];	20 kDa	9	49.40%
52694650	ref|NP_001004768.1 cell surface glycoprotein MUC18 precursor [Gallus gallus];	69 kDa	10	13.70%
45383822	ref|NP_989478.1 matrin-3 [Gallus gallus];	101 kDa	10	10.90%
57530465	ref|NP_001006314.1 tyrosine--tRNA ligase, cytoplasmic [Gallus gallus]	59 kDa	13	18.00%

GI Number	Protein Name	Molecular Weight	#Unique Peptide	Percent Coverage[a]
71894831	ref|NP_001026234.1 actin, alpha skeletal muscle [Gallus gallus]	42 kDa	12	28.60%
71897287	ref|NP_001026554.1 phosphoglucomutase-2 [Gallus gallus];	68 kDa	7	10.00%
119331082	ref|NP_001073196.1 heterogeneous nuclear ribonucleoprotein G [Gallus gallus];	41 kDa	11	18.70%
513227300	ref|XP_003642908.2 PREDICTED: complement factor D-like isoform X1 [Gallus gallus]	47 kDa	13	33.60%
55741594	ref|NP_001006415.1 14-3-3 protein theta [Gallus gallus]	28 kDa	11	60.00%
71896147	ref|NP_001026759.1 6-phosphogluconolactonase [Gallus gallus];	26 kDa	10	64.80%
45382339	ref|NP_990183.1 histone-binding protein RBBP4 [Gallus gallus]	48 kDa	11	30.10%
206597434	ref|NP_001073182.2 collagen alpha-2(I) chain precursor [Gallus gallus]	129 kDa	8	6.75%
46048885	ref|NP_990121.1 collagen alpha-1(V) chain precursor [Gallus gallus];	184 kDa	2	1.31%
482661642	ref|NP_001264798.1 coronin-1C isoform 2 [Gallus gallus];	53 kDa	13	32.30%
118092977	ref|XP_421751.2 PREDICTED: xaa-Pro aminopeptidase 1 isoform X4 [Gallus gallus];	70 kDa	20	31.80%
45382077	ref|NP_990082.1 radixin [Gallus gallus]	69 kDa	13	27.30%
347921933	ref|NP_990626.2 high mobility group protein B3 [Gallus gallus]	25 kDa	8	32.30%
45383177	ref|NP_989825.1 dihydropyrimidinase-related protein 2 [Gallus gallus];	73 kDa	11	22.30%
61098266	ref|NP_001012800.1 glutaminyl-tRNA synthetase [Gallus gallus];	88 kDa	9	11.50%
313661364	ref|NP_001186382.1 thrombospondin-1 precursor [Gallus gallus]	130 kDa	6	5.28%
71895375	ref|NP_001026618.1 threonyl-tRNA synthetase, cytoplasmic [Gallus gallus];	82 kDa	13	17.30%
46048961	ref|NP_989636.1 glyceraldehyde-3-phosphate dehydrogenase [Gallus gallus]	36 kDa	13	31.80%
57524844	ref|NP_001005834.1 anamorsin [Gallus gallus]	33 kDa	9	43.10%
57529350	ref|NP_001006289.1 14-3-3 protein beta/alpha [Gallus gallus]	28 kDa	9	55.70%
45382337	ref|NP_990182.1 spondin-1 precursor [Gallus gallus]	91 kDa	8	14.00%

GI Number	Protein Name	Molecular Weight	#Unique Peptide	Percent Coverage[a]
152031574	sp|P02457.3|CO1A1_CHICK RecName: Full=Collagen alpha-1(I) chain; AltName: Full=Alpha-1 type I collagen;	138 kDa	9	7.85%
45384378	ref|NP_990263.1 keratin, type II cytoskeletal cochleal [Gallus gallus]	54 kDa	11	13.60%
45384386	ref|NP_990265.1 gelsolin precursor [Gallus gallus]	86 kDa	6	9.64%
124249432	ref|NP_001074340.1 rho GDP-dissociation inhibitor 1 [Gallus gallus];	23 kDa	10	56.40%
46048916	ref|NP_989972.1 peptidyl-prolyl cis-trans isomerase FKBP3 [Gallus gallus];	25 kDa	12	45.80%
50800573	ref|XP_424134.1 PREDICTED: 60S acidic ribosomal protein P2 [Gallus gallus]	12 kDa	11	92.20%
363742430	ref|XP_003642632.1 PREDICTED: adenylyl cyclase-associated protein 1 isoform X1 [Gallus gallus]	58 kDa	10	19.20%
45383856	ref|NP_989456.1 sulfhydryl oxidase 1 precursor [Gallus gallus]	83 kDa	4	7.27%
46048665	ref|NP_990738.1 receptor-type tyrosine-protein phosphatase delta precursor [Gallus gallus];	169 kDa	3	2.40%
122692295	ref|NP_001073681.1 ubiquitin carboxyl-terminal hydrolase isozyme L1 [Gallus gallus];	25 kDa	7	47.80%
45384316	ref|NP_990351.1 proteasome subunit alpha type-1 [Gallus gallus]	29 kDa	11	32.30%
71894957	ref|NP_001026030.1 NSFL1 cofactor p47 [Gallus gallus]	41 kDa	9	28.70%
45383562	ref|NP_989620.1 endoplasmin precursor [Gallus gallus]	92 kDa	2	4.78%
145046232	ref|NP_001077389.1 plasminogen activator inhibitor type 1, member 2 precursor [Gallus gallus]	49 kDa	7	17.40%
71896465	ref|NP_001026164.1 programmed cell death 6-interacting protein [Gallus gallus];	97 kDa	6	8.28%
71897175	ref|NP_001026576.1 coatomer subunit alpha [Gallus gallus];	139 kDa	4	2.45%
72535134	ref|NP_001025707.1 cytoplasmic aconitate hydratase [Gallus gallus]	98 kDa	10	15.70%
126165290	ref|NP_001075173.1 hemoglobin subunit epsilon [Gallus gallus]	17 kDa	9	93.20%
71894765	ref|NP_001026348.1 transaldolase [Gallus gallus];	38 kDa	12	26.40%

GI Number	Protein Name	Molecular Weight	#Unique Peptide	Percent Coverage[a]
61097989	ref|NP_001012914.1 AP-2 complex subunit alpha-2 [Gallus gallus];	104 kDa	12	10.30%
57524990	ref|NP_001006144.1 histidyl-tRNA synthetase, cytoplasmic [Gallus gallus];	56 kDa	12	26.40%
45383530	ref|NP_989639.1 amyloid beta A4 protein precursor [Gallus gallus];	85 kDa	11	14.00%
45383309	ref|NP_989757.1 collagen alpha-1(II) chain precursor [Gallus gallus];	135 kDa	3	2.82%
71894959	ref|NP_001026031.1 microtubule-associated protein RP/EB family member 1 [Gallus gallus]	29 kDa	15	39.10%
302488427	ref|NP_001180598.1 Sjogren syndrome antigen B (autoantigen La) isoform 1 [Gallus gallus]	46 kDa	16	42.60%
313747471	ref|NP_001186415.1 cysteine and glycine-rich protein 3 [Gallus gallus]	21 kDa	6	29.90%
71896025	ref|NP_001026735.1 UMP-CMP kinase [Gallus gallus]	22 kDa	10	38.30%
46048696	ref|NP_990648.1 carbonic anhydrase 2 [Gallus gallus]	29 kDa	11	52.70%
45382027	ref|NP_990792.1 peptidyl-prolyl cis-trans isomerase B precursor [Gallus gallus]	22 kDa	9	43.00%
513163070	ref|XP_416752.3 PREDICTED: cystathionine beta-synthase [Gallus gallus]	63 kDa	5	6.53%
513192634	ref|XP_004942453.1 PREDICTED: collagen alpha-2(V) chain isoform X1 [Gallus gallus]	145 kDa	2	2.27%
45382603	ref|NP_990544.1 hepatocyte growth factor-like protein precursor [Gallus gallus];	79 kDa	6	6.82%
45384120	ref|NP_990447.1 myosin-binding protein C, cardiac-type [Gallus gallus]	142 kDa	2	2.36%
50758444	ref|XP_415925.1 PREDICTED: thioredoxin domain-containing protein 17 isoform X2 [Gallus gallus]	14 kDa	5	43.40%
57525148	ref|NP_001006180.1 ubiquitin-conjugating enzyme E2 L3 [Gallus gallus];	18 kDa	6	63.60%
513216375	ref|XP_004946758.1 PREDICTED: glyoxalase domain-containing protein 4 [Gallus gallus]	35 kDa	7	21.20%
52138663	ref|NP_001004380.1 F-actin-capping protein subunit alpha-2 [Gallus gallus]	33 kDa	8	34.30%
46048771	ref|NP_990440.1 adenylate kinase isoenzyme 1 [Gallus gallus]	22 kDa	8	36.10%

GI Number	Protein Name	Molecular Weight	#Unique Peptide	Percent Coverage[a]
147902704	ref|NP_001091009.1 dystroglycan precursor [Gallus gallus];	98 kDa	3	6.47%
60302824	ref|NP_001012610.1 heterogeneous nuclear ribonucleoprotein H3 [Gallus gallus];	37 kDa	8	26.00%
45384102	ref|NP_990456.1 dickkopf-related protein 3 precursor [Gallus gallus]	39 kDa	10	27.40%
57529473	ref|NP_001006311.1 nuclear migration protein nudC [Gallus gallus]	39 kDa	14	33.70%
45383528	ref|NP_989638.1 actin-related protein 3 [Gallus gallus]	47 kDa	14	29.70%
45384138	ref|NP_990435.1 bleomycin hydrolase [Gallus gallus]	53 kDa	15	25.70%
45383884	ref|NP_989442.1 UTP--glucose-1-phosphate uridylyltransferase [Gallus gallus]	57 kDa	10	17.10%
319655747	ref|NP_990831.2 cystatin precursor [Gallus gallus]	16 kDa	8	62.30%
363741115	ref|XP_003642446.1 PREDICTED: eukaryotic translation initiation factor 4H-like isoformX2 [Gallus gallus]	25 kDa	4	25.40%
61098334	ref|NP_001012828.1 ubiquitin-conjugating enzyme E2 N [Gallus gallus];	17 kDa	8	47.40%
71896651	ref|NP_001026323.1 alcohol dehydrogenase class-3 [Gallus gallus];	40 kDa	9	26.50%
45382931	ref|NP_989944.1 proteasome subunit alpha type-7 [Gallus gallus]	28 kDa	9	38.20%
45383077	ref|NP_989880.1 eukaryotic initiation factor 4A-II [Gallus gallus]	46 kDa	10	22.60%
60302812	ref|NP_001012601.1 cysteine--tRNA ligase, cytoplasmic [Gallus gallus]	86 kDa	3	4.28%
52138659	ref|NP_001004378.1 guanine nucleotide-binding protein subunit beta-2-like 1 [Gallus gallus]	35 kDa	17	46.70%
45384222	ref|NP_990621.1 heat shock protein beta-1 [Gallus gallus]	22 kDa	6	31.10%
60302796	ref|NP_001012592.1 SH3 domain-binding glutamic acid-rich-like protein [Gallus gallus];	13 kDa	7	59.60%
71897305	ref|NP_001026550.1 small glutamine-rich tetratricopeptide repeat-containing protein alpha [Gallus gallus];	34 kDa	7	29.40%

GI Number	Protein Name	Molecular Weight	#Unique Peptide	Percent Coverage[a]
71894995	ref|NP_001026254.1 synaptotagmin binding, cytoplasmic RNA interacting protein [Gallus gallus];	50 kDa	12	23.40%
57525015	ref|NP_001006150.1 ras GTPase-activating protein-binding protein 1 [Gallus gallus];	52 kDa	10	24.80%
212549669	ref|NP_001131122.1 calpastatin [Gallus gallus];	81 kDa	2	2.99%
47087173	ref|NP_998746.1 nuclear ubiquitous casein and cyclin-dependent kinases substrate [Gallus gallus];	33 kDa	9	32.20%
363733121	ref|XP_426283.3 PREDICTED: peptidyl-prolyl cis-trans isomerase D isoform X1 [Gallus gallus]	40 kDa	13	24.10%
45384130	ref|NP_990441.1 DNA topoisomerase 1 [Gallus gallus];	91 kDa	4	5.74%
52138655	ref|NP_001004376.1 hemoglobin subunit alpha-A [Gallus gallus];	15 kDa	7	58.50%
57529654	ref|NP_001006539.1 alcohol dehydrogenase [NADP(+)] [Gallus gallus]	37 kDa	7	20.20%
310750337	ref|NP_001185531.1 proteasome subunit alpha type-4 [Gallus gallus]	29 kDa	8	37.20%
71896205	ref|NP_001026770.1 isocitrate dehydrogenase [NADP], mitochondrial [Gallus gallus];	50 kDa	6	12.40%
119331100	ref|NP_001073198.1 alpha-adducin [Gallus gallus]; Duplicate proteins: gi|60098761	81 kDa	3	6.14%
45382981	ref|NP_990860.1 adenylosuccinate lyase [Gallus gallus];	52 kDa	8	24.40%
513167116	ref|XP_418480.4 PREDICTED: microtubule-associated protein 4 isoform X2 [Gallus gallus]	112 kDa	5	6.94%
57529969	ref|NP_001006477.1 eukaryotic translation initiation factor 2 subunit 1 [Gallus gallus];	33 kDa	7	25.30%
45384220	ref|NP_990617.1 lamin-B1 [Gallus gallus]	67 kDa	6	10.40%
513183353	ref|XP_003641248.2 PREDICTED: alpha-fetoprotein [Gallus gallus]	65 kDa	7	16.00%
45383674	ref|NP_989558.1 cadherin-5 precursor [Gallus gallus];	87 kDa	5	10.10%
513191005	ref|XP_004942138.1 PREDICTED: protein transport protein Sec24C isoform X7 [Gallus gallus]	122 kDa	3	3.84%
228008358	ref|NP_001153170.1 heat shock 105kDa [Gallus gallus]	96 kDa	9	14.60%

GI Number	Protein Name	Molecular Weight	#Unique Peptide	Percent Coverage[a]
45384002	ref|NP_990508.1 cathepsin D precursor [Gallus gallus]	43 kDa	6	18.30%
483968188	ref|NP_001264840.1 40S ribosomal protein S12 [Gallus gallus]	14 kDa	10	60.30%
343790924	ref|NP_001230519.1 aldo-keto reductase family 1, member B1-like [Gallus gallus]	36 kDa	12	47.20%
50745031	ref|XP_419952.1 PREDICTED: protein disulfide-isomerase A6 isoform 2 [Gallus gallus]	49 kDa	8	21.00%
513221874	ref|XP_004947973.1 PREDICTED: porphobilinogen deaminase isoform X3 [Gallus gallus]	33 kDa	10	46.00%
513191054	ref|XP_426503.4 PREDICTED: PDZ and LIM domain protein 1 isoformX4 [Gallus gallus]	36 kDa	10	34.90%
45383504	ref|NP_989655.1 lissencephaly-1 homolog [Gallus gallus]	47 kDa	7	21.50%
45382141	ref|NP_990768.1 capping protein (actin filament) muscle Z-line, beta isoform 1 [Gallus gallus]	31 kDa	9	38.30%
475807701	ref|NP_001264322.1 3-oxo-5-beta-steroid 4-dehydrogenase [Gallus gallus]	37 kDa	9	34.00%
513190075	ref|XP_421471.4 PREDICTED: nidogen-2, partial [Gallus gallus]	161 kDa	6	3.62%
71895723	ref|NP_001026206.1 inactive tyrosine-protein kinase 7 precursor [Gallus gallus]	116 kDa	4	4.00%
429836849	ref|NP_001258861.1 peroxiredoxin-1 [Gallus gallus]	22 kDa	10	44.70%
513202085	ref|XP_004943987.1 PREDICTED: acidic leucine-rich nuclear phosphoprotein 32 family member A isoform X6 [Gallus gallus]	24 kDa	15	58.60%
363738006	ref|XP_001232348.2 PREDICTED: splicing factor 3B subunit 3 isoform X1 [Gallus gallus];	135 kDa	3	3.29%
513193412	ref|XP_004942649.1 PREDICTED: 10 kDa heat shock protein, mitochondrial-like isoform X2 [Gallus gallus];	11 kDa	6	47.10%
71895543	ref|NP_001026648.1 14-3-3 protein gamma [Gallus gallus]	28 kDa	5	42.10%
478486799	ref|NP_001264608.1 60S ribosomal protein L12 [Gallus gallus]	18 kDa	7	55.20%
71894743	ref|NP_001025809.1 phosphoglycolate phosphatase [Gallus gallus]	33 kDa	5	21.50%

GI Number	Protein Name	Molecular Weight	#Unique Peptide	Percent Coverage[a]
57529899	ref|NP_001006491.1 proteasome subunit alpha type-3 [Gallus gallus];	28 kDa	6	17.60%
45382251	ref|NP_990156.1 ubiquitin carboxyl-terminal hydrolase isozyme L3 [Gallus gallus];	26 kDa	5	28.70%
56118302	ref|NP_001007906.1 proteasome subunit beta type-1 [Gallus gallus];	26 kDa	7	38.80%
167860105	ref|NP_001006564.2 acidic leucine-rich nuclear phosphoprotein 32 family member E [Gallus gallus]	29 kDa	6	30.90%
45382875	ref|NP_990838.1 creatine kinase M-type [Gallus gallus]	43 kDa	9	18.60%
45384294	ref|NP_990367.1 transforming growth factor-beta-induced protein ig-h3 precursor [Gallus gallus];	74 kDa	4	5.00%
476007906	ref|NP_001264359.1 protein phosphatase 1 regulatory subunit 7 isoform 3 [Gallus gallus]	40 kDa	11	24.90%
513218001	ref|XP_004947128.1 PREDICTED: exportin-2 isoform X4 [Gallus gallus]	107 kDa	9	11.40%
363731606	ref|XP_419556.3 PREDICTED: nidogen-1 [Gallus gallus]	137 kDa	4	2.56%
71897167	ref|NP_001026578.1 proteasome subunit alpha type-5 [Gallus gallus];	26 kDa	6	35.70%
45382529	ref|NP_990256.1 natriuretic peptides A precursor [Gallus gallus]	16 kDa	3	42.10%
476007876	ref|NP_001264372.1 proteasome subunit alpha type-6 [Gallus gallus]	27 kDa	8	24.40%
71897051	ref|NP_001026518.1 cold-inducible RNA-binding protein [Gallus gallus];	21 kDa	8	38.90%
363744073	ref|XP_001233320.2 PREDICTED: carbonic anhydrase 9 isoform X1 [Gallus gallus]	44 kDa	7	24.50%
118092623	ref|XP_001232700.1 PREDICTED: inorganic pyrophosphatase isoform X1 [Gallus gallus]	33 kDa	3	12.80%
118082574	ref|XP_425455.2 PREDICTED: histone H2A-IV [Gallus gallus];	14 kDa	9	58.90%
118083310	ref|XP_416513.2 PREDICTED: ubiquitin carboxyl-terminal hydrolase 5 isoform 2 [Gallus gallus]	93 kDa	5	9.50%
50760435	ref|XP_418020.1 PREDICTED: 60S ribosomal protein L10a isoform X5 [Gallus gallus]	25 kDa	13	40.60%

GI Number	Protein Name	Molecular Weight	#Unique Peptide	Percent Coverage[a]
363744275	ref|XP_424802.3 PREDICTED: phosphoglucomutase 5 [Gallus gallus]	63 kDa	10	15.90%
513164688	ref|XP_004938636.1 PREDICTED: importin-5 isoform X9 [Gallus gallus]	120 kDa	6	8.14%
45384218	ref|NP_990395.1 superoxide dismutase [Cu-Zn] [Gallus gallus]	16 kDa	5	42.90%
71894843	ref|NP_001026060.1 fatty acid-binding protein, heart [Gallus gallus];	15 kDa	8	49.60%
513241059	ref|XP_003644004.2 PREDICTED: citrate synthase, mitochondrial [Gallus gallus]	42 kDa	9	27.00%
71895697	ref|NP_001026087.1 methylosome protein 50 [Gallus gallus];	39 kDa	6	25.60%
303227902	ref|NP_001034376.2 acetyl-CoA acetyltransferase, cytosolic [Gallus gallus]	41 kDa	7	20.10%
513221075	ref|XP_004947782.1 PREDICTED: chloride intracellular channel protein 4 isoform X5 [Gallus gallus]	27 kDa	12	47.50%
45384338	ref|NP_990646.1 tubulin beta-7 chain [Gallus gallus]	50 kDa	11	28.70%
513236572	ref|XP_423851.3 PREDICTED: UPF0160 protein MYG1, mitochondrial [Gallus gallus]	42 kDa	7	31.10%
57524880	ref|NP_001005842.1 vacuolar protein sorting-associated protein 35 [Gallus gallus];	92 kDa	5	29.60%
57529974	ref|NP_001006474.1 apoptosis inhibitor 5 [Gallus gallus]	59 kDa	10	4.27%
4033470	sp|Q90987.1|STMN2_CHICK RecName: Full=Stathmin-2;	21 kDa	2	22.80%
45383688	ref|NP_989547.1 DNA damage-binding protein 1 [Gallus gallus]	127 kDa	7	4.91%
513200936	ref|XP_001233064.3 PREDICTED: mannose-6-phosphate isomerase, partial [Gallus gallus]	46 kDa	7	16.30%
513161782	ref|XP_004938293.1 PREDICTED: coproporphyrinogen-III oxidase, mitochondrial isoform X3 [Gallus gallus]	40 kDa	3	8.73%
513199422	ref|XP_422695.4 PREDICTED: procollagen-lysine,2-oxoglutarate 5-dioxygenase 2 isoform X2 [Gallus gallus]	85 kDa	2	2.59%
60593028	ref|NP_001012719.1 U5 small nuclear ribonucleoprotein 200 kDa helicase [Gallus gallus]	70 kDa	5	11.20%

GI Number	Protein Name	Molecular Weight	#Unique Peptide	Percent Coverage[a]
372266122	ref|NP_990286.2 aggrecan core protein precursor [Gallus gallus]	221 kDa	3	1.91%
513225742	ref|XP_418071.4 PREDICTED: C-type mannose receptor 2, partial [Gallus gallus]	165 kDa	3	2.76%
56605972	ref|NP_001008479.1 activated RNA polymerase II transcriptional coactivator p15 [Gallus gallus]	14 kDa	3	34.10%
363743365	ref|XP_003642828.1 PREDICTED: myosin light chain, embryonic [Gallus gallus]	21 kDa	4	29.20%
381214362	ref|NP_001244213.1 actin-related protein 2/3 complex subunit 4 [Gallus gallus]	20 kDa	7	35.10%
478431055	ref|NP_001264515.1 programmed cell death protein 5 [Gallus gallus]	14 kDa	4	34.10%
256419027	ref|NP_001157867.1 eukaryotic translation initiation factor 3 subunit I [Gallus gallus]	36 kDa	7	18.50%
513235217	ref|XP_003643296.2 PREDICTED: importin subunit beta-1 isoform X1 [Gallus gallus]	84 kDa	7	12.20%
480540346	ref|NP_001264720.1 S-formylglutathione hydrolase [Gallus gallus];	32 kDa	10	36.90%
513170472	ref|XP_004939698.1 PREDICTED: adenylyl cyclase-associated protein 2 isoform X5 [Gallus gallus]	50 kDa	10	23.60%
513211258	ref|XP_004934529.1 PREDICTED: AP-1 complex subunit beta-1 isoform X8 [Gallus gallus]	103 kDa	3	11.60%
312032350	ref|NP_990787.2 tenascin precursor [Gallus gallus]	199 kDa	3	2.93%
45382053	ref|NP_990784.1 thioredoxin [Gallus gallus]	12 kDa	7	55.20%
513211940	ref|XP_004945820.1 PREDICTED: delta-aminolevulinic acid dehydratase isoform X2 [Gallus gallus]	36 kDa	7	34.80%
363734612	ref|XP_003641424.1 PREDICTED: plasma protease C1 inhibitor isoform X1 [Gallus gallus]	54 kDa	2	5.57%
444189297	ref|NP_001263235.1 prostaglandin E synthase 3 [Gallus gallus]; Duplicate proteins: gi|1362727	19 kDa	7	28.10%
513220600	ref|XP_424381.3 PREDICTED: proline synthase co-transcribed bacterial homolog protein [Gallus gallus]	35 kDa	5	19.40%

GI Number	Protein Name	Molecular Weight	#Unique Peptide	Percent Coverage[a]
363737227	ref|XP_422784.3 PREDICTED: actin-like 6A [Gallus gallus]	47 kDa	2	5.36%
57530433	ref|NP_001006382.1 fumarate hydratase, mitochondrial [Gallus gallus];	54 kDa	7	16.00%
513221584	ref|XP_004947910.1 PREDICTED: adenylate kinase 2, mitochondrial isoform X8 [Gallus gallus]	26 kDa	5	29.00%
71897339	ref|NP_001026542.1 serine/threonine-protein phosphatase 2A activator [Gallus gallus];	37 kDa	8	34.60%
50755563	ref|XP_414797.1 PREDICTED: 28 kDa heat- and acid-stable phosphoprotein isoform X2 [Gallus gallus]	21 kDa	2	17.80%
513179629	ref|XP_004935960.1 PREDICTED: cathepsin B isoform X7 [Gallus gallus]	38 kDa	4	12.00%
61098372	ref|NP_001012934.1 60 kDa heat shock protein, mitochondrial precursor [Gallus gallus]	61 kDa	8	21.10%
71897111	ref|NP_001025899.1 nicotinamide phosphoribosyltransferase [Gallus gallus]	56 kDa	5	11.60%
513166780	ref|XP_428185.4 PREDICTED: cyclic nucleotide-gated cation channel alpha-4 [Gallus gallus]	70 kDa	2	5.64%
444299628	ref|NP_001263232.1 nascent polypeptide-associated complex alpha subunit [Gallus gallus]	23 kDa	6	35.80%
71897241	ref|NP_001025838.1 D-dopachrome decarboxylase [Gallus gallus]	13 kDa	4	45.80%
45383878	ref|NP_989447.1 brain acid soluble protein 1 homolog [Gallus gallus]	25 kDa	6	28.30%
45382083	ref|NP_990777.1 tropomyosin beta chain [Gallus gallus]; Duplicate proteins: gi|212811	29 kDa	9	35.10%
123891643	sp|Q25C36.1|OLFL3_CHICK RecName: Full=Olfactomedin-like protein 3;	45 kDa	2	6.89%
57530211	ref|NP_001006425.1 hematological and neurological expressed 1 protein [Gallus gallus];	16 kDa	7	45.50%
45382979	ref|NP_990859.1 destrin [Gallus gallus]	19 kDa	7	29.10%
1708386	sp|P49705.1|IBP2_CHICK RecName: Full=Insulin-like growth factor-binding protein 2	34 kDa	2	29.80%
72535161	ref|NP_001026943.1 EF-hand domain-containing protein D1 [Gallus gallus];	27 kDa	8	40.80%

GI Number	Protein Name	Molecular Weight	#Unique Peptide	Percent Coverage[a]
60302768	ref|NP_001012577.1 septin-7 [Gallus gallus]	49 kDa	7	24.20%
118405190	ref|NP_001072967.1 coatomer subunit delta [Gallus gallus]	57 kDa	5	6.86%
84619526	ref|NP_001033782.1 phosphoglucomutase-1 [Gallus gallus]	67 kDa	2	4.48%
48976107	ref|NP_001001755.1 thrombospondin-2 precursor [Gallus gallus]	132 kDa	2	3.48%
57529406	ref|NP_001006296.1 VAMP (vesicle-associated membrane protein)-associated protein B and C [Gallus gallus];	27 kDa	2	5.76%
119331154	ref|NP_001073228.1 profilin-2 [Gallus gallus]	15 kDa	5	35.70%
513218571	ref|XP_417465.4 PREDICTED: bactericidal permeability-increasing protein isoform X3 [Gallus gallus]	58 kDa	2	5.67%
71894903	ref|NP_001026374.1 epididymal secretory protein E1 precursor [Gallus gallus]	16 kDa	4	33.80%
50729975	ref|XP_416732.1 PREDICTED: SH3 domain-binding glutamic acid-rich protein isoform X2 [Gallus gallus]	20 kDa	3	23.80%
71895027	ref|NP_001026019.1 eukaryotic translation initiation factor 6 [Gallus gallus];	27 kDa	6	30.60%
189233525	ref|NP_001121534.1 galanin receptor type 1 [Gallus gallus];	40 kDa	2	4.48%
45383776	ref|NP_989501.1 proliferating cell nuclear antigen [Gallus gallus]	29 kDa	8	31.30%
45384354	ref|NP_990651.1 avidin precursor [Gallus gallus]	17 kDa	5	32.20%
45382147	ref|NP_990111.1 protein syndesmos precursor [Gallus gallus]	34 kDa	8	25.30%
118101676	ref|XP_001232935.1 PREDICTED: splicing factor 3A subunit 3 [Gallus gallus];	59 kDa	2	5.99%
513177250	ref|XP_004940296.1 PREDICTED: receptor-type tyrosine-protein phosphatase kappa isoform X24 [Gallus gallus]	162 kDa	2	2.35%
60592998	ref|NP_001006578.2 succinyl-CoA:3-ketoacid-coenzyme A transferase 1, mitochondrial [Gallus gallus];	56 kDa	5	7.54%
50752104	ref|XP_422654.1 PREDICTED: septin-2 isoform X2 [Gallus gallus]	42 kDa	5	17.70%

GI Number	Protein Name	Molecular Weight	#Unique Peptide	Percent Coverage[a]
77736639	ref|NP_001029998.1 ADP-ribosyltransferase 1 precursor [Gallus gallus];	34 kDa	1	14.80%
118094989	ref|XP_422637.2 PREDICTED: coatomer subunit beta' [Gallus gallus]	103 kDa	5	3.18%
45382971	ref|NP_989928.1 eukaryotic translation initiation factor 2 subunit 2 [Gallus gallus]	38 kDa	4	11.40%
513175079	ref|XP_004935408.1 PREDICTED: echinoderm microtubule associated protein like 4 isoform X7 [Gallus gallus]	106 kDa	2	1.98%
363740226	ref|XP_003642282.1 PREDICTED: macrophage migration inhibitory factor [Gallus gallus]	12 kDa	8	50.40%
513184692	ref|XP_420760.4 PREDICTED: extracellular superoxide dismutase [Cu-Zn] [Gallus gallus]	26 kDa	5	29.80%
475505726	ref|NP_001264304.1 glutathione S-transferase omega-1 [Gallus gallus]	27 kDa	4	17.60%
45383996	ref|NP_990598.1 nucleophosmin [Gallus gallus]	33 kDa	5	20.10%
45384320	ref|NP_990639.1 fatty acid-binding protein, brain [Gallus gallus]	15 kDa	6	47.00%
71895347	ref|NP_001025780.1 clathrin light chain B [Gallus gallus]	28 kDa	2	6.95%
513196791	ref|XP_003641719.2 PREDICTED: UDP-N-acetylhexosamine pyrophosphorylase, partial [Gallus gallus]	51 kDa	3	7.64%
71896741	ref|NP_001026313.1 heterogeneous nuclear ribonucleoprotein D-like [Gallus gallus]	33 kDa	5	15.00%
363735530	ref|XP_001233764.2 PREDICTED: nucleoplasmin-3 isoform X1 [Gallus gallus]	16 kDa	7	56.10%
71894971	ref|NP_001026029.1 tumor protein D54 [Gallus gallus];	22 kDa	9	33.20%
33312179	gb|AAQ04021.1|AF419846_1 midkine precursor [Gallus gallus]	16 kDa	3	23.90%
71896361	ref|NP_001026105.1 acidic leucine-rich nuclear phosphoprotein 32 family member B [Gallus gallus]	30 kDa	8	27.10%
261490822	ref|NP_001159797.1 coactosin-like protein [Gallus gallus]	16 kDa	9	66.20%
71894963	ref|NP_001026385.1 glia maturation factor beta [Gallus gallus];	17 kDa	6	42.30%

GI Number	Protein Name	Molecular Weight	#Unique Peptide	Percent Coverage[a]
475504687	ref|NP_001264293.1 rho GDP-dissociation inhibitor 2 [Gallus gallus]	23 kDa	3	25.00%
45383590	ref|NP_989605.1 connective tissue growth factor precursor [Gallus gallus];	37 kDa	2	2.91%
45384190	ref|NP_990404.1 translin [Gallus gallus]	26 kDa	7	32.30%
45383173	ref|NP_989827.1 heterogeneous nuclear ribonucleoprotein H [Gallus gallus]	57 kDa	4	12.10%
71895881	ref|NP_001026711.1 ubiquitin-conjugating enzyme E2 K [Gallus gallus]	22 kDa	7	40.00%
356991151	ref|NP_001025862.2 protein SET [Gallus gallus]	32 kDa	8	27.10%
363746921	ref|XP_003643851.1 PREDICTED: hsp70-binding protein 1-like isoform X1 [Gallus gallus]	26 kDa	9	35.00%
57530095	ref|NP_001006447.1 COP9 signalosome complex subunit 4 [Gallus gallus]	47 kDa	7	16.80%
45382731	ref|NP_990813.1 hyaluronan and proteoglycan link protein 1 precursor [Gallus gallus]	41 kDa	11	26.80%
363733143	ref|XP_420392.3 PREDICTED: carboxypeptidase E [Gallus gallus]	52 kDa	7	10.70%
513165046	ref|XP_417016.3 PREDICTED: exosome complex exonuclease RRP44 isoform X2 [Gallus gallus]	113 kDa	2	2.31%
60302722	ref|NP_001012553.1 eukaryotic translation initiation factor 3 subunit L [Gallus gallus]	67 kDa	2	4.08%
475506756	ref|NP_001264313.1 glutaredoxin-3 [Gallus gallus]	37 kDa	7	19.80%
513192585	ref|XP_001233435.2 PREDICTED: LOW QUALITY PROTEIN: BAG family molecular chaperone regulator 3 isoform 1 [Gallus gallus]	61 kDa	3	8.05%
45382219	ref|NP_990142.1 proactivator polypeptide precursor [Gallus gallus];	58 kDa	5	12.90%
55741612	ref|NP_001006235.1 lamina-associated polypeptide 2, isoform beta [Gallus gallus];	50 kDa	2	6.50%
52138637	ref|NP_001004371.1 cadherin-11 precursor [Gallus gallus]	88 kDa	4	9.34%
62899037	ref|NP_001017413.1 pentraxin-related protein PTX3 precursor [Gallus gallus]	47 kDa	6	14.30%
57525024	ref|NP_001006152.1 serine/threonine-protein phosphatase 2A catalytic subunit alpha isoform [Gallus gallus]	36 kDa	6	19.40%

GI Number	Protein Name	Molecular Weight	#Unique Peptide	Percent Coverage[a]
57530009	ref|NP_001006469.1 nucleosome assembly protein 1-like 4 [Gallus gallus]	43 kDa	9	13.30%
71895709	ref|NP_001026681.1 glycine--tRNA ligase [Gallus gallus];	78 kDa	2	3.80%
71897163	ref|NP_001025820.1 eukaryotic initiation factor 4A-III [Gallus gallus]	47 kDa	4	15.30%
45383800	ref|NP_989489.1 caldesmon [Gallus gallus];	87 kDa	8	6.61%
71897077	ref|NP_001025883.1 uncharacterized protein LOC417536 precursor [Gallus gallus];|AH221	10 kDa	5	51.60%
118092580	ref|XP_421577.2 PREDICTED: vacuolar protein sorting-associated protein 26A [Gallus gallus]	38 kDa	4	14.70%
164452937	ref|NP_001006160.2 nudix (nucleoside diphosphate linked moiety X)-type motif 1 [Gallus gallus]	18 kDa	4	34.00%
478431053	ref|NP_001264514.1 3,2-trans-enoyl-CoA isomerase, mitochondrial [Gallus gallus]	34 kDa	2	7.14%
513223965	ref|XP_004948460.1 PREDICTED: prefoldin subunit 2 isoform X2 [Gallus gallus]	21 kDa	7	29.20%
61098378	ref|NP_001012937.1 aspartyl aminopeptidase [Gallus gallus];	52 kDa	3	8.03%
57530593	ref|NP_001006339.1 coatomer subunit epsilon [Gallus gallus]	34 kDa	3	13.00%
71896957	ref|NP_001026494.1 eukaryotic translation initiation factor 2A [Gallus gallus]	65 kDa	4	9.04%
363733172	ref|XP_420496.3 PREDICTED: aminoacyl tRNA synthase complex-interacting multifunctional protein 1 isoform X2 [Gallus gallus]	35 kDa	6	19.60%
513220310	ref|XP_004947590.1 PREDICTED: phosphopantothenate--cysteine ligase isoform X2 [Gallus gallus]	40 kDa	3	9.02%
513217819	ref|XP_004947087.1 PREDICTED: embryonic polyadenylate-binding protein-like isoform X4 [Gallus gallus]	38 kDa	8	28.20%
513164985	ref|XP_004938693.1 PREDICTED: ES1 protein homolog, mitochondrial isoform X3 [Gallus gallus]	19 kDa	9	60.00%
49169816	ref|NP_001001777.1 glutathione S-transferase [Gallus gallus]	25 kDa	4	20.40%

GI Number	Protein Name	Molecular Weight	#Unique Peptide	Percent Coverage[a]
206597436	ref|NP_990711.2 collagen alpha-1(III) chain precursor [Gallus gallus]	139 kDa	4	5.21%
45382755	ref|NP_990817.1 high mobility group protein B2 [Gallus gallus]	24 kDa	7	36.70%
118097222	ref|XP_414511.2 PREDICTED: eukaryotic peptide chain release factor subunit 1 [Gallus gallus]	49 kDa	8	22.70%
347800736	ref|NP_001006247.2 serine-threonine kinase receptor-associated protein [Gallus gallus]	38 kDa	6	19.10%
45384112	ref|NP_990453.1 serine/threonine-protein phosphatase PP1-beta catalytic subunit [Gallus gallus]	37 kDa	10	28.10%
50752600	ref|XP_422851.1 PREDICTED: tubulin alpha-3 chain [Gallus gallus]	50 kDa	10	21.80%
57530697	ref|NP_001006358.1 basic leucine zipper and W2 domain-containing protein 2 [Gallus gallus]	48 kDa	6	20.80%
513197616	ref|XP_004936755.1 PREDICTED: receptor-type tyrosine-protein phosphatase F isoform X10 [Gallus gallus]	200 kDa	2	1.29%
513200587	ref|XP_004943685.1 PREDICTED: beta-2-microglobulin isoform X1 [Gallus gallus]	13 kDa	4	41.20%
309951118	ref|NP_001006317.2 amyloid-like protein 2 precursor [Gallus gallus]	86 kDa	1	2.66%
45382569	ref|NP_990555.1 actin-related protein 2 [Gallus gallus]	45 kDa	4	6.85%
478621110	ref|NP_001264603.1 cleavage and polyadenylation specificity factor subunit 5-like [Gallus gallus]	26 kDa	3	15.90%
513224250	ref|XP_004934895.1 PREDICTED: troponin I, slow skeletal muscle isoform X6 [Gallus gallus]	19 kDa	2	18.70%
86129442	ref|NP_001034360.1 cleavage and polyadenylation specificity factor subunit 6 [Gallus gallus]	59 kDa	3	7.80%
45383540	ref|NP_989631.1 protein enabled homolog [Gallus gallus]	85 kDa	2	3.06%
363742094	ref|XP_424534.3 PREDICTED: V-type proton ATPase subunit B, brain isoform [Gallus gallus]	56 kDa	5	13.80%
71896363	ref|NP_001026106.1 polypyrimidine tract-binding protein 1 [Gallus gallus]	57 kDa	3	8.37%

GI Number	Protein Name	Molecular Weight	#Unique Peptide	Percent Coverage[a]
57530004	ref|NP_001006468.1 nucleobindin-2 precursor [Gallus gallus];	54 kDa	2	4.84%
513160723	ref|XP_423856.4 PREDICTED: LOW QUALITY PROTEIN: tetratricopeptide repeat protein 38 [Gallus gallus]	52 kDa	6	20.20%
50756597	ref|XP_415233.1 PREDICTED: v-crk sarcoma virus CT10 oncogene homolog-like [Gallus gallus]	34 kDa	4	15.80%
363747239	ref|XP_423673.3 PREDICTED: drebrin-like [Gallus gallus]	53 kDa	2	6.47%
307746908	ref|NP_001182714.1 thymosin beta 15 [Gallus gallus];	5 kDa	4	62.20%
45383834	ref|NP_989472.1 60S ribosomal protein L22 [Gallus gallus]	15 kDa	4	25.80%
513216944	ref|XP_415748.4 PREDICTED: complement component 1 Q subcomponent-binding protein, mitochondrial [Gallus gallus]	25 kDa	3	23.30%
45382847	ref|NP_989974.1 chromobox protein homolog 3 [Gallus gallus];	20 kDa	5	35.10%
513222324	ref|XP_004948127.1 PREDICTED: cell adhesion molecule 1 isoform X16 [Gallus gallus]	47 kDa	6	14.40%
363744612	ref|XP_429175.3 PREDICTED: UV excision repair protein RAD23 homolog B isoform X4 [Gallus gallus]	43 kDa	4	11.40%
45383966	ref|NP_990589.1 GTP-binding nuclear protein Ran [Gallus gallus]	24 kDa	5	25.90%
71896121	ref|NP_001026753.1 proteasome inhibitor PI31 subunit [Gallus gallus]	29 kDa	2	9.59%
513240635	ref|XP_004951026.1 PREDICTED: poly(rC)-binding protein 2-like isoform X16 [Gallus gallus]	32 kDa	3	13.40%
118405166	ref|NP_001072956.1 deoxyuridine 5'-triphosphate nucleotidohydrolase, mitochondrial [Gallus gallus];	18 kDa	6	39.80%
45384366	ref|NP_990336.1 calmodulin [Gallus gallus]	17 kDa	8	62.40%
471434827	ref|NP_001264206.1 chromosome 1 open reading frame, human C11orf54 [Gallus gallus]	35 kDa	3	12.00%
429544679	ref|NP_001258859.1 inosine triphosphate pyrophosphatase [Gallus gallus]	22 kDa	5	45.80%

GI Number	Protein Name	Molecular Weight	#Unique Peptide	Percent Coverage[a]
513204573	ref|XP_003642020.2 PREDICTED: putative RNA-binding protein 15B [Gallus gallus]	87 kDa	2	3.47%
50748450	ref|XP_421250.1 PREDICTED: protein transport protein Sec23A isoform X3 [Gallus gallus]	86 kDa	2	3.53%
118405172	ref|NP_001072962.1 AP-2 complex subunit mu [Gallus gallus]	49 kDa	3	11.30%
313747537	ref|NP_001186454.1 dnaJ homolog subfamily C member 9 [Gallus gallus]	30 kDa	4	18.10%
45384350	ref|NP_990653.1 60S acidic ribosomal protein P1 [Gallus gallus]	11 kDa	2	66.70%
45383498	ref|NP_989661.1 peptidyl-prolyl cis-trans isomerase FKBP1A [Gallus gallus];	12 kDa	3	31.50%
478732979	ref|NP_001264621.1 14 kDa phosphohistidine phosphatase isoform 1 [Gallus gallus]	14 kDa	4	37.60%
45382283	ref|NP_990164.1 ELAV-like protein 1 [Gallus gallus];	36 kDa	4	14.40%
513172280	ref|XP_419226.4 PREDICTED: gamma-glutamyl hydrolase [Gallus gallus]	48 kDa	6	9.34%
363742288	ref|XP_003642616.1 PREDICTED: proteasome subunit beta type-2 isoform 1 [Gallus gallus]	20 kDa	6	28.40%
45384330	ref|NP_990348.1 ras-related C3 botulinum toxin substrate 1 [Gallus gallus]	21 kDa	6	30.70%
86129490	ref|NP_001034380.1 low molecular weight phosphotyrosine protein phosphatase [Gallus gallus]	18 kDa	5	38.60%
45382483	ref|NP_990236.1 pterin-4-alpha-carbinolamine dehydratase [Gallus gallus]	12 kDa	4	45.20%
57524801	ref|NP_001005827.1 ras-related protein Rab-11A [Gallus gallus]	24 kDa	6	28.70%
61098232	ref|NP_001012789.1 eukaryotic translation initiation factor 3 subunit J [Gallus gallus]	29 kDa	4	17.10%
118088894	ref|XP_001234709.1 PREDICTED: 40S ribosomal protein S7 isoformX2 [Gallus gallus];	22 kDa	7	25.30%
513185558	ref|XP_420655.4 PREDICTED: eukaryotic translation initiation factor 4E [Gallus gallus]	27 kDa	7	20.20%
50740506	ref|XP_419481.1 PREDICTED: lactoylglutathione lyase [Gallus gallus]	21 kDa	5	30.00%

GI Number	Protein Name	Molecular Weight	#Unique Peptide	Percent Coverage[a]
118093746	ref|XP_426598.2 PREDICTED: actin-related protein 2/3 complex subunit 2 [Gallus gallus]	34 kDa	4	16.30%
57525383	ref|NP_001006237.1 ran GTPase-activating protein 1 [Gallus gallus]	63 kDa	3	6.21%
45384398	ref|NP_990675.1 heme oxygenase 1 [Gallus gallus]	34 kDa	2	7.77%
47575885	ref|NP_001001195.1 keratin, type II cytoskeletal 5 [Gallus gallus];	62 kDa	2	10.20%
363742391	ref|XP_427366.3 PREDICTED: regulator of chromosome condensation [Gallus gallus]	44 kDa	4	13.40%
50736564	ref|XP_419132.1 PREDICTED: mRNA cap guanine-N7 methyltransferase isoform X2 [Gallus gallus]	48 kDa	6	16.40%
71895115	ref|NP_001026002.1 paraspeckle component 1 [Gallus gallus]	58 kDa	3	8.03%
475503508	ref|NP_001264284.1 N-alpha-acetyltransferase 38, NatC auxiliary subunit [Gallus gallus]	10 kDa	3	38.50%
513208660	ref|XP_001234358.3 PREDICTED: LOW QUALITY PROTEIN: C-type lectin domain family 19 member A isoform 2 [Gallus gallus]	21 kDa	3	17.10%
45382329	ref|NP_990729.1 translationally-controlled tumor protein homolog [Gallus gallus]	20 kDa	5	21.50%
485049501	ref|NP_990340.2 keratin, type I cytoskeletal 19 [Gallus gallus]	46 kDa	3	7.33%
60302750	ref|NP_001012568.1 proteasome activator complex subunit 3 [Gallus gallus]	29 kDa	4	18.90%
71895783	ref|NP_001026692.1 adenylosuccinate synthetase isozyme 2 [Gallus gallus]	49 kDa	3	9.53%
513193723	ref|XP_004942717.1 PREDICTED: elongation factor 1-beta isoform X1 [Gallus gallus]	25 kDa	5	41.50%
57530666	ref|NP_001006352.1 ADP-ribosylation factor 1 [Gallus gallus]	21 kDa	5	37.00%
513172523	ref|XP_004939993.1 PREDICTED: inositol monophosphatase 1 isoform X5 [Gallus gallus]	30 kDa	5	9.71%
513196126	ref|XP_422218.4 PREDICTED: cysteine-rich protein 2 [Gallus gallus]	26 kDa	5	45.00%
57529758	ref|NP_001006519.1 cytoplasmic dynein 1 intermediate chain 2 [Gallus gallus]	68 kDa	2	6.90%

GI Number	Protein Name	Molecular Weight	#Unique Peptide	Percent Coverage[a]
513161834	ref|XP_416605.2 PREDICTED: mitochondrial import receptor subunit TOM70 [Gallus gallus]	73 kDa	5	11.00%
45383339	ref|NP_989742.1 growth factor receptor-bound protein 2 [Gallus gallus]	25 kDa	5	34.10%
513168933	ref|XP_418734.4 PREDICTED: secernin-1 isoform X2 [Gallus gallus];	56 kDa	3	6.93%
56119012	ref|NP_001007887.1 AP-1 complex subunit mu-1 [Gallus gallus]	49 kDa	2	5.67%
71896747	ref|NP_001026310.1 general vesicular transport factor p115 [Gallus gallus]	106 kDa	2	2.63%
513183226	ref|XP_420591.3 PREDICTED: septin-11 isoform X2 [Gallus gallus]	51 kDa	4	8.60%
513164434	ref|XP_004938589.1 PREDICTED: ADP-ribosylhydrolase like 1 isoform X3 [Gallus gallus]	216 kDa	7	5.53%
310772242	ref|NP_001185580.1 CD99 antigen precursor [Gallus gallus]	18 kDa	2	17.60%
50759498	ref|XP_417666.1 PREDICTED: gastrokine-2 [Gallus gallus]	21 kDa	3	19.70%
363738949	ref|XP_414534.3 PREDICTED: stanniocalcin-2 [Gallus gallus]	33 kDa	5	26.10%
347920951	ref|NP_001026082.2 platelet-activating factor acetylhydrolase IB subunit beta [Gallus gallus]	27 kDa	3	11.20%
57525160	ref|NP_001006183.1 ran-specific GTPase-activating protein [Gallus gallus];	24 kDa	3	14.90%
513193476	ref|XP_004942661.1 PREDICTED: NIF3-like protein 1 isoform X3 [Gallus gallus]	41 kDa	3	12.10%
57529509	ref|NP_001006566.1 dihydropteridine reductase [Gallus gallus]; Duplicate proteins: gi|53130724	25 kDa	3	8.40%
52138699	ref|NP_001004400.1 tubulin beta-2 chain [Gallus gallus]	50 kDa	4	29.70%
513173559	ref|XP_004940097.1 PREDICTED: translation initiation factor IF-2 isoform X13 [Gallus gallus];	37 kDa	4	20.10%
118101125	ref|XP_417628.2 PREDICTED: aflatoxin B1 aldehyde reductase member 2 [Gallus gallus]	37 kDa	5	12.00%
48976117	ref|NP_001001760.1 cadherin-13 precursor [Gallus gallus]; Duplicate proteins: gi|386363	79 kDa	2	2.79%

GI Number	Protein Name	Molecular Weight	#Unique Peptide	Percent Coverage[a]
86129600	ref|NP_001034420.1 pre-mRNA-processing factor 19 [Gallus gallus]	55 kDa	4	11.70%
57529492	ref|NP_001006571.1 3-ketoacyl-CoA thiolase, mitochondrial [Gallus gallus];	42 kDa	4	15.90%
71895267	ref|NP_001025966.1 carbonyl reductase [NADPH] 1 [Gallus gallus];	30 kDa	3	12.70%
363738555	ref|XP_003642026.1 PREDICTED: ras-related protein Rab-7a isoform 1 [Gallus gallus]	24 kDa	7	29.50%
71895095	ref|NP_001026007.1 40S ribosomal protein S3 [Gallus gallus]	27 kDa	7	26.60%
57529904	ref|NP_001006488.1 eukaryotic translation initiation factor 5 [Gallus gallus]	49 kDa	4	9.07%
166091440	ref|NP_001107213.1 serine/arginine-rich splicing factor 1 [Gallus gallus]	28 kDa	5	23.00%
513223680	ref|XP_004948396.1 PREDICTED: selenium-binding protein 1-A-like isoform X2 [Gallus gallus];	52 kDa	2	7.01%
513159418	ref|XP_004937833.1 PREDICTED: eukaryotic translation initiation factor 3 subunit D isoform X2 [Gallus gallus]	64 kDa	2	4.39%
513166013	ref|XP_417163.4 PREDICTED: cullin-5 [Gallus gallus]	88 kDa	2	2.64%
363744458	ref|XP_001231514.2 PREDICTED: UPF0553 protein C9orf64 isoform 1 [Gallus gallus]	39 kDa	2	8.50%
45382905	ref|NP_990846.1 F-actin-capping protein subunit alpha-1 [Gallus gallus]	33 kDa	4	23.80%
45383494	ref|NP_989663.1 chromobox protein homolog 1 [Gallus gallus];	22 kDa	3	30.80%
118093267	ref|XP_001232694.1 PREDICTED: malonyl-CoA O-methyltransferase BioC isoformX1 [Gallus gallus]	30 kDa	5	17.00%
45383366	ref|NP_989728.1 proteasome subunit beta type-7 [Gallus gallus]	30 kDa	5	16.20%
57529848	ref|NP_001006501.1 adenosine kinase [Gallus gallus];	40 kDa	3	8.08%
61098428	ref|NP_001012961.1 syntaxin-7 [Gallus gallus];	29 kDa	4	14.30%
45382613	ref|NP_990056.1 caspase-3 [Gallus gallus]	32 kDa	3	12.40%
118102948	ref|XP_418119.2 PREDICTED: proteasome subunit beta type-3 [Gallus gallus]	23 kDa	7	33.20%

GI Number	Protein Name	Molecular Weight	#Unique Peptide	Percent Coverage[a]
268607704	ref|NP_001161224.1 myoglobin [Gallus gallus]	17 kDa	3	22.70%
57529764	ref|NP_001006516.1 basic leucine zipper and W2 domain-containing protein 1 [Gallus gallus]	48 kDa	3	4.55%
229606091	ref|NP_001153454.1 calcineurin-like phosphoesterase domain containing 1 [Gallus gallus]	36 kDa	3	14.30%
57524906	ref|NP_001006129.1 NEDD8-activating enzyme E1 regulatory subunit [Gallus gallus]	60 kDa	3	7.48%
71896903	ref|NP_001025928.1 hsc70-interacting protein [Gallus gallus]	40 kDa	5	15.20%
363728304	ref|XP_416476.3 PREDICTED: alpha-2-macroglobulin isoform X3 [Gallus gallus]	165 kDa	2	1.76%
45382073	ref|NP_990780.1 troponin T, cardiac muscle isoforms [Gallus gallus]	36 kDa	3	9.93%
57524852	ref|NP_001005836.1 alanyl-tRNA synthetase, cytoplasmic [Gallus gallus]	101 kDa	2	3.18%
363732737	ref|XP_420200.3 PREDICTED: cysteine and histidine-rich domain-containing protein 1 isoform X3 [Gallus gallus]	42 kDa	2	5.28%
45384518	ref|NP_990326.1 retinal dehydrogenase 2 [Gallus gallus]	55 kDa	5	11.40%
513215594	ref|XP_415774.4 PREDICTED: protein unc-45 homolog B isoform X2 [Gallus gallus]	104 kDa	2	2.47%
45382431	ref|NP_990217.1 myotrophin [Gallus gallus]	13 kDa	3	30.50%
71897327	ref|NP_001026545.1 histone H2A.Z [Gallus gallus]	14 kDa	3	53.90%
513217471	ref|XP_417328.3 PREDICTED: dynein light chain roadblock-type 1 isoform X2 [Gallus gallus]	11 kDa	3	44.80%
513239668	ref|XP_004950832.1 PREDICTED: keratin, type I cytoskeletal 18-like [Gallus gallus]	19 kDa	2	15.40%
482513648	ref|NP_001264782.1 glutathione peroxidase 1 [Gallus gallus]	22 kDa	4	30.80%
363747068	ref|XP_003643901.1 PREDICTED: LOW QUALITY PROTEIN: transgelin-2-like [Gallus gallus]	22 kDa	2	13.10%

GI Number	Protein Name	Molecular Weight	#Unique Peptide	Percent Coverage[a]
363738693	ref|XP_003642054.1 PREDICTED: cAMP-dependent protein kinase type II-alpha regulatory subunit [Gallus gallus]	46 kDa	4	9.50%
71896943	ref|NP_001025918.1 decorin precursor [Gallus gallus]	40 kDa	2	7.00%
45383544	ref|NP_989629.1 metalloproteinase inhibitor 2 precursor [Gallus gallus]	24 kDa	2	6.82%
118101327	ref|XP_001232615.1 PREDICTED: neurofilament light polypeptide isoform 1 [Gallus gallus]	54 kDa	2	6.21%
513172077	ref|XP_426083.4 PREDICTED: desmoglein-2 isoform X2 [Gallus gallus]	118 kDa	3	3.19%
86129544	ref|NP_001034402.1 clathrin light chain A [Gallus gallus]; Duplicate proteins: gi|53136794	24 kDa	2	18.10%
513212083	ref|XP_004945852.1 PREDICTED: syntaxin-binding protein 1 isoform X2 [Gallus gallus]	67 kDa	2	3.90%
312596918	ref|NP_001006272.2 calcium binding protein 39-like [Gallus gallus]	39 kDa	3	8.68%
57525156	ref|NP_001006182.1 septin-2 [Gallus gallus]	40 kDa	4	19.80%
71894779	ref|NP_001025803.1 actin-related protein 2/3 complex subunit 1B [Gallus gallus]	41 kDa	2	11.70%
50748536	ref|XP_421292.1 PREDICTED: activator of 90 kDa heat shock protein ATPase homolog 1 isoformX2 [Gallus gallus]	38 kDa	8	26.80%
118405182	ref|NP_001072966.1 small ubiquitin-related modifier 3 precursor [Gallus gallus]	11 kDa	2	27.70%
513216292	ref|XP_004946738.1 PREDICTED: tax1-binding protein 3 isoform X3 [Gallus gallus]	12 kDa	2	29.50%
480306426	ref|NP_001264684.1 60S ribosomal protein L31 [Gallus gallus]	14 kDa	2	18.40%
56118966	ref|NP_001007968.1 60S ribosomal protein L30 [Gallus gallus]	13 kDa	3	24.30%
478733026	ref|NP_001264641.1 copper transport protein ATOX1 [Gallus gallus]	8 kDa	4	76.10%
513221877	ref|XP_004947974.1 PREDICTED: histone H2A.x-like [Gallus gallus]	15 kDa	3	53.10%
71896335	ref|NP_001026100.1 60S ribosomal protein L19 [Gallus gallus]	23 kDa	3	16.80%

GI Number	Protein Name	Molecular Weight	#Unique Peptide	Percent Coverage[a]
429535826	ref|NP_001258858.1 myosin regulatory light chain 2A, cardiac muscle isoform [Gallus gallus]	19 kDa	4	17.00%
47604946	ref|NP_001001315.1 thymosin, beta 4 [Gallus gallus];	5 kDa	3	44.40%
50760001	ref|XP_417859.1 PREDICTED: m7GpppX diphosphatase [Gallus gallus]	37 kDa	4	16.40%
513174694	ref|XP_423931.3 PREDICTED: aldose 1-epimerase isoformX2 [Gallus gallus];	38 kDa	3	11.30%
513158256	ref|XP_004937637.1 PREDICTED: nucleosome assembly protein 1-like 1 isoform X9 [Gallus gallus]	44 kDa	5	19.50%
50749406	ref|XP_421624.1 PREDICTED: eukaryotic translation initiation factor 3 subunit F [Gallus gallus]	35 kDa	3	10.80%
45383023	ref|NP_989912.1 60S ribosomal protein L5 [Gallus gallus]	34 kDa	2	8.08%
444741647	ref|NP_001263253.1 endoplasmic reticulum resident protein 29 precursor [Gallus gallus]	28 kDa	3	19.80%
513196058	ref|XP_422209.4 PREDICTED: olfactomedin-like 2B [Gallus gallus]	81 kDa	2	4.73%
444741724	ref|NP_001263291.1 pleiotrophin precursor [Gallus gallus]	19 kDa	3	31.50%
363742157	ref|XP_427212.3 PREDICTED: MOB kinase activator 1A [Gallus gallus]	25 kDa	3	16.20%
52138719	ref|NP_001004411.1 neuroserpin precursor [Gallus gallus]	47 kDa	3	8.05%
218664505	ref|NP_001136320.1 draxin precursor [Gallus gallus]	39 kDa	2	4.87%
513174887	ref|XP_004935373.1 PREDICTED: transforming growth factor beta-2 isoform X2 [Gallus gallus]	50 kDa	1	2.13%
56119060	ref|NP_001007839.1 small nuclear ribonucleoprotein Sm D3 [Gallus gallus];	14 kDa	2	14.30%
45383045	ref|NP_989898.1 peptidyl-prolyl cis-trans isomerase FKBP1B [Gallus gallus];	12 kDa	3	31.50%
74048411	ref|NP_001027570.1 eukaryotic translation elongation factor 1 alpha 2 [Gallus gallus]	50 kDa	3	16.60%
513220885	ref|XP_004947725.1 PREDICTED: SH3 domain binding glutamic acid-rich protein like 3 isoform X4 [Gallus gallus]	17 kDa	3	16.10%

GI Number	Protein Name	Molecular Weight	#Unique Peptide	Percent Coverage[a]
363746230	ref|XP_001236782.2 PREDICTED: ubiquitin thioesterase OTUB1 [Gallus gallus]	31 kDa	2	9.26%
475808444	ref|NP_001264336.1 beta-lactamase-like protein 2 [Gallus gallus]	32 kDa	3	11.10%
133778969	ref|NP_001006584.2 dihydrofolate reductase [Gallus gallus]	22 kDa	5	28.90%
363730689	ref|XP_003640848.1 PREDICTED: ras-related protein Rab-12 [Gallus gallus]	28 kDa	3	12.80%
45382667	ref|NP_990035.1 transforming protein RhoA [Gallus gallus]	22 kDa	3	17.60%
118091445	ref|XP_421073.2 PREDICTED: protein FADD [Gallus gallus]	23 kDa	4	22.60%
513182216	ref|XP_004941026.1 PREDICTED: U6 snRNA-associated Sm-like protein LSm6 isoform X4 [Gallus gallus];	9 kDa	5	35.00%
513177075	ref|XP_419539.4 PREDICTED: heterogeneous nuclear ribonucleoprotein U, partial [Gallus gallus]	68 kDa	3	4.98%
45382323	ref|NP_990732.1 tropomyosin alpha-1 chain [Gallus gallus]; Duplicate proteins: gi|212813,gi|833619	33 kDa	2	19.40%
56119058	ref|NP_001007838.1 vacuolar protein sorting-associated protein 29 [Gallus gallus]	21 kDa	2	11.30%
71897245	ref|NP_001025840.1 ras-related protein Rab-35 [Gallus gallus]	23 kDa	2	20.90%
50745986	ref|XP_420327.1 PREDICTED: prefoldin subunit 3 isoform X3 [Gallus gallus]	22 kDa	2	11.50%
45382783	ref|NP_990825.1 transgelin [Gallus gallus]	22 kDa	3	18.50%
50744564	ref|XP_419778.1 PREDICTED: 5'-nucleotidase domain-containing protein 1 isoformX2 [Gallus gallus]	52 kDa	5	16.70%
477555784	ref|NP_001264415.1 actin-related protein 2/3 complex subunit 3 [Gallus gallus]	21 kDa	4	15.20%
513224225	ref|XP_419249.3 PREDICTED: tubulin alpha-1C chain isoform X2 [Gallus gallus]	46 kDa	3	21.30%
71896007	ref|NP_001026732.1 actin-related protein 2/3 complex subunit 5 [Gallus gallus]	16 kDa	4	49.70%
513239573	ref|XP_003643857.2 PREDICTED: UV excision repair protein RAD23 homolog A-like [Gallus gallus]	24 kDa	2	19.40%
56605932	ref|NP_001008466.1 ras-related protein Rab-33B [Gallus gallus]	26 kDa	3	13.60%

GI Number	Protein Name	Molecular Weight	#Unique Peptide	Percent Coverage[a]
57525187	ref|NP_001006190.1 serine/threonine-protein phosphatase PP1-gamma catalytic subunit [Gallus gallus]	37 kDa	4	23.80%
347300441	ref|NP_001005823.1 U2 small nuclear ribonucleoprotein A' [Gallus gallus]	28 kDa	2	9.41%
513240689	ref|XP_004951037.1 PREDICTED: peptidyl-prolyl cis-trans isomerase-like 1 isoform X4 [Gallus gallus];	16 kDa	2	11.60%
479277984	ref|NP_001264658.1 isoamyl acetate-hydrolyzing esterase 1 homolog [Gallus gallus]	28 kDa	4	24.50%
513223962	ref|XP_004948459.1 PREDICTED: V-type proton ATPase catalytic subunit A-like isoform X5 [Gallus gallus]	58 kDa	2	6.20%
57530393	ref|NP_001006387.1 transcription elongation factor A protein 1 [Gallus gallus]	34 kDa	2	13.80%
118405170	ref|NP_001072959.1 flap endonuclease 1 [Gallus gallus]	43 kDa	2	7.09%
363746026	ref|XP_003643500.1 PREDICTED: partner of Y14 and mago-like [Gallus gallus]	23 kDa	2	12.60%
57530543	ref|NP_001006334.1 7-methylguanosine phosphate-specific 5'-nucleotidase [Gallus gallus]	33 kDa	2	9.00%
513172980	ref|XP_003640897.2 PREDICTED: nudC domain-containing protein 1 isoform X1 [Gallus gallus]	78 kDa	3	6.39%
46048964	ref|NP_989618.1 thymocyte nuclear protein 1 [Gallus gallus]	28 kDa	3	16.90%
45382561	ref|NP_990559.1 ras-related protein Rab-2A [Gallus gallus]	24 kDa	3	21.70%
71896625	ref|NP_001026324.1 ubiquitin-conjugating enzyme E2 D3 [Gallus gallus]	17 kDa	3	36.10%
71897303	ref|NP_001026551.1 poly(U)-binding-splicing factor PUF60 [Gallus gallus]	39 kDa	2	10.40%
513181601	ref|XP_003641126.2 PREDICTED: histone H1 [Gallus gallus]	23 kDa	2	17.50%
45382473	ref|NP_990233.1 high mobility group protein B1 [Gallus gallus]	25 kDa	2	16.70%
46048708	ref|NP_990627.1 histone H3.3 [Gallus gallus];	15 kDa	3	40.40%
487439656	ref|NP_001264927.1 small nuclear ribonucleoprotein Sm D1 [Gallus gallus]	12 kDa	2	29.50%

GI Number	Protein Name	Molecular Weight	#Unique Peptide	Percent Coverage[a]
513179623	ref|XP_004935958.1 PREDICTED: cathepsin B isoform X5 [Gallus gallus]	41 kDa	2	22.20%
348591875	emb|CCC15116.1 chemokine [Gallus gallus]	10 kDa	5	52.10%
57525011	ref|NP_001006153.1 S-phase kinase-associated protein 1 [Gallus gallus]	19 kDa	2	12.90%
71895205	ref|NP_001025983.1 phosducin-like protein 3 [Gallus gallus]	28 kDa	2	9.58%
363731011	ref|XP_418373.3 PREDICTED: collagen triple helix repeat-containing protein 1 [Gallus gallus]	29 kDa	2	7.52%
118101780	ref|XP_425786.2 PREDICTED: adenylate kinase 2, mitochondrial isoform X4 [Gallus gallus]	26 kDa	4	40.40%
61098292	ref|NP_001012811.1 guanine nucleotide-binding protein subunit beta-like protein 1 [Gallus gallus]	36 kDa	2	6.10%
478621062	ref|NP_001264573.1 sel1 repeat-containing protein 1 isoform 2 [Gallus gallus]	20 kDa	2	15.20%
56118978	ref|NP_001007954.1 glutamate--cysteine ligase regulatory subunit [Gallus gallus]	30 kDa	2	8.49%
363738196	ref|XP_427969.3 PREDICTED: vesicle amine transport protein 1 homolog (T. californica)-like isoform X2 [Gallus gallus]	46 kDa	4	17.50%
56119006	ref|NP_001007889.1 transcription elongation factor B polypeptide 1 [Gallus gallus]	12 kDa	3	34.80%
348591869	emb|CCC15113.1 chemokine [Gallus gallus]|CCLI7	10 kDa	2	27.50%
363740917	ref|XP_001232214.2 PREDICTED: 39S ribosomal protein L12, mitochondrial [Gallus gallus]	21 kDa	2	25.80%
45383812	ref|NP_989481.1 mitogen-activated protein kinase 1 [Gallus gallus]	42 kDa	2	8.42%
269784818	ref|NP_001161481.1 cathepsin L1 precursor [Gallus gallus]	40 kDa	1	3.97%
71895207	ref|NP_001026073.1 stromal membrane-associated protein 2 [Gallus gallus]	46 kDa	2	9.81%
460838684	ref|NP_001264077.1 prefoldin subunit 1 isoform 3 [Gallus gallus]	13 kDa	2	16.50%
513236547	ref|XP_004950295.1 PREDICTED: prefoldin subunit 5 isoform X5 [Gallus gallus]	12 kDa	2	21.80%

GI Number	Protein Name	Molecular Weight	#Unique Peptide	Percent Coverage[a]
45383556	ref|NP_989621.1 fatty acid-binding protein, adipocyte [Gallus gallus]	15 kDa	3	37.10%
513228208	ref|XP_414700.4 PREDICTED: haloacid dehalogenase-like hydrolase domain containing 2 isoform X1 [Gallus gallus]	28 kDa	2	10.00%
71895237	ref|NP_001025975.1 eukaryotic translation initiation factor 1A, Y chromosome [Gallus gallus]	16 kDa	2	27.80%
513221687	ref|XP_004947931.1 PREDICTED: polyadenylate-binding protein 4 isoform X13 [Gallus gallus]	34 kDa	4	24.50%
57530631	ref|NP_001006346.1 fatty acid binding protein 5 (psoriasis-associated) [Gallus gallus]	15 kDa	3	23.90%
57525368	ref|NP_001006233.1 methionine aminopeptidase 2 [Gallus gallus]	53 kDa	4	13.20%
45384136	ref|NP_990437.1 non-histone chromosomal protein HMG-14B [Gallus gallus]	11 kDa	3	18.40%
307078119	ref|NP_001182483.1 splicing factor, arginine/serine-rich 3 [Gallus gallus]	19 kDa	3	22.00%
82231235	sp|Q5F470.1|RAB8A_CHICK RecName: Full=Ras-related protein Rab-8A; Flags: Precursor;	24 kDa	2	5.31%
118102009	ref|XP_001234052.1 PREDICTED: 40S ribosomal protein S25 isoform X1 [Gallus gallus]	14 kDa	2	15.20%
356460917	ref|NP_001239055.1 40S ribosomal protein S8 [Gallus gallus]	24 kDa	3	15.40%
513227132	ref|XP_004948855.1 PREDICTED: perilipin-3-like isoform X3 [Gallus gallus]	45 kDa	2	4.90%
57530311	ref|NP_001006403.1 translin-associated protein X [Gallus gallus]	19 kDa	2	16.90%
513220016	ref|XP_004947540.1 PREDICTED: transmembrane and coiled-coil domain-containing protein 4 isoform X7 [Gallus gallus]	75 kDa	2	5.47%
513239492	ref|XP_004950803.1 PREDICTED: SUMO-activating enzyme subunit 1-like, partial [Gallus gallus]	17 kDa	2	14.60%
118096822	ref|XP_414333.2 PREDICTED: transketolase isoform X4 [Gallus gallus]	68 kDa	3	33.80%
45384530	ref|NP_990332.1 high mobility group protein HMGI-C [Gallus gallus]	12 kDa	3	54.10%

GI Number	Protein Name	Molecular Weight	#Unique Peptide	Percent Coverage[a]
71895261	ref|NP_001025969.1 ES1 protein homolog, mitochondrial [Gallus gallus]	27 kDa	2	13.50%
153792017	ref|NP_001074329.2 tubulin beta-3 chain [Gallus gallus]	50 kDa	2	23.40%
45382333	ref|NP_990179.1 hypoxanthine-guanine phosphoribosyltransferase [Gallus gallus]	25 kDa	2	11.90%
478621070	ref|NP_001264579.1 adenine phosphoribosyltransferase-like isoform 2 [Gallus gallus]	17 kDa	2	13.20%
513220000	ref|XP_004947538.1 PREDICTED: microfibrillar-associated protein 2 isoform X4 [Gallus gallus]	23 kDa	1	4.90%
71895243	ref|NP_001025972.1 renin receptor [Gallus gallus]	37 kDa	2	9.01%
57525076	ref|NP_001006165.1 phosphoribosyl pyrophosphate synthase-associated protein 2 [Gallus gallus]	41 kDa	2	8.40%
45384212	ref|NP_990612.1 lysozyme C precursor [Gallus gallus]	16 kDa	2	21.10%
363740987	ref|XP_003642414.1 PREDICTED: ras and EF-hand domain-containing protein homolog isoform X1 [Gallus gallus]	23 kDa	2	14.20%
113206120	ref|NP_001038133.1 ladybird-like homeobox 3 [Gallus gallus]	23 kDa	2	12.70%
71896731	ref|NP_001026314.1 heterogeneous nuclear ribonucleoprotein D0 [Gallus gallus]	29 kDa	2	9.34%
513211241	ref|XP_415310.4 PREDICTED: neurofilament heavy polypeptide [Gallus gallus]	103 kDa	2	3.91%
269784810	ref|NP_001161477.1 acylphosphatase-1 [Gallus gallus]	11 kDa	2	24.20%
363732860	ref|XP_420326.3 PREDICTED: LOW QUALITY PROTEIN: ras-related protein Rab-39B [Gallus gallus]	25 kDa	2	15.50%
45382571	ref|NP_990556.1 40S ribosomal protein S6 [Gallus gallus]	29 kDa	2	9.64%
71895291	ref|NP_001025790.1 40S ribosomal protein S14 [Gallus gallus]	16 kDa	2	15.90%
45383836	ref|NP_989466.1 small ubiquitin-related modifier 1 precursor [Gallus gallus]	12 kDa	2	18.80%
119331144	ref|NP_001073222.1 tumor protein D52 [Gallus gallus]	20 kDa	2	15.80%

GI Number	Protein Name	Molecular Weight	#Unique Peptide	Percent Coverage[a]
71895139	ref|NP_001025998.1 ubiquitin-fold modifier 1 precursor [Gallus gallus]	9 kDa	2	50.60%
363729733	ref|XP_003640692.1 PREDICTED: guanylate kinase isoform X3 [Gallus gallus];	22 kDa	2	21.70%
478694653	ref|NP_001264634.1 uncharacterized protein LOC770635 [Gallus gallus]	6 kDa	2	98.20%
45384108	ref|NP_990455.1 serine/threonine-protein phosphatase 2A catalytic subunit alpha isoform [Gallus gallus]	36 kDa	2	16.20%
45383105	ref|NP_989866.1 osteopontin precursor [Gallus gallus]	29 kDa	2	13.30%

[a] Percent coverage is the percentage of the whole protein sequence covered by matched peptides identified in the 2D-LC-MS/MS.

Appendix B. EHE secretome

TABLE IV. EHE SECRETOME

GI Number	Gene Symbol	Protein Name	Location	Type(s)
363728304	A2M	alpha-2-macroglobulin	Extracellular Space	transporter
372266122	ACAN	Aggrecan	Extracellular Space	Other
45382569	ACTR2	ARP2 actin-related protein 2 homolog (yeast)	Plasma Membrane	Other
45383528	ACTR3	ARP3 actin-related protein 3 homolog (yeast)	Plasma Membrane	Other
513183353	AFP	alpha fetoprotein	Extracellular Space	transporter
71897077	AH221	uncharacterized protein LOC417536 precursor /Chemokine ah221	unmapped by IPA	
363733172	AIMP1	aminoacyl tRNA synthetase complex-interacting multifunctional protein 1	Extracellular Space	cytokine
61097989	AP2B1	adaptor related protein complex 2 beta 1 subunit	Plasma Membrane	transporter
309951118	APLP2	amyloid beta (A4) precursor-like protein 2	Cytoplasm	Other
45382961	APOA1	apolipoprotein A-I	Extracellular Space	transporter
45383530	APP	amyloid beta precursor protein	Plasma Membrane	Other
77736639	ART1	ADP-ribosyltransferase 1	Plasma Membrane	Enzyme
513223962	ATP6V1A	ATPase, H+ transporting, lysosomal 70kDa, V1 subunit A	Plasma Membrane	transporter
45384354	AVD	avidin precursor	unmapped by IPA	
513200587	B2M	beta-2-microglobulin	Plasma Membrane	transmembrane receptor
513218571	BPI	bactericidal/permeability-increasing protein	Plasma Membrane	transporter
363744073	CA9	carbonic anhydrase IX	Nucleus	Enzyme
513222324	CADM1	cell adhesion molecule 1	Plasma Membrane	Other
45383800	Cald1	caldesmon 1	Plasma Membrane	Other

GI Number	Gene Symbol	Protein Name	Location	Type(s)
44969651	CALR	Calreticulin	Cytoplasm	transcription regulator
363742430	CAP1	CAP, adenylate cyclase-associated protein 1 (yeast)	Plasma Membrane	Other
513170472	CAP2	CAP, adenylate cyclase-associated protein, 2 (yeast)	Plasma Membrane	Other
348591875	CCLI10	PREDICTED: C-C motif chemokine 3-like 1	unmapped by IPA	
348591869	CCLI7	PREDICTED: C-C motif chemokine 3	unmapped by IPA	
310772242	CD99	CD99 molecule	Plasma Membrane	Other
52138637	CDH11	cadherin 11	Plasma Membrane	Other
48976117	CDH13	cadherin 13	Plasma Membrane	Other
48675901	CDH2	cadherin 2	Plasma Membrane	Other
45383674	CDH5	cadherin 5	Plasma Membrane	Other
513227300	CFD	complement factor D (adipsin)	Extracellular Space	peptidase
52138701	CFL2	cofilin 2 (muscle)	Extracellular Space	Other
513221075	CLIC4	chloride intracellular channel 4	Plasma Membrane	ion channel
308081945	CLSTN1	calsyntenin 1	Plasma Membrane	Other
86129544	CLTA	clathrin, light chain A	Plasma Membrane	Other
124339781	CLTC	clathrin, heavy chain (Hc)	Plasma Membrane	Other
513166780	CNGA4	PREDICTED: cyclic nucleotide-gated cation channel alpha-4	Plasma Membrane	ion channel
45383788	COL18A1	collagen, type XVIII, alpha 1	Extracellular Space	Other
206597434	COL1A2	collagen, type I, alpha 2	Extracellular Space	Other
45383309	COL2A1	collagen, type II, alpha 1	Extracellular Space	Other
206597436	COL3A1	collagen, type III, alpha 1	Extracellular Space	Other
46048885	COL5A1	collagen, type V, alpha 1	Extracellular Space	Other

GI Number	Gene Symbol	Protein Name	Location	Type(s)
513192634	COL5A2	collagen, type V, alpha 2	Extracellular Space	Other
363733143	CPE	carboxypeptidase E	Cytoplasm	peptidase
513196126	Crip2	cysteine rich protein 2	Plasma Membrane	Other
319655747	CST3	cystatin C	Extracellular Space	Other
45383590	CTGF	connective tissue growth factor	Extracellular Space	growth factor
363731011	CTHRC1	collagen triple helix repeat containing 1	Extracellular Space	Other
513179629	CTSB	cathepsin B	Cytoplasm	peptidase
45384002	CTSD	cathepsin D	Cytoplasm	peptidase
269784818	CTSV	cathepsin V	Cytoplasm	peptidase
147902704	DAG1	dystroglycan 1	Plasma Membrane	transmembrane receptor
71896943	DCN	Decorin	Extracellular Space	Other
45384102	DKK3	dickkopf WNT signaling pathway inhibitor 3	Extracellular Space	cytokine
218664505	DRAXIN	dorsal inhibitory axon guidance protein	Extracellular Space	Other
513172079	DSG2	desmoglein 2	Plasma Membrane	Other
444741647	ERP29	endoplasmic reticulum protein 29	Cytoplasm	transporter
45382429	EZR	Ezrin	Plasma Membrane	Other
513173562	FAM49B	family with sequence similarity 49 member B	Extracellular Space	Other
45383790	FBLN1	fibulin 1	Extracellular Space	Other
513204938	FBLN2	fibulin 2	Extracellular Space	Other
513226445	FBN2	fibrillin 2	Extracellular Space	Other
311213923	FN1	fibronectin 1	Extracellular Space	enzyme
513161428	FSTL1	follistatin like 1	Extracellular Space	Other
189233525	GALR1	galanin receptor 1	Plasma Membrane	G-protein coupled receptor

GI Number	Gene Symbol	Protein Name	Location	Type(s)
50759498	GKN2	gastrokine 2	Extracellular Space	Other
57524920	GPI	glucose-6-phosphate isomerase	Extracellular Space	enzyme
45384386	GSN	Gelsolin	Extracellular Space	Other
45382731	HAPLN1	hyaluronan and proteoglycan link protein 1	Extracellular Space	Other
363737594	HAPLN3	hyaluronan and proteoglycan link protein 3	Extracellular Space	Other
363742669	HDGF	hepatoma-derived growth factor	Extracellular Space	growth factor
45383562	HSP90B1	heat shock protein 90kDa beta family member 1	Cytoplasm	Other
45382769	HSPA5	heat shock protein family A (Hsp70) member 5	Cytoplasm	enzyme
61098372	HSPD1	heat shock protein family D (Hsp60) member 1	Cytoplasm	enzyme
94536813	HSPG2	heparan sulfate proteoglycan 2	Extracellular Space	enzyme
1708386	IGFBP2	insulin like growth factor binding protein 2	Extracellular Space	Other
363733410	IGFBP7	insulin like growth factor binding protein 7	Extracellular Space	transporter
195539501	ITIH2	inter-alpha-trypsin inhibitor heavy chain 2	Extracellular Space	Other
45382221	LCN8	extracellular fatty acid-binding protein (lipocalin 8)	Extracellular Space	transporter
513175427	LTBP1	latent transforming growth factor beta binding protein 1	Extracellular Space	Other
45384212	LYZ	Lysozyme	Extracellular Space	enzyme
52694650	MCAM	melanoma cell adhesion molecule	Plasma Membrane	Other
33312179	MDK	midkine (neurite growth-promoting factor 2)	Extracellular Space	growth factor
513220000	MFAP2	microfibrillar associated protein 2	Extracellular Space	Other
363740226	MIF	macrophage migration inhibitory factor (glycosylation-inhibiting factor)	Extracellular Space	cytokine
45383321	MMP2	matrix metallopeptidase 2	Extracellular Space	peptidase

GI Number	Gene Symbol	Protein Name	Location	Type(s)
363742157	MOB1A	MOB kinase activator 1A	Plasma Membrane	Other
513225742	MRC2	mannose receptor, C type 2	Plasma Membrane	transmembrane receptor
45382603	MST1	macrophage stimulating 1	Extracellular Space	growth factor
71897111	NAMPT	nicotinamide phosphoribosyltransferase	Extracellular Space	cytokine
383387814	NCAM1	neural cell adhesion molecule 1	Plasma Membrane	Other
363731606	NID1	nidogen 1	Extracellular Space	Other
513190075	NID2	nidogen 2	Extracellular Space	Other
71894903	NPC2	Niemann-Pick disease, type C2	Extracellular Space	Other
45382529	NPPA	natriuretic peptide A	Extracellular Space	Other
57530004	NUCB2	nucleobindin 2	Nucleus	Other
164452937	NUDT1	nudix hydrolase 1	Extracellular Space	phosphatase
45382147	NUDT16L1	nudix hydrolase 16 like 1	Cytoplasm	Other
513196058	OLFML2B	olfactomedin like 2B	Extracellular Space	Other
123891643	OLFML3	olfactomedin like 3	Extracellular Space	Other
312283582	P4HB	prolyl 4-hydroxylase, beta polypeptide	Cytoplasm	enzyme
45383890	PDIA3	protein disulfide isomerase family A member 3	Cytoplasm	peptidase
50745031	PDIA6	protein disulfide isomerase family A member 6	Cytoplasm	enzyme
54111425	PLOD1	procollagen-lysine, 2-oxoglutarate 5-dioxygenase 1	Cytoplasm	enzyme
513240689	PNOC	Prepronociceptin	Extracellular Space	Other
71896385	POSTN	periostin, osteoblast specific factor	Extracellular Space	Other
45382027	PPIB	peptidylprolyl isomerase B	Cytoplasm	enzyme
513240689	PPIL1	peptidylprolyl isomerase like 1	Plasma Membrane	enzyme

GI Number	Gene Symbol	Protein Name	Location	Type(s)
45382219	PSAP	Prosaposin	Extracellular Space	Other
71895723	PTK7	protein tyrosine kinase 7 (inactive)	Plasma Membrane	kinase
444741724	PTN	Pleiotrophin	Extracellular Space	growth factor
513197616	PTPRF	protein tyrosine phosphatase, receptor type F	Plasma Membrane	phosphatase
513177250	PTPRK	protein tyrosine phosphatase, receptor type K	Plasma Membrane	phosphatase
46048665	PTPRS	protein tyrosine phosphatase, receptor type S	Plasma Membrane	phosphatase
62899037	PTX3	pentraxin 3	Extracellular Space	Other
513178768	PXDN	Peroxidasin	Extracellular Space	enzyme
45383856	QSOX1	quiescin sulfhydryl oxidase 1	Cytoplasm	enzyme
363732860	RAB39B	RAB39B, member RAS oncogene family	Plasma Membrane	enzyme
82231235	RAB8A	RAB8A, member RAS oncogene family	Plasma Membrane	enzyme
45384330	RAC1	ras-related C3 botulinum toxin substrate 1	Plasma Membrane	enzyme
57529989	RNH1	ribonuclease/angiogenin inhibitor 1	Cytoplasm	Other
145046232	SERPINE 2	serpin peptidase inhibitor, clade E , member 2	Extracellular Space	Other
363734612	SERPING 1	serpin peptidase inhibitor, clade G (C1 inhibitor), member 1	Extracellular Space	Other
52138719	SERPINI1	serpin peptidase inhibitor, clade I (neuroserpin), member 1	Extracellular Space	Other
45384218	SOD1	superoxide dismutase 1, soluble	Cytoplasm	enzyme
513184692	SOD3	superoxide dismutase 3, extracellular	Extracellular Space	enzyme
45383337	SPARC	secreted protein, acidic, cysteine-rich (osteonectin)	Extracellular Space	Other
45382337	SPON1	spondin 1	Extracellular Space	Other
45383105	SPP1	secreted phosphoprotein 1	Extracellular Space	cytokine
110227609	SPTAN1	spectrin alpha, non-erythrocytic 1	Plasma Membrane	Other

GI Number	Gene Symbol	Protein Name	Location	Type(s)
313661476	SPTBN1	spectrin beta, non-erythrocytic 1	Plasma Membrane	Other
363738949	STC2	stanniocalcin 2	Extracellular Space	Other
4033470	STMN2	stathmin 2	Plasma Membrane	Other
347800736	STRAP	serine/threonine kinase receptor associated protein	Plasma Membrane	Other
61098428	STX7	syntaxin 7	Plasma Membrane	transporter
45385813	TF	Transferrin	Extracellular Space	transporter
45383950	TFRC	transferrin receptor	Plasma Membrane	transporter
513174887	TGFB2	transforming growth factor beta 2	Extracellular Space	growth factor
45384294	TGFBI	transforming growth factor beta induced	Extracellular Space	Other
313661364	THBS1	thrombospondin 1	Extracellular Space	Other
48976107	THBS2	thrombospondin 2	Extracellular Space	Other
45383544	TIMP2	TIMP metallopeptidase inhibitor 2	Extracellular Space	Other
45383127	TLN1	talin 1	Plasma Membrane	Other
47604946	TMSB4X	thymosin beta 4, X-linked	unmapped by IPA	
312032350	TNC	tenascin C	Extracellular Space	Other
45382329	TPT1	tumor protein, translationally-controlled 1	Cytoplasm	Other
57530789	TXNDC5	thioredoxin domain containing 5	Cytoplasm	Enzyme
57529406	VAPB	VAMP (vesicle-associated membrane protein)-associated protein B and C	Plasma Membrane	Other
46048882	VCAN	Versican	Extracellular Space	Other
45382123	VCL	Vinculin	Plasma Membrane	Enzyme
52138693	WDR1	WD repeat domain 1	Extracellular Space	Other

Appendix C. Over-represented IPA Canonical Pathways in the EHE secretome

TABLE V. OVER-REPRESENTED IPA CANONICAL PATHWAYS[1] (P-VALUE < 0.05) IN THE EHE SECRETOME

Ingenuity Canonical Pathways	-log(p-value)	Ratio	Molecules
Hepatic Fibrosis / Hepatic Stellate Cell Activation	8.28E00	6.56E-02	COL5A1,COL1A2,COL5A2,FN1,CTGF,COL2A1,TGFB2,MMP2,COL18A1,A2M,COL3A1,TIMP2
Clathrin-mediated Endocytosis Signaling	6.2E00	5.41E-02	ACTR2,LYZ,ACTR3,APOA1,TF,CLTA,AP2B1,CLTC,RAC1,TFRC
Lipid Antigen Presentation by CD1*	6.07E00	1.92E-01	B2M,CALR,PDIA3,AP2B1,PSAP
RhoGDI Signaling[#]	5.49E00	5.2E-02	ACTR2,CDH2,ACTR3,CFL2,CDH5,EZR,RAC1,CDH13,CDH11
Inhibition of Matrix Metalloproteases[#]	5.16E00	1.28E-01	HSPG2,THBS2,MMP2,A2M,TIMP2
Actin Cytoskeleton Signaling	4.72E00	4.17E-02	ACTR2,ACTR3,FN1,CFL2,EZR,RAC1,TLN1,VCL,GSN
Virus Entry via Endocytic Pathways	4.46E00	6.74E-02	B2M,CLTA,AP2B1,CLTC,RAC1,TFRC
Signaling by Rho Family GTPases[#]	4.44E00	3.85E-02	ACTR2,CDH2,ACTR3,CFL2,CDH5,EZR,RAC1,CDH13,CDH11
Intrinsic Prothrombin Activation Pathway	4.35E00	1.38E-01	COL1A2,COL2A1,COL18A1,COL3A1
Germ Cell-Sertoli Cell Junction Signaling	3.91E00	4.38E-02	CDH2,CFL2,RAC1,TGFB2,VCL,GSN,A2M
Atherosclerosis Signaling	3.66E00	4.84E-02	COL1A2,LYZ,APOA1,COL2A1,COL18A1,COL3A1
Endoplasmic Reticulum Stress Pathway*	3.41E00	1.43E-01	CALR,HSP90B1,HSPA5
Leukocyte Extravasation Signaling	3.35E00	3.54E-02	CD99,CDH5,EZR,RAC1,MMP2,VCL,TIMP2
Fcγ Receptor-mediated Phagocytosis in Macrophages and Monocytes	3.34E00	5.38E-02	ACTR2,ACTR3,EZR,RAC1,TLN1
Unfolded protein response*	3.28E00	7.41E-02	CALR,P4HB,HSP90B1,HSPA5
Epithelial Adherens Junction Signaling	3.28E00	4.11E-02	ACTR2,CDH2,ACTR3,RAC1,TGFB2,VCL
Regulation of Cellular Mechanics by Calpain Protease	3.19E00	7.02E-02	CNGA4,EZR,TLN1,VCL
Acute Phase Response Signaling	2.95E00	3.55E-02	SERPING1,FN1,APOA1,TF,ITIH2,A2M
Superoxide Radicals Degradation*	2.89E00	2.5E-01	SOD1,SOD3
Dendritic Cell Maturation	2.84E00	3.39E-02	B2M,COL1A2,PDIA3,COL2A1,COL18A1,COL3A1

Ingenuity Canonical Pathways	-log(p-value)	Ratio	Molecules
Antigen Presentation Pathway*	2.68E00	8.11E-02	B2M,CALR,PDIA3
Integrin Signaling#	2.5E00	2.9E-02	ACTR2,ACTR3,RAC1,TLN1,VCL,GSN
CTLA4 Signaling in Cytotoxic T Lymphocytes*	2.49E00	4.55E-02	B2M,CLTA,AP2B1,CLTC
Regulation of Actin-based Motility by Rho	2.44E00	4.4E-02	ACTR2,ACTR3,RAC1,GSN
Rac Signaling	2.24E00	3.85E-02	ACTR2,ACTR3,CFL2,RAC1
Actin Nucleation by ARP-WASP Complex	2.17E00	5.36E-02	ACTR2,ACTR3,RAC1
Role of Tissue Factor in Cancer	2.15E00	3.64E-02	P4HB,CTGF,CFL2,RAC1
Gα12/13 Signaling	2.06E00	3.42E-02	CDH2,CDH5,CDH13,CDH11
Sperm Motility*	2.01E00	3.31E-02	CNGA4,PDIA3,NPPA,PTK7
Agranulocyte Adhesion and Diapedesis	2E00	2.65E-02	CD99,FN1,CDH5,EZR,MMP2
RhoA Signaling#	2E00	3.28E-02	ACTR2,ACTR3,CFL2,EZR
Remodeling of Epithelial Adherens Junctions	1.94E00	4.41E-02	ACTR2,ACTR3,VCL
Glucocorticoid Receptor Signaling	1.92E00	2.18E-02	HSP90B1,RAC1,TGFB2,NPPA,HSPA5,A2M
IL-12 Signaling and Production in Macrophages	1.87E00	3.01E-02	LYZ,APOA1,TGFB2,MST1
Ephrin B Signaling#	1.85E00	4.11E-02	CFL2,RAC1,CAP1
Thyroid Hormone Biosynthesis*	1.69E00	3.33E-01	CTSD
Oxidized GTP and dGTP Detoxification*	1.69E00	3.33E-01	NUDT1
Aldosterone Signaling in Epithelial Cells*	1.68E00	2.63E-02	HSP90B1,PDIA3,HSPD1,HSPA5
FAK Signaling	1.65E00	3.45E-02	RAC1,TLN1,VCL
Inhibition of Angiogenesis by TSP1*	1.64E00	5.88E-02	HSPG2,THBS1
Complement System*	1.57E00	5.41E-02	CFD,SERPING1
Glutathione Redox Reactions II*	1.56E00	2.5E-01	PDIA3
Tight Junction Signaling	1.55E00	2.4E-02	RAC1,TGFB2,SPTAN1,VCL
Cdc42 Signaling#	1.55E00	2.4E-02	B2M,ACTR2,ACTR3,CFL2
IGF-1 Signaling#	1.52E00	3.10E-02	CTGF, IGFBP2, IGFBP7
Wnt/β-catenin Signaling#	1.52E00	2.37E-02	CDH2,CDH5,DKK3,TGFB2
Neuroprotective Role of THOP1 in Alzheimer's Disease*	1.5E00	5.00E-02	APP, PNOC
Ephrin Receptor Signaling	1.49E00	2.3E-02	ACTR2,ACTR3,CFL2,RAC1
Paxillin Signaling	1.49E00	2.97E-02	RAC1,TLN1,VCL
Eumelanin Biosynthesis*	1.47E00	2E-01	MIF

Ingenuity Canonical Pathways	-log(p-value)	Ratio	Molecules
PPARα/RXRα Activation	1.46E00	2.30E-02	HSP90B1,APOA1,PDIA3,TGFB2
Granulocyte Adhesion and Diapedesis	1.46E00	2.26E-02	CD99,CDH5,EZR,MMP2
Sertoli Cell-Sertoli Cell Junction Signaling	1.46E00	2.25E-02	RAC1,SPTAN1,VCL,A2M
NRF2-mediated Oxidative Stress Response*	1.44E00	2.22E-02	ERP29,PPIB,SOD1,SOD3
fMLP Signaling in Neutrophils	1.41E00	2.78E-02	ACTR2,ACTR3,RAC1
phagosome formation	1.4E00	2.75E-02	FN1,MRC2,PDIA3
NAD Biosynthesis III*	1.39E00	1.67E-01	NAMPT
GDP-mannose Biosynthesis*	1.39E00	1.67E-01	GPI
Ephrin A Signaling	1.36E00	4.17E-02	CFL2,RAC1
CD28 Signaling in T Helper Cells	1.32E00	2,54E-02	ACTR2,ACTR3,RAC1

[*] For these pathways, none of the identified molecules has been previously implicated in epicardial-myocardial signaling

[#] For these pathways, which have known roles in epicardial-myocardial signaling, MS identified one or more regulatory components that have not been previously implicated in the process.

[1] As defined in the IPA library.

Appendix D. Primers used in qRT-PCR

TABLE VI. PRIMERS USED IN QRT-PCR

Gene	Sense primer (5'-3')	Anti-sense primer (5'-3')
GAPDH	ACGGGAAACTTGTGATCAATGGGC	TCAGATGAGCCCCAGCCTTCTC
WT1	AACCAAATGAACCTGGGATCCACG	CGTCGGACATCTTGTATGCCTCTAAAG
MMP2	TGCCTTTGCCCGAGCCTTTAAAG	GCCAGGAGACCATCTTTGCCA
DCN	GAACTAGGCACCAATCCACTCAAGAG	AGGTGAAGCTCAGTAAGGGATGGAG

Appendix E. Primers used for reverse-transcriptase PCR

TABLE VII. PRIMERS USED FOR REVERSE-TRANSCRIPTASE PCR

Gene	Sense primer (5'-3')	Anti-sense primer (5'-3')
CST3	AGCTGCGAATTCCACGATGA	CCAAGAGAGGCTTACTGGCA
THBS1	TGTAGACCAGAGGGACACAGA	TCACAGGCATCACCTTTTCCA
NAMPT	TGCATAGGACACCTGCTGGA	TCAGCCTGGCATTTTGCCTT
CTGF	CCGCCTACAGACTGGAAGAC	TGGAGATTTTTGGGGTGCGA
FSTL1	CTCAGCCCATCCTTCAACCC	ATTGCAGTGCACACCCAGTT
PTX3	CCCAAGAAACAGCTTTCCAGC	CTTTCTGGAGCGCATTGGGA
DRAXIN	CTCTTGCTGTGACTTGCGTG	CTCTCCATTGGCCGACTCAG
IGFBP2	CCCATCACAACCACGAGGAC	TGCTTGTCACAGTTGGGGAT
IGFBP7	AGTCATTGGCATCCCAACCC	TACCCAGCCGGTCACTTCAT
DCN	ACCTAGTGGGTTGGGTGAAC	TGGTGTTGTAGCCAAGAGGG
DKK3	TCACCTGGGAACTGGGAACCT	GCACTTCCTGAATGACGCTG
MDK	TGGTCTATGTGAGCAAGCCC	GAGGCACATGTGTCCGGG
SPP1	GAACAGCCGGACTTTCCTGA	CCTCAATGAGCTTCCTGGCA
MIF	TTGGCAAAATTGGAGGGCAG	TCTATGCAAAGGTGGAACCGT
TGFBI	CCACAGGGGGAACTCAACAA	TGTCTCCCTGCATGGACTTG
AIMP1	TTGGAGAAGCGAGCCCAA	AACTGGGGGAGCCAGAATTT
PTN	CCTGCAACTGGAAGAAGCAAT	GCAAATTGAAATTACCTTGAGGT
mTGFBR	GCCAGACGGCTACGAAGATTT	AACACTACCACTCCAGCACGG
mβMHC	TCTCCTGCTGTTTCCTTACTTGCT	CAGGCCTGTAGGAGAGCTGTACTC
mαMHC	GTCACCAACAACCCATACGACTAC	CAGCACATCAAAGGCACTATCAGT
mANP	AGGAGAAGATGCCGGTAGAAGA	GCTTCCTCAGTCTGCTCACTCA
mACTC1	ACCCAGATCATGTTTGAGACC	TTACACCATCGCCAGAATCC
mGJA1	GAAAGGCGTGAGGGAAGTAC	GAAAATGAAGAGCACCGACAG

Appendix F. Investigation of ASXL2's protein interactions

Purpose and objective

ASXL2 is an epigenetic regulator belonging to the Enhancers of Trithorax and Polycomb (ETP) group. ETP proteins play dual roles in transcriptional activation and repression. Previous studies in our lab have shown that ASXL2 is highly expressed in the heart and plays important roles in heart development and function (Baskind et al., 2009; Khan et al., 2014; Lai et al., 2012). To understand the molecular mechanisms underlying ASXL2's functions in the heart, a yeast-two hybrid screening was performed previously in the lab to identify candidates of ASXL2 protein partners (Khan et al., 2014). The screen identified genetic interaction between the C-terminal of ASXL2 with the N-terminal of ZMIZ1(Khan, 2014) as well as confirmed interaction between ASXL2 and the histone deubiquitinase BAP1 (Alonso et al., 2010; Lai and Wang, 2013). Since the Drosophila homolog of ZMIZ1 genetically interacts with the TrxG gene *brahma* and is required for proper Hox gene expression (Gutiérrez et al., 2003), here I asked whether ASXL2 interact with ZMIZ1 in mammalian cells.

Materials and methods

Plasmids

pYX-Asc-BAP1 was obtained from Invitrogen. Full length BAP1 cDNAs was subcloned in frame into pDONR221 vector and subsequently transferred into a destination vector pT-REX-DEST30, generating the pT-REX-DEST30-BAP1. The mouse $ASXL2_{731\text{-}1370}$ cDNA was generated via PCR and subcloned into the pCDNA3 vector (Invitrogen), generating the pCDNA3-FLAG-ASXL2-C plasmid. pCS2-HA-ZMIZ1 was generous gift from Dr. Zijie Sun (Stanford University). FLAG-$ASXL2_{1\text{-}720}$ was inserted into pCAG vector to generate pCDNA3-FLAG-ASXL2-N.

Appendix F. Investigation of ASXL2's protein interactions (continued)

Co-immunoprecipitations (co-IPs)

HEK293 cells were seeded with ~20% confluency and cultured overnight before adding 1 ml DMEM, 9 ug total plasmid DNA and 27 ul branched polyethylenimine (PEI) (Sigma-Aldrich). HEK293 cells were harvested 48 hours post-transfection by centrifugation at 1000 g at 4°C for 5 minutes. The pellet was re-suspended in 1 ml low salt lysis buffer (150 mM NaCl; 1% Triton-X 100; 50 mM Tris-Cl, pH 7.4) supplemented with protease inhibitor cocktail (Calbiochem). After 20 minutes of lysis, solution was centrifuged and the supernatant is the input (inp) for immunoprecipitation (IP). The supernatant was incubated with 30 ul anti-FLAG M2 magnetic beads (Sigma-Aldrich) and incubated overnight at 4°C on a rotating platform. The next day, beads were separated by a magnetic separator and were washed 3 times in wash buffer (50 mM Tris-HCl, pH 7.4; 150 mM NaCl). The flow through (FT) of the first wash was saved. After the last wash, 50 ul SDS sample buffer (Sigma-Aldrich) was added to samples and boiled for 5 minutes to elute the proteins before storage at -20°C. The samples were now ready for SDS-PAGE and immunoblotting using antibodies against the tagged proteins.

Results and conclusions

Co-IP assays were performed to determine whether ASXL2 interacts with ZMIZ1 in mammalian cells. Co-IP using BAP1 and FLAG-ASXL2-N was performed as positive control (Fig 42A, Appendix F). FLAG-ASXL2-C did not co-IP with HA-tagged ZMIZ1 in double transfected cells, instead HA-tagged ZMIZ1 was detected in the flow through fraction (Fig 42B, Appendix F). This result indicates that ZMIZ1 doesn't interact with C-terminal of ASXL2 in the experimental setting used.

Appendix F. Investigation of ASXL2's protein interactions (continued)

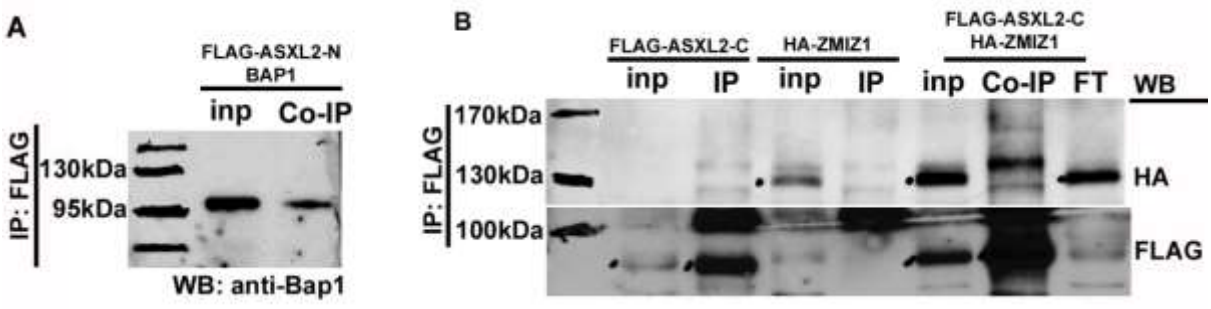

Figure 42. Biochemical characterization of ASXL2 and ZMIZ1 interaction. (A) HEK293 cells were transiently transfected with FALG-ASXL2-N and BAP1. Proteins were IPed using anti-FLAG beads. (B) FLAG-ASXL2-C, HA-ZMIZ1 or both constructs. Proteins were IPed using anti-FLAG beads. Input (inp), IP fractions and flow through (FT) were used for SDS-PAGE followed by Western blot (WB) analysis.

Appendix G. Establish culture of a cardiac muscle cell line HL-1

Purpose and objective

Previous studies in our lab have shown that ASXL2 is highly expressed in the heart and plays important roles in heart development and function (Baskind et al., 2009; Khan et al., 2014; Lai et al., 2012). The fundamental cell type that supports the function of the mammalian heart is the cardiomyocyte. Therefore, it was important to investigate the mechanism of ASXL2 function in the context of cardiomyocytes. Here I describe the protocol of culturing a cardiac muscle cell line HL-1 as a cell model for these investigations.

Materials and methods

Culture of HL-1 Cells

HL-1 cells were HL-1 cells derived from mouse atrial cardiac muscle cells (a generous gift from Dr. William Claycomb, Louisiana State University Health Sciences Center, New Orleans, LA, USA) were cultured in tissue culture incubator with 5% CO2 at 37°C in Claycomb medium (Sigma, #51800C) supplemented with 10% FBS, Penicillin/Streptomycin (100 μg/ml), Norepinephrine (0.1mM) and L-Glutamine (2mM). HL-1 cells were seeded in fibronectin/gelatin-precoated dishes as described in the protocol provided by Claycomb lab. The cultures are split 1:2 only after full confluence.

Reverse transcriptase PCR

Total RNA was extracted from HL-1 cells or neonatal mouse heart tissue using the RNeasy mini kit (Qiagen, CA, USA). Reverse transcriptase PCR was performed using the OneStep RT-PCR kit (Qiagen, CA, USA). QuantumRNA Universal 18S Internal Standard (Applied Biosystems) was used to analyze 18s rRNA.

Appendix G. Establish culture of a cardiac muscle cell line HL-1 (continued)

Western blotting

HL-1 cells were lysed and homogenized by passing through 21-gauge needle in RIPA buffer (Sigma) supplemented with protease inhibitors cocktail (EMD Millipore). Cell lysate was suspended with 2x Laemmli sample buffer, separated by SDS-PAGE and detected using the following primary antibodies: anti-cardiac troponin T (Thermo Scientific, MS-295), anti-cardiac α-actinin (Sigma). Appropriate HRP-conjugated secondary antibodies (Jackson ImmunoResearch) were then used. The reactivity was revealed by Immobilon Western chemiluminescence (Millipore).

Infection

Recombinant adenovirus expressing GFP (AdGFP) was used to infect HL-1 cells. Cells were incubated in complete medium supplemented with adenoviral particles (MOI=500) for 48 h before examined under fluorescent microscope.

Results and conclusions

To confirm that the HL-1 cells we received indeed possess phenotypic characteristics of adult cardiomyocytes, I performed cell morphological and expression analyses of cardiac specific genes. Cultured HL-1 cells exhibited synchronous beating in confluent cultures (data not shown). Western blot analysis revealed that HL-1 cells express cardiac troponin T and α-actinin (Fig 43A, Appendix G), which are expected to be expressed in cardiomyocytes. RT-PCR analysis further showed that HL-1 cells express the adult isoform of MHC (α-MHC) but not the embryonic isoform of myosin (β-MHC) (Fig 43B,C). Similar to adult mouse ventricle cells, HL-1 cells also express

α-cardiac actin, ANF and connexin43 (the major protein of the adult gap junction) (Fig 43C, Appendix G). AdGFP

infection of HL-1 cells showed a high infection rate (>80%) (Fig 43D, Appendix G). These results indicate that HL-1 cells at least partially retained features of adult atrial cardiomyocytes and can be genetically manipulated by adenovirus infection.

Appendix G. Establish culture of a cardiac muscle cell line HL-1 (continued)

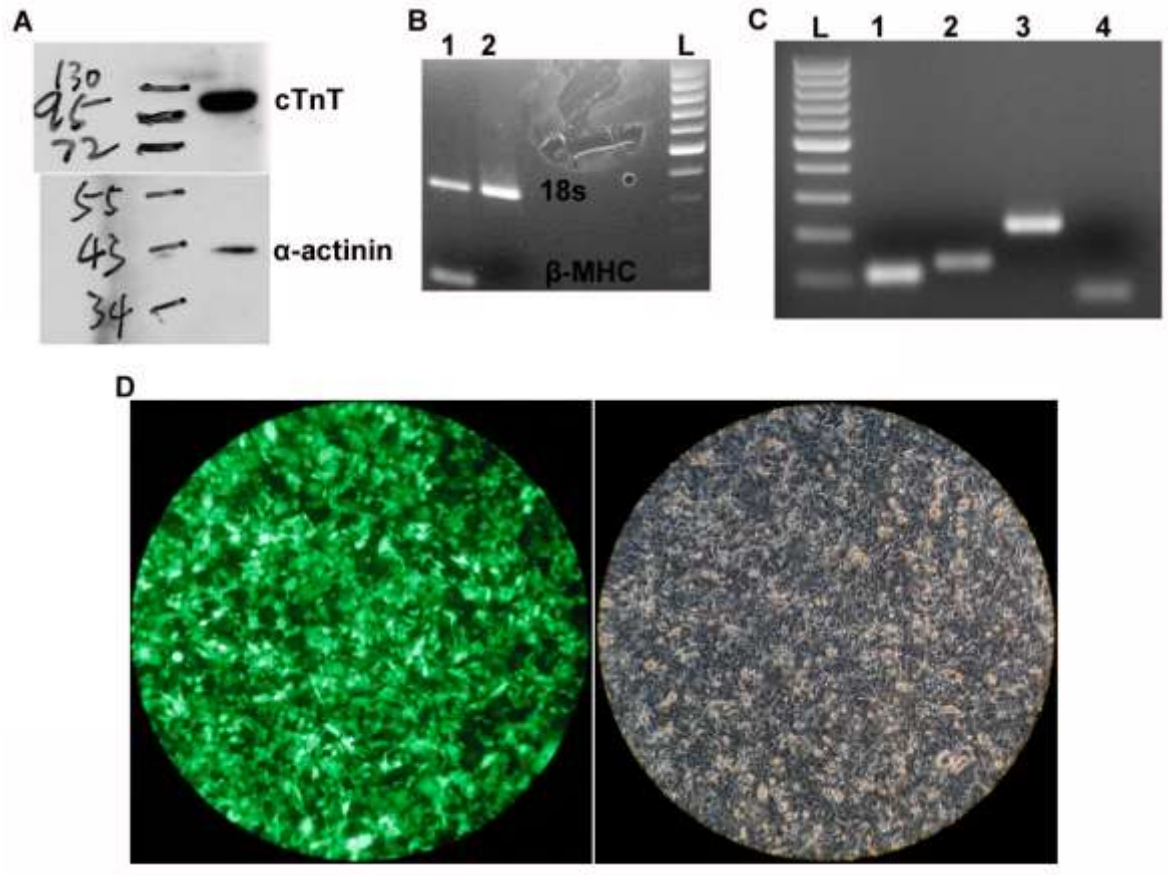

Figure 43. Culture and characterization of HL-1 cells. (A) Western blot analysis of cardiac Troponin T (cTnT) and α-actinin. (B) RT-PCR analysis for transcription of β-MHC. L: 100bp DNA ladder; lane 1 = RNA isolated from neonatal mouse heart tissue; lane 2 = RNA isolated from HL-1 cells. (C) RT-PCR analysis for transcription of select genes. L: 100bp DNA ladder; lane 1 = α-MHC (adult isoform); lane 2 = α-cardic actin; lane 3 = connexin43 (the major protein of the adult gap junction); lane 4, atrial natriuretic factor (ANF). (D) HL-1 cells infected with AdGFP (left) and corresponding phase contrast image (right).

Appendix H. Creative Commons Attribution License

Creative Commons Legal Code

Attribution 4.0 International

Official translations of this license are available in other languages.

Creative Commons Corporation ("Creative Commons") is not a law firm and does not provide legal services or legal advice. Distribution of Creative Commons public licenses does not create a lawyer-client or other relationship. Creative Commons makes its licenses and related information available on an "as-is" basis. Creative Commons gives no warranties regarding its licenses, any material licensed under their terms and conditions, or any related information. Creative Commons disclaims all liability for damages resulting from their use to the fullest extent possible.

Using Creative Commons Public Licenses

Creative Commons public licenses provide a standard set of terms and conditions that creators and other rights holders may use to share original works of authorship and other material subject to copyright and certain other rights specified in the public license below. The following considerations are for informational purposes only, are not exhaustive, and do not form part of our licenses.

Considerations for licensors: *Our public licenses are intended for use by those authorized to give the public permission to use material in ways otherwise restricted by copyright and certain other rights. Our licenses are irrevocable. Licensors should read and understand the terms and conditions of the license they choose before applying it. Licensors should also secure all rights necessary before applying our licenses so that the public can reuse the material as expected. Licensors should clearly mark any material not subject to the license. This includes other CC-licensed material, or material used under an exception or limitation to copyright. More considerations for licensors.*

Considerations for the public: *By using one of our public licenses, a licensor grants the public permission to use the licensed material under specified terms and conditions. If the licensor's permission is not necessary for any reason–for example, because of any applicable exception or limitation to copyright–then that use is not regulated by the license. Our licenses grant only permissions under copyright and certain other rights that a licensor has authority to grant. Use of the licensed material may still be restricted for other reasons, including because others have copyright or other rights in the material. A licensor may make special requests, such as asking that all changes be marked or described. Although not required by our licenses, you are encouraged to respect those requests where reasonable. More considerations for the public.*

Creative Commons Attribution 4.0 International Public License

By exercising the Licensed Rights (defined below), You accept and agree to be bound by the terms and conditions of this Creative Commons Attribution 4.0 International Public License ("Public License"). To the extent this Public License may be interpreted as a contract, You are granted the Licensed Rights in consideration of Your acceptance of these terms and conditions, and the Licensor grants You such rights in consideration of benefits the Licensor receives from making the Licensed Material available under these terms and conditions.

Appendix H. Creative Commons Attribution License (continued)

Section 1 – Definitions.

a. **Adapted Material** means material subject to Copyright and Similar Rights that is derived from or based upon the Licensed Material and in which the Licensed Material is translated, altered, arranged, transformed, or otherwise modified in a manner requiring permission under the Copyright and Similar Rights held by the Licensor. For purposes of this Public License, where the Licensed Material is a musical work, performance, or sound recording, Adapted Material is always produced where the Licensed Material is synched in timed relation with a moving image.
b. **Adapter's License** means the license You apply to Your Copyright and Similar Rights in Your contributions to Adapted Material in accordance with the terms and conditions of this Public License.
c. **Copyright and Similar Rights** means copyright and/or similar rights closely related to copyright including, without limitation, performance, broadcast, sound recording, and Sui Generis Database Rights, without regard to how the rights are labeled or categorized. For purposes of this Public License, the rights specified in Section 2(b)(1)-(2) are not Copyright and Similar Rights.
d. **Effective Technological Measures** means those measures that, in the absence of proper authority, may not be circumvented under laws fulfilling obligations under Article 11 of the WIPO Copyright Treaty adopted on December 20, 1996, and/or similar international agreements.
e. **Exceptions and Limitations** means fair use, fair dealing, and/or any other exception or limitation to Copyright and Similar Rights that applies to Your use of the Licensed Material.
f. **Licensed Material** means the artistic or literary work, database, or other material to which the Licensor applied this Public License.
g. **Licensed Rights** means the rights granted to You subject to the terms and conditions of this Public License, which are limited to all Copyright and Similar Rights that apply to Your use of the Licensed Material and that the Licensor has authority to license.
h. **Licensor** means the individual(s) or entity(ies) granting rights under this Public License.
i. **Share** means to provide material to the public by any means or process that requires permission under the Licensed Rights, such as reproduction, public display, public performance, distribution, dissemination, communication, or importation, and to make material available to the public including in ways that members of the public may access the material from a place and at a time individually chosen by them.
j. **Sui Generis Database Rights** means rights other than copyright resulting from Directive 96/9/EC of the European Parliament and of the Council of 11 March 1996 on the legal protection of databases, as amended and/or succeeded, as well as other essentially equivalent rights anywhere in the world.
k. **You** means the individual or entity exercising the Licensed Rights under this Public License. **Your** has a corresponding meaning.

Section 2 – Scope.

a. **License grant.**
    1. Subject to the terms and conditions of this Public License, the Licensor hereby grants You a worldwide, royalty-free, non-sublicensable, non-exclusive, irrevocable license to exercise the Licensed Rights in the Licensed Material to:
        A. reproduce and Share the Licensed Material, in whole or in part; and
        B. produce, reproduce, and Share Adapted Material.
    2. Exceptions and Limitations. For the avoidance of doubt, where Exceptions and Limitations apply to Your use, this Public License does not apply, and You do not need to comply with its terms and conditions.
    3. Term. The term of this Public License is specified in Section 6(a).
    4. Media and formats; technical modifications allowed. The Licensor authorizes You to exercise the Licensed Rights in all media and formats whether now known or hereafter created, and to make technical modifications necessary to do so. The Licensor waives and/or agrees not to assert any right or authority to forbid You from making technical modifications necessary to exercise the Licensed Rights, including technical modifications necessary to circumvent Effective Technological Measures. For purposes of this Public License, simply making modifications authorized by this Section 2(a)(4) never produces Adapted Material.
    5. Downstream recipients.
        A. Offer from the Licensor – Licensed Material. Every recipient of the Licensed Material

Appendix H. Creative Commons Attribution License (continued)

automatically receives an offer from the Licensor to exercise the Licensed Rights under the terms and conditions of this Public License.

B. No downstream restrictions. You may not offer or impose any additional or different terms or conditions on, or apply any Effective Technological Measures to, the Licensed Material if doing so restricts exercise of the Licensed Rights by any recipient of the Licensed Material.

6. No endorsement. Nothing in this Public License constitutes or may be construed as permission to assert or imply that You are, or that Your use of the Licensed Material is, connected with, or sponsored, endorsed, or granted official status by, the Licensor or others designated to receive attribution as provided in Section 3(a)(1)(A)(i).

b. **Other rights**.

1. Moral rights, such as the right of integrity, are not licensed under this Public License, nor are publicity, privacy, and/or other similar personality rights; however, to the extent possible, the Licensor waives and/or agrees not to assert any such rights held by the Licensor to the limited extent necessary to allow You to exercise the Licensed Rights, but not otherwise.
2. Patent and trademark rights are not licensed under this Public License.
3. To the extent possible, the Licensor waives any right to collect royalties from You for the exercise of the Licensed Rights, whether directly or through a collecting society under any voluntary or waivable statutory or compulsory licensing scheme. In all other cases the Licensor expressly reserves any right to collect such royalties.

Section 3 – License Conditions.

Your exercise of the Licensed Rights is expressly made subject to the following conditions.

a. **Attribution**.

1. If You Share the Licensed Material (including in modified form), You must:

A. retain the following if it is supplied by the Licensor with the Licensed Material:
i. identification of the creator(s) of the Licensed Material and any others designated to receive attribution, in any reasonable manner requested by the Licensor (including by pseudonym if designated);
ii. a copyright notice;
iii. a notice that refers to this Public License;
iv. a notice that refers to the disclaimer of warranties;
v. a URI or hyperlink to the Licensed Material to the extent reasonably practicable;

B. indicate if You modified the Licensed Material and retain an indication of any previous modifications; and

C. indicate the Licensed Material is licensed under this Public License, and include the text of, or the URI or hyperlink to, this Public License.

2. You may satisfy the conditions in Section 3(a)(1) in any reasonable manner based on the medium, means, and context in which You Share the Licensed Material. For example, it may be reasonable to satisfy the conditions by providing a URI or hyperlink to a resource that includes the required information.
3. If requested by the Licensor, You must remove any of the information required by Section 3(a)(1)(A) to the extent reasonably practicable.
4. If You Share Adapted Material You produce, the Adapter's License You apply must not prevent recipients of the Adapted Material from complying with this Public License.

Section 4 – Sui Generis Database Rights.

Where the Licensed Rights include Sui Generis Database Rights that apply to Your use of the Licensed Material:

a. for the avoidance of doubt, Section 2(a)(1) grants You the right to extract, reuse, reproduce, and Share all or a substantial portion of the contents of the database;
b. if You include all or a substantial portion of the database contents in a database in which You have

Appendix H. Creative Commons Attribution License (continued)

Sui Generis Database Rights, then the database in which You have Sui Generis Database Rights (but not its individual contents) is Adapted Material; and

c. You must comply with the conditions in Section 3(a) if You Share all or a substantial portion of the contents of the database.

For the avoidance of doubt, this Section 4 supplements and does not replace Your obligations under this Public License where the Licensed Rights include other Copyright and Similar Rights.

Section 5 – Disclaimer of Warranties and Limitation of Liability.

a. **Unless otherwise separately undertaken by the Licensor, to the extent possible, the Licensor offers the Licensed Material as-is and as-available, and makes no representations or warranties of any kind concerning the Licensed Material, whether express, implied, statutory, or other. This includes, without limitation, warranties of title, merchantability, fitness for a particular purpose, non-infringement, absence of latent or other defects, accuracy, or the presence or absence of errors, whether or not known or discoverable. Where disclaimers of warranties are not allowed in full or in part, this disclaimer may not apply to You.**

b. **To the extent possible, in no event will the Licensor be liable to You on any legal theory (including, without limitation, negligence) or otherwise for any direct, special, indirect, incidental, consequential, punitive, exemplary, or other losses, costs, expenses, or damages arising out of this Public License or use of the Licensed Material, even if the Licensor has been advised of the possibility of such losses, costs, expenses, or damages. Where a limitation of liability is not allowed in full or in part, this limitation may not apply to You.**

c. The disclaimer of warranties and limitation of liability provided above shall be interpreted in a manner that, to the extent possible, most closely approximates an absolute disclaimer and waiver of all liability.

Section 6 – Term and Termination.

a. This Public License applies for the term of the Copyright and Similar Rights licensed here. However, if You fail to comply with this Public License, then Your rights under this Public License terminate automatically.

b. Where Your right to use the Licensed Material has terminated under Section 6(a), it reinstates:

   1. automatically as of the date the violation is cured, provided it is cured within 30 days of Your discovery of the violation; or
   2. upon express reinstatement by the Licensor.

   For the avoidance of doubt, this Section 6(b) does not affect any right the Licensor may have to seek remedies for Your violations of this Public License.

c. For the avoidance of doubt, the Licensor may also offer the Licensed Material under separate terms or conditions or stop distributing the Licensed Material at any time; however, doing so will not terminate this Public License.

d. Sections 1, 5, 6, 7, and 8 survive termination of this Public License.

Section 7 – Other Terms and Conditions.

a. The Licensor shall not be bound by any additional or different terms or conditions communicated by You unless expressly agreed.

b. Any arrangements, understandings, or agreements regarding the Licensed Material not stated herein are separate from and independent of the terms and conditions of this Public License.

Section 8 – Interpretation.

a. For the avoidance of doubt, this Public License does not, and shall not be interpreted to, reduce, limit, restrict, or impose conditions on any use of the Licensed Material that could lawfully be made without permission under this Public License.

b. To the extent possible, if any provision of this Public License is deemed unenforceable, it shall be

Appendix H. Creative Commons Attribution License (continued)

automatically reformed to the minimum extent necessary to make it enforceable. If the provision cannot be reformed, it shall be severed from this Public License without affecting the enforceability of the remaining terms and conditions.

c. No term or condition of this Public License will be waived and no failure to comply consented to unless expressly agreed to by the Licensor.

d. Nothing in this Public License constitutes or may be interpreted as a limitation upon, or waiver of, any privileges and immunities that apply to the Licensor or You, including from the legal processes of any jurisdiction or authority.

Creative Commons is not a party to its public licenses. Notwithstanding, Creative Commons may elect to apply one of its public licenses to material it publishes and in those instances will be considered the "Licensor." The text of the Creative Commons public licenses is dedicated to the public domain under the CC0 Public Domain Dedication. Except for the limited purpose of indicating that material is shared under a Creative Commons public license or as otherwise permitted by the Creative Commons policies published at creativecommons.org/policies, Creative Commons does not authorize the use of the trademark "Creative Commons" or any other trademark or logo of Creative Commons without its prior written consent including, without limitation, in connection with any unauthorized modifications to any of its public licenses or any other arrangements, understandings, or agreements concerning use of licensed material. For the avoidance of doubt, this paragraph does not form part of the public licenses.

Creative Commons may be contacted at creativecommons.org.

Additional languages available: Bahasa Indonesia, Deutsch, français, hrvatski, Nederlands, norsk, polski, suomeksi, svenska, te reo Māori, Türkçe, українська, العربية, 日本語. Please read the FAQ for more information about official translations.

Appendix I. Animal care committee letter of approval

UIC UNIVERSITY OF ILLINOIS AT CHICAGO

February 28, 2013

Qun-Tian Wang
Biological Sciences
M/C 567

Office of Animal Care and
Institutional Biosafety Committees (MC 672)
Office of the Vice Chancellor for Research
206 Administrative Office Building
1737 West Polk Street
Chicago, Illinois 60612-7227

Dear Dr. Wang:

The protocol indicated below was reviewed at a convened ACC meeting in accordance with the Animal Care Policies of the University of Illinois at Chicago on **2/19/2013**. *The protocol was not initiated until final clarifications were reviewed and approved on* **2/28/2013**. *The protocol is approved for a period of 3* years with annual continuation.

Title of Application: Proteomic Characterization of Epicardial-Myocardial Signaling

ACC Number: 13-002

Initial Approval Period: 2/28/2013 to 2/19/2014

Current Funding: ***Portions of this protocol are supported by the funding sources indicated in the table below.***
Number of funding sources: 1

Funding Agency	**Funding Title**			**Portion of Proposal Matched**
Chicago Biomedical Consortium	*Proteomic Characterization of Epicardial-Myocardial Signaling and Regenerative Activity*			*UIC portion of the grant is matched*
Funding Number	**Current Status**	**UIC PAF NO.**	**Performance Site**	**Funding PI**
C-036	*Funded*	*2013-03505*	*UIC and NWU (not subcontracted)*	*Qun-Tian Wang*

This institution has Animal Welfare Assurance Number A3460.01 on file with the Office of Laboratory Animal Welfare (OLAW), NIH. **This letter may only be provided as proof of IACUC approval for those specific funding sources listed above in which all portions of the funding proposal are matched to this ACC protocol.**

In addition, all investigators are responsible for ensuring compliance with all federal and institutional policies and regulations related to use of animals under this protocol and the funding sources listed on this protocol. Please use OLAW's "*What Investigators Need to Know about the Use of Animals*" (http://grants.nih.gov/grants/olaw/InvestigatorsNeed2Know.pdf) as a reference guide. Thank you for complying with the Animal Care Policies and Procedures of UIC.

Sincerely yours,

Bradley Merrill, PhD
Chair, Animal Care Committee
BM/*ss*
cc: BRL, ACC File, **PAF #2013-03505**

Phone (312) 996-1972 • Fax (312) 996-9088 • www.research.uic.edu

CITED LITERATURE

Abu-Issa, R., Kirby, M.L., 2008. Patterning of the heart field in the chick. Dev. Biol. 319, 223–233. doi:10.1016/j.ydbio.2008.04.014

Acharya, A., Baek, S.T., Banfi, S., Eskiocak, B., Tallquist, M.D., 2011. Efficient inducible Cre-mediated recombination in Tcf21 cell lineages in the heart and kidney. Genesis 49, 870–7. doi:10.1002/dvg.20750

Acharya, A., Baek, S.T., Huang, G., Eskiocak, B., Goetsch, S., Sung, C.Y., Banfi, S., Sauer, M.F., Olsen, G.S., Duffield, J.S., Olson, E.N., Tallquist, M.D., 2012. The bHLH transcription factor Tcf21 is required for lineage-specific EMT of cardiac fibroblast progenitors. Development 139, 2139–2149. doi:10.1242/dev.079970

Ahmed, G., Shinmyo, Y., Ohta, K., Islam, S.M., Hossain, M., Naser, I. Bin, Riyadh, M.A., Su, Y., Zhang, S., Tessier-Lavigne, M., Tanaka, H., 2011. Draxin inhibits axonal outgrowth through the netrin receptor DCC. J. Neurosci. 31, 14018–23. doi:10.1523/JNEUROSCI.0943-11.2011

Alonso, D.A., Oktaba, K., Ly-hartig, N., Scheuermann, J.C., Mcginty, R.K., Fraterman, S., Wilm, M., Muir, T.W., 2010. Histone H2A deubiquitinase activity of the Polycomb repressive complex PR-DUB 465. doi:10.1038/nature08966

Angel, P.M., Baldwin, H.S., Gottlieb Sen, D., Su, Y.R., Mayer, J.E., Bichell, D., Drake, R.R., 2016. Advances in MALDI imaging mass spectrometry of proteins in cardiac tissue, including the heart valve. Biochim. Biophys. Acta - Proteins Proteomics 1865, 927–935. doi:10.1016/j.bbapap.2017.03.009

Arthur, H.M., Bamforth, S.D., 2011. TGFbeta signaling and congenital heart disease: Insights from mouse studies. Birth Defects Res. Part A - Clin. Mol. Teratol. 91, 423–434. doi:10.1002/bdra.20794

Austin, A.F., Compton, L. a, Love, J.D., Brown, C.B., Barnett, J. V, 2008. Primary and immortalized mouse epicardial cells undergo differentiation in response to TGFbeta. Dev. Dyn. 237, 366–76. doi:10.1002/dvdy.21421

Bakalarski, C.E., Kirkpatrick, D.S., 2016. A Biologist's Field Guide to Multiplexed Quantitative Proteomics. Mol. Cell. Proteomics 13975, 1–31. doi:10.1074/mcp.O115.056986

Baskind, H. a, Na, L., Ma, Q., Patel, M.P., Geenen, D.L., Wang, Q.T., 2009. Functional conservation of Asxl2, a murine homolog for the Drosophila enhancer of trithorax and polycomb group gene Asx. PLoS One 4, e4750. doi:10.1371/journal.pone.0004750

Bax, N.A.M., Van Oorschot, A.A.M., Maas, S., Braun, J., Van Tuyn, J., De Vries, A.A.F., Gittenberger-De Groot, A.C., Goumans, M.J., 2011. In vitro epithelial-to-mesenchymal transformation in human adult epicardial cells is regulated by TGFβ-signaling and WT1. Basic Res. Cardiol. 106, 829–847. doi:10.1007/s00395-011-0181-0

Bax, N. a M., Lie-Venema, H., Vicente-Steijn, R., Bleyl, S.B., Van Den Akker, N.M.S., Maas, S.,

Poelmann, R.E., Gittenberger-de Groot, A.C., 2009. Platelet-derived growth factor is involved in the differentiation of second heart field-derived cardiac structures in chicken embryos. Dev. Dyn. 238, 2658–69. doi:10.1002/dvdy.22073

Beg, A.A., Sha, W.C., Bronson, R.T., Ghosh, S., Baltimore, D., 1995. Embryonic lethality and liver degeneration in mice lacking the RelA component of NF-kappa B. Nature. doi:10.1038/376167a0

Bin-Nun, N., Lichtig, H., Malyarova, A., Levy, M., Elias, S., Frank, D., 2014. PTK7 modulates Wnt signaling activity via LRP6. Development 141, 410–21. doi:10.1242/dev.095984

Blanco, M.A., LeRoy, G., Khan, Z., Alečković, M., Zee, B.M., Garcia, B. a, Kang, Y., 2012. Global secretome analysis identifies novel mediators of bone metastasis. Cell Res. 22, 1339–1355. doi:10.1038/cr.2012.89

Blaze, M., Aydin, B., Carlson, P., Hanley, L., 2012. Identification and imaging of peptides and proteins on Enterococcus faecalis biofilms by matrix assisted laser desorption ionization mass spectrometry † 5018–5025. doi:10.1039/c2an35922g

Brade, T., Kumar, S., Cunningham, T.J., Chatzi, C., Zhao, X., Cavallero, S., Li, P., Sucov, H.M., Ruiz-lozano, P., Duester, G., 2011. Retinoic acid stimulates myocardial expansion by induction of hepatic erythropoietin which activates epicardial Igf2 148, 139–148. doi:10.1242/dev.054239

Brade, T., Männer, J., Kühl, M., 2006. The role of Wnt signalling in cardiac development and tissue remodelling in the mature heart. Cardiovasc. Res. 72, 198–209. doi:10.1016/j.cardiores.2006.06.025

Brand, T., 2003. Heart development: Molecular insights into cardiac specification and early morphogenesis. Dev. Biol. 258, 1–19. doi:10.1016/S0012-1606(03)00112-X

Brutsaert, D.L., 2003. Cardiac endothelial-myocardial signaling: its role in cardiac growth, contractile performance, and rhythmicity. Physiol. Rev. 83, 59–115. doi:10.1152/physrev.00017.2002

Buckingham, M., Meilhac, S., Zaffran, S., 2005. Building the mammalian heart from two sources of myocardial cells. Nat. Rev. Genet. 6, 826–837. doi:10.1038/nrg1710

Burke, J.R., Pattoli, M. a., Gregor, K.R., Brassil, P.J., MacMaster, J.F., McIntyre, K.W., Yang, X., Iotzova, V.S., Clarke, W., Strnad, J., Qiu, Y., Zusi, F.C., 2003. BMS-345541 is a highly selective inhibitor of IκB kinase that binds at an allosteric site of the enzyme and blocks NF-κB-dependent transcription in mice. J. Biol. Chem. 278, 1450–1456. doi:10.1074/jbc.M209677200

Calvano, S.E., Xiao, W., Richards, D.R., Felciano, R.M., Baker, H. V., Cho, R.J., Chen, R.O., Brownstein, B.H., Cobb, J.P., Tschoeke, S.K., Miller-Graziano, C., Moldawer, L.L., Mindrinos, M.N., Davis, R.W., Tompkins, R.G., Lowry, S.F., Inflamm and Host Response to Injury Large Scale Collaborative Research Program, 2005. A network-based analysis of systemic inflammation in humans. Nature 437, 1032–1037. doi:10.1038/nature03985

Caprioli, R.M., Farmer, T.B., Gile, J., 1997. Molecular Imaging of Biological Samples: Localization of Peptides and Proteins Using MALDI-TOF MS. Anal. Chem. 69, 4751–4760. doi:10.1021/ac970888i

Casadonte, R., Caprioli, R.M., 2011. Proteomic analysis of formalin-fixed paraffin- embedded tissue by MALDI imaging mass spectrometry. Nat. Protoc. 6, 1695–1709. doi:10.1038/nprot.2011.388

Chevallet, M., Diemer, H., Van Dorssealer, A., Villiers, C., Rabilloud, T., 2007. Toward a better analysis of secreted proteins: the example of the myeloid cells secretome. Proteomics 7, 1757–70. doi:10.1002/pmic.200601024

Chevallet, M., Luche, S., Rabilloud, T., 2006. Silver staining of proteins in polyacrylamide gels. Nat Protoc 1, 1852–1858. doi:10.1038/nprot.2006.288

Christoffels, V.M., Hoogaars, W.M.H., Moorman, A.F.M., 2010. Patterning and Development of the Conduction System of the Heart. Origins of the Conduction System in Development, Heart Development and Regeneration. Elsevier Inc. doi:10.1016/B978-0-12-381332-9.00008-6

Chughtai, K., Heeren, R.M.A., 2011. Mass Spectrometric Imaging for biomedical tissue analysis 110, 3237–3277. doi:10.1021/cr100012c.Mass

Cillero-Pastor, B., Heeren, R.M. a, 2013. Matrix Assisted Laser Desorption Ionization Mass Spectrometry Imaging for Peptide and Protein Analyses: a Critical Review of on-Tissue Digestion. J. Proteome Res. doi:10.1021/pr400743a

Clark, C.R., Robinson, J.Y., Sanchez, N.S., Townsend, T.A., Arrieta, J.A., Merryman, W.D., Trykall, D.Z., Olivey, H.E., Hong, C.C., Barnett, J. V., 2016. Common pathways regulate type III TGFβ receptor–dependent cell invasion in epicardial and endocardial cells. Cell. Signal. 28, 688–698. doi:10.1016/j.cellsig.2016.03.004

Compton, L.A., Potash, D.A., Mundell, N.A., Barnett, J. V., 2006. Transforming growth factor-β induces loss of epithelial character and smooth muscle cell differentiation in epicardial cells. Dev. Dyn. 235, 82–93. doi:10.1002/dvdy.20629

Cooley, J.R., Yatskievych, T.A., Antin, P.B., 2014. Embryonic expression of the transforming growth factor beta ligand and receptor genes in chicken. Dev. Dyn. 243, 497–508. doi:10.1002/dvdy.24085

Cortesio, C.L., Chan, K.T., Perrin, B.J., Burton, N.O., Zhang, S., Zhang, Z.-Y., Huttenlocher, A., 2008. Calpain 2 and PTP1B function in a novel pathway with Src to regulate invadopodia dynamics and breast cancer cell invasion. J. Cell Biol. 180, 957–71. doi:10.1083/jcb.200708048

Cottrell, J.S., 2011. Protein identification using MS / MS data. J. Proteomics 74, 1842–1851. doi:10.1016/j.jprot.2011.05.014

Craig, E. a, Austin, A.F., Vaillancourt, R.R., Barnett, J. V, Camenisch, T.D., 2010. TGFβ2-mediated production of hyaluronan is important for the induction of epicardial cell

differentiation and invasion. Exp. Cell Res. 316, 3397–405. doi:10.1016/j.yexcr.2010.07.006

Crispino, J.D., Lodish, M.B., Thurberg, B.L., Litovsky, S.H., Collins, T., Molkentin, J.D., Orkin, S.H., 2001. Proper coronary vascular development and heart morphogenesis depend on interaction of GATA-4 with FOG cofactors Proper coronary vascular development and heart morphogenesis depend on interaction of GATA-4 with FOG cofactors 839–844. doi:10.1101/gad.875201

Darehzereshki, A., Rubin, N., Gamba, L., Kim, J., Fraser, J., Huang, Y., Billings, J., Mohammadzadeh, R., Wood, J., Warburton, D., Kaartinen, V., Lien, C.L., 2015. Differential regenerative capacity of neonatal mouse hearts after cryoinjury. Dev. Biol. 399, 91–99. doi:10.1016/j.ydbio.2014.12.018

Das, D.S., Wadhwa, N., Kunj, N., Sarda, K., Pradhan, B.S., Majumdar, S.S., 2013. Dickkopf Homolog 3 (DKK3) Plays a Crucial Role Upstream of WNT/β-CATENIN Signaling for Sertoli Cell Mediated Regulation of Spermatogenesis. PLoS One 8. doi:10.1371/journal.pone.0063603

Dawn, B., Xuan, Y.T., Marian, M., Flaherty, M.P., Murphree, S.S., Smith, T.L., Bolli, R., Jones, W.K., 2001. Cardiac-specific abrogation of NF- kappa B activation in mice by transdominant expression of a mutant I kappa B alpha. J. Mol. Cell. Cardiol. 33, 161–173. doi:10.1006/jmcc.2000.1291

DeLaughter, D.M., Clark, C.R., Christodoulou, D.C., Seidman, C.E., Baldwin, H.S., Seidman, J.G., Barnett, J. V., 2016. Transcriptional Profiling of Cultured, Embryonic Epicardial Cells Identifies Novel Genes and Signaling Pathways Regulated by TGFβR3 In Vitro. PLoS One 11, e0159710. doi:10.1371/journal.pone.0159710

Dettman, R.W., Denetclaw, W., Ordahl, C.P., Bristow, J., 1998. Common epicardial origin of coronary vascular smooth muscle, perivascular fibroblasts, and intermyocardial fibroblasts in the avian heart. Dev. Biol. 193, 169–81. doi:10.1006/dbio.1997.8801

Diehl, H.C., Beine, B., Elm, J., Trede, D., Ahrens, M., Eisenacher, M., Marcus, K., Meyer, H.E., Henkel, C., 2015. The challenge of on-tissue digestion for MALDI MSI- a comparison of different protocols to improve imaging experiments. Anal. Bioanal. Chem. 407, 2223–2243. doi:10.1007/s00216-014-8345-z

Dokic, D., Dettman, R.W., 2006. VCAM-1 inhibits TGFbeta stimulated epithelial-mesenchymal transformation by modulating Rho activity and stabilizing intercellular adhesion in epicardial mesothelial cells. Dev. Biol. 299, 489–504. doi:10.1016/j.ydbio.2006.08.054

Durr, E., Yu, J., Krasinska, K.M., Carver, L. a, Yates, J.R., Testa, J.E., Oh, P., Schnitzer, J.E., 2004. Direct proteomic mapping of the lung microvascular endothelial cell surface in vivo and in cell culture. Nat. Biotechnol. 22, 985–992. doi:10.1038/nbt993

Firlej, V., Mathieu, J.R.R., Gilbert, C., Lemonnier, L., Nakhlé, J., Gallou-Kabani, C., Guarmit, B., Morin, A., Prevarskaya, N., Delongchamps, N.B., Cabon, F., 2011. Thrombospondin-1 triggers cell migration and development of advanced prostate tumors. Cancer Res. 71, 7649–58. doi:10.1158/0008-5472.CAN-11-0833

Foglia, M.J., Poss, K.D., 2016. Building and re-building the heart by cardiomyocyte proliferation. Development 143, 729–740. doi:10.1242/dev.132910

Foster, M.W., Morrison, L.D., Todd, J.L., Snyder, L.D., Thompson, J.W., Soderblom, E.J., Plonk, K., Weinhold, K.J., Townsend, R., Minnich, A., Moseley, M.A., 2015. Quantitative proteomics of bronchoalveolar lavage fluid in idiopathic pulmonary fibrosis. J. Proteome Res. 14, 1238–1249. doi:10.1021/pr501149m

Franco, S.J., Huttenlocher, A., 2005. Regulating cell migration: calpains make the cut. J. Cell Sci. 118, 3829–38. doi:10.1242/jcs.02562

Garriock, R.J., Mikawa, T., Yamaguchi, T.P., 2014. Isolation and culture of mouse proepicardium using serum-free conditions. Methods 66, 365–369. doi:10.1016/j.ymeth.2013.06.030

Gassmann, M., Casagranda, F., Orioli, D., Simon, H., Lai, C., Klein, R., Lemke, G., 1995. Aberrant neural and cardiac development in mice lacking the ErbB4 neuregulin receptor. Nature 378, 390–394. doi:10.1038/378390a0

Germani, A., Foglio, E., Capogrossi, M.C., Russo, M.A., Limana, F., 2015. Generation of cardiac progenitor cells through epicardial to mesenchymal transition. J. Mol. Med. 93, 735–748. doi:10.1007/s00109-015-1290-2

Gessert, S., Kühl, M., 2010. The multiple phases and faces of Wnt signaling during cardiac differentiation and development. Circ. Res. 107, 186–199. doi:10.1161/CIRCRESAHA.110.221531

Ghosh, S., May, M.J., Kopp, E.B., 1998. NF- κ B AND REL PROTEINS : Evolutionarily Conserved Mediators of Immune Responses. Annu. Rev. iImunology 16, 225–260. doi:10.1146/annurev.immunol.16.1.225

Gilmore, R., 1993. Protein translocation across the endoplasmic reticulum: A tunnel with toll booths at entry and exit. Cell 75, 589–592. doi:10.1016/0092-8674(93)90476-7

Gilmore, T.D., 2006. Introduction to NF-κB: players, pathways, perspectives. Oncogene 25, 6680–6684. doi:10.1038/sj.onc.1209954

Govind, S., 1999. Control of development and immunity by rel transcription factors in Drosophila. Oncogene 18, 6875–6887. doi:10.1038/sj.onc.1203223

Green, M.L., Karp, P.D., 2006. The outcomes of pathway database computations depend on pathway ontology. Nucleic Acids Res. 34, 3687–3697. doi:10.1093/nar/gkl438

Grego-Bessa, J., Luna-Zurita, L., del Monte, G., Bolós, V., Melgar, P., Arandilla, A., Garratt, A.N., Zang, H., Mukouyama, Y. suke, Chen, H., Shou, W., Ballestar, E., Esteller, M., Rojas, A., Pérez-Pomares, J.M., de la Pompa, J.L., 2007. Notch Signaling Is Essential for Ventricular Chamber Development. Dev. Cell 12, 415–429. doi:10.1016/j.devcel.2006.12.011

Gregson, C., 2009. Optimization of MALDI tissue imaging and correlation with immunohistochemistry in rat kidney sections 2, 134–146.

Greutmann, M., Tobler, D., Kovacs, A.H., Greutmann-Yantiri, M., Haile, S.R., Held, L., Ivanov, J., Williams, W.G., Oechslin, E.N., Silversides, C.K., Colman, J.M., 2015. Increasing mortality burden among adults with complex congenital heart disease. Congenit. Heart Dis. 10, 117–127. doi:10.1111/chd.12201

Groot, A.C.G., Peeters, M.-P.F.M.V., Bergwerff, M., Mentink, M.M.T., Poelmann, R.E., 2000. Epicardial Outgrowth Inhibition Leads to Compensatory Mesothelial Outflow Tract Collar and Abnormal Cardiac Septation and Coronary Formation 3615–3621. doi:10.1039/b005411i

Groseclose, M.R., Andersson, M., Hardesty, W.M., Caprioli, R.M., 2007. Identification of proteins directly from tissue : in situ tryptic digestions coupled with imaging mass spectrometry 254–262. doi:10.1002/jms

Gutiérrez, L., Zurita, M., Kennison, J.A., Vázquez, M., 2003. The Drosophila trithorax group gene tonalli (tna) interacts genetically with the Brahma remodeling complex and encodes an SP-RING finger protein. Development 343–354. doi:10.1242/dev.00222

Harvey, R.P., 2002. Organogenesis: Patterning the vertebrate heart. Nat. Rev. Genet. 3, 544–556. doi:10.1038/nrg843

Hayden, M.S., Ghosh, S., 2012. NF-κB, the first quarter-century: remarkable progress and outstanding questions. Genes Dev. 26, 203–34. doi:10.1101/gad.183434.111

Heeren, R.M.A., Smith, D.F., Stauber, J., Kükrer-Kaletas, B., MacAleese, L., 2009. Imaging Mass Spectrometry: Hype or Hope? J. Am. Soc. Mass Spectrom. 20, 1006–1014. doi:10.1016/j.jasms.2009.01.011

Hernandez-Gutierrez., Garcıa-Pel´ aez, A. Zentella-Dehesa · M. Ramos-Kuri · P.Hern´, andezFranco · F., Rojas, andez-S. anchez · E., 2006. NF-κB signaling blockade by Bay 11-7085 during early cardiac morphogenesis induces alterations of the outflow tract in chicken heart. Apoptosis 11, 1101–1109. doi:10.1007/s10495-006-6984-z

Hikoso, S., Yamaguchi, O., Nakano, Y., Takeda, T., Omiya, S., Mizote, I., Taneike, M., Oka, T., Tamai, T., Oyabu, J., Uno, Y., Matsumura, Y., Nishida, K., Suzuki, K., Kogo, M., Hori, M., Otsu, K., 2009. The IκB Kinase beta/Nuclear factor κb signaling pathway protects the heart from hemodynamic stress mediated by the regulation of manganese superoxide dismutase expression. Circ. Res. 105, 70–79. doi:10.1161/CIRCRESAHA.108.193318

Hill, C.R., Sanchez, N.S., Love, J.D., Arrieta, J. a., Hong, C.C., Brown, C.B., Austin, A.F., Barnett, J. V., 2012. BMP2 signals loss of epithelial character in epicardial cells but requires the Type III TGFβ receptor to promote invasion. Cell. Signal. 24, 1012–1022. doi:10.1016/j.cellsig.2011.12.022

Hiruma, T., Hirakow, R., 1989. Epicardial formation in embryonic chick heart: computer-aided reconstruction, scanning, and transmission electron microscopic studies. Am. J. Anat. 184, 129–138. doi:10.1002/aja.1001840204

Hoffman, J.I.E., Kaplan, S., 2002. The incidence of congenital heart disease. J. Am. Coll. Cardiol. 39, 1890–1900. doi:10.1016/S0735-1097(02)01886-7

Hoos, M.D., Richardson, B.M., Foster, M.W., Everhart, A., Thompson, J.W., Moseley, M.A., Colton, C. a, 2013. Longitudinal study of differential protein expression in an Alzheimer's mouse model lacking inducible nitric oxide synthase. J. Proteome Res. 12, 4462–4477. doi:10.1021/pr4005103

Huang, D.W., Lempicki, R. a, Sherman, B.T., 2009. Systematic and integrative analysis of large gene lists using DAVID bioinformatics resources. Nat. Protoc. 4, 44–57. doi:10.1038/nprot.2008.211

Huang, R., Fang, P., Hao, Z., Kay, B.K., 2016. Directed evolution of a highly specific FN3 monobody to the SH3 domain of human lyn tyrosine kinase. PLoS One 11, 1–22. doi:10.1371/journal.pone.0145872

Huang, Y., Hoque, M.O., Wu, F., Trink, B., Ratovitski, E.A., 2008. Midkine induces epithelial-mesenchymal transition through Notch2/Jak2-Stat3 signaling in human keratinocytes 4101. doi:10.4161/cc.7.11.5952

Huber, M. a, Azoitei, N., Baumann, B., Grünert, S., Sommer, A., Pehamberger, H., Kraut, N., Beug, H., Wirth, T., 2004. NF- κ B is essential for epithelial- mesenchymal transition and metastasis in a model of breast cancer progression. J. Clin. Invest. 114, 569–581. doi:10.1172/JCI200421358.The

Ieda, M., Tsuchihashi, T., Ivey, K.N., Ross, R.S., Hong, T.-T., Shaw, R.M., Srivastava, D., 2009. Cardiac fibroblasts regulate myocardial proliferation through beta1 integrin signaling. Dev. Cell 16, 233–44. doi:10.1016/j.devcel.2008.12.007

Ishii, Y., Garriock, R.J., Navetta, A.M., Coughlin, L.E., Mikawa, T., 2010. BMP signals promote proepicardial protrusion necessary for recruitment of coronary vessel and epicardial progenitors to the heart. Dev. Cell 19, 307–316. doi:10.1016/j.devcel.2010.07.017

Jensen, B., Wang, T., Christoffels, V.M., Moorman, A.F.M., 2013. Evolution and development of the building plan of the vertebrate heart. Biochim. Biophys. Acta - Mol. Cell Res. 1833, 783–794. doi:10.1016/j.bbamcr.2012.10.004

Jiang, W., Xiang, C., Cazacu, S., Brodie, C., Mikkelsen, T., 2008. Insulin-like Growth Factor Binding Protein 7 Mediates Glioma Cell Growth and Migration 1 10, 1335–1342. doi:10.1593/neo.08694

Kale, S., Raja, R., Thorat, D., Soundararajan, G., Patil, T. V, Kundu, G.C., 2013. Osteopontin signaling upregulates cyclooxygenase-2 expression in tumor-associated macrophages leading to enhanced angiogenesis and melanoma growth via a 9 b 1 integrin 33, 2295–2306. doi:10.1038/onc.2013.184

Kanegae, Y., Tavares, A.T., Izpisúa Belmonte, J.C., Verma, I.M., 1998. Role of Rel/NF-kappaB transcription factors during the outgrowth of the vertebrate limb. Nature 392, 611–4. doi:10.1038/33429

Kelley, M.W., 2008. Leading Wnt down a PCP path: Cthrc1 acts as a coreceptor in the Wnt-PCP pathway. Dev. Cell 15, 7–8. doi:10.1016/j.devcel.2008.06.008

Kelly, R.G., 2012. The Second Heart Field, Current Topics in Developmental Biology. Elsevier Inc. doi:10.1016/B978-0-12-387786-4.00002-6

Kelly, R.G., Buckingham, M.E., 2002. The anterior heart-forming field: Voyage to the arterial pole of the heart. Trends Genet. 18, 210–216. doi:10.1016/S0168-9525(02)02642-2

Keyte, A., Redmond, M., 2012. The neural crest in cardiac congenital anomalies. Differentiation 84, 25–40. doi:10.1016/j.diff.2012.04.005

Khan, F.F., 2014. Identification and Characterization of the Protein Interaction between ASXL2 and WTIP. Dissertation 2014, 0–1.

Khan, F.F., Li, Y., Balyan, A., Wang, Q.T., 2014. WTIP interacts with ASXL2 and blocks ASXL2-mediated activation of retinoic acid signaling. Biochem. Biophys. Res. Commun. 451, 101–106. doi:10.1016/j.bbrc.2014.07.080

Kikuchi, K., 2014. Advances in understanding the mechanism of zebrafish heart regeneration. Stem Cell Res. 13, 542–555. doi:10.1016/j.scr.2014.07.003

Kolditz, D.P., Wijffels, M.C.E.F., Blom, N.A., Van Der Laarse, A., Hahurij, N.D., Lie-Venema, H., Markwald, R.R., Poelmann, R.E., Schalij, M.J., Gittenberger-De Groot, A.C., 2008. Epicardium-derived cells in development of annulus fibrosis and persistence of accessory pathways. Circulation 117, 1508–1517. doi:10.1161/CIRCULATIONAHA.107.726315

Krainock, M., Toubat, O., Danopoulos, S., Beckham, A., Warburton, D., Kim, R., 2016. Epicardial Epithelial-to-Mesenchymal Transition in Heart Development and Disease. J. Clin. Med. 5, 27. doi:10.3390/jcm5020027

Kraut, B., Maier, H.J., Kókai, E., Fiedler, K., Boettger, T., Illing, A., Kostin, S., Walther, P., Braun, T., Wirth, T., 2015. Cardiac-specific activation of IKK2 leads to defects in heart development and embryonic lethality. PLoS One 10, 1–17. doi:10.1371/journal.pone.0141591

Kwee, L., Baldwin, H.S., Shen, H.M., Stewart, C.L., Buck, C., Buck, C. a, Labow, M. a, 1995. Defective development of the embryonic and extraembryonic circulatory systems in vascular cell adhesion molecule (VCAM-1) deficient mice. Development 121, 489–503. doi:10.1016/1074-7613(94)90076-0

Lai, H.-L., Grachoff, M., McGinley, A.L., Khan, F.F., Warren, C.M., Chowdhury, S. a K., Wolska, B.M., Solaro, R.J., Geenen, D.L., Wang, Q.T., 2012. Maintenance of adult cardiac function requires the chromatin factor Asxl2. J. Mol. Cell. Cardiol. 53, 734–41. doi:10.1016/j.yjmcc.2012.08.014

Lai, H.L., Wang, Q.T., 2013. Additional Sex Combs-Like 2 Is Required for Polycomb Repressive Complex 2 Binding at Select Targets. PLoS One 8, 1–13. doi:10.1371/journal.pone.0073983

Lavine, K.J., Ornitz, D.M., 2007. The Epicardial Signaling Center in Development and Disease, in: Heart Development and Regeneration. Elsevier Inc., pp. 345–359. doi:10.1016/B978-0-12-381332-9.00017-7

Lavine, K.J., Yu, K., White, A.C., Zhang, X., Smith, C., Partanen, J., Ornitz, D.M., 2005.

Endocardial and epicardial derived FGF signals regulate myocardial proliferation and differentiation in vivo. Dev. Cell 8, 85–95. doi:10.1016/j.devcel.2004.12.002

Lemaire, R., Desmons, a, Tabet, J.C., Day, R., Salzet, M., Fournier, I., 2007. Direct Analysis and MALDI Imaging of Formalin-Fixed , Paraffin-Embedded Tissue Sections research articles 1295–1305.

Levéen, P., Pekny, M., Gebre-Medhin, S., Swolin, B., Larsson, E., Betsholtz, C., 1994. Mice deficient for PDGF B show renal, cardiovascular, and hematological abnormalities. Genes Dev. 8, 1875–1887. doi:10.1101/gad.8.16.1875

Li, P., Cavallero, S., Gu, Y., Chen, T.H.P., Hughes, J., Hassan, a B., Brüning, J.C., Pashmforoush, M., Sucov, H.M., 2011. IGF signaling directs ventricular cardiomyocyte proliferation during embryonic heart development. Development 138, 1795–805. doi:10.1242/dev.054338

Li, Q., Lu, Q., Hwang, J.Y., Büscher, D., Lee, K.F., Izpisua-Belmonte, J.C., Verma, I.M., 1999. IKK1-deficient mice exhibit abnormal development of skin and skeleton. Genes Dev. 13, 1322–1328. doi:10.1101/gad.13.10.1322

Lietz, C.B., Gemperline, E., Li, L., 2008. Qualitative and quantitative mass spectrometry imaging of. Growth (Lakeland) 23, 1–7. doi:10.1038/jid.2014.371

Lim, S., Yoo, B.K., Kim, H.-S., Gilmore, H.L., Lee, Y., Lee, H., Kim, S.-J., Letterio, J., Lee, H., O'Brien, R., Wong, P., Hardy, J., Higgins, G., Strooper, B. De, Annaert, W., Jacobsen, K., Iverfeldt, K., Sheng, B., Song, B., Zheng, Z., Zhou, F., Lu, G., Zhao, N., Zhang, X., Gong, Y., Sosa, L., Bergman, J., Estrada-Bernal, A., Glorioso, T., Kittelson, J., Pfenninger, K., Baratchi, S., Evans, J., Tate, W., Abraham, W., Connor, B., Hoffmann, J., Twiesselmann, C., Kummer, M., Romagnoli, P., Herzog, V., Pietrzik, C., Hoffmann, J., Stober, K., Chen, C., Bauer, C., Otero, D., Roch, J., Herzog, V., Meng, J., Kataoka, H., Itoh, H., Koono, M., Hansel, D., Rahman, A., Wehner, S., Herzog, V., Yeo, C., Maitra, A., Krause, K., Karger, S., Sheu, S., Aigner, T., Kursawe, R., Gimm, O., Schmid, K., Dralle, H., Fuhrer, D., Takayama, K., Tsutsumi, S., Suzuki, T., Horie-Inoue, K., Ikeda, K., Kaneshiro, K., Fujimura, T., Kumagai, J., Urano, T., Sakaki, Y., Shirahige, K., Sasano, H., Takahashi, S., Kitamura, T., Ouchi, Y., Aburatani, H., Inoue, S., Venkataramani, V., Rossner, C., Iffland, L., Schweyer, S., Tamboli, I., Walter, J., Wirths, O., Bayer, T., Takagi, K., Ito, S., Miyazaki, T., Miki, Y., Shibahara, Y., Ishida, T., Watanabe, M., Inoue, S., Sasano, H., Suzuki, T., Young-Pearse, T., Bai, J., Chang, R., Zheng, J., LoTurco, J., Selkoe, D., Young-Pearse, T., Chen, A., Chang, R., Marquez, C., Selkoe, D., Jemal, A., Bray, F., Center, M., Ferlay, J., Ward, E., Forman, D., Hong, S., Lim, S., Li, A., Lee, C., Lee, Y., Lee, E., Park, S., Wang, X., Kim, S., Harris, J., Devidze, N., Verret, L., Ho, K., Halabisky, B., Thwin, M., Kim, D., Hamto, P., Lo, I., Yu, G., Palop, J., Masliah, E., Mucke, L., Minn, A., Gupta, G., Siegel, P., Bos, P., Shu, W., Giri, D., Viale, A., Olshen, A., Gerald, W., Massague, J., Tang, B., Vu, M., Booker, T., Santner, S., Miller, F., Anver, M., Wakefield, L., Miller, F., Soule, H., Tait, L., Pauley, R., Wolman, S., Dawson, P., Heppner, G., Aslakson, C., Miller, F., Mattson, M., Kummer, C., Wehner, S., Quast, T., Werner, S., Herzog, V., Sherr, C., Roberts, J., Caldon, C., Daly, R., Sutherland, R., Musgrove, E., Chu, I., Hengst, L., Slingerland, J., Wander, S., Zhao, D., Slingerland, J., Mahalingam, D., Szegezdi, E., Keane, M., Jong, S. de, Samali, A., Joensuu, H., Gligorov, J., Lee, G., Kenny, P., Lee, E., Bissell, M., Schmeichel, K., Bissell, M., Weigelt, B., Bissell, M., Kenny, P., Lee,

G., Myers, C., Neve, R., Semeiks, J., Spellman, P., Lorenz, K., Lee, E., Barcellos-Hoff, M., Petersen, O., Gray, J., Bissell, M., Hollestelle, A., Elstrodt, F., Nagel, J., Kallemeijn, W., Schutte, M., Chakrabarty, A., Bhola, N., Sutton, C., Ghosh, R., Kuba, M., Dave, B., Chang, J., Arteaga, C., Rexer, B., Arteaga, C., Tzivion, G., Dobson, M., Ramakrishnan, G., Clarke, R., Zheng, H., Jiang, M., Trumbauer, M., Hopkins, R., Sirinathsinghji, D., Stevens, K., Conner, M., Slunt, H., Sisodia, S., Chen, H., Ploeg, L. Van der, Goodarzi, H., Zhang, S., Buss, C., Fish, L., Tavazoie, S., Tavazoie, S., King, T., Suto, M., Li, Y., Incassati, A., Chandramouli, A., Eelkema, R., Cowin, P., Yang, J., Hung, M., Srinivasula, S., Ashwell, J., Jimenez, S., Torres, M., Vizuete, M., Sanchez-Varo, R., Sanchez-Mejias, E., Trujillo-Estrada, L., Carmona-Cuenca, I., Caballero, C., Ruano, D., Gutierrez, A., Vitorica, J., Larue, L., Bellacosa, A., Gilles, C., Polette, M., Mestdagt, M., Nawrocki-Raby, B., Ruggeri, P., Birembaut, P., Foidart, J., Roxanis, I., 2014. Amyloid-β precursor protein promotes cell proliferation and motility of advanced breast cancer. BMC Cancer 14, 928. doi:10.1186/1471-2407-14-928

Londhe, V.A., Maisonet, T.M., Lopez, B., Jeng, J.-M., Xiao, J., Li, C., Minoo, P., 2011. Conditional deletion of epithelial IKKβ impairs alveolar formation through apoptosis and decreased VEGF expression during early mouse lung morphogenesis. Respir. Res. 12, 134. doi:10.1186/1465-9921-12-134

Londhe, V.A., Nguyen, H.T., Jeng, J.M., Li, X., Li, C., Tiozzo, C., Zhu, N., Minoo, P., 2008. NF-kB induces lung maturation during mouse lung morphogenesis. Dev. Dyn. 237, 328–338. doi:10.1002/dvdy.21413

Ma, Y., Visser, L., Roelofsen, H., Vries, M. De, Diepstra, A., Imhoff, G. Van, Wal, V. Der, Luinge, M., Alvarez-llamas, G., Vos, H., Poppema, S., Vonk, R., Dc, W., Ma, Y., Visser, L., Roelofsen, H., Vries, M. De, Diepstra, A., Imhoff, G. Van, Wal, T. Van Der, 2013. Proteomics analysis of Hodgkin lymphoma : identification of new players involved in the cross-talk between HRS cells and infiltrating lymphocytes. Blood 111, 2339–2346. doi:10.1182/blood-2007-09-112128

Maier, H.J., Schmidt-Straßburger, U., Huber, M. a., Wiedemann, E.M., Beug, H., Wirth, T., 2010. NF-κB promotes epithelial-mesenchymal transition, migration and invasion of pancreatic carcinoma cells. Cancer Lett. 295, 214–228. doi:10.1016/j.canlet.2010.03.003

Maleszewska, M., Moonen, J.R.A.J., Huijkman, N., van de Sluis, B., Krenning, G., Harmsen, M.C., 2013. IL-1β and TGF2β synergistically induce endothelial to mesenchymal transition in an NFkB-dependent manner. Immunobiology 218, 443–454. doi:10.1016/j.imbio.2012.05.026

Martinsen, B.J., 2005. Reference guide to the stages of chick heart embryology. Dev. Dyn. 233, 1217–1237. doi:10.1002/dvdy.20468

Masters, M., Riley, P.R., 2014. The epicardium signals the way towards heart regeneration. Stem Cell Res. 13, 683–692. doi:10.1016/j.scr.2014.04.007

Meding, S., Walch, A., 2013. MALDI Imaging Mass Spectrometry for Direct Tissue Analysis 931, 537–546. doi:10.1007/978-1-62703-056-4

Meilhac, S.M., Lescroart, F., Blanpain, C.D., Buckingham, M.E., 2014. Cardiac cell lineages that form the heart. Cold Spring Harb. Perspect. Med. 4. doi:10.1101/cshperspect.a013888

Mellman, I., Warren, G., 2000. The road taken: past and future foundations of membrane traffic. Cell 100, 99–112. doi:10.1016/S0092-8674(00)81687-6

Mercer, S.E., Odelberg, S.J., Simon, H.G., 2013. A dynamic spatiotemporal extracellular matrix facilitates epicardial-mediated vertebrate heart regeneration. Dev. Biol. 382, 457–469. doi:10.1016/j.ydbio.2013.08.002

Merki, E., Zamora, M., Raya, A., Kawakami, Y., Wang, J., Zhang, X., Burch, J., Kubalak, S.W., Kaliman, P., Izpisua Belmonte, J.C., Chien, K.R., Ruiz-Lozano, P., 2005. Epicardial retinoid X receptor alpha is required for myocardial growth and coronary artery formation. Proc. Natl. Acad. Sci. U. S. A. 102, 18455–60. doi:10.1073/pnas.0504343102

Mikawa, T., Brand, T., 2005. Epicardial Lineage : Origins and Fates, in: Heart Development and Regeneration. Elsevier Inc., pp. 325–344. doi:10.1016/B978-0-12-381332-9.00016-5

Miquerol, L., Kelly, R.G., 2013. Organogenesis of the vertebrate heart. Wiley Interdiscip. Rev. Dev. Biol. 2, 17–29. doi:10.1002/wdev.68

Mitra, S.K., Hanson, D.A., Schlaepher, D.D., 2005. Focal Adhesion Kinase: In command and Control of Cell Motility. Mol Cell Bio 6, 56–68. doi:10.1038/nrm1549

Molin, D.G.M., Bartram, U., Van der Heiden, K., Van Iperen, L., Speer, C.P., Hierck, B.P., Poelmann, R.E., Gittenberger-de-Groot, A.C., 2003. Expression patterns of Tgfβ1-3 associate with myocardialisation of the outflow tract and the development of the epicardium and the fibrous heart skeleton. Dev. Dyn. 227, 431–444. doi:10.1002/dvdy.10314

Moore, A.W., McInnes, L., Kreidberg, J., Hastie, N.D., Schedl, A., 1999. YAC complementation shows a requirement for Wt1 in the development of epicardium, adrenal gland and throughout nephrogenesis. Development 126, 1845–1857.

Moorman, A.F.M., Christoffels, V.M., 2003. Cardiac Chamber Formation: Development, Genes, and Evolution. Physiol. Rev. 83, 1223–1267. doi:10.1152/physrev.00006.2003

Morabito, C.J., Dettman, R.W., Kattan, J., Collier, J.M., Bristow, J., 2001. Positive and negative regulation of epicardial-mesenchymal transformation during avian heart development. Dev. Biol. 234, 204–15. doi:10.1006/dbio.2001.0254

Moynihan, K., Stockdale, F., Bader, D., 2010. An overview of Avian Heart Structure and Development, Heart Development and Regeneration. Elsevier Inc. doi:10.1016/B978-0-12-381332-9.00005-0

Muraoka, R.S., Bushdid, P.B., Brantley, D.M., Yull, F.E., Kerr, L.D., 2000. Mesenchymal expression of nuclear factor-kappaB inhibits epithelial growth and branching in the embryonic chick lung. Dev. Biol. 225, 322–38. doi:10.1006/dbio.2000.9824

Nickel, W., 2010. Pathways of unconventional protein secretion. Curr. Opin. Biotechnol. 21, 621–626. doi:10.1016/j.copbio.2010.06.004

Niehrs, C., 2006. Function and biological roles of the Dickkopf family of Wnt modulators. Oncogene 25, 7469–81. doi:10.1038/sj.onc.1210054

Nimesh, S., Mohottalage, S., Vincent, R., Kumarathasan, P., 2013. Current status and future perspectives of mass spectrometry imaging. Int. J. Mol. Sci. 14, 11277–11301. doi:10.3390/ijms140611277

O'Meara, C.C., Wamstad, J.A., Gladstone, R.A., Fomovsky, G.M., Butty, V.L., Shrikumar, A., Gannon, J.B., Boyer, L.A., Lee, R.T., 2015. Transcriptional reversion of cardiac myocyte fate during mammalian cardiac regeneration. Circ. Res. 116, 804–815. doi:10.1161/CIRCRESAHA.116.304269

Ohta, S., Misawa, A., Fukaya, R., Inoue, S., Kanemura, Y., 2012. Macrophage migration inhibitory factor (MIF) promotes cell survival and proliferation of neural stem / progenitor cells.

Olivey, H.E., Svensson, E.C., 2010. Epicardial-myocardial signaling directing coronary vasculogenesis. Circ. Res. 106, 818–32. doi:10.1161/CIRCRESAHA.109.209197

Pae, S.H., Dokic, D., Dettman, R.W., 2008. Communication between integrin receptors facilitates epicardial cell adhesion and matrix organization. Dev. Dyn. 237, 962–78. doi:10.1002/dvdy.21488

Pennisi, D.J., Ballard, V.L.T., Mikawa, T., 2003. Epicardium is required for the full rate of myocyte proliferation and levels of expression of myocyte mitogenic factors FGF2 and its receptor, FGFR-1, but not for transmural myocardial patterning in the embryonic chick heart. Dev. Dyn. 228, 161–72. doi:10.1002/dvdy.10360

Perez-Pinera, P., Alcantara, S., Dimitrov, T., Vega, J. a, Deuel, T.F., 2006. Pleiotrophin disrupts calcium-dependent homophilic cell-cell adhesion and initiates an epithelial-mesenchymal transition. Proc. Natl. Acad. Sci. U. S. A. 103, 17795–17800. doi:10.1073/pnas.0607299103

Pérez-Pomares, J.M., de la Pompa, J.L.J.L., Perez-Pomares, J.M., de la Pompa, J.L.J.L., 2011. Signaling during epicardium and coronary vessel development. Circ. Res. 109, 1429–1442. doi:10.1161/CIRCRESAHA.111.245589

Person, A.D., Garriock, R.J., Krieg, P.A., Runyan, R.B., Klewer, S.E., 2005. Frzb modulates Wnt-9a-mediated β-catenin signaling during avian atrioventricular cardiac cushion development. Dev. Biol. 278, 35–48. doi:10.1016/j.ydbio.2004.10.013

Petersen, T.N., Brunak, S., von Heijne, G., Nielsen, H., 2011. SignalP 4.0: discriminating signal peptides from transmembrane regions. Nat. Methods 8, 785–786. doi:10.1038/nmeth.1701

Poelmann, R.E.., Lie-Venema, Heleen; Gittenberger-de Groot, A., 2002. The Role of the Epicardium and Neural Crest. Texas Hear. Inst. J. 29, 255–261.

Polacek, M., Bruun, J.A., Johansen, O., Martinez, I., 2010. Differences in the secretome of cartilage explants and cultured chondrocytes unveiled by SILAC technology. J. Orthop. Res. 28, 1040–1049. doi:10.1002/jor.21067

Porrello, E.R., Olson, E.N., 2014. A neonatal blueprint for cardiac regeneration. Stem Cell Res. 13, 556–570. doi:10.1016/j.scr.2014.06.003

Ramjee, V., Li, D., Manderfield, L.J., Liu, F., Engleka, K.A., Aghajanian, H., Rodell, C.B., Lu,

W., Ho, V., Wang, T., Li, L., Singh, A., Cibi, D.M., Burdick, J.A., Singh, M.K., Jain, R., Epstein, J.A., 2017. Epicardial YAP / TAZ orchestrate an immunosuppressive response following myocardial infarction 127, 1–13. doi:10.1172/JCI88759.

Reymond, A., Marigo, V., Yaylaoglu, M.B., Leoni, A., Ucla, C., Scamuffa, N., Caccioppoli, C., Dermitzakis, E.T., Lyle, R., Banfi, S., Eichele, G., Antonarakis, S.E., Ballabio, A., 2002. Human chromosome 21 gene expression atlas in the mouse. Nature 420, 582–586. doi:10.1038/nature01178

Ronca, R., Di Salle, E., Giacomini, A., Leali, D., Alessi, P., Coltrini, D., Ravelli, C., Matarazzo, S., Ribatti, D., Vermi, W., Presta, M., 2013. Long pentraxin-3 inhibits epithelial-mesenchymal transition in melanoma cells. Mol. Cancer Ther. 12, 2760–71. doi:10.1158/1535-7163.MCT-13-0487

Ross, R.S., Borg, T.K., 2001. Integrins and the myocardium. Circ. Res. 88, 1112–9. doi:10.1161/hh1101.091862

Ruiz-Villalba, A., Pérez-Pomares, J.M., 2012. The expanding role of the epicardium and epicardial-derived cells in cardiac development and disease. Curr. Opin. Pediatr. 24, 569–576. doi:10.1097/MOP.0b013e328357a532

Ryzhakov, G., Teixeira, A., Saliba, D., Blazek, K., Muta, T., Ragoussis, J., Udalova, I.A., 2013. Cross-species analysis reveals evolving and conserved features of the nuclear factor κb (NF-κB) proteins. J. Biol. Chem. 288, 11546–11554. doi:10.1074/jbc.M113.451153

Sánchez, N.S., Barnett, J. V, 2012. TGFβ and BMP-2 regulate epicardial cell invasion via TGFβR3 activation of the Par6/Smurf1/RhoA pathway. Cell. Signal. 24, 539–48. doi:10.1016/j.cellsig.2011.10.006

Sanford, L.P., Ormsby, I., Groot, A.C.G., Sariola, H., Friedman, R., Boivin, G.P., Cardell, E. Lou, Doetschman, T., 1997. TGFβ2 knockout mice have multiple developmental defects that are non-overlapping with other TGFβ knockout phenotypes. Development 124, 2659–2670.

Sarkar, P., Randall, S.M., Muddiman, D.C., Rao, B.M., 2012. Targeted Proteomics of the Secretory Pathway Reveals the Secretome of Mouse Embryonic Fibroblasts and Human Embryonic Stem Cells. Mol. Cell. Proteomics 11, 1829–1839. doi:10.1074/mcp.M112.020503

Schober, Y., Schramm, T., Spengler, B., Römpp, A., 2011. Protein identification by accurate mass matrix-assisted laser desorption/ionization imaging of tryptic peptides. Rapid Commun. Mass Spectrom. 25, 2475–2483. doi:10.1002/rcm.5135

Schwamborn, K., Caprioli, R.M., 2010. Molecular imaging by mass spectrometry — looking beyond classical histology. Nat. Publ. Gr. 10, 639–646. doi:10.1038/nrc2917

Schwartz, S.A., Reyzer, M.L., Caprioli, R.M., 2003. SPECIAL FEATURE : Direct tissue analysis using matrix-assisted laser desorption / ionization mass spectrometry : practical aspects of sample preparation 699–708. doi:10.1002/jms.505

Sedmera, David; McQuinn, T., 2008. Embryogenesis of heart muscle. Heart Fail. Clin. 4, 235–

245. doi:10.1016/j.hfc.2008.02.007.Embryogenesis

Seeley, E.H., Caprioli, R.M., 2011. MALDI imaging mass spectrometry of human tissue: Method challenges and clinical perspectives. Trends Biotechnol. 29, 136–143. doi:10.1016/j.tibtech.2010.12.002

Seeley, E.H., Oppenheimer, S.R., Mi, D., Chaurand, P., Caprioli, R.M., 2008. Enhancement of Protein Sensitivity for MALDI Imaging Mass Spectrometry After Chemical Treatment of Tissue Sections. J. Am. Soc. Mass Spectrom. 19, 1069–1077. doi:10.1016/j.jasms.2008.03.016

Sha, W.C., Liou, H.C., Tuomanen, E.I., Baltimore, D., 1995. Targeted disruption of the p50 subunit of NF-κB leads to multifocal defects in immune responses. Cell 80, 321–330. doi:10.1016/0092-8674(95)90415-8

Shin, H.M., Kim, M.H., Kim, B.H., Jung, S.H., Kim, Y.S., Park, H.J., Hong, J.T., Min, K.R., Kim, Y., 2004. Inhibitory action of novel aromatic diamine compound on lipopolysaccharide-induced nuclear translocation of NF-κB without affecting IκB degradation. FEBS Lett. 571, 50–54. doi:10.1016/j.febslet.2004.06.056

Singh, M., Foster, C.C.R., Dalal, S., Singh, K., 2010. Osteopontin: role in extracellular matrix deposition and myocardial remodeling post-MI. J. Mol. Cell. … 48, 538–543. doi:10.1016/j.yjmcc.2009.06.015.Osteopontin

Smart, N., Bollini, S., Dubé, K.N., Vieira, J.M., Zhou, B., Riegler, J., Price, A.N., Lythgoe, M.F., Davidson, S., Yellon, D., Pu, W.T., Riley, P.R., 2012. Myocardial regeneration: Expanding the repertoire of thymosin β4 in the ischemic heart. Ann. N. Y. Acad. Sci. 1269, 92–101. doi:10.1111/j.1749-6632.2012.06708.x

Smart, N., Risebro, C. a, Melville, A. a D., Moses, K., Schwartz, R.J., Chien, K.R., Riley, P.R., 2007. Thymosin beta4 induces adult epicardial progenitor mobilization and neovascularization. Nature 445, 177–182. doi:10.1038/nature05383

Smith, C.L., Baek, S.T., Sung, C.Y., Tallquist, M.D., 2011. Epicardial-derived cell epithelial-to-mesenchymal transition and fate specification require PDGF receptor signaling. Circ. Res. 108, e15-26. doi:10.1161/CIRCRESAHA.110.235531

Sofeu Feugaing, D.D., Götte, M., Viola, M., 2013. More than matrix: the multifaceted role of decorin in cancer. Eur. J. Cell Biol. 92, 1–11. doi:10.1016/j.ejcb.2012.08.004

Sokol, J.P., Neil, J.R., Schiemann, B.J., Schiemann, W.P., 2005. The use of cystatin C to inhibit epithelial-mesenchymal transition and morphological transformation stimulated by transforming growth factor-beta. Breast Cancer Res. 7, R844-53. doi:10.1186/bcr1312

Soncini, D., Caffa, I., Zoppoli, G., Cea, M., Cagnetta, A., Passalacqua, M., Mastracci, L., Boero, S., Montecucco, F., Sociali, G., Lasigliè, D., Damonte, P., Grozio, A., Mannino, E., Poggi, A., D'Agostino, V.G., Monacelli, F., Provenzani, A., Odetti, P., Ballestrero, A., Bruzzone, S., Nencioni, A., 2014. Nicotinamide phosphoribosyltransferase promotes epithelial-to-mesenchymal transition as a soluble factor independent of its enzymatic activity. J. Biol.

Chem. 0–27. doi:10.1074/jbc.M114.594721

Sonnylal, S., Xu, S., Jones, H., Tam, A., Sreeram, V.R., Ponticos, M., Norman, J., Agrawal, P., Abraham, D., de Crombrugghe, B., 2013. Connective tissue growth factor causes EMT-like cell fate changes in vivo and in vitro. J. Cell Sci. 126, 2164–75. doi:10.1242/jcs.111302

Sridurongrit, S., Larsson, J., Schwartz, R., Ruiz-Lozano, P., Kaartinen, V., 2008. Signaling via the Tgf-beta type I receptor Alk5 in heart development. Dev. Biol. 322, 208–18. doi:10.1016/j.ydbio.2008.07.038

Stastna, M., Van Eyk, J.E., 2012. Investigating the secretome lessons about the cells that comprise the heart. Circ. Cardiovasc. Genet. 5, 8–19. doi:10.1161/CIRCGENETICS.111.960187

Stuckmann, I., Evans, S., Lassar, A.B., 2003. Erythropoietin and retinoic acid, secreted from the epicardium, are required for cardiac myocyte proliferation. Dev. Biol. 255, 334–349. doi:10.1016/S0012-1606(02)00078-7

Sucov, H.M., Gu, Y., Thomas, S., Li, P., Pashmforoush, M., 2009. Epicardial control of myocardial proliferation and morphogenesis. Pediatr. Cardiol. 30, 617–25. doi:10.1007/s00246-009-9391-8

Sundaram, G.M., Common, J.E.A., Gopal, F.E., Srikanta, S., Lakshman, K., 2013. "See-saw" expression of microRNA-198 and FSTL1 from a single transcript in wound healing. Nature 495, 103–106. doi:10.1038/nature11890

Tanaka, K., Waki, H., Ido, Y., Akita, S., Yoshida, Y., Yoshida, T., Matsuo, T., 1988. Protein and polymer analyses up to *m/z* 100 000 by laser ionization time-of-flight mass spectrometry. Rapid Commun. Mass Spectrom. 2, 151–153. doi:10.1002/rcm.1290020802

Tao, J., Doughman, Y., Yang, K., Ramirez-Bergeron, D., Watanabe, M., 2013. Epicardial HIF signaling regulates vascular precursor cell invasion into the myocardium. Dev. Biol. 376, 136–49. doi:10.1016/j.ydbio.2013.01.026

Tian, X., Pu, W.T., Zhou, B., 2015. Cellular origin and developmental program of coronary angiogenesis. Circ. Res. 116, 515–530. doi:10.1161/CIRCRESAHA.116.305097

Van Den Akker, N.M.S., Lie-Venema, H., Maas, S., Eralp, I., DeRuiter, M.C., Poelmann, R.E., Gittenberger-De Groot, A.C., 2005. Platelet-derived growth factors in the developing avian heart and maturating coronary vasculature. Dev. Dyn. 233, 1579–88. doi:10.1002/dvdy.20476

van den Berg, G., Somi, S., Buffing, A. a M., Moorman, A.F.M., van den Hoff, M.J.B., 2007. Patterns of expression of the Follistatin and Follistatin-like1 genes during chicken heart development: a potential role in valvulogenesis and late heart muscle cell formation. Anat. Rec. (Hoboken). 290, 783–7. doi:10.1002/ar.20559

Vega-Hernández, M., Kovacs, A., De Langhe, S., Ornitz, D.M., 2011. FGF10/FGFR2b signaling is essential for cardiac fibroblast development and growth of the myocardium. Development 138, 3331–40. doi:10.1242/dev.064410

Verma, I.M., Stevenson, J.K., Schwarz, E.M., Antwerp, D. Van, 1995. R~~/NF-KB /IKB familv: intimate tales of association and dissociation. Genes Dev. 2723–2735.

Visel, A., Thaller, C., Eichele, G., 2004. GenePaint.org: an atlas of gene expression patterns in the mouse embryo. Nucleic Acids Res. 32, D552-6. doi:e

von Gise, A., Pu, W.T., Gise, A. Von, Pu, W.T., 2012. Endocardial and epicardial epithelial to mesenchymal transitions in heart development and disease. Circ. Res. 110, 1628–1645. doi:10.1161/CIRCRESAHA.111.259960

von Gise, A., Zhou, B., Honor, L.B., Ma, Q., Petryk, A., Pu, W.T., 2011. WT1 regulates epicardial epithelial to mesenchymal transition through β-catenin and retinoic acid signaling pathways. Dev. Biol. 356, 421–31. doi:10.1016/j.ydbio.2011.05.668

Waldo, K.L., Hutson, M.R., Ward, C.C., Zdanowicz, M., Stadt, H.A., Kumiski, D., Abu-Issa, R., Kirby, M.L., 2005. Secondary heart field contributes myocardium and smooth muscle to the arterial pole of the developing heart. Dev. Biol. 281, 78–90. doi:10.1016/j.ydbio.2005.02.012

Waldo, K.L., Kumiski, D.H., Wallis, K.T., Stadt, H.A., Hutson, M.R., Platt, D.H., Kirby, M.L., 2001. Conotruncal myocardium arises from a secondary heart field. Development 128, 3179–3188.

Walsh, S., Pontén, A., Fleischmann, B.K., Jovinge, S., 2010. Cardiomyocyte cell cycle control and growth estimation in vivo-An analysis based on cardiomyocyte nuclei. Cardiovasc. Res. 86, 365–373. doi:10.1093/cvr/cvq005

Wang, G.K., Hu, L., Fuller, G.N., Zhang, W., 2006. An interaction between insulin-like growth factor-binding protein 2 (IGFBP2) and integrin alpha5 is essential for IGFBP2-induced cell mobility. J. Biol. Chem. 281, 14085–91. doi:10.1074/jbc.M513686200

Wang, J., Greene, S.B., Martin, J.F., 2011. BMP signaling in congenital heart disease: New developments and future directions. Birth Defects Res. Part A - Clin. Mol. Teratol. 91, 441–448. doi:10.1002/bdra.20785

Wang, J., Karra, R., Dickson, A.L., Poss, K.D., 2013. Fibronectin is deposited by injury-activated epicardial cells and is necessary for zebrafish heart regeneration. Dev. Biol. 382, 427–435. doi:10.1016/j.ydbio.2013.08.012

Warkman, A.S., 2009. Xenopus as a model system for vertebrate heart development. Motor Control 27, 590–609. doi:10.1016/j.humov.2008.02.015.Changes

Watrous, J., 2011. The evolving field of imaging mass spectrometry and its impact on future biological research. … Mass Spectrom. 46, 209–222. doi:10.1002/jms.1876.The

Weeke-Klimp, A., Bax, N. a M., Bellu, A.R., Winter, E.M., Vrolijk, J., Plantinga, J., Maas, S., Brinker, M., Mahtab, E. a F., Gittenberger-de Groot, A.C., van Luyn, M.J. a, Harmsen, M.C., Lie-Venema, H., 2010. Epicardium-derived cells enhance proliferation, cellular maturation and alignment of cardiomyocytes. J. Mol. Cell. Cardiol. 49, 606–16. doi:10.1016/j.yjmcc.2010.07.007

Wei, K., Serpooshan, V., Hurtado, C., Diez-Cunado, M., Zhao, M., Maruyama, S., Zhu, W., Fajardo, G., Noseda, M., Nakamura, K., Tian, X., Liu, Q., Wang, A., Matsuura, Y., Bushway, P., Cai, W., Savchenko, A., Mahmoudi, M., Schneider, M.D., van den Hoff, M.J.B., Butte, M.J., Yang, P.C., Walsh, K., Zhou, B., Bernstein, D., Mercola, M., Ruiz-Lozano, P., 2015. Epicardial FSTL1 reconstitution regenerates the adult mammalian heart. Nature 525, 479–485. doi:10.1038/nature15372

Welikson, R.E., Kaestner, S., Evans, A.M., Hauschka, S.D., 2007. Embryonic cardiomyocyte expression of endothelial genes. Dev. Dyn. 236, 2512–2522. doi:10.1002/dvdy.21276

Wenke, J.L., Rose, K.L., Spraggins, J.M., Schey, K.L., 2017. MALDI Imaging Mass Spectrometry Spatially Maps Age- Related Deamidation and Truncation of Human Lens. doi:10.1167/iovs.15-18117

Werner Bouschen, Schulz, O., 2010. N-Nitrosopiperazines form at high pH in post-combustion capture solutions containing piperazine: a low-energy collisional behaviour study. Rapid Commun. Mass Spectrom. 24, 3567–3577. doi:10.1002/rcm

Wessels, A., van den Hoff, M.J.B., Adamo, R.F., Phelps, A.L., Lockhart, M.M., Sauls, K., Briggs, L.E., Norris, R.A., van Wijk, B., Perez-Pomares, J.M., Dettman, R.W., Burch, J.B.E., 2012. Epicardially derived fibroblasts preferentially contribute to the parietal leaflets of the atrioventricular valves in the murine heart. Dev. Biol. 366, 111–124. doi:10.1016/j.ydbio.2012.04.020

Wetzel-Strong, S.E., Li, M., Klein, K.R., Nishikimi, T., Caron, K.M., 2014. Epicardial-derived adrenomedullin drives cardiac hyperplasia during embryogenesis. Dev. Dyn. 243, 243–256. doi:10.1002/dvdy.24065

Winter, E.M., Grauss, R.W., Hogers, B., Tuyn, J. Van, Geest, R. Van Der, F, A.A., Steendijk, P., Doevendans, P.A., Laarse, A. Van Der, 2007. Preservation of Left Ventricular Function and Attenuation of Remodeling After Transplantation of Human Epicardium-Derived Cells Into the Infarcted Mouse Heart. doi:10.1161/CIRCULATIONAHA.106.668178

Wittig, J., Münsterberg, A., 2016. The Early Stages of Heart Development: Insights from Chicken Embryos. J. Cardiovasc. Dev. Dis. 3, 12. doi:10.3390/jcdd3020012

Wu, H., Lee, S.H., Gao, J., Liu, X., Iruela-Arispe, M.L., 1999. Inactivation of erythropoietin leads to defects in cardiac morphogenesis. Development 126, 3597–3605.

Wu, M., Smith, C.L., Hall, J. a, Lee, I., Luby-Phelps, K., Tallquist, M.D., 2010. Epicardial spindle orientation controls cell entry into the myocardium. Dev. Cell 19, 114–25. doi:10.1016/j.devcel.2010.06.011

Yang, J., Caprioli, R.M., 2011. Spectrometry at High Spatial Resolution 5728–5734.

Yang, J.T., Rayburn, H., Hynes, R.O., 1995. Cell adhesion events mediated by alpha 4 integrins are essential in placental and cardiac development. Development 121, 549–60.

Zavalin, A., Yang, J., Hayden, K., Vestal, M., Caprioli, R.M., 2015. Tissue protein imaging at 1 μ m laser spot diameter for high spatial resolution and high imaging speed using transmission

geometry MALDI TOF MS 2337–2342. doi:10.1007/s00216-015-8532-6

Zhou, B., Honor, L.B., He, H., Ma, Q., Oh, J., Butterfield, C., Lin, R., Melero-martin, J.M., Dolmatova, E., Duffy, H.S., Gise, A. Von, Zhou, P., Hu, Y.W., Wang, G., Zhang, B., Wang, L., Hall, J.L., Moses, M.A., Mcgowan, F.X., Pu, W.T., 2011. Adult mouse epicardium modulates myocardial injury by secreting paracrine factors. J. Clin. Invest. 121. doi:10.1172/JCI45529DS1

Zhou, B., Honor, L.B., Ma, Q., Oh, J.-H., Lin, R.-Z., Melero-Martin, J.M., von Gise, A., Zhou, P., Hu, T., He, L., Wu, K.H., Zhang, H., Zhang, Y., Pu, W.T., 2012. Thymosin beta 4 treatment after myocardial infarction does not reprogram epicardial cells into cardiomyocytes. J. Mol. Cell. Cardiol. 52, 43–7. doi:10.1016/j.yjmcc.2011.08.020

Zhou, B., von Gise, A., Ma, Q., Hu, Y.W., Pu, W.T., 2010. Genetic fate mapping demonstrates contribution of epicardium-derived cells to the annulus fibrosis of the mammalian heart. Dev. Biol. 338, 251–261. doi:10.1016/j.ydbio.2009.12.007

VITA

EDUCATION

Ph.D. Candidate in Molecular, Cell and Developmental Biology (MCDB) Program

University of Illinois at Chicago (UIC), Chicago, IL, 2010-2017

B.S. in Biochemistry and Molecular Biology

China Agricultural University (CAU), Beijing, China, 2006-2010

RESEARCH EXPERIENCE

Doctoral research. Department of Biological Sciences**,** University of Illinois at Chicago (UIC), 2010-2017

Undergraduate Researcher. Tsinghua University, Beijing, 08/2009-06/2010

Undergraduate Researcher. National Institute of Biological Sciences (NIBS), Beijing, 10/2008-04*/2009*

AWARDS and HONORS

- UIC Research Achievement Award, 2017
- UIC Graduate Student Council Travel Award, 2014, 2015, 2016
- UIC Department of Biological Sciences Travel Award, 2014, 2015, 2016
- UIC Research Image Competition, final list, 2014
- National Inspirational Awards for Disadvantaged Outstanding Students, 2007, 2008
- NIBS-CAU Scholarship, 2006

TEACHING EXPERIENCE

Teaching Assistant

University of Illinois at Chicago (UIC), 2010-20017

- Genetics Laboratory, 6 semesters
- Molecular & Mendelian Genetics, 2 semesters
- Cell Biology Laboratory, 2 semesters
- Microbiology Laboratory, 1 semester

CONFERENCE PRESENTATIONS

- **Yanyang Li**, Devin Midura, Alexander Urban, Hans-Georg Simon, Q. Tian Wang. Proteomic Characterization of Epicardial-Myocardial Signaling Reveals Novel Regulatory Networks Including a Role for NF-κB in Epicardial EMT. 2017. ASBMB Annual Meeting. Chicago, IL
- **Yanyang Li**, Devin Midura, Alexander Urban, Hans-Georg Simon, Q. Tian Wang. Proteomic

Characterization of Epicardial-Myocardial Signaling Reveals Novel Regulatory Networks Including a Role for NF-κB in Epicardial EMT. 2016. ASCB Annual Meeting. San Francisco, CA

- **Yanyang Li,** Devin Midura, Alexander Urban, Hans-Georg Simon, Q. Tian Wang. Global Characterization of Epicardial-Myocardial Signaling Reveals an Essential Role of NF-κB in Epithelial-to-Mesenchymal Transition. 2016. Weinstein conference. Durham, NC
- **Yanyang Li,** Devin Midura, Alexander Urban, Hans-Georg Simon, Q. Tian Wang. Proteomics analysis of primary chicken epicardium-myocardium explant conditioned medium. 2015. Weinstein conference. Boston, MA
- **Yanyang Li**, Devin Midura, Hans-Georg Simon, Q. Tian Wang. Identifying Secreted Factors Mediating Epicardial-Myocardial Signaling. 2014. Midwest Society for Developmental Biology Meeting. St. Louis, MO
- **Yanyang Li**, Devin Midura, Yang Cui, Luke Hanley, Hans-Georg Simon, Q. Tian Wang. Identifying Secreted Factors Mediating Epicardial-Myocardial Signaling. 2014. 1st Annual MBRB Retreat. Chicago, IL

PUBLICATIONS

- **Li Y**, Urban A, Midura D, Simon HG, Wang QT (2017) Proteomic characterization of epicardial-myocardial signaling reveals novel regulatory networks including a role for NF-κB in epicardial EMT. PLOS ONE 12(3): e0174563.
- Khan FF, **Li Y**, Balyan A, Wang QT. WTIP interacts with ASXL2 and blocks ASXL2-mediated activation of retinoic acid signaling. Biochem Biophys Res Commun. 2014 Aug 15; 451(1):101-6.
- McGinley AL, **Li Y**, Deliu Z, Wang QT. Additional sex combs-like family genes are required for normal cardiovascular development. Genesis. 2014 Jul; 52(7):671-86.